AD-A184 074   GAS-SOLID TRANSPORT IN A 08508 M PIPE AT VARIOUS   1/3
INCLINATIONS WITH AND WITHOUT ELECTROSTATICS(U) ARMY
MILITARY PERSONNEL CENTER ALEXANDRIA VA C A MYLER
UNCLASSIFIED AUG 85   F/G 13/11   NL

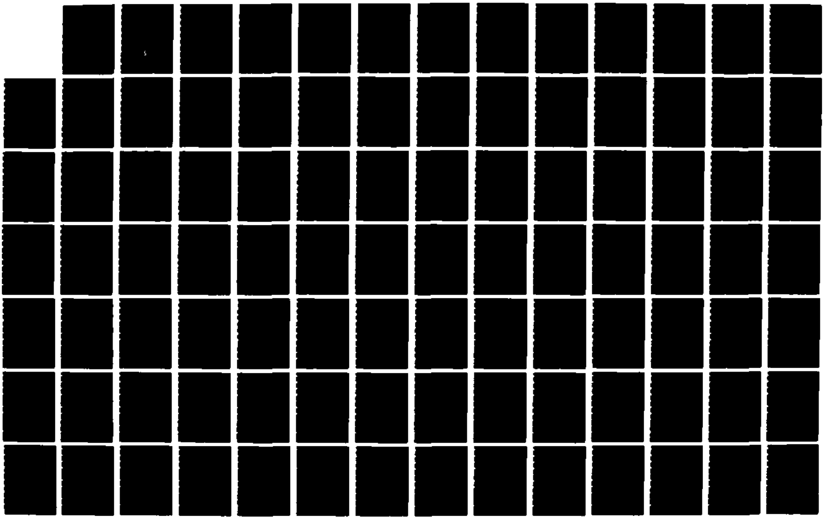

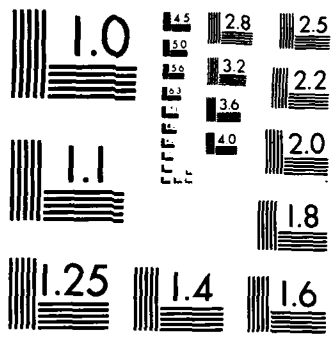

MICROCOPY RESOLUTION TEST CHART
NATIONAL BUREAU OF STANDARDS-1963-A

(2)

GAS-SOLID TRANSPORT IN A 0.0508 m PIPE AT VARIOUS INCLINATIONS WITH AND WITHOUT ELECTROSTATICS

Captain Craig A. Myler
HQDA, MILPERCEN(DAPC-OPA-E)
200 Stovall Street
Alexandria, VA 22332

Final Report AUG 85

A thesis submitted to the University of Pittsburgh in partial fulfillment of the requirements for the degree of Master of Science in Chemical Engineering

SECURITY CLASSIFICATION OF THIS PAGE (When Data Entered)

REPORT DOCUMENTATION PAGE		READ INSTRUCTIONS BEFORE COMPLETING FORM
1. REPORT NUMBER	2. GOVT ACCESSION NO. AD-A184074	3. RECIPIENT'S CATALOG NUMBER
4. TITLE (and Subtitle) Gas-Solid Transport in a 0.058m Pipe at various Inclinations with and Without Electrostatics		5. TYPE OF REPORT & PERIOD COVERED Thesis / Aug 85
		6. PERFORMING ORG. REPORT NUMBER
7. AUTHOR(s) Craig A. Myler		8. CONTRACT OR GRANT NUMBER(s)
9. PERFORMING ORGANIZATION NAME AND ADDRESS Student, HQDA, MILPERCEN (DAPC-OPA-E), 200 Stovall Street, Alexandria, Virginia 22332		10. PROGRAM ELEMENT, PROJECT, TASK AREA & WORK UNIT NUMBERS
11. CONTROLLING OFFICE NAME AND ADDRESS HQDA, MILPERCEN, ATTN: DAPC-OPA-E, 200 Stovall Street, Alexandria, Virginia 22332		12. REPORT DATE Aug 85
		13. NUMBER OF PAGES 238
14. MONITORING AGENCY NAME & ADDRESS (if different from Controlling Office)		15. SECURITY CLASS. (of this report) UNCLASS
		15a. DECLASSIFICATION/DOWNGRADING SCHEDULE

16. DISTRIBUTION STATEMENT (of this Report)

Approved for Public Release; distribution unlimited

17. DISTRIBUTION STATEMENT (of the abstract entered in Block 20, if different from Report)

18. SUPPLEMENTARY NOTES M.S. Thesis, University of Pittsburgh

19. KEY WORDS (Continue on reverse side if necessary and identify by block number)

Choking, Electrostatics, Horizontal, Inclined, Linear Stability, Particle Velocity, Pressure Drop, Vertical

20. ABSTRACT (Continue on reverse side if necessary and identify by block number)

Pneumatic transport of fine solids by air was conducted in a 0.058m pipe at 90°, 45°, and 0° from the horizontal. Particle velocities, pressure drop, gas velocities, and solid feed rate were measured. Analysis includes pressure drop relationships and stability. Electrostatic effects were controlled through humidity control.

DD FORM 1 JAN 73 1473 EDITION OF 1 NOV 65 IS OBSOLETE

SECURITY CLASSIFICATION OF THIS PAGE (When Data Entered)

SECURITY CLASSIFICATION OF THIS PAGE(*When Data Entered*)

SECURITY CLASSIFICATION OF THIS PAGE(*When Data Entered*)

GAS-SOLID TRANSPORT IN A 0.0508 m PIPE AT VARIOUS

INCLINATIONS WITH AND WITHOUT ELECTROSTATICS

by

Craig A. Myler

B.S. in Chemistry, Virginia Military Institute, 1979

Submitted to the Graduate Faculty

of the School of Engineering

in partial fulfillment of

the requirements for the degree of

Master of Science
in
Chemical Engineering

University of Pittsburgh

1985

Signed

ACKNOWLEDGEMENTS

I would like to thank Dr. G.E. Klinzing for having the faith to let me try, the patience when I failed, and the encouragement I needed to continue. I would also like to thank Dr. M.P. Mathur and Dr. B. Morsi for their time and expertise in evaluating this thesis.

To Abdi Zaltash I owe a great deal, and I sincerely thank him for his time and effort in assisting me throughout my research.

I would like to thank Mr. Larry Herman and Mrs. Pye Pajewski for their assistance in technical matters. I also thank Miss Suxuan Huang for her performing the particle analysis.

Finally, I would like to thank my wife, Janice, for silently accepting the long hours I kept and the irritable disposition I often displayed.

ABSTRACT

Signature George E Klinzing

GAS-SOLID TRANSPORT IN A 0.0508 m PIPE AT VARIOUS INCLINATIONS WITH AND WITHOUT ELECTROSTATICS

Craig A. Myler, M.S.

University of Pittsburgh

The transport of solid particles by air through a 0.0508 m pipe was studied in vertical, horizontal, and 45° orientations. Through control of the air humidity, the effects of electrostatic charging was observed. Pressure drop and particle velocities were measured. Particles used included 79µm, 125µm, and 450µm glass beads and 128µm Plexiglas beads.

Analysis of particle velocity, pressure drop, pressure drop fluctuation, electrostatic pressure drop, choking, and saltation was performed. Visual observations of the flow patterns and behavior were made. A linear stability analysis for the three orientations was performed.

DESCRIPTORS

Choking

Electrostatics

Horizontal

Inclined

Linear Stability

Particle Velocity

Pressure Drop

Saltation

Vertical

TABLE OF CONTENTS

LIST OF FIGURES

LIST OF TABLES

NOMENCLATURE

C_{DS}	Drag coefficient of single particle (dimensionless)
D_p	Particle diameter (m)
D_t	Tube diameter (m)
f_g	Gas friction factor (dimensionless)
f_{pc}	Particle friction factor at choking (dimensionless)
f_s	Solid friction factor (dimensionless)
g	Gravitational acceleration (m/s^2)
Δm_g	Mass of gas in differential length of tube (kg)
Δm_p	Mass of solids in differential length of tube (kg)
ΔP_E	Electrostatic pressure drop (Pa)
ΔP_T	Total pressure drop (Pa)
q	Charge/particle (C)

R	Solids loading (kg solids/kg air)
Re_p	Particle Reynolds number (dimensionless)
Re_t	Terminal Reynolds number (dimensionless)
t	Time (s)
U_f	Actual fluid velocity (m/s)
U_{fs}	Steady state fluid velocity (m/s)
$\hat{U}_f$	Fluid velocity fluctuation (m/s)
U_{fc}	Actual fluid velocity at choking (m/s)
U_g	Superficial gas velocity (m/s)
U_{gsalt}	Superficial gas velocity at saltation (m/s)
U_{gc}	Superficial gas velocity at choking (m/s)
U_p	Particle velocity (m/s)
U_{ps}	Steady state particle velocity (m/s)
$\hat{U}_p$	Particle velocity fluctuation (m/s)
U_s	Slip velocity (m/s)

U_t	Terminal velocity (m/s)
V_p	Volume of a particle (m^3)
Z_o	Contact distance (m)
W_s	Solid flow rate (kg/s)

Greek Letters

ε	Gas voidage (dimensionless)
ε_c	Gas voidage at choking (dimensionless)
ε_o	Permittivity of free space (farad/m)
ρ_f	Fluid density (kg/m^3)
ρ_p	Particle density (kg/m^3)
μ	Fluid viscosity (kg/ms)
$\frac{:P}{:x}$	Pressure gradient in axial direction (Pa/m)
π	Constant equal to 3.14159265
θ	Angle from the horizontal (degrees)

Ψ_p Particle–Particle collision factor (dimensionless)

Ψ_f Friction factor (dimensionless)

Ψ_w Wall collision factor (dimensionless)

1.0 INTRODUCTION

In the transport of solid particles by a gas stream, numerous forces act on the system. The direction and magnitude of these forces significantly affects the behaviour of the flow. Two such forces which arise in gas-solid transport, and not significantly in single phase gas flow, are those of gravity and electrostatics. The major problem with these two forces is that they affect the solid particles almost exclusively.

Gravity imposes a constant downward acceleration on the particles. To overcome the force caused by this acceleration, the gas must equal and overcome this force by exerting a drag force on the particles. When the drag force is no longer sufficient to overcome the force of gravity, and other forces present, the particles fall, and transport ceases. This falling of the particles is dependent on the orientation of the pipe through which they are being transported. In vertical upflow, the particles can fall unimpeded by the pipe itself, whereas in horizontal flow, the maximum descent is the diameter of the pipe. At other orientations, the particles can continue to fall while in contact with the pipe wall. The effect of gravity is different in different orientations and therefore must be accounted for in conjunction with that orientation.

Electrostatic forces are not as easily defined. The contacting of the solid particles with the pipe wall causes static electrification. As the particles themselves are moving and charged, the magnitude and direction of the electric field is difficult to define, even for a homogeous dispersion of the particles. Combined with the effect of gravity, the electrostatic forces can affect the flow differently with pipe orientaiton.

The purpose of this study is to examine the affects of pipe orientation on gas-solid transport with and without electrostatics. Additionally, the use of electrostatic ring probes for the measurement of solid particle velocity in a 0.0508 m pipe will be assessed.

2.0 LITERATURE REVIEW

Investigations into pneumatic transport have generally taken two approaches. The first is an attempt to empirically correlate data from these systems into workable expressions. The second approach is through theoretical modeling. The first approach suffers from the number of variables, and therefore, the number of groupings required to describe a given system. The second approach is hampered by a lack of fundamental knowledge.

2.1 BALANCE OF FORCES

An application of Newton's second law to the particles shown in figure 2-1 provides the following equation:

$$\Delta m_p dU_p/dt = dF_D - dF_g \sin\theta - dF_f - \Delta m_p/\rho_p \, \partial P/\partial x \pm F_{add} \tag{2-1}$$

Similarly, the gas must also have a balance of forces, which can be described by:

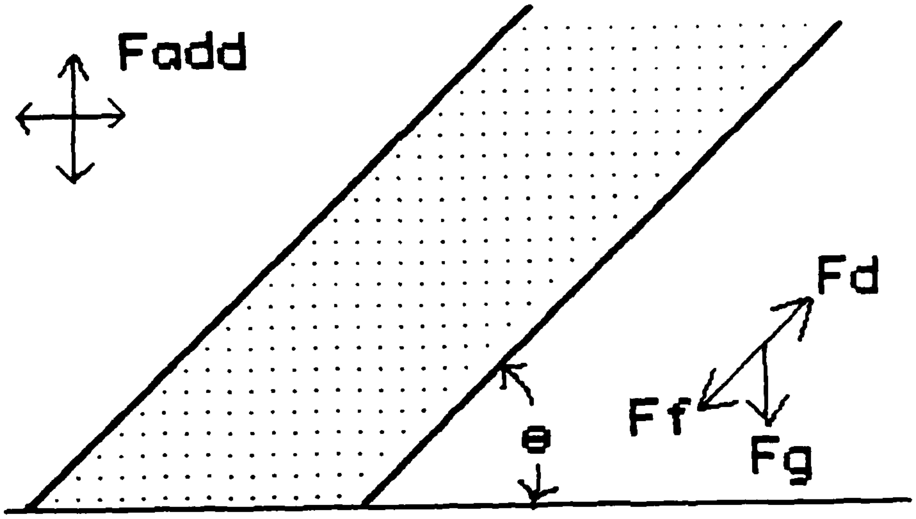

Figure 2-1: Force Balance on a Gas-Solid Flow in a Pipe at Inclination θ

$$\Delta m_g dU_f/dt = -dF_D - dF_g \sin\theta - dF_f - \Delta m_g/\rho_f \partial P/\partial x \qquad (2\text{-}2)$$

The first term on the RHS of equation 2-1 is the force due to drag on the particles. For a single particle, this term is described by:

$$dF_D = 3/4 C_{DS} \rho_f (U_{fs} - U_{ps}) \Delta m_p / [(\rho_p - \rho_f) D_p] \tag{2-3}$$

Wen and Yu[1]* suggest a modification to the single particle drag coefficient of:

$$C_{DS}(\text{modified}) = \varepsilon^{-4.7} C_{DS}(\text{single particle}) \tag{2-4}$$

This gives:

$$dF_D = 3/4\ \varepsilon^{-4.7}\ C_{DS} \rho_f (U_{fs} - U_{ps}) \Delta m_p / [(\rho_p - \rho_f) D_p] \tag{2-5}$$

The second term on the RHS of equation 2-1 is a gravity force. Direct application of Newton's law gives:

---

*Parenthetical references placed superior to the line of text refer to the bibliography.

$$dF_g = \Delta m_p g \tag{2-6}$$

which is the weight of the particles in the tube.

The third term on the RHS of equation 2-1 is the force due to friction. Using a friction factor for the solids, this force can be described as:

$$dF_f = 2f_s U_p^2 \Delta m_p / D_t \tag{2-7}$$

The fourth term on the RHS of equation 2-1 is the force due to the pressure gradient along the axis of the pipe.

Additional forces are present in the flow system and are often significant. They include forces due to electrostatic generation, external fields of force (such as magneto static fields), lift forces due to rotation, and cohesive forces. The electrostatic forces will be discussed later. The other forces are assumed to be negligible for this discussion and will be neglected.

Substitution of the expessions above into equation 2-1 and rearrangement yields:

$$dU_p/dt = 3/4\varepsilon^{-4.7}C_{DS}\rho_f(U_f - U_p)^2/[(\rho_p - \rho_f)D_p] - g\sin\theta - 2f_sU_p^2/D_t - 1/\rho_p\,\partial P/\partial x \tag{2-8}$$

For steady flow, and neglecting the pressure term, this becomes:

$$3/4\varepsilon^{-4.7}C_{DS}\rho_f(U_f - U_p)^2/[(\rho_p - \rho_f)D_p] - g\sin\theta - 2f_sU_p^2/D_t = 0 \tag{2-9}$$

As the voidage can be expressed as:

$$\varepsilon = 1 - 4W_s/(\rho_p\pi D_t^2U_p) \tag{2-10}$$

equation 2-9 can be made explicit for the particle velocity. There are, however, two terms in equation 2-9 which make the solution for the particle velocity difficult. They are the drag coefficient and the solid friction factor. The drag coefficient is dependent on the air flow rate. The friction factor is apparently strongly influenced by pipe orientation, particle diameter, particle and pipe material, and possibly other factors.

2.2 PRESSURE DROP

The pressure drop across a length of a pneumatic transport line is a very important design parameter. The introduction of solids into a gas stream causes, for most conditions, an increase in the pressure drop over that of air alone. Cases of pressure drop reduction to below that of air alone have been reported[2, 3], however, the conditions for this phenomena are very specialized. For steady flow conditions, the pressure drop can be obtained by adding the reduced forms of equations 2-1 and 2-2 as a sum of the forces in the system. This gives:

$$\Delta m_p g\sin\theta + \Delta m_g g\sin\theta + \Delta m_p 2f_s U_p^2/D_t \tag{2-11}$$

$$+ \Delta m_g 2f_g U_f^2/D_t + (\Delta m_p/\rho_p + \Delta m_g/\rho_g)\partial P/\partial x = 0$$

Note that in formulating equation 2-11, the force due to drag on the particles is equal and opposite the force causing the drag by the fluid, and therefore, cancels. Also, the additional force terms have been omitted. The mass terms in equation 2-11 can be expressed in terms of the voidage as:

$$\Delta m_p = (1-\varepsilon)\rho_p V_t \tag{2-12}$$

$$\Delta m_g = \varepsilon\rho_g V_t \tag{2-13}$$

and equation 2-11 becomes:

$$(1-\varepsilon)\rho_p g \sin\theta + \varepsilon\rho_g g \sin\theta \tag{2-14}$$

$$+(1-\varepsilon)\rho_p\ 2f_s U_p^2/D_t$$

$$+\varepsilon\rho_g\ 2f_g U_f^2/D_t + \partial P/\partial x = 0$$

Integrating equation 2-14 over a length L, rearranging, and noting the sign convention of the pressure drop, yields:

$$\Delta P = [(1-\varepsilon)\rho_p + \varepsilon\rho_g]\, Lg\sin\theta \tag{2-15}$$

$$+2\rho_p f_s (1-\varepsilon) L U_p^2/D_t$$

$$+2\rho_p f_g \varepsilon L U_f^2/D_t$$

The apparent simplicity of equation 2-15 is misleading. First, the particle velocity must be known. As mentioned before, the solids friction factor is apparently influenced by many factors, and therefore makes solution for the particle velocity from equation 2-8 difficult. Measuring the particle velocity is also difficult. Methods used have included the use of radioactive tracers[4], electrostatic signal cross-correlation[5, 6, 7], ultrasonic cross-correlation[8], and Laser-Doppler velocimeters.[9] All of these methods have drawbacks and/or difficulties in measuring the particle velocity. The additional forces

which were left out of equation 2-15 are sometimes very significant. The electrostatic forces which can be generated in pneumatic systems are often very large and have a significant impact on the pressure drop. These forces will be discussed further on.

2.3 PARTICLE PATH APPROACH

Molerus[10] has taken the force balance on particles in pneumatic transport a step further. He has considered the path of flight of a particle and the different interactions of the particle in different phases of its motion. A particle is considered to undergo the following flight phases:

Flight under the influence of gravity

Particle-Particle Collision

Particle-Wall Collision

Slide along the pipe wall

Pressure Gradient effects

From these possible interactions, equation 2-16 is obtained.

$$\Delta P/\rho_p + 3\rho_f C_{DS}(Re_p)U_f^2 L/(4D_p\rho_p) = \qquad (2\text{-}16)$$

$$(1-\rho_f/\rho_p)gL(\sin\theta + \psi_f\cos\theta)$$

$$+\psi_p(\rho_f\mu/\rho_p)^{1/3}LU_g^2/D_p$$

$$+\psi_w LU_g^2/D_t$$

where

Ψ_f = friction coefficient

Ψ_p = Particle–Particle collision coefficient

Ψ_w = Wall collision coefficient

Comparison of equation 2–16 with equation 2–8 at steady state is obvious. The major difference is in the frictional terms. Molerus provides simplifications to equation 2–16 for different flow conditions; however, the empirical nature of the friction factors required remains.

2.4 THERMODYNAMIC ANALOGY APPROACH

A different approach to describing pneumatic systems was initiated by Tuba.[11] This approach treats the pneumatic system by a thermodynamic phase equilibrium analogy. The solids flux, fluid flux, and voidage are used in the format of the Van der Waals equation of state. In this format, the critical properties of the system, and hence the constants for the equation, can be determined.

2.5 VERTICAL SYSTEMS

2.5.1 Force Balance on Vertical System

The force balance equation for the particles in a verticle section of pipe is:

$$\Delta m_p dU_p/dt = dF_D - dF_g - dF_f - \Delta m_p/\rho_p \partial P/\partial x \pm F_{add} \tag{2-17}$$

For dilute systems, the pressure term is normally negligible due to the relatively large particle density and small amount of particles in the system. Neglecting additional forces and substituting the appropriate expressions for the forces, this expression becomes:

$$dU_p/dt= \; 3/4\ \varepsilon^{-4.7} C_{DS}\rho_f(U_f-U_p)^2/[(\rho_p - \rho_f)D_p] - g - \tag{2-18}$$

$$2f_s U_p^2/D_t - 1/\rho_p \partial P/\partial x$$

At steady state, and with values for the drag coefficient and solids friction factor, this equation can be solved for the particle velocity.

The pressure drop equation is:

$$\Delta P=[(1-\varepsilon)\rho_p+\varepsilon\rho_g]Lg \tag{2-19}$$

$$+2\rho_p f_s(1-\varepsilon)LU_p^2/D_t$$

$$+2\rho_p f_g \varepsilon LU^2/D_t$$

Solution for the pressure drop requires a gas friction factor, f_g, which can be obtained from single phase correllations such as the Blasius or Koo equations. The particle velocity and solids friction factor are not so easily determined. Table 2-1 lists some of the expressions available and the systems from which they were obtained. The Institute of Gas Technology performed testing of various correlations and recommends the modified Konno-Saito correlation.

Table 2-1: Various Correlations Available for Pneumatic Systems

INVESTIGATOR	SYSTEM	RESULTS
Konno and Saito[12]	D_p=.1 to 1.0 mm ρ_p=1440 to 2500 kg/m^3 D_t=26.5 and 46.8 mm Vertical and Horizontal	$f_s = 0.0285(gD_t)^{1/2}/U_p$
Yang[13]	Vertical D_t=6.78 and 13.5 mm	$f_s = 0.00515(1-\varepsilon)/\varepsilon^3[(1-\varepsilon U_t/U_p]^{-0.869}$
	Horizontal D_t=50.8 and 76.2 cm	$f_s = 0.02925(1-\varepsilon)/\varepsilon^3$ x $[(1-\varepsilon U_t/U_p U_f/(gD_t)^{1/2}]^{-1.15}$
Leung and Wiles[14]	Vertical Avg of results from van Swaaij, Reddy and Pai, and Konno-Saito	$f_s = 0.05/U_p$
Van Swaaij, et.al.[15]	D_t=0.18 m	$f_s = 0.08/U_p$
Reddy and Pai[16]	D_t=0.10 m D_p=100 to 270 µm Glass Beads	$f_s = 0.046/U_p$

Capes and Nakamura[17]	D_t=0.0381 m D_p=256 to 3400 μm ρ_p=0.911 to 7.7 gm/cm^3	$f_s = 0.048/U_p^{1.22}$
Stemerding[18]	D_t=0.0508 m D_p=20 to 150 μm ρ_p=1.6 gm/cm^3	$f_s = 0.003$
Molerus[19]	Horizontal D=.04 and .01 m	State Diagram from which P can be read
Morikawa and Tsuji[20]	Vertical D_t=40 mm (acrylic) D_p=1.11 to 3.43 mm ρ_p=923 to 969 kg/m^3	$f_s = 1.503(U_p/(gD_t)^{1/2})^{-1.831}$
	Horizontal same as above	$f_s = 0.805(U_p/(gD_t)^{1/2})^{-1.883}$
	Inclined same as above (30,45,and 60 degrees)	Figure from which f_s can be read
Marcus, et.al.[4]	Horizontal D_t=0.1 m D_p=30μm ρ_p=1500 kg/m^3	$U_p = U_g(1-0.0221D_p^{0.3}\rho_p^{0.5})$
Yang[13]	Vertical D=.267 to 1.023 in D_p=109 to 2024μm ρ_p=53.7 to 169 lb/ft^3	$U_p = U_g - [(1+2f_sU_p^2/D) \times 4/3(\rho_p-\rho_f d_p\varepsilon^{4.7}/(\rho_f C_{DS})]^{1/2}$

Konno and Saito[12]	Vertical and Horizontal	$U_p = U_g - U_t$
IGT[21] (Modified Hinkle)	Vertical Multiple systems	$U_p = U_g(1 - D_p^{0.92} \rho_p^{0.5} \rho_f^{-0.2} D_t^{-0.54})$
IGT[21] (Modified Konno and Saito)	Vertical ultiple Systems	$\Delta P = 2f_g \rho_f U_g^2 L / g_c D_t + 0.057 U_g \rho_f L/(g D_t)^{1/2} + W_s L/U_p + \rho_f L$

2.6 HORIZONTAL SYSTEMS

The force balance for the particles in a horizontal system ($\theta=0$) is:

$$\Delta m_p dU_p/dt = dF_D - dF_f - \Delta m_p/\rho_p \, \partial P/\partial x \pm F_{add} \qquad (2\text{-}20)$$

Again, neglecting the pressure term and additional forces, this becomes:

$$dU_p/dt = 3/4\varepsilon^{-4.7} C_{DS} \rho_f (U_f - U_p)^2 \Delta m_p/(\rho_p - \rho_f) D_p - 2f_s U_p^2/D_t - \Delta m_p/\rho_p \, \partial P/\partial x \qquad (2\text{-}21)$$

The effects of gravity are not immediately apparent in equation 2-21. The effects are

incorporated in the solid friction factor. The expression derived by Molerus[10] does contain a term in the horizontal case which is gravity dependent. The pressure drop equation for horizontal transport is:

$$\Delta P = 2\rho_p f_s (1-\varepsilon) L U_p^2 / D_t + 2\rho_f f_g \varepsilon L U_f^2 / D_t \qquad (2\text{-}22)$$

Some correlations applicable to horizontal systems are given in table 2-1. Again, the system from which the correlations were obtained is a key factor as to the applicability of the correlation.

2.7 INCLINED SYSTEMS

The most general form of the force balance on the particles in pneumatic transport is for the inclined geometry. Here, the gravity effect is present in both a vertical and horizontal sense. The force balance and the pressure drop equations are given by equations 2-9 and 2-15. There seems to be a general lack of data on inclined systems, and therefore, very few correlations to describe them. The work done by Morikawa and Tsuji[20] used data from pipes at three inclinations. Their results give a correlation in terms of a figure of friction factor and loading versus particle Froude number. The work of Molerus[10] is capable of describing the inclined system, however, the difficulties in obtaining the separate friction factors in the equation would be severe.

2.8 ELECTROSTATICS

During the course of transporting solid particles through a pipe, there occurs a substantial amount of contacting between the particles and the pipe wall. If the particles and the pipe are of different materials, then electrostatic charging occurs. The extent to which this charging proceeds is dependent on many factors. These include the condition of the pipe wall, the condition of the solid particles, the relative humidity of the carrier gas, the particle size, and the particle velocity. These conditions often allow for a significant amount of charging. The effect of this charging may in some cases be useful, while in other cases, detrimental. A particular use of the charging in pneumatic transport is in measuring devices for solids flow.[22, 5] The detrimental effects normally appear as increases in the pressure drop of the system. Another detrimental effect is that of discharge of static electricity which can lead to explosions.

Klinzing[23] gives the force attributable to electrostatics on a single particle as:

$$F_{e,i} = Eq \tag{2-23}$$

with the resulting force for a system of n particles as:

$$F_e = \sum_{i=1}^{n} F_{e,i} = \sum_{i=1}^{n} Eq\Delta m \tag{2-24}$$

This force can be inserted into equation 2-1 to determine the force balance for a sys-

tem involving electrostatics. A problem arises, however, when trying to evaluate the charge per particle and the electric field strength. Also, the direction which this force is exerted is not easily determined.

Ally[24] has given a theoretical analysis of this type system. He assumes that the particles in the system are, on an average, contained at $D_t/4$. His analysis results in pressure drop due to electrostatics of:

$$\Delta P_E = 45(1-\varepsilon)^2 q^2 D_t / (16\pi^2 \varepsilon_0 D_p^6) \qquad (2\text{-}25)$$

with q given as:

$$q = \int \sum_{i=1}^{k} (\partial\lambda/\partial\xi_i)_{x_{j=i}} d\xi_i + q_a \qquad (2\text{-}26)$$

Where ξ is representative of each of the variables which q is a function of. The first limitation of equation 2-25 is the complexity which equation 2-26 imparts. Additionally, the assumption of a uniform concentration of particles at $D_t/4$ is obviously unsuited to flow in horizontal and inclined pipes where a significant density gradient can exist.

2.9 STABILITY

As the gas velocity is decreased in a pneumatic system, the balance of forces is maintained by a decrease in the system voidage. There is a point at which the drag force which is suspending the particles becomes insufficient to balance the forces of gravity, friction, and pressure. At this point the system can no longer be maintained in a steady state. The range of instabilities which occur at and near this point are described in different ways depending on the orientation of the pneumatic system. In vertical systems it is known as choking. In horizontal systems it is called saltation. In all cases, it is a difficult situation to define and predict.

2.9.1 Choking

The phenomenon of choking in vertical pneumatic transport is best described by the pressure drop observed as the gas velocity is decreased. Figure 2-2 shows the relationship.

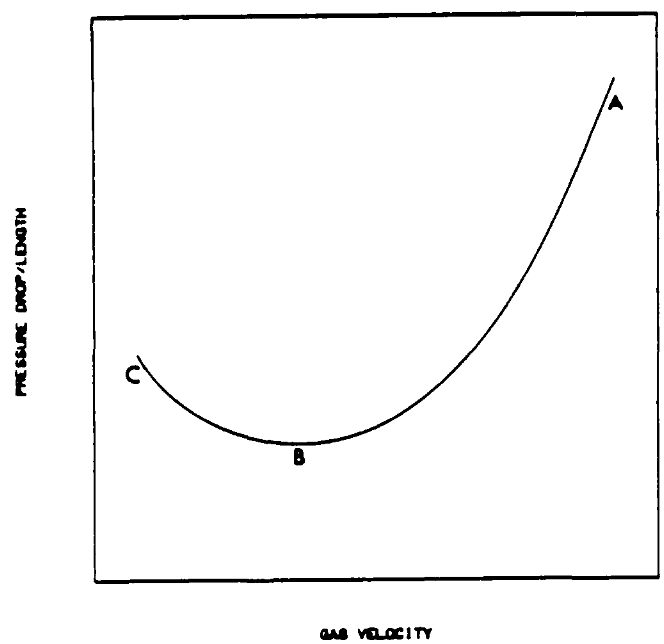

Figure 2-2: Pressure Drop vs. Gas Velocity Near the Choking Point

As the gas velocity is decreased from point A to point B, the pressure drop decreases to a minimium at point B. Further decrease in the gas velocity from B to C shows an increase in pressure drop. Point B is called the choking point. This point, as described by Yang[25], is by no means as precise as shown in figure 2-2 due to the number of variables which determine it. Yang gives the following correlation to determine the choking parameters in vertical flow:

$$2gD_t(\varepsilon_c^{-4.7} - 1)/U_{fc}-U_t)^2 = 6.81 \times 10^5(\rho_f/\rho_p)^{2.2} \tag{2-27}$$

2.9.2 Saltation

The stability of a horizontal pneumatic system is somewhat different than the vertical case. As the gas velocity is decreased, the particles begin to separate to the lower portion of the pipe. Further decrease in the gas velocity causes some particles to actually deposit on the bottom of the pipe. This deposition is known as saltation. If the gas velocity is decreased enough, the particles will eventually fill the crosssection of the pipe and flow will stop.

Jones and Leung[26] compared various correlations for determining the saltation velocity. They recommend the Rizk correlation which is given as:

$$U_{gsalt} = (gD_t)^{1/2}\left[R/(0.1)^{1.44D_p+1.96}\right]^{1/(1.1D_p+2.5)} \tag{2-28}$$

where: D_p is in mm.

This correlation was recommended for it simplicity and because the resultant accuracy was approximately equal to that of other more complicated expressions.

2.9.3 Stability Analysis

Another approach to describing the stability of a pneumatic transport system is through the use of the basic dynamic equations of the flow. The velocities of the gas and solids can be expressed as a steady state term plus a fluctuation from that steady state by:

$$U_p = U_{ps} + \hat{U}_p \tag{2-29}$$
$$U_g = U_{gs} + \hat{U}_f$$

If the fluctuating terms can be shown to decay, then the system is said to be stable. If the fluctuating terms grow, then the system is said to be unstable.

a. Linear Stability. The linear stability approach utilizies Taylor Series expansion to linearize the non-linear terms in equations 2-8 and 2-2. Klinzing[27] first performed this operation on a vertical system without electrostatics, and then on a system containing electrostatics. The result of this analysis was the following second order differential equation:

$$d^2U_p/dt^2 + \lambda_1 \, dU_p/dt + \lambda_2 U_p = \lambda_3 \qquad (2\text{-}30)$$

where:

$$\lambda_1 = a_1 - a_2 - b_1 - b_2$$

$$\lambda_2 = a_2b_1 + a_2b_2 - a_1b_2$$

$$\lambda_3 = a_1b_0 - a_0b_1 - a_0b_0$$

and

$$a_0 = 3/4\varepsilon^{-4.7}C_{DS}\rho_f(U_{fs}-U_{ps})/[(\rho_p-\rho_f)D_p] - g\sin\theta - 2f_sU_{ps}^2/D_t - 1/\rho_p\,\partial P/\partial x$$

$$a_1 = 6\varepsilon^{-4.7}C_{DS}\rho_f(U_{fs}-U_{ps})/4\rho_pD_p$$

$$a_2 = -4f_sU_{ps}/D_t$$

$$b_0 = -3/4\varepsilon^{-4.7}C_{DS}(1-\varepsilon)(U_{fs}-U_{ps})^2/4\varepsilon D_p - g\sin\theta - 2f_gU_{fs}^2/D_t - 1/\rho_f\,\partial P/\partial x$$

$$b_1 = -3\varepsilon^{-4.7}C_{DS}(1-\varepsilon)(U_{fs}-U_{ps})/4\varepsilon D_p$$

$$b_2 = -2f_gU_{fs}/D_t$$

The eigenvalues of equation 2-30 determine the stability of system without electrostatics. They are determined from:

$$m_{1,2} = [-\gamma_1 \pm (\gamma_1^2 - 4\gamma_2^{1/2}]/2 \qquad (2\text{-}31)$$

For the system to be linearly stable, m_1 and m_2 must both be negative. By including the force due to electrostatics in a vertical system given by equation 2-25, the analysis can be extended to systems containing electrostatics.

<u>b. Liapunov Stability.</u> Another approach to determining the stability of a pneumatic transport system is through the use of the second method of Liapunov. This method was first applied to pneumatic transport by Joseph[28]. This method determines regions of stability around a steady state value.

3.0 EXPERIMENTAL METHODS

This study investigates the flow of spherical solid particles in a 0.0508 m (2 inch nominal), Excelon (PVC) pipe at three different inclinations. Air for the system was supplied by a 7.5 horsepower Roots blower followed by a conditioning system capable of adjusting the water content of the air. The solid particles were introduced into the air stream by means of a live-bin vibrating-screw feeder unit. The gas-solid stream was transported through a 0.0508 m (PVC) pipe which included a 3.05m (10 foot) test section of translucent Excelon pipe. This test section included pressure taps at each end and contained two aluminum probes used for determining the solid particle velocity. The gas- solids stream was separated in a cyclone separator, the air stream being passed to the atmosphere, and the solids stream passed to a storage tank mounted on a platform scale. The system is illustrated in figure 3-1.

3.1 THE TEST SECTION

The main test section consisted of a schedule 40, Excelon pipe, 3.05 m long with an internal diameter of 0.0508 m. The ends of the pipe were fitted with two inch nominal, schedule 80, PVC flanges. Pressure taps were made in the flanges with a 3.175 mm hole through to the test section.

Probes used to obtain velocity measurements were fitted to the test section ensuring continuity between the probe wall and the inner pipe wall. The probes were constructed from free machining aluminum rod. The probe construction and dimensions are shown in figure 3-2. The first probe was located 0.6096 m from the downstream end of the main test section. The second probe was located 0.6605 m upstream of the first probe.

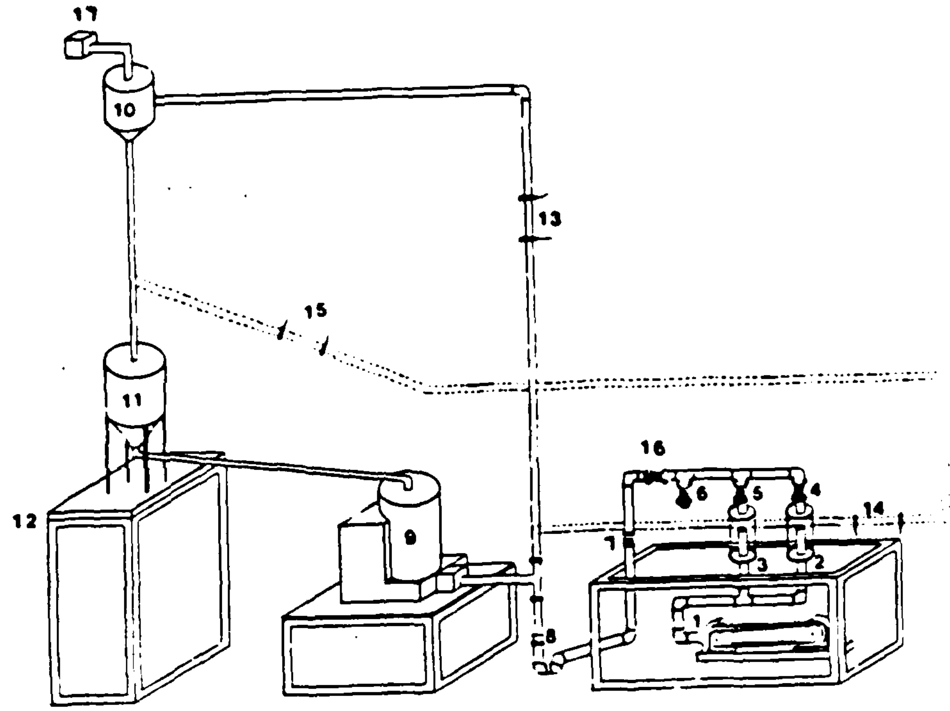

1-ROOTS BLOWER
2-DEHUMIDIFICAION COLUMN
3-HUMIDIFICAION COLUMN
4-CONTROL VALVE
5-CONTROL VALVE
6-THROTTLE
7-TURBINE METER
8-3" TO 2" REDUCER
9-SOLIDS FEEDER
10-CYCLONE SEPARATOR
11-CONICAL BOTTOM STORAGE TANK
12-PLATFORM SCALE
13-VERTICAL TEST SECTION
14-HORIZONTAL TEST SECTION
15-INCLINED TEST SECTION
16-CONTROL VALVE
17-AIR FILTER

Figure 3-1: Experimental Test Loop

3.2 AIR DELIVERY SYSTEM

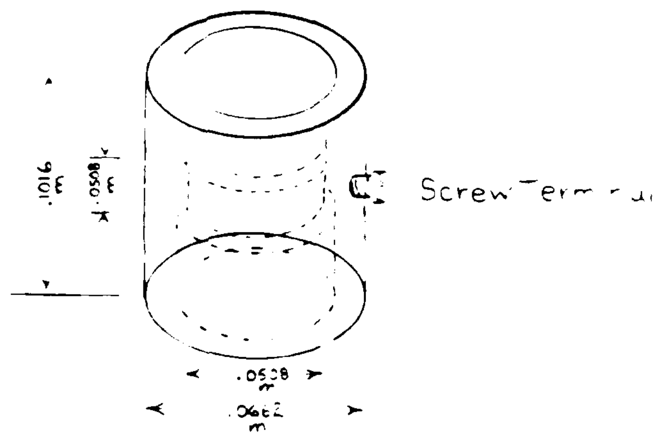

Figure 3-2: Electrostatic Ring Probe

3.2.1 Blower

The air delivery system was a stand alone unit centered around a Roots-Connersville, Model 2406J, Whispair Blower, mounted on a baseplate. The blower was powered by a 7.5 horsepower, 220 V, 3 phase electric motor through a drive belt pulley system. The blower operated at 3600 RPM, delivering 250 SCFM of air at 6 psig. As the blower is a positive displacement, rotary lobe type blower, a pulsation in air delivery was encountered with a frequency of 240 Hz. This pulsation was partially damped by the humidity control columns and the control valves used in the air delivery system.

3.2.2 Humidity Control and Measurement

Air from the blower was passed through two packed columns used to control the humidity. Each column was constructed from 0.2794 m diameter Plexiglas tube with 1.905 cm aluminum end plates. The first column was packed with 1.905 cm ceramic, Intalox saddles. Water was delivered to the center of this column through tygon tubing. An outlet at the bottom of this column allowed water to be passed continuously through the column. The second column was packed with 1.905 cm ceramic Intalox saddles and Dryrite, to adsorb moisture from the incoming air. At the top of each column was a three inch nominal, PVC Gate Valve. The flow through each column could be controlled by the positioning of these valves. Thus, the total air stream humidity could be adjusted by manually positioning these two valves. Immediately downstream of the humidity control columns was a thermometer mounted in the pipe. Following the thermometer was a humidity probe connected to a Hydrodynamics Hygrometer, Model 15-3050. By the proper choice of sensing elements, the humidity of the air stream was able to be determined. The range of measurable humidities for this meter was 12 to 90%. Dial readings from the hygrometer and the air temperature are used with charts to determine the percent relative humidity.

3.2.3 Air Flowrate Control and Measurement

Air from the humidity control columns flowed to a tee-fitting where a bypass valve allowed the control of air discharged to the atmosphere, thus controlling the amount of air through the test section. This valve was a three inch nominal, PVC gate valve identical to the valves used in the humidity control section. Another three inch nominal, PVC gate valve was in line with the feed line to the test section. This valve allowed the flow of air to the test section to be reduced to zero. One of either of these valves was required to be fully open during operation of the blower to avoid overpressurizing the blower. Prior to the discharge end of the air delivery system was an Elster, Model Q160 turbine meter, used to measure the flow rate of air to the test section. This meter had an 8-digit roller counter which displayed the volume of gas passed through the meter. By reading the counter at the beginning and end of a known time interval, the volumetric flow rate of air was obtained.

3.2.4 Piping for the Air Delivery System

All piping in the air delivery system was three inch nominal, schedule 40, PVC. Flanges to valves and the turbine meter were three inch nominal, schedule 80 PVC. A three inch to two inch reducer coupling was attached to the discharge end of the air delivery system to accomadate the two inch test section.

3.3 SOLIDS FEEDING SYSTEM

The solids feeding system consisted of a Vibra-Screw, Inc., Live Bin Volumetric Screw Feeder mounted on a steel frame. The bin capacity of this feeder was three cubic feet. The feeder was modified to make use of an auger type screw which allowed for higher back pressures on the screw feeder than was possible with the manufacturers screw. The auger screw was mounted in a chuck which used teflon tipped set screws to secure the screw. If the screw was impeded due to excessive pressure or a blockage, the chuck continued turning without turning the screw until the blockage was eliminated. The rate of revolution of the screw, and thus, the volumetric feed rate of the solids, was controlled by a dial setting on the feeder unit.

The discharge from the screw feeder was injected into the test section through a two inch nominal y-fitting. This allowed the solids to be injected downward into the test section, thereby reducing blockages in the screw feeder.

3.4 SOLIDS RECOVERY AND WEIGHING SYSTEM

Solids recovery from the test section was accomplished with a Federal Classifications Systems Cyclone Separator. The air stream from the cyclone was passed through an MSA absolute filter to the atmosphere. The solids from the bottom of the cyclone fell into a 15 gallon, conical bottom storage tank which was mounted on a Circuts and Systems, Inc., Model sx-501 platform scale. A valve was located at the base of the storage tank which allowed the solid mass rate to be determined. With the valve open,

the solids from the storage tank passed by gravity, back to the bin of the screw feeder, thus completing the loop.

3.5 PRESSURE MEASUREMENT

The pressure drop through the test section was measured by the use of a Viatran Model 215 pressure transducer. The range of this transducer was 0 to 5 inches of water. Pressure taps were located at a ten foot interval of the test section. The output signal from the transducer was connected to a Hewlett-Packard Model 7702B Strip-chart Recorder which provided a graphical output of the pressure response.

3.6 PARTICLE VELOCITY MEASUREMENT

Measurement of particle velocity in the test section was accomplished using electrostatic ring probes.[5] This method involves the use of cross-correlation techniques to determine time of flight through a known distance. The probes used were constructed from three inch diameter, free-machining, aluminum rod. The contact length of each probe was two inches. The probe separation was 2.167 feet.

Signals from the electrostatic probes were processed through two Keithly 610C Electrometers. The output from the electrometers was recorded on magnetic tape. This provided a simultaneous record of each probe which could be processed by computer to determine the particle velocity.

The computer used for processing the data was a Digital Equipment Corporation MNC/Declab-23 system. This system contained an analog to digital converter through which recorded signals were converted to digital signal files. The digital signal files were then correlated using a FORTRAN computer program. The computer programs used for data input to the computer and for determining the particle velocity are included in Appendix C.

3.7 EXPERIMENTAL PROCEDURE

The experimental procedure involved three overall steps: Start-up, Experimental Data Acquisition, and Shut-down. The start-up and shut-down procedures were completed at the beginning and end of each operating period. The steps taken for experimental data aquisition were completed for each condition. Refer to figure 3-1 for equipment numbers.

3.7.1 Start-up Procedures

The following steps were completed at the beginning of each experimental day:

- Check equipment for breakage, stray objects, etc.

- Electronic equipment warm-up (approximately 15 minutes)

- Check pressure transducer calibration

- Install desired humidity sensor

- Check valves

  * Valves 4 , 5 , and 6 should be fully open and valve 16 should be fully closed

- Blower start-up

  * Caution should be made when starting the blower that proper ear protection is observed. The noise level of the blower exceeds 80 decibels at 5 feet.

- Humidity adjustment

    * The humidity meter is turned to on. For lower humidity runs, valve 5 is slowly closed until the desired humidity is achieved. For high humidity, the water inlet line is connected to the water supply and the needle valve is adjusted for proper water flow. Valve 4 is then slowly closed until the desired humidity is achieved.

    * Care must be taken not to allow water to become entrained in the air stream as damage to the humidity probe could result.

3.7.2 Experimental Data Acquisition

Data acquisition was accomplished using pre-printed data acquisition forms. A sample form is shown in appendix . Preset conditions for each run were first made. These included the test section orientation, humidity, and particle size. The air flow rate was approximated by the use of a manometer, which read the air pressure at the outlet of the air delivery system. The following steps were taken for each run:

1. The date, time, tape number, and particle information were recorded.

2. Valve 16 was slowly opened completely.

3. Valve 6 was closed until the desired air flow rate was achieved.

4. The temperature and humidity were noted.

5. The solids feeder was turned to on and the dial reading recorded.

6. The turbine meter counter reading was recorded and time was begun on a stopwatch

7. The scale was reset to zero if required and the valve located at the bottom of the storage tank was closed. The time on the stopwatch was noted for the time of solids weighing.

8. The tape counter number on the tape recorder was noted and the recorder started. After a sufficient time period (at least 8 seconds), the tape recorder was stopped and the counter number again noted. The tape recorder was then advanced to provide spacing between signals for each run.

9. Visual observations were then made through the glass viewing section.

10. The scale reading was taken and the time period from the stopwatch was recorded. The valve located at the base of the storage tank was opened.

11. The turbine meter counter reading was taken and the time period from the stopwatch recorded.

12. Humidity and Temperature were again noted.

13. The ending time of the experimental run was then recorded.

14. The solids feeder was turned to off and valve 6 fully opened.

3.7.3 Shutdown Procedure

There were no unusual shutdown procedures other than shutting off of the equipment, except in the case of high humidity experiments. For these cases, the humidification column had to be purged to prevent water from leaking back into the blower. This was accomplished by stopping the water supply to column 3 and allowing the blower to run with valve 4 fully closed, and valve 5 fully open. When the water in the column was eliminated, valves 4 and 5 were opened fully and the blower stopped.

4.0 RESULTS AND ANALYSIS

4.1 PARTICLE SIZE

Experiments were conducted using four particle sizes. Three of these were glass beads while the fourth was Plexiglas. A particle size analysis was conducted on these particles prior to the experiments and after completion of the experiments. Table 4-1 shows the results of the analysis and the particle size used. The results of the analysis are included in Appendix .

4.2 FLOW BEHAVIOR AND PATTERNS

The three different test section orientations showed a marked difference as to the flow behavior and flow patterns of the different particles. There were some general aspects common to all particles in a given orientation. In the vertical pipe, as the gas velocity was lowered, the particles could be seen to deviate from streamlined flow lines. Pulsations occurred in the system where denser slugs of material moved through the pipe with lengths of lesser particle density between them.

In the horizontal test section, decrease in the gas velocity caused a radial separation in the pipe. The bottom of the pipe had a higher particle density than the top, even before saltation occurred.

As the gas velocity was decreased in the inclined orientation, a reverse flow behavior was observed. Particles formed retrograde dunes which slid downwards and were either reduced by entrainment, or were destroyed by partially plugging the entrance to the test section where they were redispersed into the gas stream.

Table 4-1: Particle Size Analysis

Weight Mean Particle Diameter (μm)

Before	After			Used
79.1 (Glass)	90.8	67.8	(avg=79.3)	79
125.0 (Glass)	133.8	100.7	(avg=117.3)	125
446.3 (Glass)	447.8	343.1	(avg=395.5)	450
128.6 (Plexiglas)	126.7	100.9	(avg=113.8)	128

a. Vertical Systems. The 79μm glass beads tended to pulse through the system even at higher velocities. These pulsations could be termed slugging; however, the density of the slugs was only slightly greater than that of the flow between them and they occured at higher frequencies. Definite slugging was observed at lower gas velocities. An additional observation at lower velocities was an internal radial motion of the particles. This motion became more pronounced as the gas velocity was further decreased. This radial motion set in at much higher gas velocities for the systems at high humidity. It appeared that the presence of electrostatics in the system stabilized this motion.

The 125μm glass beads acted much the same as the 79μm glass beads except that definite slugging occurred at higher gas velocities. Again, the radial motions were damped by the presence of electrostatics, but the formation of dense slugs occurred at

higher gas velocities. Wall interactions were also more pronounced with the 125μm glass beads. At low gas velocities, particles hit the walls and then rebounded into the main stream of flow with increasingly lower tragectories. At the lowest gas velocities, some particles hit the wall and traveled downward in the pipe.

Wall interactions were most pronounced with the 450μm glass beads. At lower velocities, particles in-between slugs, could be seen to traverse the width of the pipe from wall collision to wall collision. Again, the presence of electrostatics seemed to dampen the internal motion of the flow. The plugging of the pipe with these particles was a very rapid phenomenon. The smaller particles seemed to drop out slowly in comparison.

b. Horizontal Systems. The 79μm glass beads were the most susceptible to saltation in the horizontal pipe. As gas velocities were decreased, the flow separated with the bottom of the pipe having a higher solids concentration than the top (See Figure 4-1). Further decrease in gas velocity caused some of the particles to salt out on the bottom of the pipe forming blunt nosed islands. A further decrease in gas velocity caused more saltation until the bottom of the pipe was covered with a layer of particles. At the onset of this condition, particles began to salt out in the vertical section and eventually plugged the vertical pipe. The presence of electrostatics caused more pulsing in the horizontal section.

The 125μm glass beads followed similar behavior to the 79μm glass beads except when saltation caused the bottom of the pipe to be covered. In this case, the small disturbances seen on the top of this layer were not observed. The layer was very smooth and particles could be seen to be lifted from this layer into the stream flowing above.

The 450μm glass beads did not salt out in the horizontal orientation. Although flow separated to the bottom of the pipe, the particles never actually stayed on the pipe wall. There was much more activity along the particle tragectories and more wall collisions were observed.

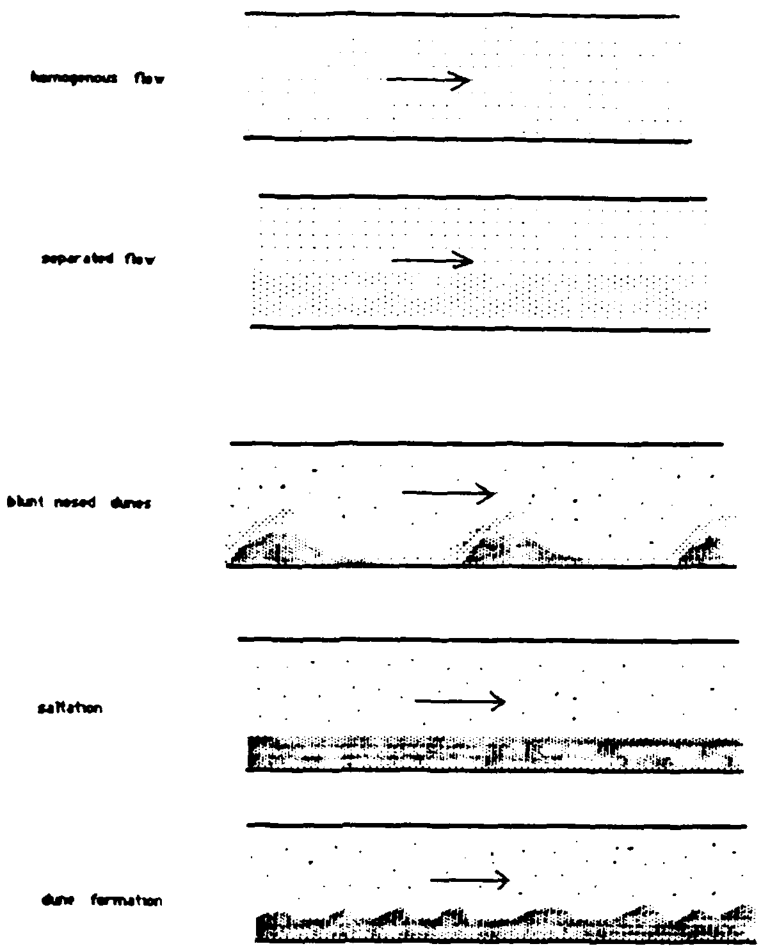

Figure 4-1: Flow Patterns in Horizontal Flow

<u>c. Inclined Systems</u>. The 79μm glass beads tended to begin salting out of the horizontal section before any deposition occured in the inclined section. When deposition did begin, it began very near the entrance to the inclined section. Eventually, retrograde dunes formed and traveled downward (See Figure 4-2).

The 125μm glass beads formed the same type retrograde dunes as the 79μm glass beads, except that the horizontal section preceeding the 45° test section salted out prior

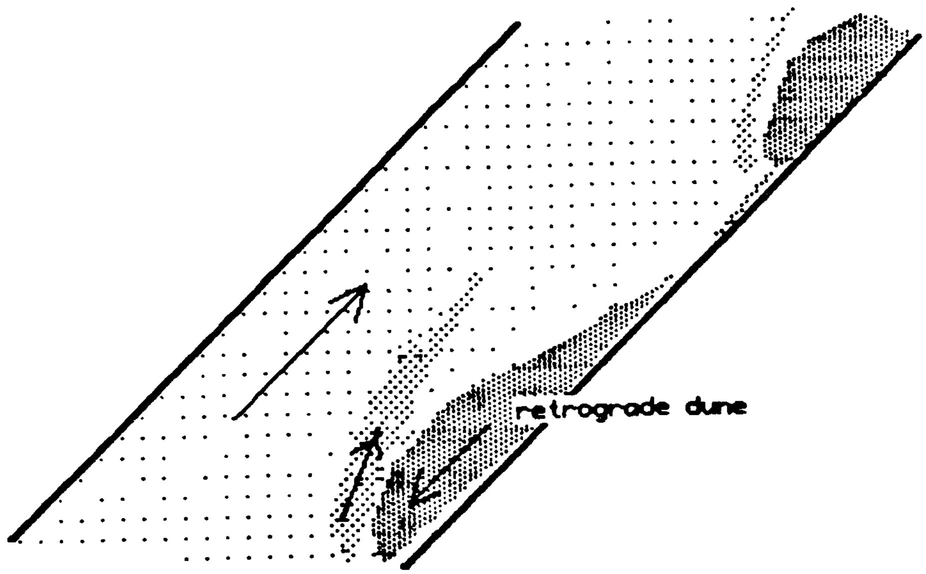

Figure 4-2: Retrograde Dunes in Inclined Flow

to formation of the retrograde dunes for high humidity cases, and after formation for the lower humidities.

The 450μm glass beads formed the retrograde dunes very quickly and their size and velocity was much higher than the smaller particles. These dunes began as a thin layer on the bottom of the pipe from which particles were entrained. This layer grew as deposition increased until a dune of sufficient size formed and slid down the pipe. The formation of the retrograde dunes in all systems concluded with the plugging of the vertical section. The smaller particle sizes took much longer for this to occur than the 450μm glass beads.

4.3 PARTICLE VELOCITY ANALYSIS

The particle velocity was obtained from cross-correlation of the signals from two electrostatic ring probes. This data has been plotted as particle velocity vs. gas velocity. The best fit of the data to a straight line was obtained by linear regression. Comparison is made between the experimental particle velocity, the expression $U_p - U_t$, and the IGT[21] recommended correlation. The particle velocity obtained for the vertical systems shows fair agreement with the correlations. Figure 4-3 shows the particle velocity for 125μm glass beads vs. gas velocity. At lower gas velocities, agreement with the correlations is within 10%. As the gas velocity increases, the experimental values tend to be less than that from either correlation with a mean deviation of approximately 20%. For the 79μm glass beads, 125μm glass beads and 128 μm Plexiglas beads, the experimental particle velocity was less than both correlations with the expression $U_g - U_t$ giving only slightly better results. For the 450μm glass beads, the experimental particle velocities were between the two correlations with the IGT over predicting. The additional particle velocity figures are included in figures A-1, A-2 and A-3.

The horizontal systems showed much the same results as the vertical systems, except that the spread of the data was much greater. The analysis for the 125μm glass beads is shown in figure 4-4. The mean deviation from the correlations has increased from 20% to 47%. The additional horizontal systems are shown in figures A-4 and A-5.

The inclined systems also show the same type deviation from the two correlations. The analysis for the 125μm glass beads is shown in figure 4-5. The additional inclined systems are shown in figures A-6 and A-7.

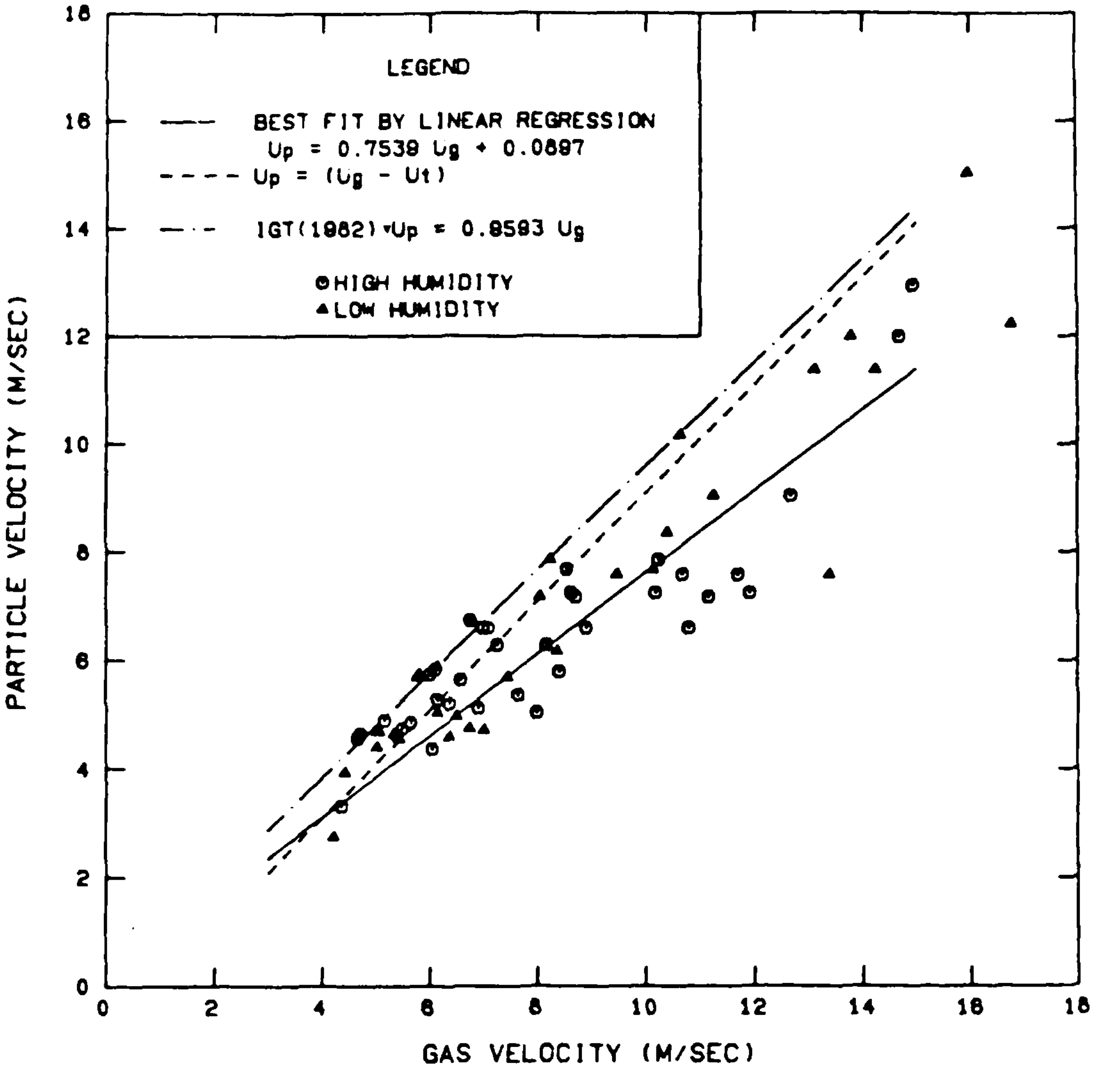

Figure 4-3: Particle Velocity vs. Gas Velocity for 125μm Glass Beads in the Vertical Orientation

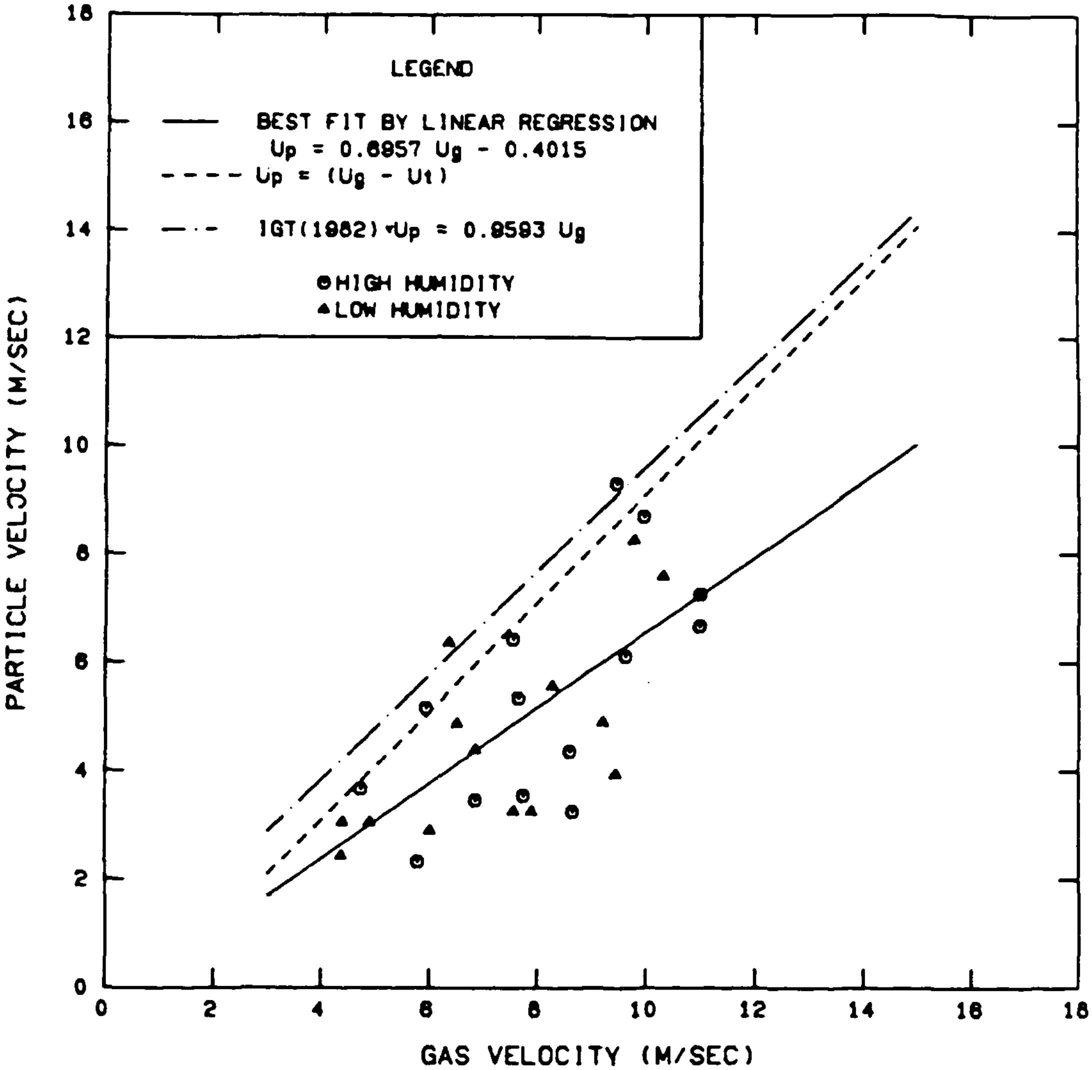

Figure 4-4: Particle Velocity vs. Gas Velocity for 125μm Glass Beads in the Horizontal Orientation

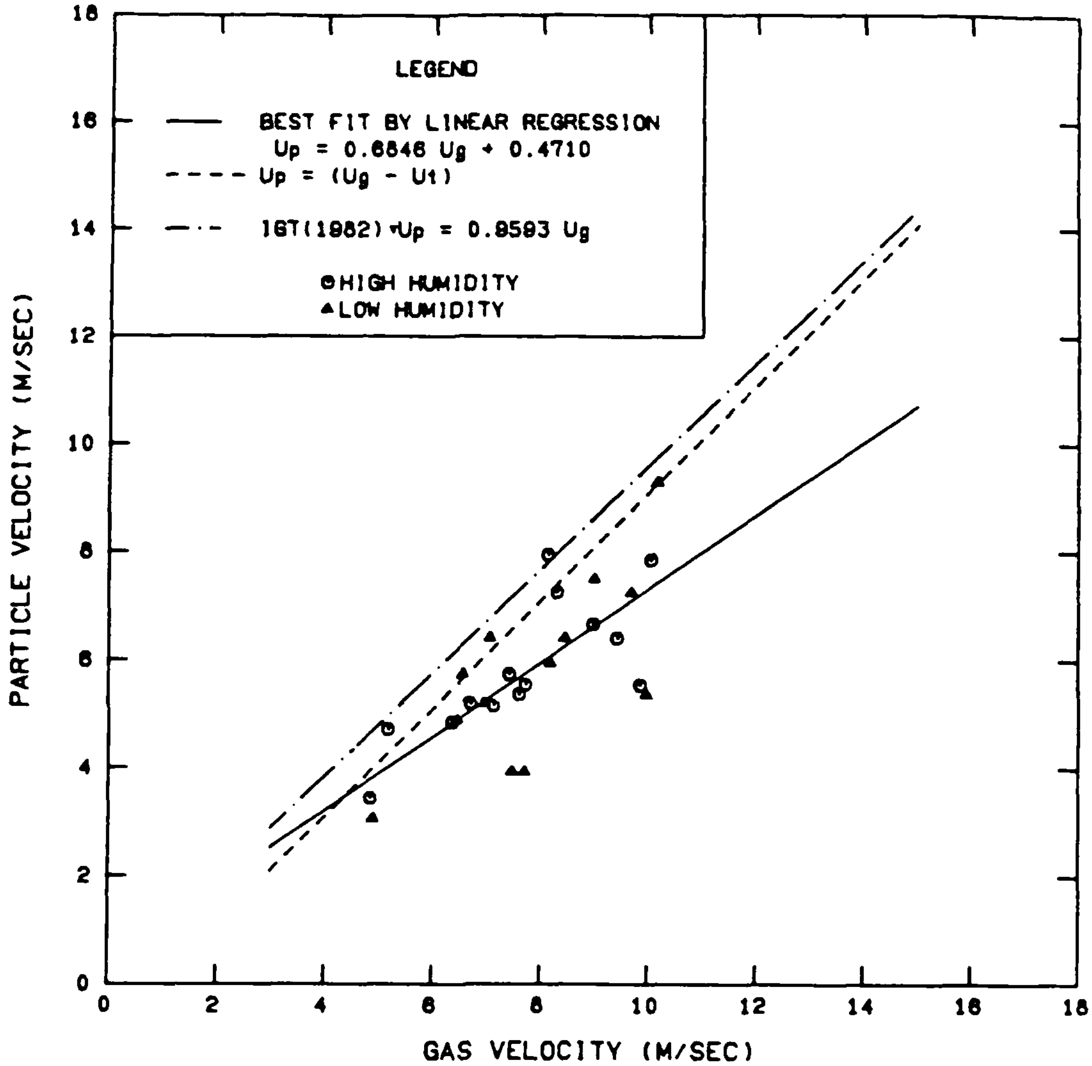

Figure 4-5: Particle Velocity vs. Gas Velocity for 125μm Glass Beads in the Inclined Orientation

4.4 PRESSURE DROP

Various pressure drop relationships were investigated to determine the effect of pipe orientation and electrostatics on the flow. These included the pressure drop vs. gas velocity relationship, the pressure drop fluctuation vs. gas velocity relationship, and the electrostatic pressure drop vs. water to air mass ratio.

4.4.1 Pressure Drop vs. Gas Velocity

As discussed in section 2.9, the pressure drop vs. gas velocity curve graphically represents the nature of a pneumatic system in terms of stability. It also provides the criterion for optimum operation. The presence of electrostatics in the system affects the pressure drop in different ways. For this study, operation at high humidity was assumed to eliminate the electrostatic effects.

a. Vertical Systems. The pressure drop vs. gas velocities for the vertical systems studied are shown in figures 4-6, A-8, A-9, and A-10. Particular attention was paid to these systems during the experiments to obtain data near the choking point. In most cases, the system was allowed to completely plug the pipe. The 79μm glass beads remained in steady flow at much lower gas velocities than the larger glass beads as expected. The instabilities near the choking point were not as dramatic as the 125μm glass beads. By visual observation, a great deal of instability in the system was seen, however, the pressure drop readings did not indicate the dramatic increase in pressure that was expected. The effects of electrostatics in this system were also not as expected. The smaller particle size should have caused the largest increase in pressure drop of all particles studied. The results, however, show only a very small increase in pressure drop due to electrostatics.

The 125μm glass beads showed a unique behavior near the choking point. Figure 4-6 shows an increasing maximum for the high humidity cases. This maximum actually exceeds the pressure drop for the low humidity experiments at the highest mass flow rate. A similar phenomenon was found in a 0.0254 m pipe by Zaltash[29]. This

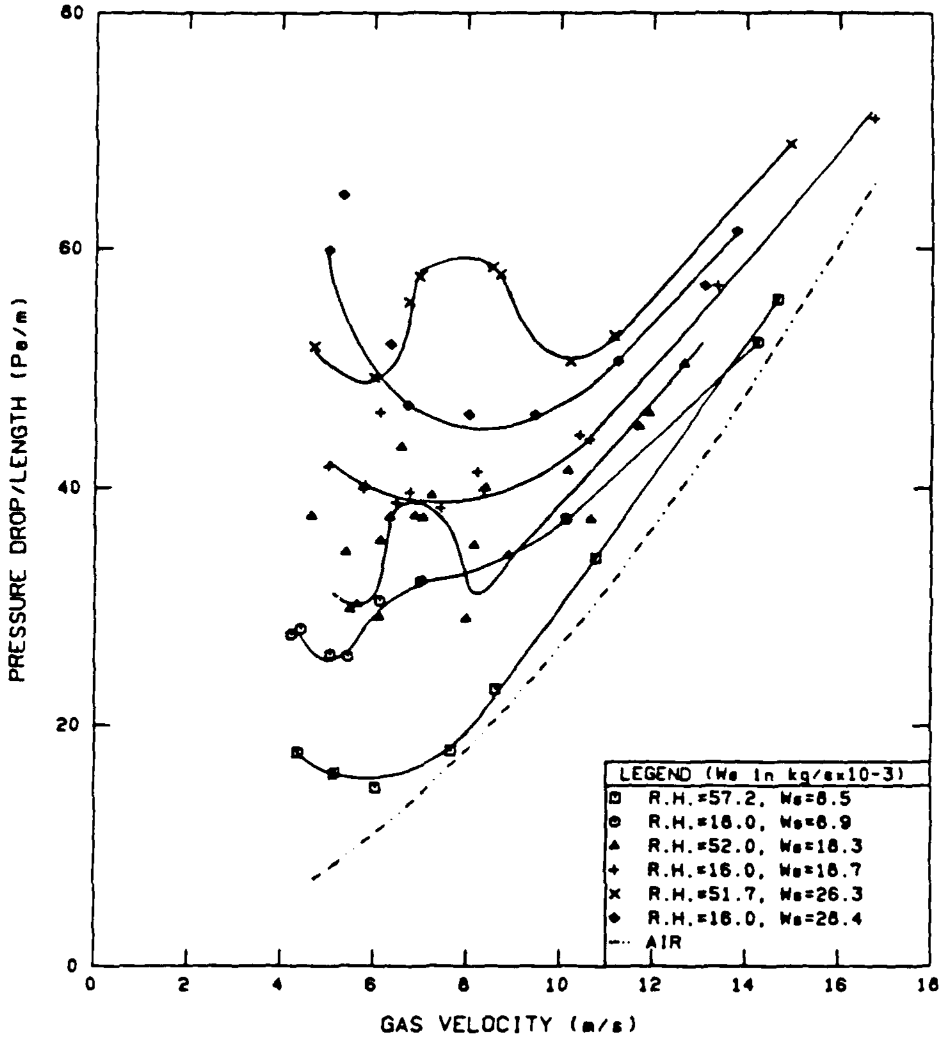

Figure 4-6: Pressure Drop vs. Gas Velocity for 125μ Glass Beads in the Vertical Orientation

phenomenon was attributed to a particle size effect. Since the Plexiglas beads had a partical size of 128µm, and this behavior was not observed for them, a density factor should be included. For Zaltash's study, the group $(D_p/D_t)(\rho_p/\rho_f)$ was equal to 6.06. In this study, the same group equals 4.79, suggesting that this group could describe a critical particle to pipe combination. This type of phenomenon has been disclaimed[2], however, most studies have not explored the region of choking that closely.

The 450µm glass beads showed results much more as expected. The range of unstable behavior was not as broad as with the smaller particles and instability leading to the plugging of the pipe occured very rapidly. For low mass flow rates, the electrostatic effect was negligible. As the mass flow rate was increased, the electrostatic contribution to the pressure drop increased.

The 128µm plexiglas particles showed very little electrostatic effects. This is due to the nature of the particle and pipe materials having very similar dielectric constants.

b. Horizontal Systems. Three particles were studied in the horizontal section. They were the 79µm, 125µm and 450µm glass beads. The Plexiglas particles were not studied due to concern over the explosive hazard they presented. The range of gas velocities was less than that of the vertical systems as the increased total line pressure prevented consistant bead feeder operation at higher velocities. As the horizontal test section was preceded by a 2.5m vertical section, the complete plugging of the horizontal section was not obtained. The pressure drop vs. gas velocity data is presented in figures 4-7, A-11, and A-12. The 79µm glass beads were the most susceptible to saltation due to the saltation gas velocities being greater than the choking velocities. The pressure drop vs. gas velocity curves are less smooth than the larger particles. The presence of electrostatics in the low humidity cases tended to dampen the fluctuations. The effect of the electrostatics on the magnitude of the pressure drop was seen to vary due to the fluctuations present in the high humidity cases.

The pressure drop vs. gas velocity data for the 125µm glass beads is shown in figure 4-7. Again, the presence of electrostatics dampened the fluctuations in the

curves. The effect of the electrostatics on the magnitude of the pressure drop is an overall decrease. This is opposite to the effect found in the vertical cases.(see Figure 4-6)

The 450μm glass beads showed a much more stable pressure drop response. This is due to the 450μm glass beads not salting out at all prior to complete plugging of the vertical section. The effect of electrostatics was found to increase the pressure drop, although, this effect was not as prominent as the decrease found for the 125μm glass beads.

<u>c. Inclined Systems</u>. The particles, mass rates, and humidities studied in the inclined section were the same as those for the horizontal section. The inclined test section was placed at the same point as the horizontal section. The test section was inclined at 45°. Due to space limitations, no entrance length after the horizontal section was included. The resultant effect of the 45° bend on the test section was not included in the analysis. The results are presented in figures A-13, 4-8 and A-14.

The 79μm glass beads showed the greatest fluctuation in the pressure drop vs. gas velocity curves. Electrostatic effects caused increased fluctuations. In the higher mass flow rate cases, the lower humidity pressure drop was greater than that of the high humidity. This is a reversal of the pattern seen in the horizontal systems.

The pressure drop vs. gas velocity data for the 125μm glass beads is shown in figure 4-8. Again, a reverse of the horizontal case was observed with electrostatics causing an increase in the pressure drop and fluctuations.

The 40μm glass beads had the least fluctuations in the pressure drop vs gas velocity curves. Also, the presence of electrostatics caused an increase in pressure drop for both mass flow rates.

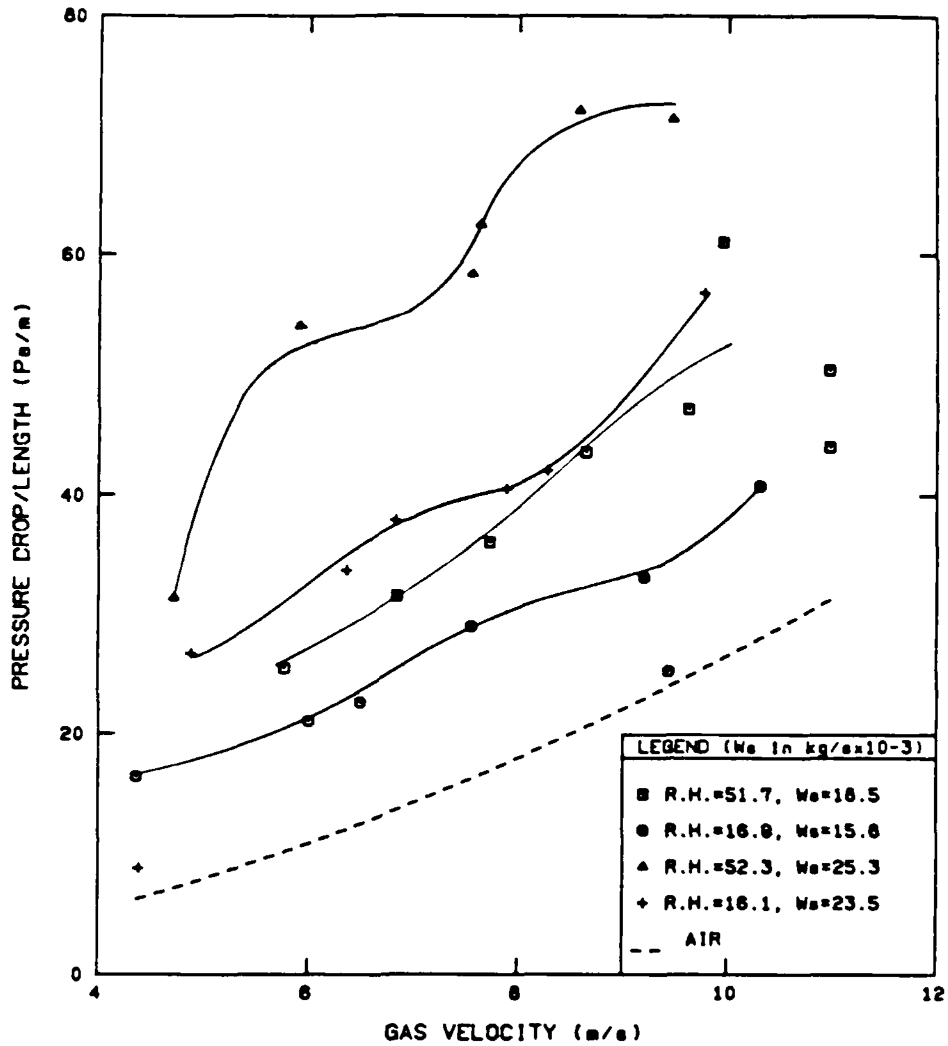

Figure 4-7: Pressure Drop vs. Gas Velocity for the 125μm Glass Beads in the Horizontal Orientation

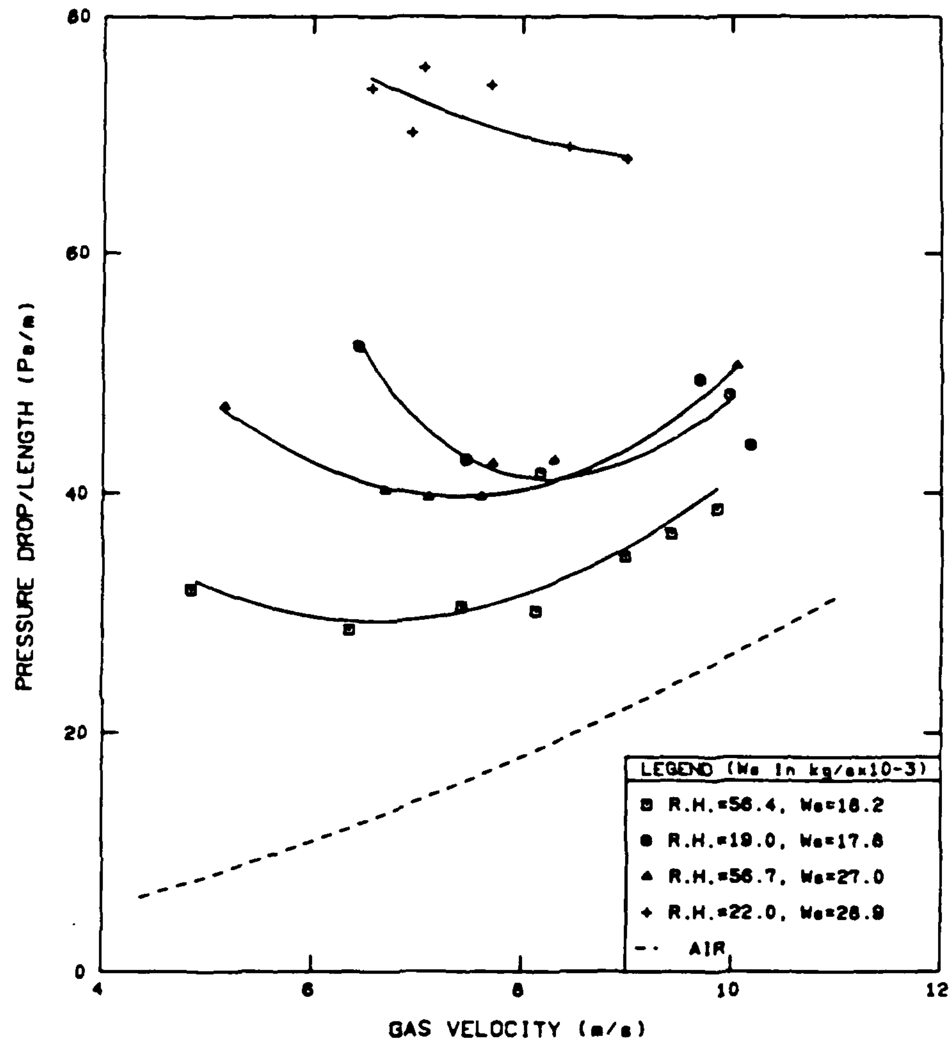

Figure 4-8: Pressure Drop vs. Gas Velocity for the 125µm Glass Beads in the Inclined Orientation

d. Combined System Analysis. Each system was compared for the effect of pipe orientation on pressure drop vs. gas velocity. This analysis shows how the pressure drop for different particle sizes varied with pipe orientation as well as electrostatic effects. This combined data is shown in figures A-15 through A-26.

For the 79µm glass beads, the horizontal orientation dominated the vertical case, except for the condition of high mass flow rates and high humidity. The effect of electrostatics dampened fluctuations in the horizontal case with little effect in the vertical cases. This can be explained by a charge distribution effect, where in the vertical case, clustering is inhibited by the charge on the particles but pressure drop is increased due to the additional electrostatic force. In the horizontal cases, the charge on the particles tends to inhibit the increase in solid concentration to the bottom of the pipe. The 45° inclined pipe showed an increase in pressure drop over both the horizontal and vertical cases for the low humidity cases. For high humidities, the pressure drops were much closer to those for the horizontal and vertical cases. This is apparently due to a combination of the repulsive forces of the particles now having an axial component and the electrostatic force terms.

The 125µm glass beads followed the same trend as the 79µm glass beads, except that now the separation between vertical and horizontal cases is not as great. The dominant orientation is not as clearly delineated, which was borne out by observation when saltation and choking occurred simultaneously.

The 450µm glass beads also follow the same pattern, except that the vertical system now dominates. This effect was observed by the vertical section choking above the saltation velocity of the particles.

4.4.2 Comparison to Correlations

The experimental pressure drop was compared to two correlations for the vertical and horizontal orientations. The Konno and Saito[12] correlation was used for both orientations. The correlations by Yang[13] were also used, one for the vertical orientation and another for the horizontal orientation. The results of this analysis have been plotted as ΔPexperimental/ΔPcalculated vs. gas velocity and are shown in Figures A-40 through A-56. Absolute mean errors and standard deviations were also calculated and are included in Tables B-1 through B-7.

In the vertical systems, the correlation of Konno and Saito had an absolute mean error range of 11.0% to 88.1%. The correlation of Yang had an error range of 11.7% to 44.3%. It is important to note that for most conditions, the values calculated using the correlation of Yang, were less than the experimental values, while the correlation of Konno and Saito usually predicted pressure drops above the experimental values.

For the horizontal systems, the correlation of Konno and Saito gave an error range from 10.2% to 55.9%. The correlation of Yang had an error range from 6.0% to 36.7%. For most conditions, the correlation of Konno and Saito was found to under-predict the pressure drop. Such a generalization could not be made for the results obtained using the correlation of Yang.

4.4.3 Pressure Drop Fluctuation

Upon introduction of the solids to the gas stream, the pressure drop began to fluctuate. This fluctuation was found to depend on particle size, humidity, pipe orientation, and solids mass flow rate.

a. Vertical Systems. The pressure drop vs. gas velocity for the 79μm glass beads in the vertical pipe is shown in figure A-28. There was little correlation between gas velocity and pressure drop fluctuation with a mean fluctuation of about 20%. The effect of electrostatics and solids mass flow rate was also indeterminate.

The 125μm glass beads (see Figure) showed an increase in pressure drop fluctuation with decrease in mass flow rate. This could be due to a decrease in particle-particle collisions allowing greater particle mobility across the pipe. The presence of electrostatics increased the pressure drop fluctuations for all cases. At the lowest mass flow rate, a maximum fluctuation was found as the gas velocity was decreased. Further decrease in gas velocity caused a decrease in fluctuation intensity. This was also the case for the next highest mass flow rate, except the maximum was not as well defined. At the highest solids mass flow rate, this maximum was not present.

The data for the 450μm glass beads is shown in figure A-29. Again, a decrease in fluctuations was found for increasing solids mass flow rate. For all cases, fluctuations increased with decreasing gas velocity. The presence of electrostatics caused an increase in fluctuations for the two lower mass flow rates but a reduction in fluctuations for the higher solids mass flow rate. In all cases this difference was less than 10%.

The 128μm Plexiglass beads showed little fluctuation in pressure drop. (see Figure A-30) A mean fluctuation of about 5% best describes this system. This is probably due to the lesser density of the Plexiglas particles (about 1/2 that of the glass beads) and the low mass flow rates studied.

b. Horizontal Systems. The results for the 79μm glass beads in the horizontal orientation are shown in figure A-32. Like the vertical case, the fluctuations appear to vary about a mean value of 20% with little effect from gas velocity or solids mass flow rate.

The results for the 125μm glass beads are shown in Figure A-31. In this case there is an increase in pressure drop fluctuation with decreasing gas velocity. For the

higher solids mass flow rate, the presence of electrostatics increases the fluctuations, but only by about 2%. In the lower mass flow rate there is not appreciable difference between the electrostatic and non-electrostatic cases.

The results for the 450μm glass beads are shown in Figure A-33. There is an increase in pressure drop fluctuation with decreasing gas velocity. Solids mass flow rate had little effect on the pressure drop fluctuations while electrostatics showed a small decrease in fluctuations.

c. Inclined Systems. The inclined systems displayed the most uniform pressure drop fluctuations for all particle sizes. In all cases, there was an increase in pressure drop fluctuation with decrease in gas velocity to a maximum. Further decrease in gas velocity caused a decrease in fluctuation. The only variation to this behavior was for the 125μm glass beads at the lower solids mass flow rate. In this case the pressure drop fluctuations decreased to a minimum, then increased to a maximum, and then decreased again as the gas velocity was decreased. The results for the inclined systems are shown in Figures A-34, A-35 and A-36.

4.4.4 Electrostatic Pressure Drop

The effect of electrostatic forces on the pressure drop was not as expected. An increase in pressure drop was anticipated for all vertical systems; however, some cases resulted in pressure drop reduction. The horizontal systems also showed pressure drop reductions for some cases. Only the 45° inclined systems showed consistent pressure drop increase with electrostatics. An explanation for this behavior lies in the particle flow conditions. Ally[30] considered the particles in his system to occupy, on an average, an annular region centered at $D_t/4$ and calculated the work required to move them to the wall. This assumption is valid for a homogenous distribution of particles moving with negligible radial velocity components. This condition is approached when D_t is small. Observations during the experiments revealed, for some cases, a considerable amount of internal motion in the flow. This apparently changes the work function due to electrostatics by altering the magnitude or direction of the eletrical field.

A comparison was made between the inclined systems which showed predominantly positive increases to the pressure drop with the results of Ally[30]. Ally found that electrostatic pressure drop increased with decreasing water to solids ratio. A minimum water to solids ratio of about 0.1 was determined above which there was no appreciable increase in pressure drop due to electrostatics. Figures A-37, A-38 and A-39 show the electrostatic pressure drop vs. water to solids mass ratio for the inclined systems. For these systems the minimum water to solids mass ratio is between 0.03 and 0.07 which agrees within 10% of Ally's result. The decrease in the minimum is probably due to the cleanliness of the particles; Ally's being cleaner.

4.5 STABILITY

The stability of the systems studied varied widely with particle size, pipe orientation and electrostatics. In the vertical systems, motions in the radial and tangential directions in the pipe became very pronounced as the system was brought to choking. The horizontal systems went through a separation across the radius of the pipe, with the bottom of the pipe having a higher solids concentration. In the 45° inclined pipe, the formation of retrograde dunes formed for all cases.

4.5.1 Choking

The phenomenon of choking has already been described as the result of a range of instabilities. It is probably better described by a range of parameters. For this study, the choking point was chosen as the point where solids first dropped out of the flow below the feed point and were not picked up by the gas stream. The instabilities leading to this point occurred before this, and small changes in the system operation could have brought about choking at different times.

Two different correlations were used to predict the choking point. They were the Yang[25] and the Rose and Duckworth[26]. The comparison of these two correlations with the experimental results is shown in Table 4-2. Both correlations are seen to under-

Table 4-2: Choking in the Vertical Systems

Particle Size (μm)	Average W_s (kg/sx10^{-3})	U_{gc}(exper) High R.H.	U_{gc}(exper) LOW R.H.	U_{gc}(calc) Yang	U_{gc}(calc) Rose and Duckworth
125	8.7	4.36	4.83	1.51	0.75
glass beads	18.3	3.25	5.02	1.68	0.93
	27.0	3.29	5.18	1.79	1.03
79	9.2	5.73	4.35	1.15	0.53
glass beads	17.4	5.57	4.89	1.30	0.64
	26.5	5.89	6.70	1.42	0.72
450	11.2	5.89	5.74	4.57	2.16
glass beads	17.4	5.85	6.24	4.71	2.57
	30.5	7.11	7.67	4.83	2.88
128	8.8	3.17	3.50	1.08	0.76
Plexiglas beads	12.6	3.22	3.78	1.14	0.84

predict the experimental choking point. The Rose and Duckworth correlation has an error range of 831% to 147%, which is clearly unsuitable for predicting choking. The Yang correlation does much better with errors from 398% to 26%. The largest errors occur for the 79μm glass beads which apparently act as clusters.

The effect of electrostatics on choking varies with particle size and mass flow rate. For the 79μm glass beads, electrostatics tend to decrease the choking gas velocity for the lower mass flow rates. This could be due to the breaking up of clusters in the system due to the like charges on the particles. For the 125μm glass beads and the 128 μm Plexiglas beads, the presence of electrostatics increases the choking gas velocity. The effects of electrostatics on the 450μm glass beads is only a slight increase in the choking gas velocity.

4.5.2 Saltation

Saltation in the horizontal pipe was determined at the superficial gas velocity where solid particles were in constant contact with the bottom of the pipe. The 450μm glass beads did not salt out in this study as the vertical section leading to the horizontal section became plugged before any saltation occurred.

Two correlations were compared to the experimental results. The correlation of Owens[26] which relates a pseudo Froude number to saltation as follows:

$$\rho_f U^2_{salt} f_g / 2\rho_p g D_p > 0.01 \qquad (4\text{-}1)$$

The second correlation is that of Rizk[26] which is:

$$U_{gsalt} = [10^{1440D_p + 1.96}(gD_t)^{550D_p + 1.25} W_s / \rho_g A]^{1/1100D_p + 3.5} \qquad (4\text{-}2)$$

Both of these expressions are implicit in saltation gas velocity and can be solved by iteration. The results of these calculations and the experimental saltation velocities are shown in Table 4-3.

Table 4-3: Saltation Velocity Analysis

Partical µm	W_s(exper) (kg/sx10^{-3}	U_{gsalt}(exper) High R.H.	Low R.H.	U_{gsalt}(calc) Owens	Rizk
125 glass beads	18.3	5.78	4.36	2.60	5.24
	27.0	5.92	4.89	2.60	5.83
79 glass beads	17.4	5.38	8.05	2.00	5.09
	26.5	5.83	6.17	2.00	5.73
450 glass beads	20.6	*	*	5.41	5.89
	30.5	*	*	5.41	6.50

* NO SALTATION OCCURRED

For the 79µm glass beads the Rizk correlation was far superior to the Owens correlation for both high and low humidity, with errors of 2% to 6% for the high humidity and 7% to 58% for the low humidity. The Owens correlation was off by 303% to 169%.

For the 125μm glass beads the Rizk correlation was again superior. Errors ranged from 2% to 17%, while the Owens correlation ranged from 68% to 128%. The Owens correlation was better for the 125μm particles than for the 79μm particles but still was less accurate than the Rizk correlation.

The 450μm glass beads had no experimental saltation velocities as the particles never salted out. Comparison of the saltation velocities obtained by the two correlations with the experimental choking velocities for 450μm glass beads shown in Table 4-2 shows that the expected saltation velocities to be below that of choking which is what was found.

4.5.3 Linear Analysis

A linear stability analysis was performed for all conditions. Values for the solids friction factor were obtained by solving equation 2-15 for f_s using the experimental pressure drop, gas velocity, and particle velocity. Equation 2-31 was then solved for m_1 and m_2. For all cases, m_2 was negative and much greater than m_1. The condition for stability was then the sign of m_1. For positive values of m_1, the flow was considered unstable. As the effect of the electrostatic forces did not always fit the form of equation 2-25, the low humidity cases were treated identically to the high humidity cases, with the electrostatic effects being combined in the solids friction factor.

a. Vertical Systems. The results of the linear analysis for the 79μm glass beads in the vertical pipe are included in tables B-20 through B-25. The analysis shows this particle to be very unstable, except at the higher gas velocities. There is considerable fluctuation in the eigenvalue m_1. This fluctuation was observed in the pulsing and twisting motions of the flow, although complete plugging of the pipe did not occur at the unstable gas velocities resulting from the analysis. The effects of electrostatics was found to be minor, except in the highest mass flow rate condition. In this case, electrostatics caused instability at higher gas velocities.

The results for the 125μm glass beads are included in tables B-8 through B-13.

This particle size showed unusual behavior with change in mass flow rate and electrostatics. Stability increased with increasing mass flow rate. At low mass flow rates, electrostatics increased stability. As mass flow rate increased, this effect was damped out.

The results for the 450μm glass beads are included in tables B-14 through B-19. A very unusual result was obtained for the lowest mass flow rate. In that case, stability was seen to increase from unstable to stable with a decrease in the gas velocity.

The results for the 128μm Plexiglas beads are included in tables B-26 through B-29. The 128μm Plexiglas beads were seen to show unusually unstable behavior by linear analysis. Stability was predicted for the higher gas flow rates, but unstable predictions occured for most of the lower gas flow rates. Again, observations of the Plexiglas beads during flow, pointed out the twisting and pulsing instabilities without plugging of the pipe.

b. Horizontal Systems. The linear analysis results for all horizontal systems are included in tables B-34 through B-41. Stable eigenvalues were obtained for all conditions. This result does not reflect the true nature of the flow conditions. The voidage used in calculations was for a uniformly dispersion of particles across the pipe. This was not the true condition as gas flow rate was decreased as the flow separated to cause an increased concentration in the bottom of the pipe. The equations for the analysis are incapable of predicting this gravity effect. A possible solution would be to use equation 2-16. This possibility, however, requires knowledge of the individual friction factors, which were not obtained.

c. Inclined Systems. The linear analysis results for the inclined systems are included in tables B-50 through B-49. The results show an increase in stability with decrease in humidity for all systems. The 79μm glass beads had unstable eigenvalues for the high humidity cases only, while the 125μm and 450μm glass beads had stable eigenvalues for all cases. In general, stability was increased with increase in gas velocity and increase

in mass flow rate. There was fluctuation in the values of the eigenvalues as gas velocity was decreased.

5.0 CONCLUSIONS

1. The use of electrostatic ring probes was found to work reasonably well in the 0.0508 m pipe. Agreement with correlations tested was within 50%. The use of this type probe in the horizontal and inclined orientations is not recommended in the probes current form as a particle density gradient can exist in these orientations which can cause significant deviations in the signals from the probes.

2. Various flow patterns were observed for the different orientations studied:

   a. In the vertical orientation, radial and tangential disturbances were observed as the system was brought toward choking.

   b. In the horizontal systems, the particle density in the lower portion of the pipe increased as saltation was approached. Prior to uniform saltation, blunt nosed dunes formed on the bottom of the pipe.

   c. In the inclined orientation, retrograde dunes formed and were observed to flow along the bottom of the pipe against the main stream.

3. The pressure drop vs. gas velocity was found to depend heavily on pipe

orientation and particle size. The vertical pipe was found to control the system in terms of stability for the largest particles. The horizontal section was found to control the system for the smaller particles. For the medium particle size, both the vertical and horizontal sections contributed to instabilities.

4. A unique behavior was found for the 125 μm glass beads. The pressure drop curve passed through a maximum as gas velocity was decreased. This behavior was compared to similar observations made by Zaltash[29] who attributed this phenomenon to a particle to tube size ratio. As this behavior was not found for the 128μm Plexiglas particles, a density factor is believed to contribute. For Zaltash's study, the group $(D_p/D_t)(\rho_p/\rho_f)$ equaled 6.06. For this study, this group equaled 4.79.

5. Fluctuations in the pressure drop were found to decrease with increasing solids mass flow rate. For the smallest particles, there was little change in the fluctuations with change in gas velocity. As particle size increased, the dependency of the fluctuations on gas velocity increased, with fluctuations increasing with decreasing gas velocity. The effect of electrostatics was found to vary considerably with particle size and pipe orientation.

6. The effect of electrostatic forces on the systems studied was found to vary considerably. The orientation, particle size, and gas velocity were found to affect the impact of electrostatics significantly.

7. The correlation of Konno and Saito was found to be comparable to that of Yang in the vertical systems studied with the advantage of over-predicting for most conditions. In the horizontal systems, the correlation of Yang for this orientation was found superior.

8. The two correlations used to predict choking gas velocities were found to be inadequate as the velocities were below the experimental velocities by as much as 831%. The use of the Yang correlation for choking velocity was found to be superior to that of Rose and Duckworth, however, both correlations under-predicted the choking point. The instabilities associated with choking cover a wide range of gas velocities, and therefore, the definition of choking should include the capacity to cover this range.

9. For predicting saltation, the correlation of Rizk was found to predict within 17% of the experimental values.

10. The linear analysis performed was found to describe the vertical systems as far as observations made. Its applicability to the horizontal and inclined orientations is questionable as the fundamental equations used do not adequately describe the system.

6.0 RECOMMENDATIONS

The following recommendations are included as possibilities for further investigation:

1. A means of verifying the velocities obtained with the electrostatic probes should be examined. This could be by such means as high speed photography.

2. A selection of particles with different densities and sizes should be studied. In conjunction with this, other pipe sizes should be included. A particle size and density range should include values of the group $(D_p/D_t)(\rho_p/\rho_f)$ within the range of the unique behavior found.

3. The role of electrostatics requires much further attention. Work in this area should attempt to evaluate the direction and magnitude of the electric field.

APPENDICES

APPENDIX A.

FIGURES REFERRED TO IN TEXT

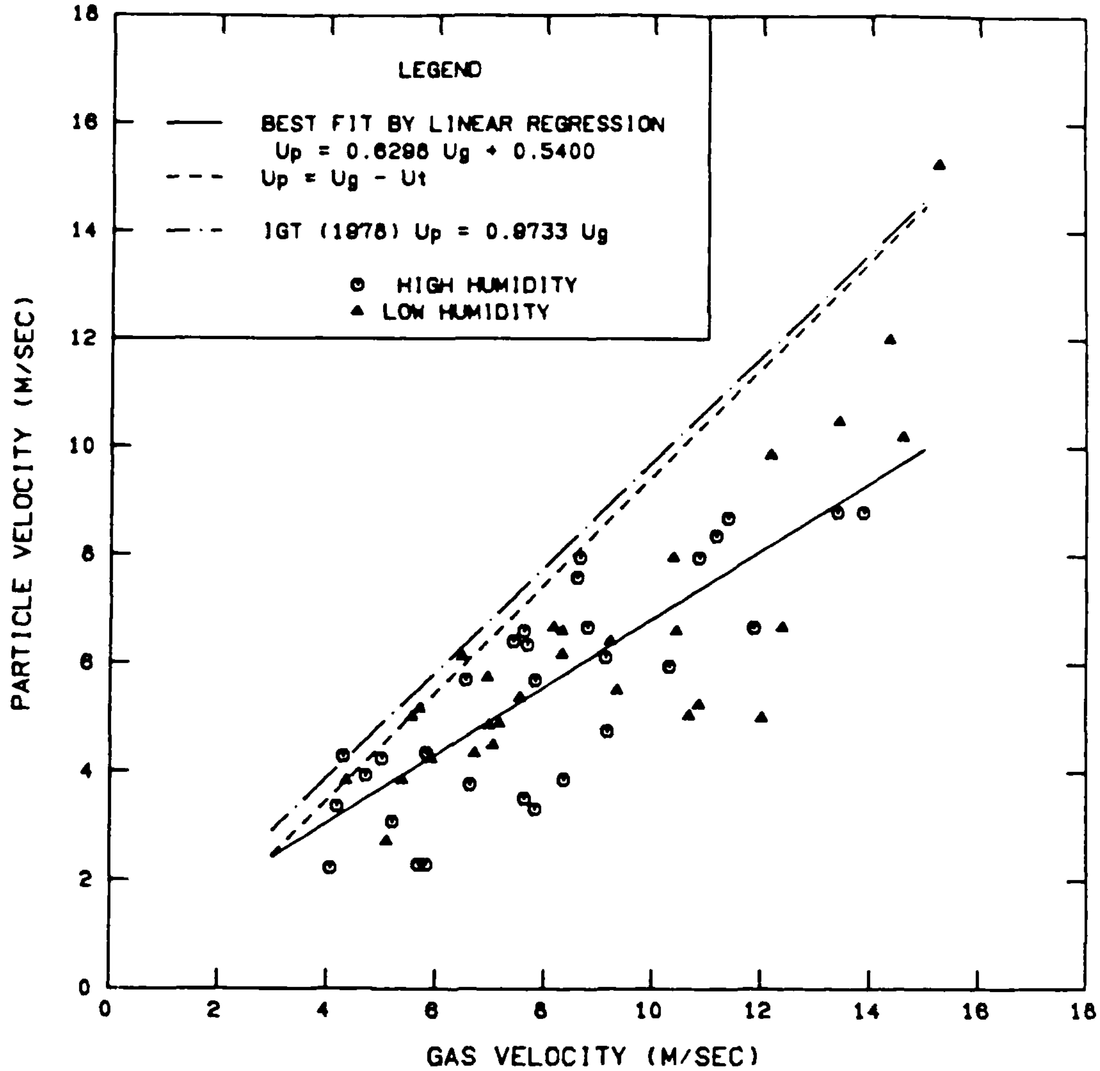

Figure A-1: Particle Velocity vs. Gas Velocity for 79μm Glass Beads in the Vertical Orientation

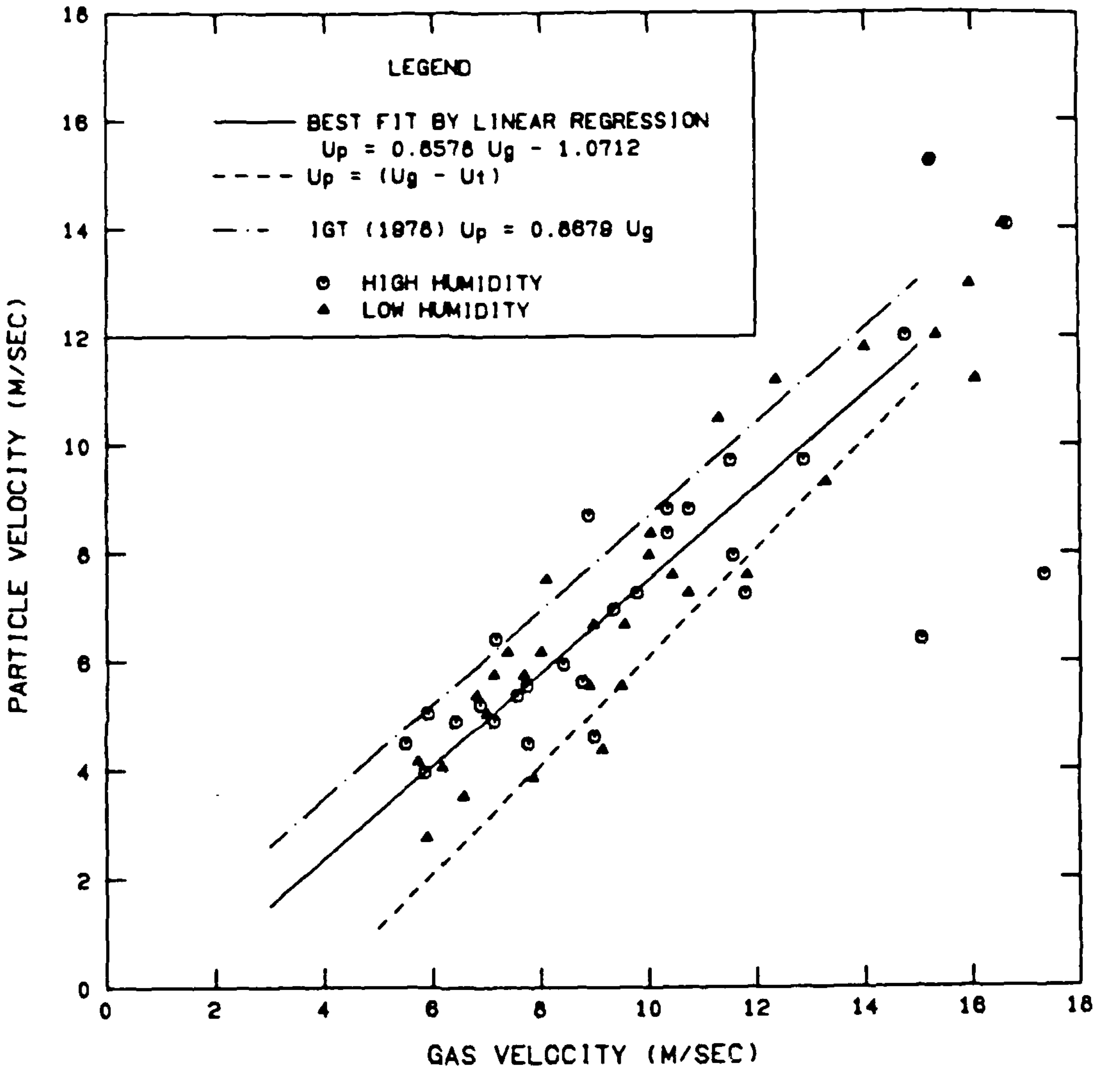

Figure A-2: Particle Velocity vs. Gas Velocity for 450μm Glass Beads in the Vertical Orientation

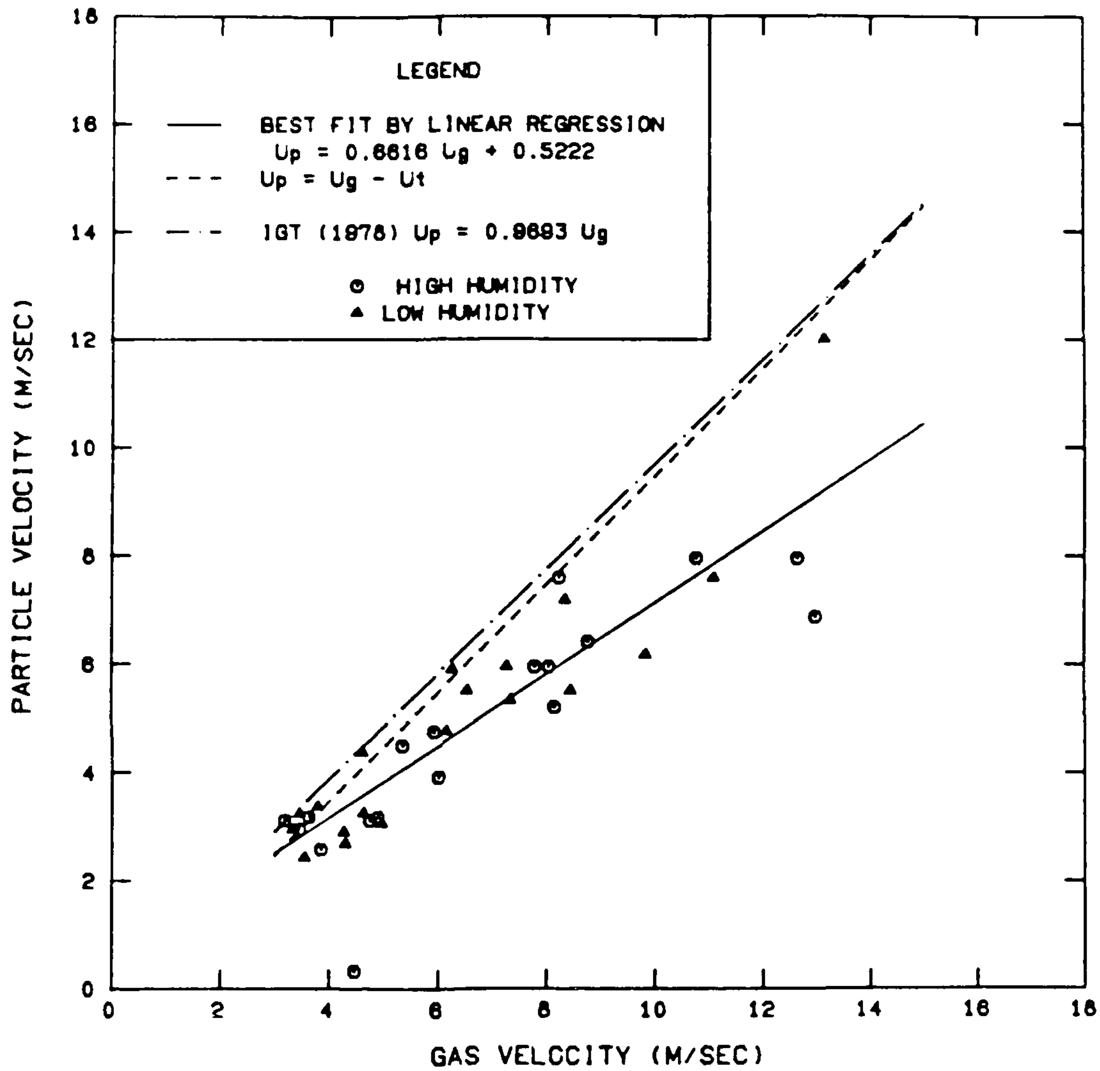

Figure A-3: Particle Velocity vs. Gas Velocity for 128μm Plexiglas Beads in the Vertical Orientation

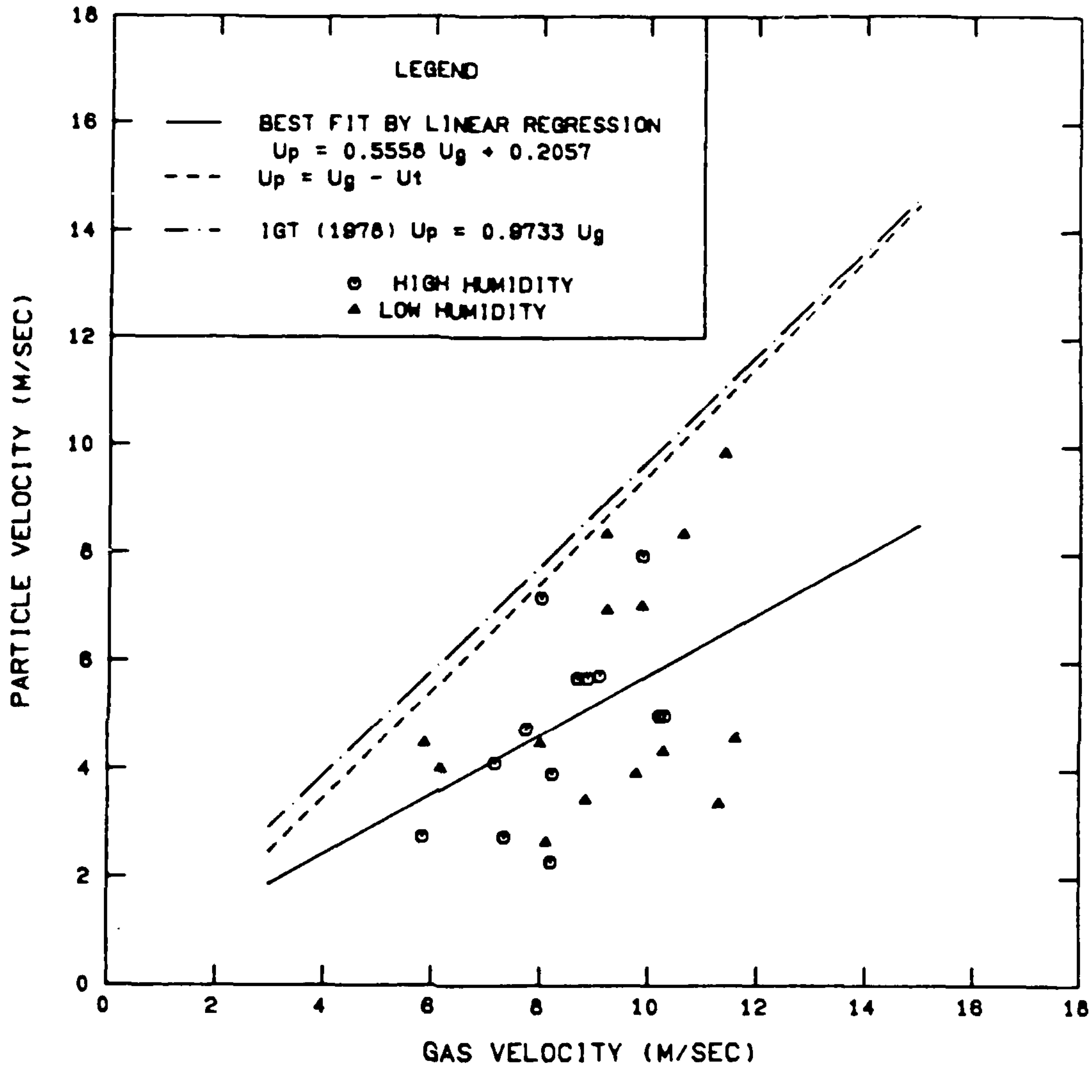

Figure A-4: Partical Velocity vs. Gas Velocity for $79\mu m$ Glass Beads in the Horizontal Orientation

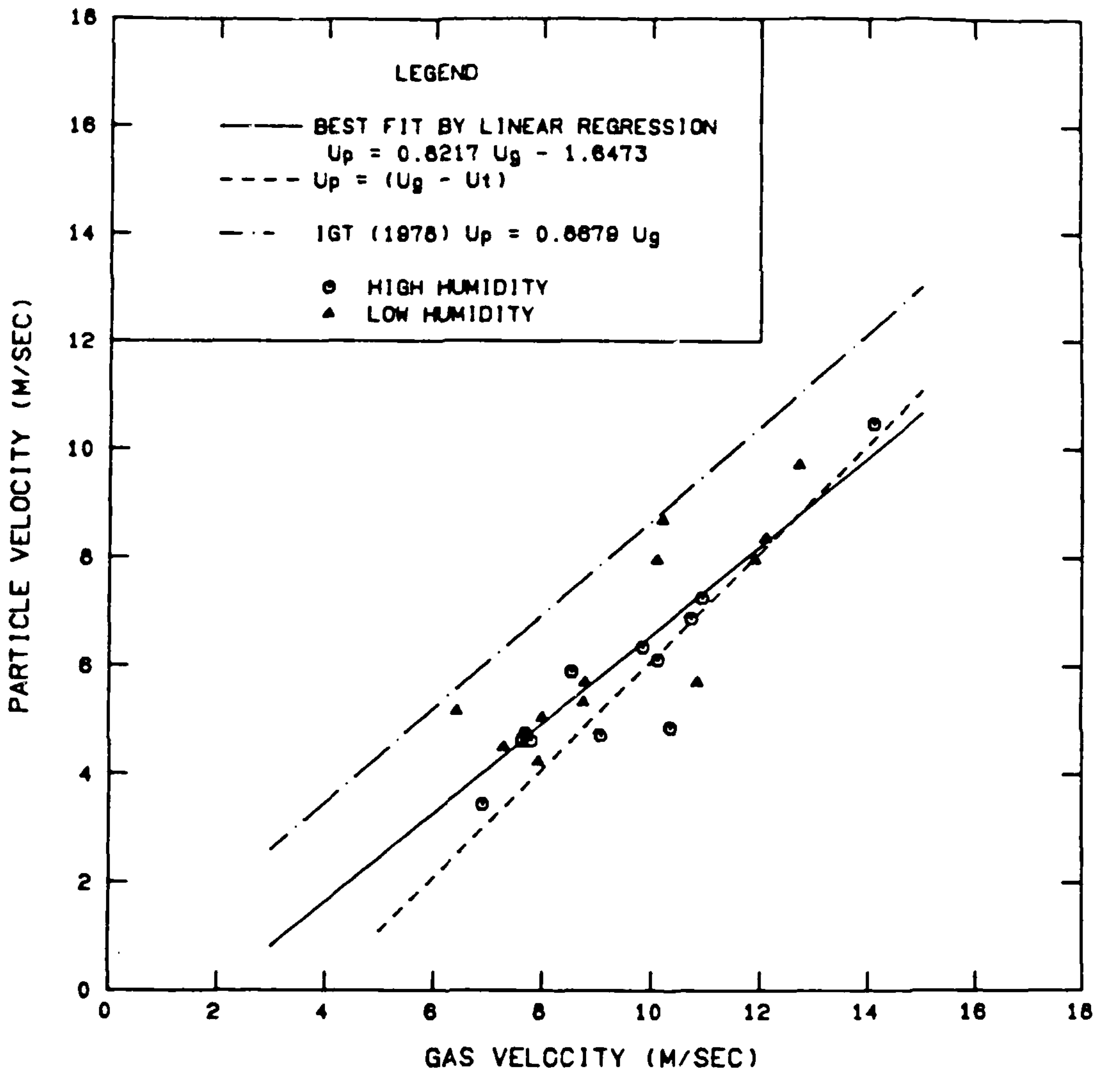

Figure A-5: Partical Velocity vs. Gas Velocity for 450µm Glass beads in the Horizontal Orientation

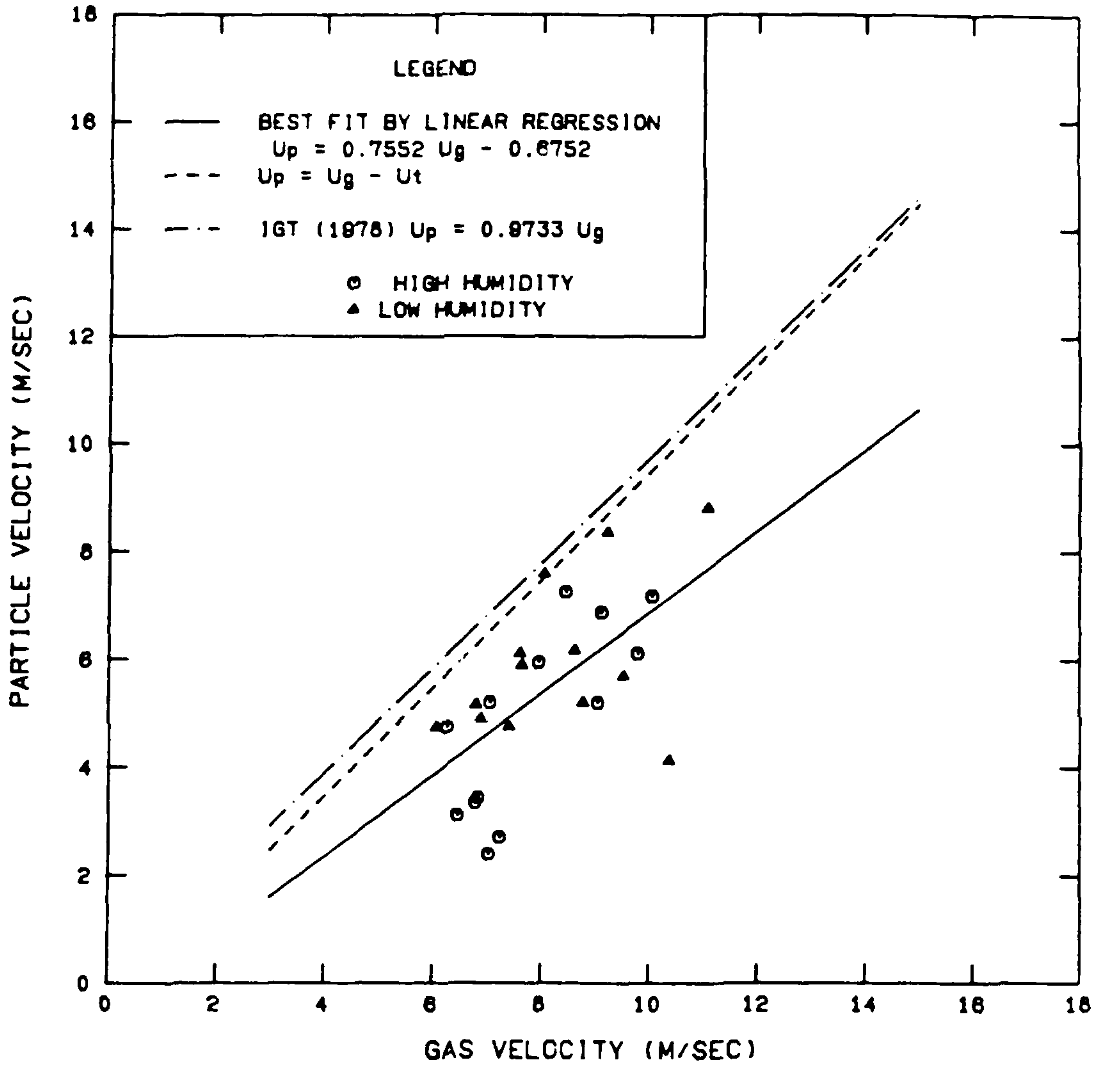

Figure A-6: Particle Velocity vs. Gas Velocity for 79μm Glass Beads in the Inclined Orientation

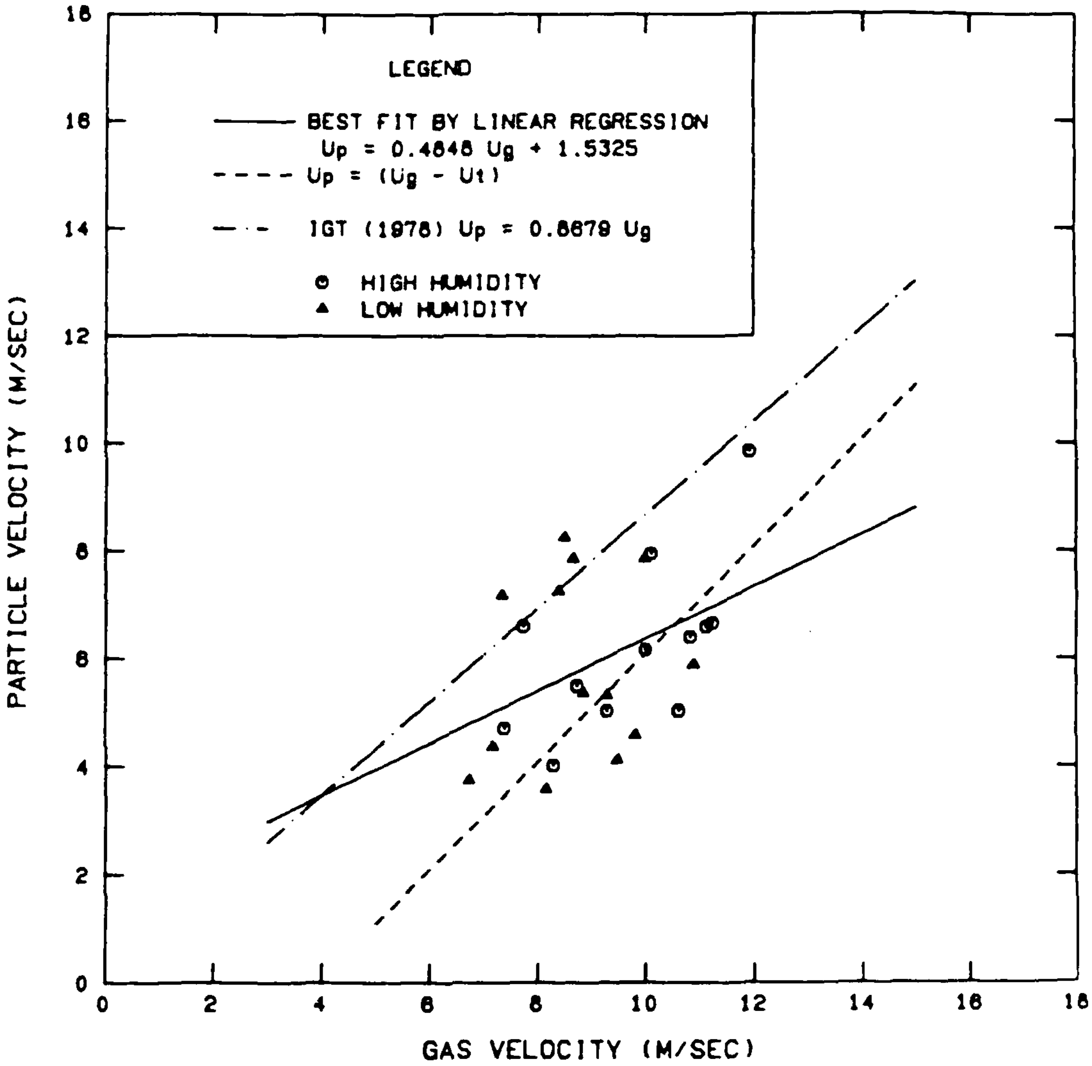

Figure A-7: Particle Velocity vs. Gas Velocity for 450μm Glass Beads in the Inclined Orientation

AD-A184 074 GAS-SOLID TRANSPORT IN A 00508 M PIPE AT VARIOUS INCLINATIONS WITH AND WITHOUT ELECTROSTATICS(U) ARMY MILITARY PERSONNEL CENTER ALEXANDRIA VA C A MYLER 2/3

UNCLASSIFIED AUG 85 F/G 13/11 NL

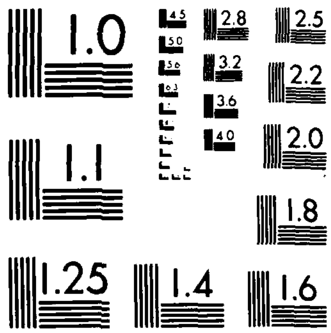

MICROCOPY RESOLUTION TEST CHART
NATIONAL BUREAU OF STANDARDS-1963-A

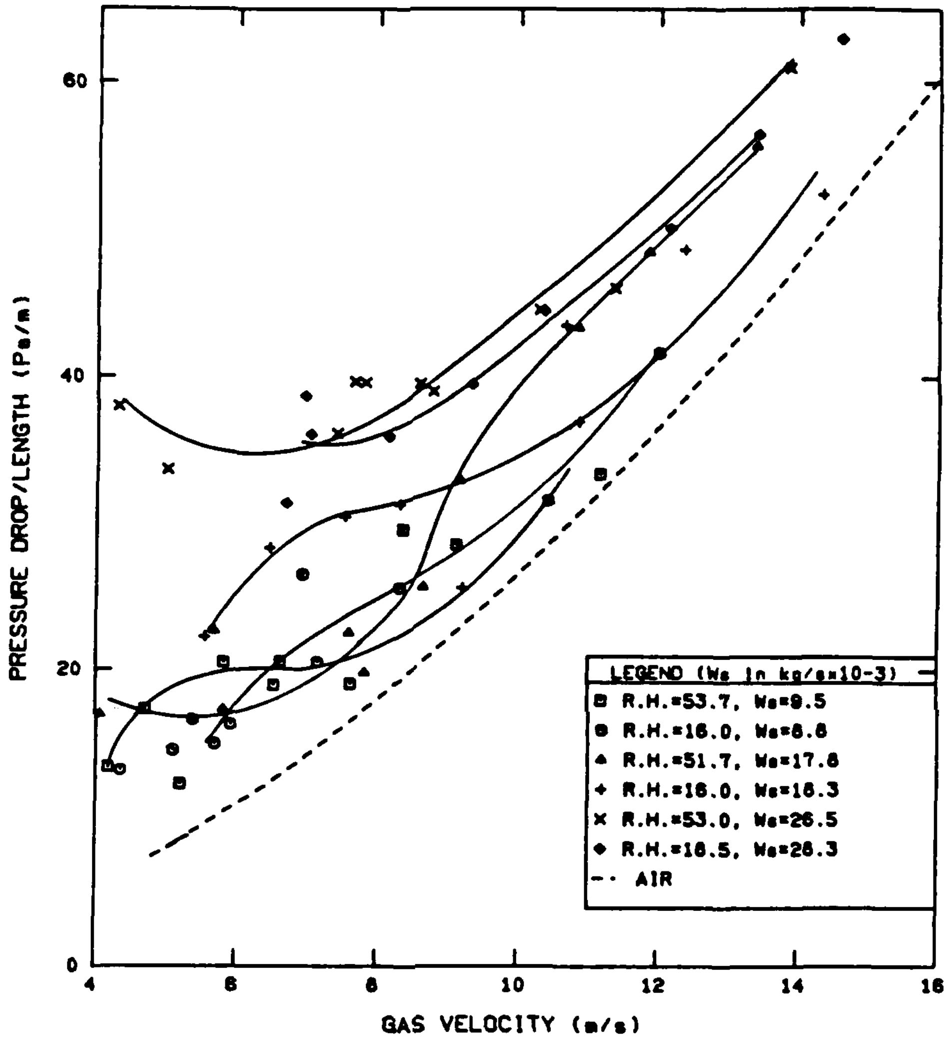

Figure A-8: Pressure Drop vs. Gas Velocity for 79μm Glass Beads in the Vertical Orientation

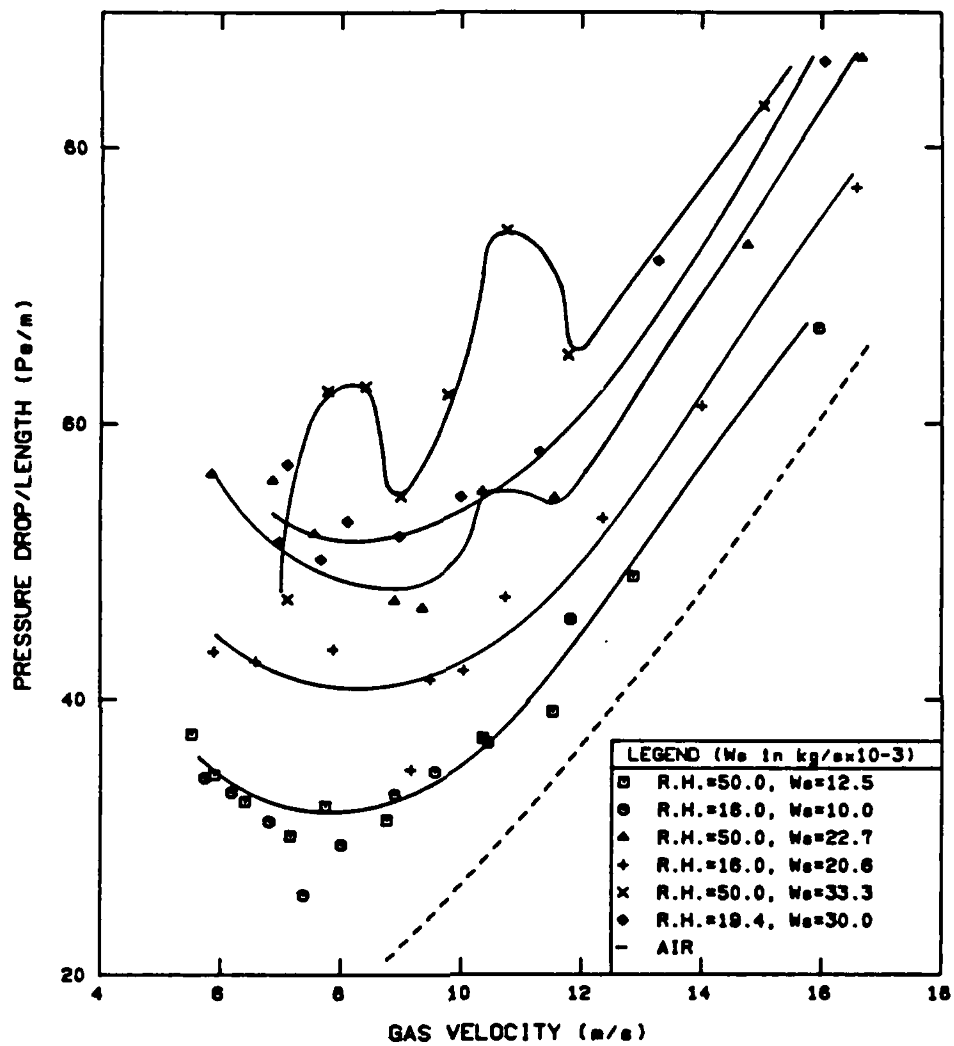

Figure A-9: Pressure Drop vs. Gas Velocity for 450µm Glass Beads in the Vertical Orientation

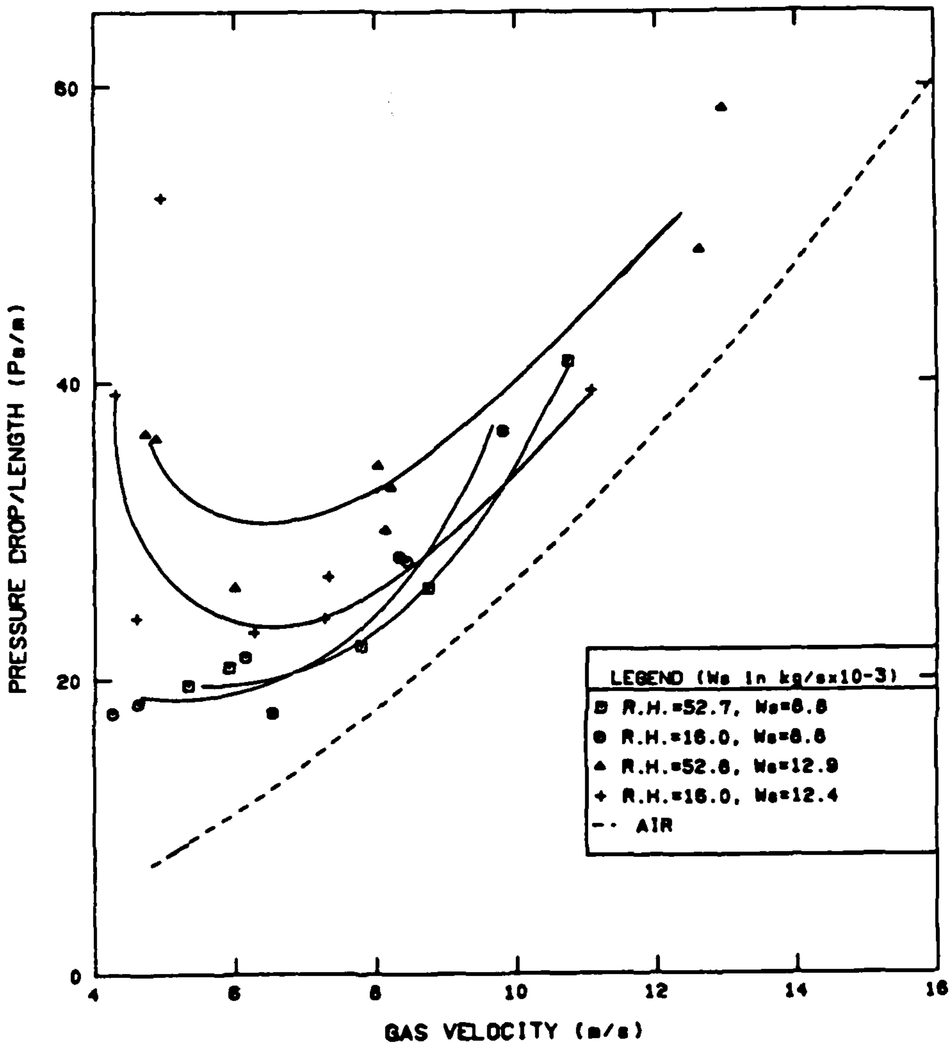

Figure A-10: Pressure Drop vs. Gas Velocity for 128μm Plexiglas Beads in the Vertical Orientation

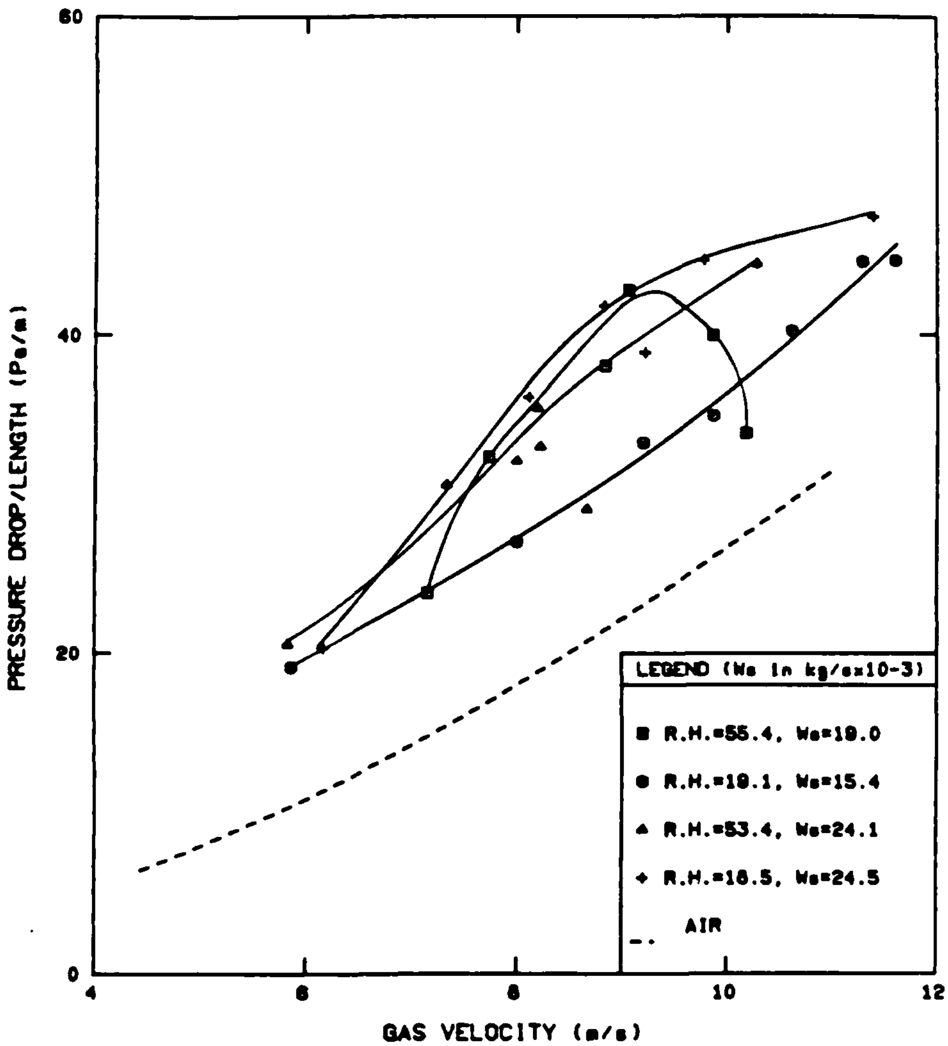

Figure A-11: Pressure Drop vs. Gas Velocity for 79μm Glass Beads in the Horizontal Orientation

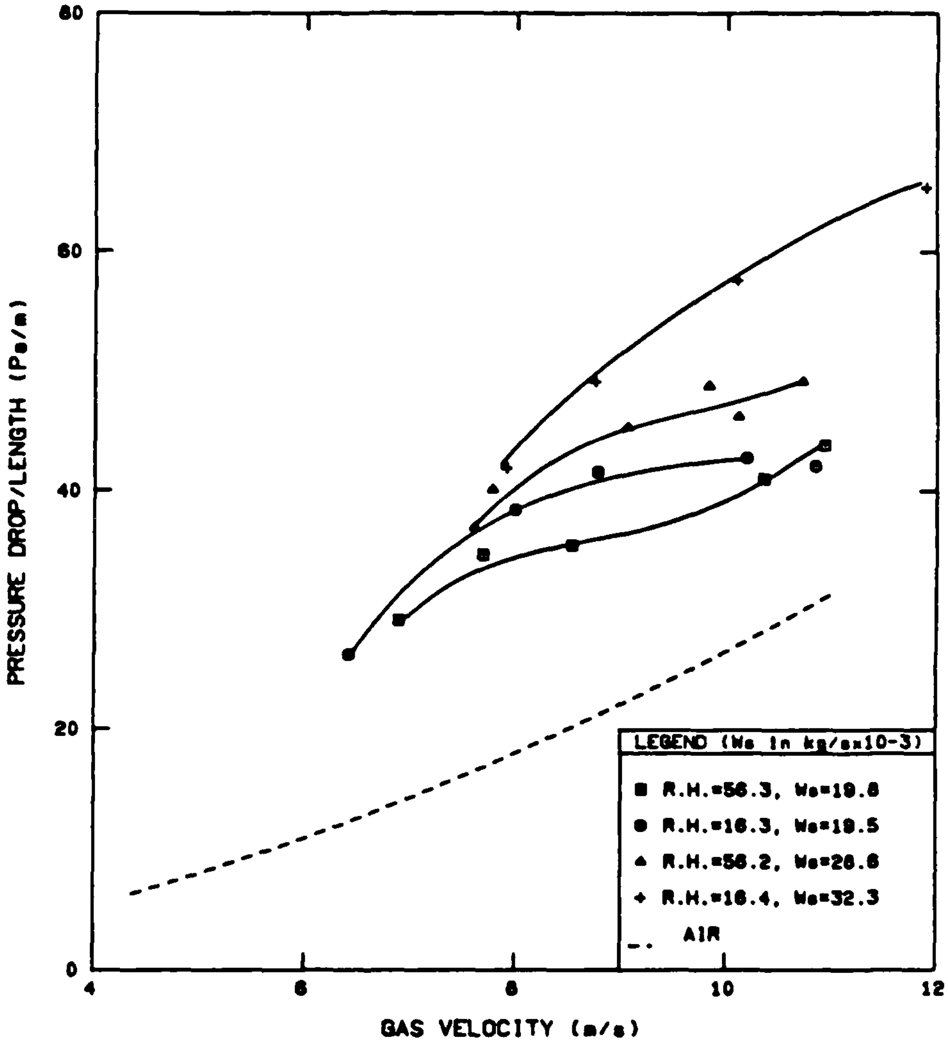

Figure A-12: Pressure Drop vs. Gas Velocity for 450μm Glass Beads in the Horizontal Orientation

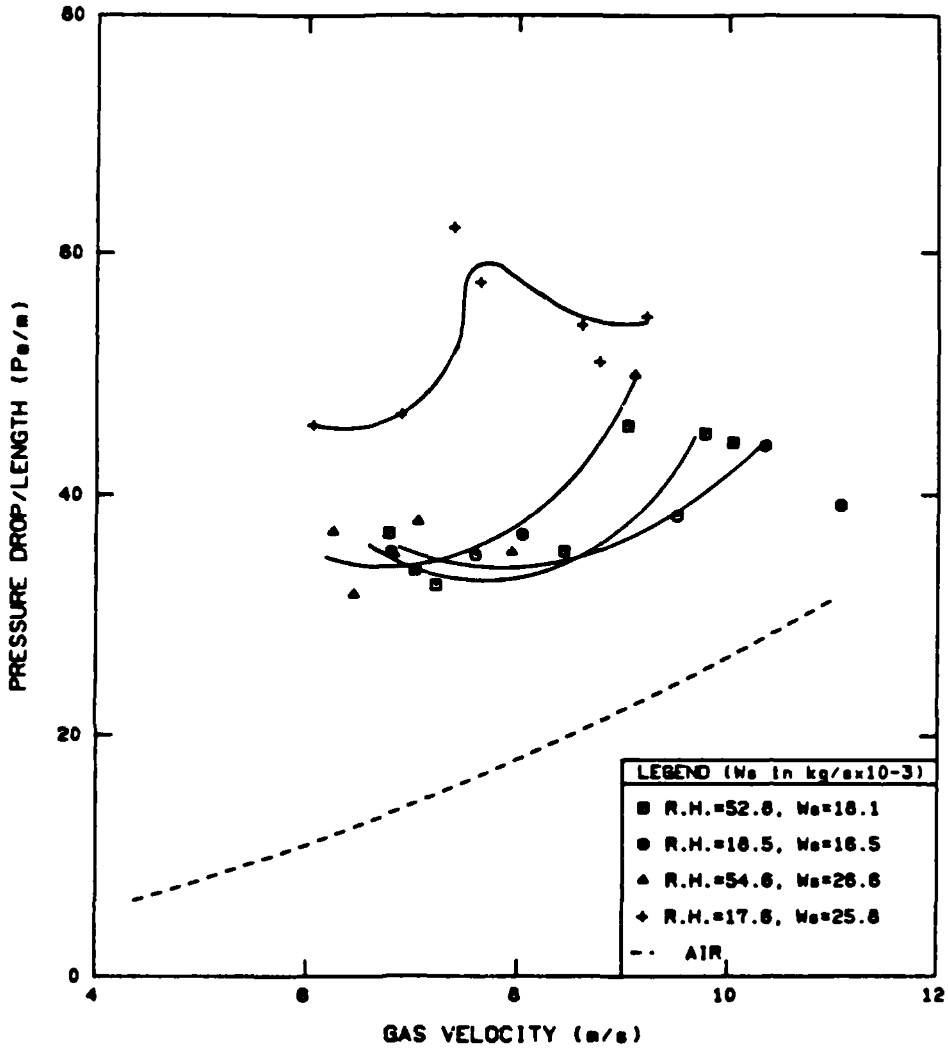

Figure A-13: Pressure Drop vs. Gas Velocity for the 79μm Glass Beads in the Inclined Orientation

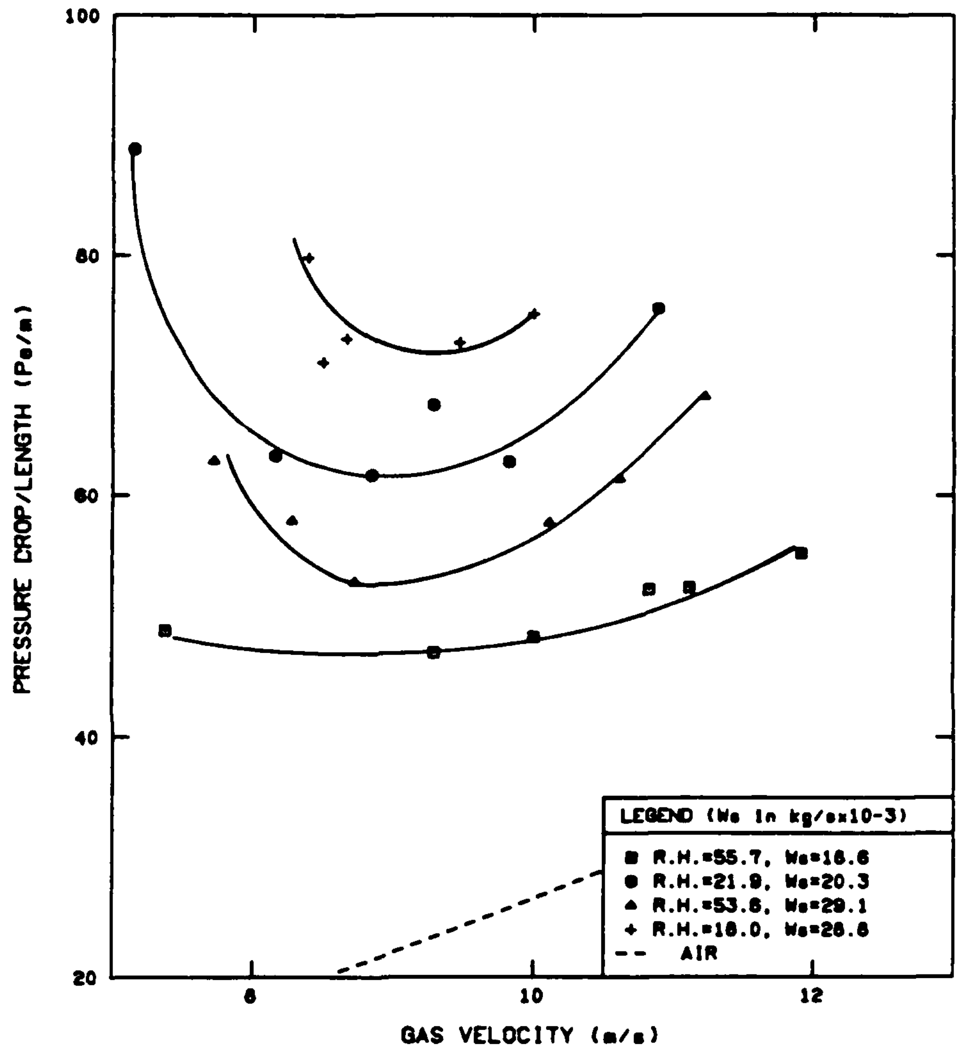

Figure A-14: Pressure Drop vs. Gas Velocity for the 450μm Glass Beads in the Inclined Orientation

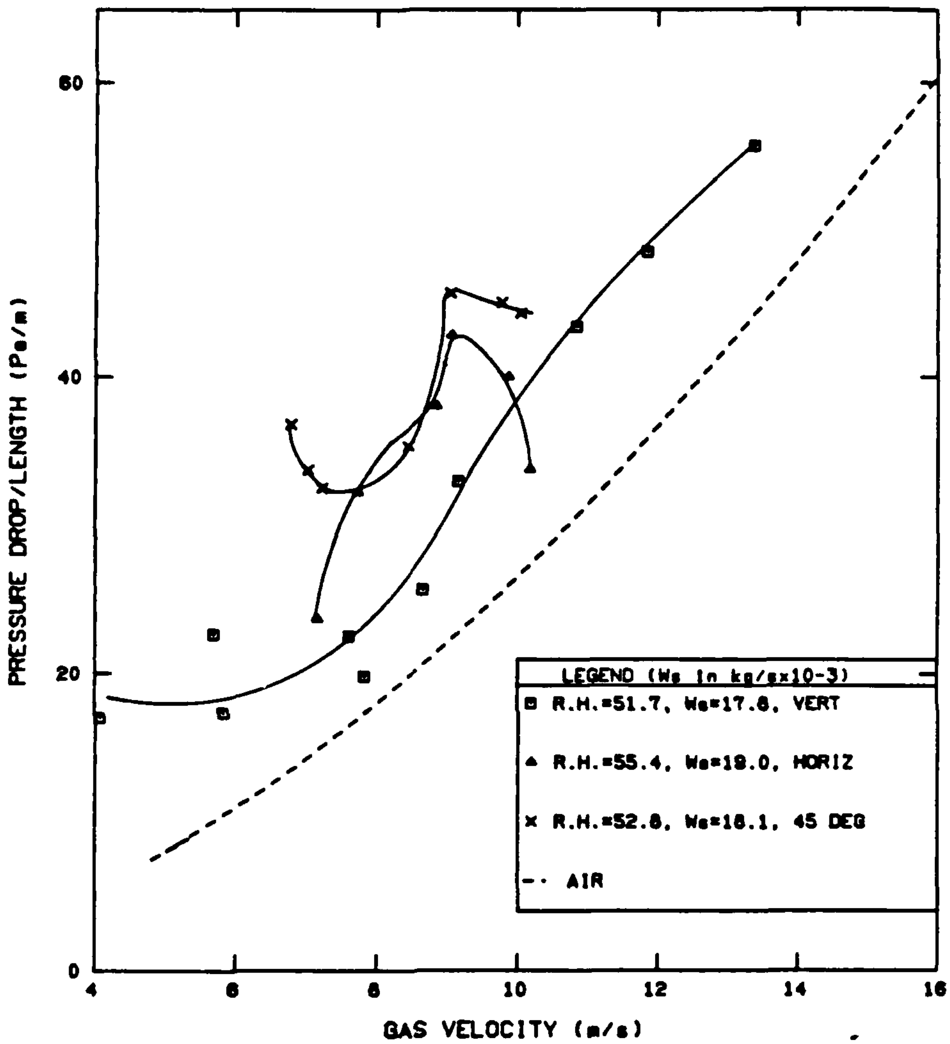

Figure A-15: Pressure Drop vs. Gas Velocity for 79µm Glass Beads for the Combined Orientations at the Lower Mass Flow Rate Without Electrostatics

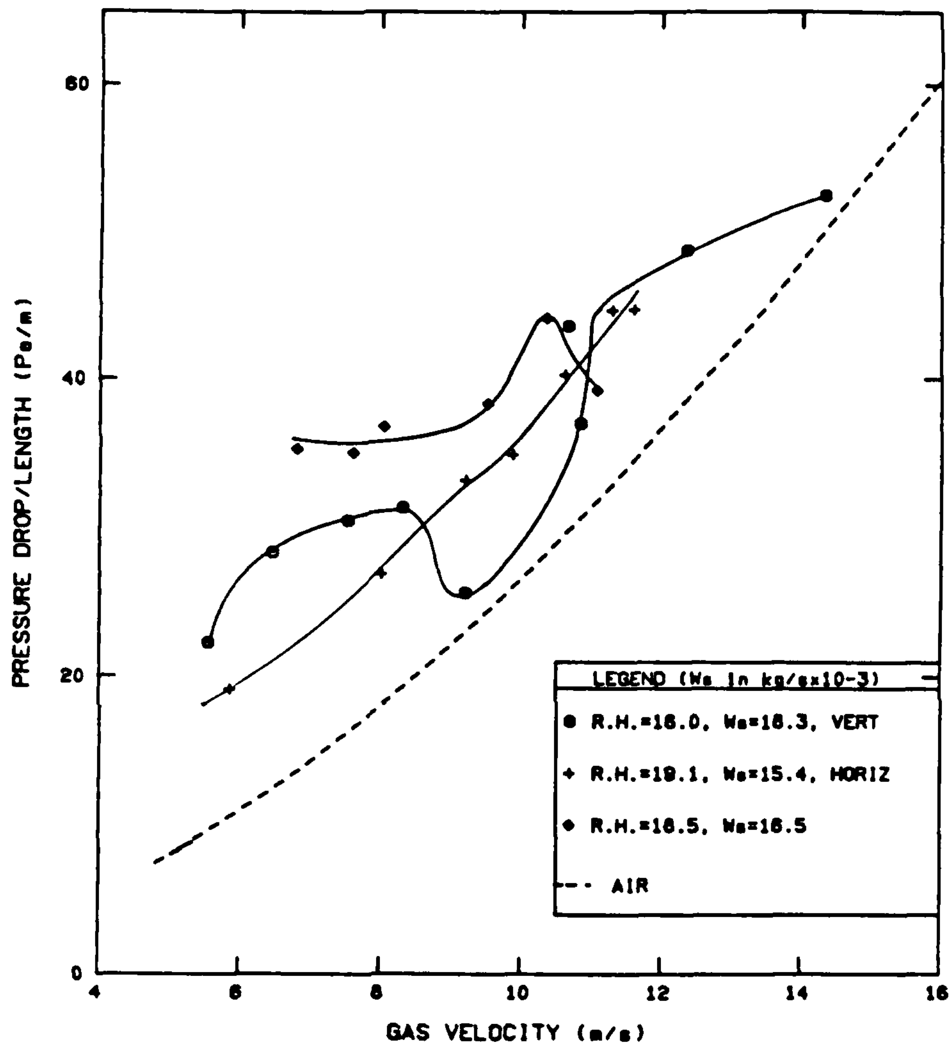

Figure A-16: Pressure Drop vs. Gas Velocity for 79μm Glass Beads for the Combined Orientations at the Lower Mass Flow Rate With Electrostatics

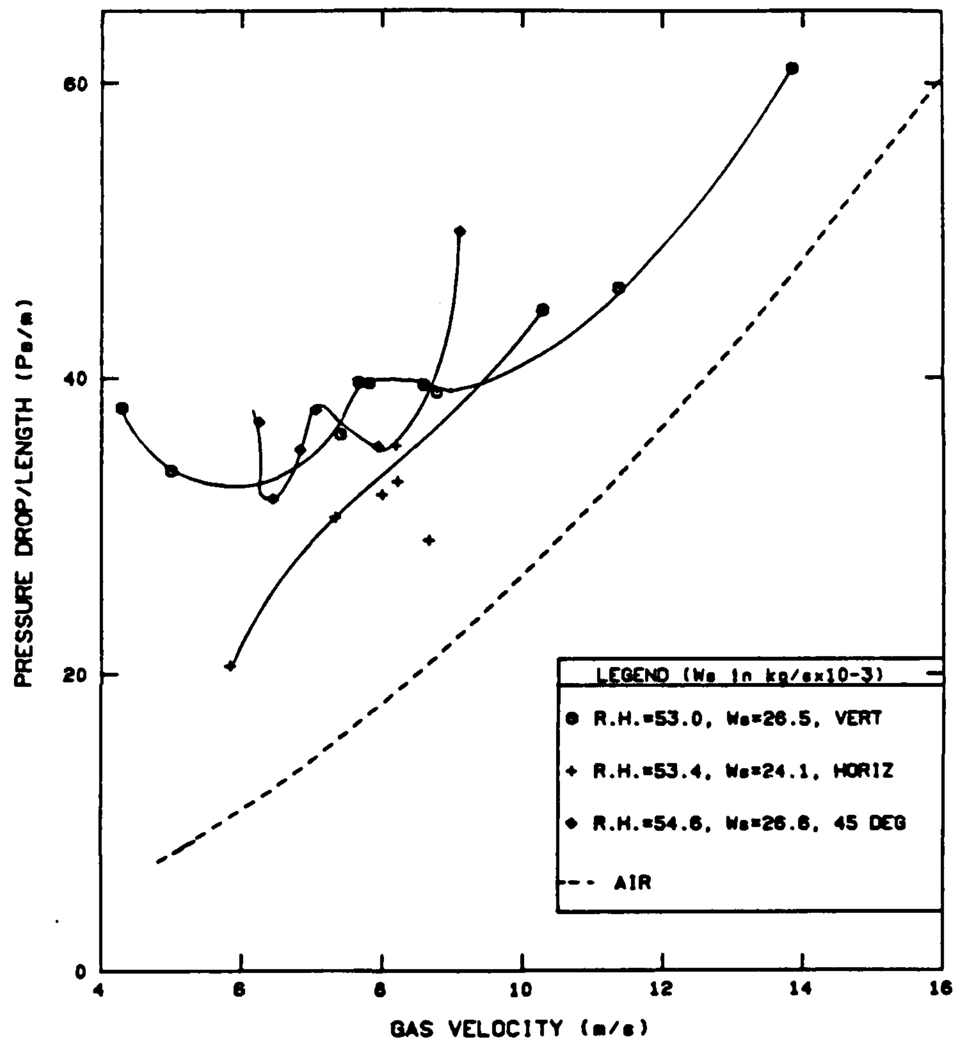

Figure A-17: Pressure Drop vs. Gas Velocity for 79μm Glass Beads for the Combined Orientations at the Higher Mass Flow Rate Without Electrostatics

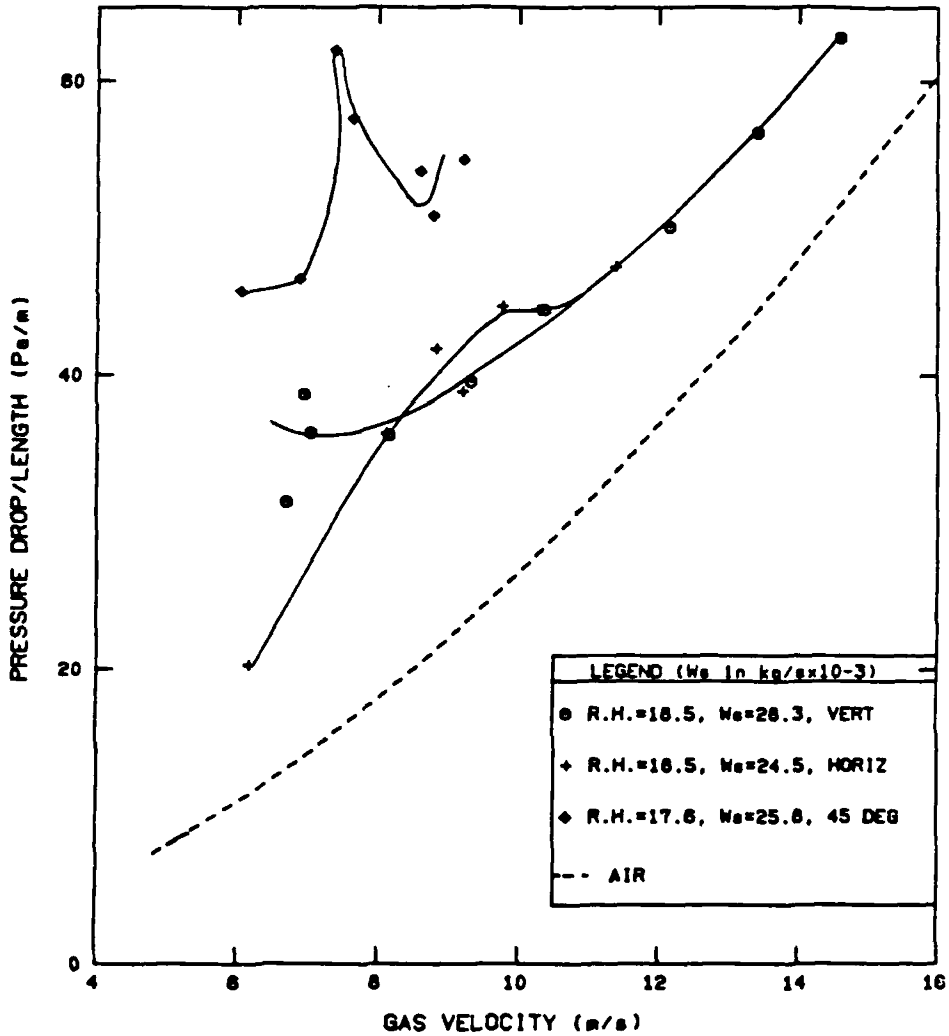

Figure A-18: Pressure Drop vs. Gas Velocity for 79μm Glass Beads for the Combined Orientations at the Higher Mass Flow Rate With Electrostatics

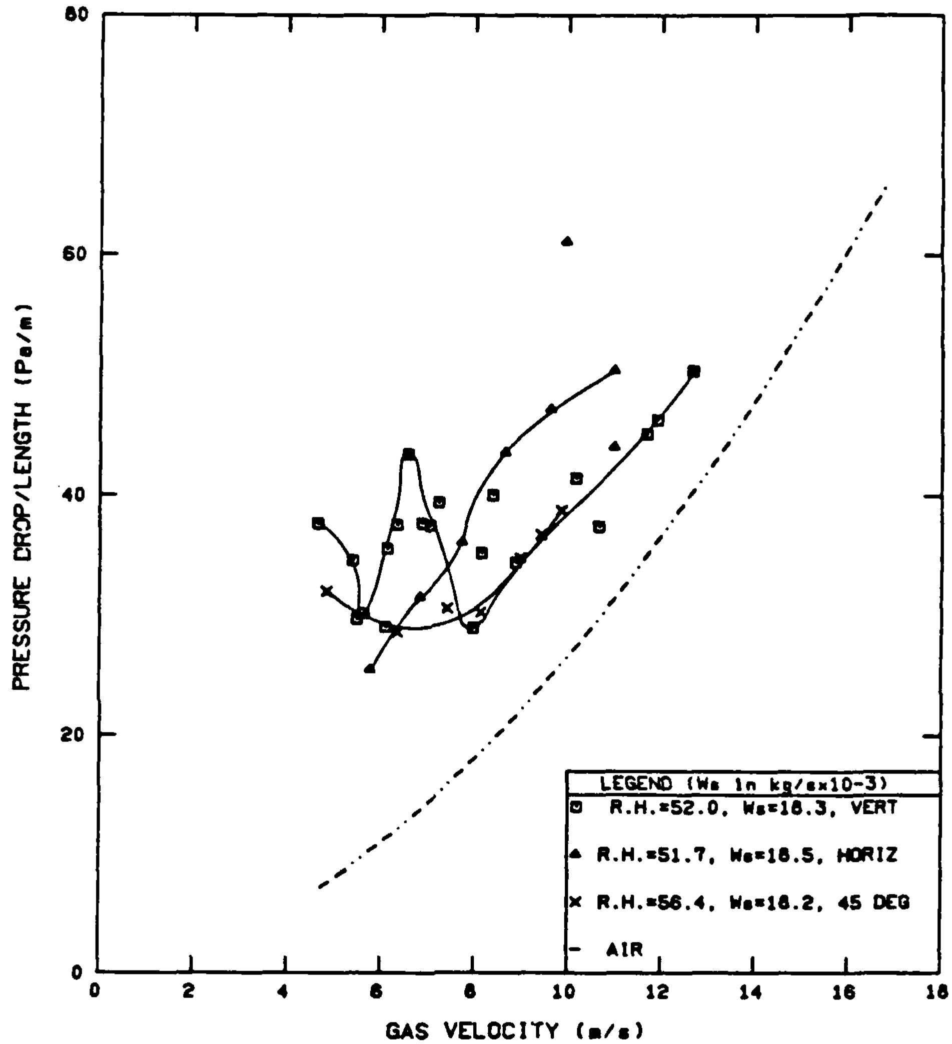

Figure A-19: Pressure Drop vs. Gas Velocity for 125μm Glass Beads for the Combined Orientations at the Lower Mass Flow Rate Without Electrostatics

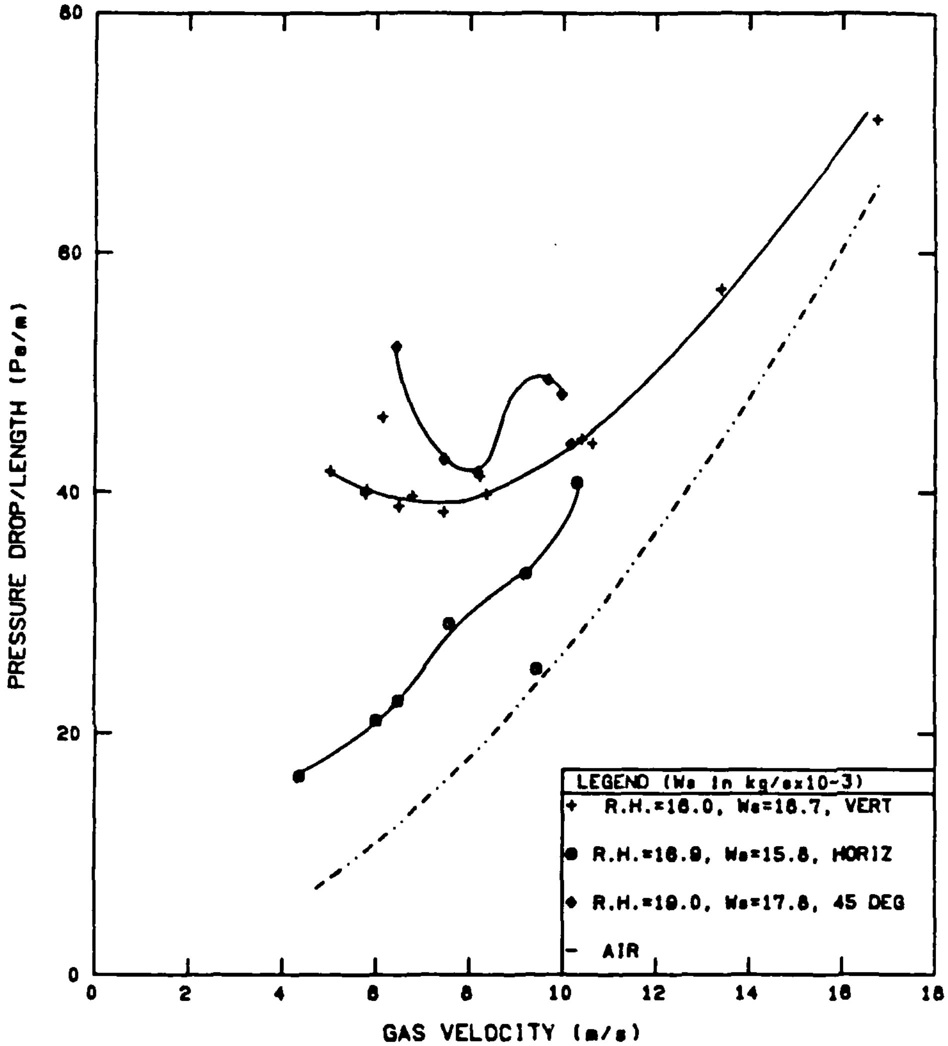

Figure A-20: Pressure Drop vs. Gas Velocity for 125μm Glass Beads for the Combined Orientations at the Lower Mass Flow Rate With Electrostatics

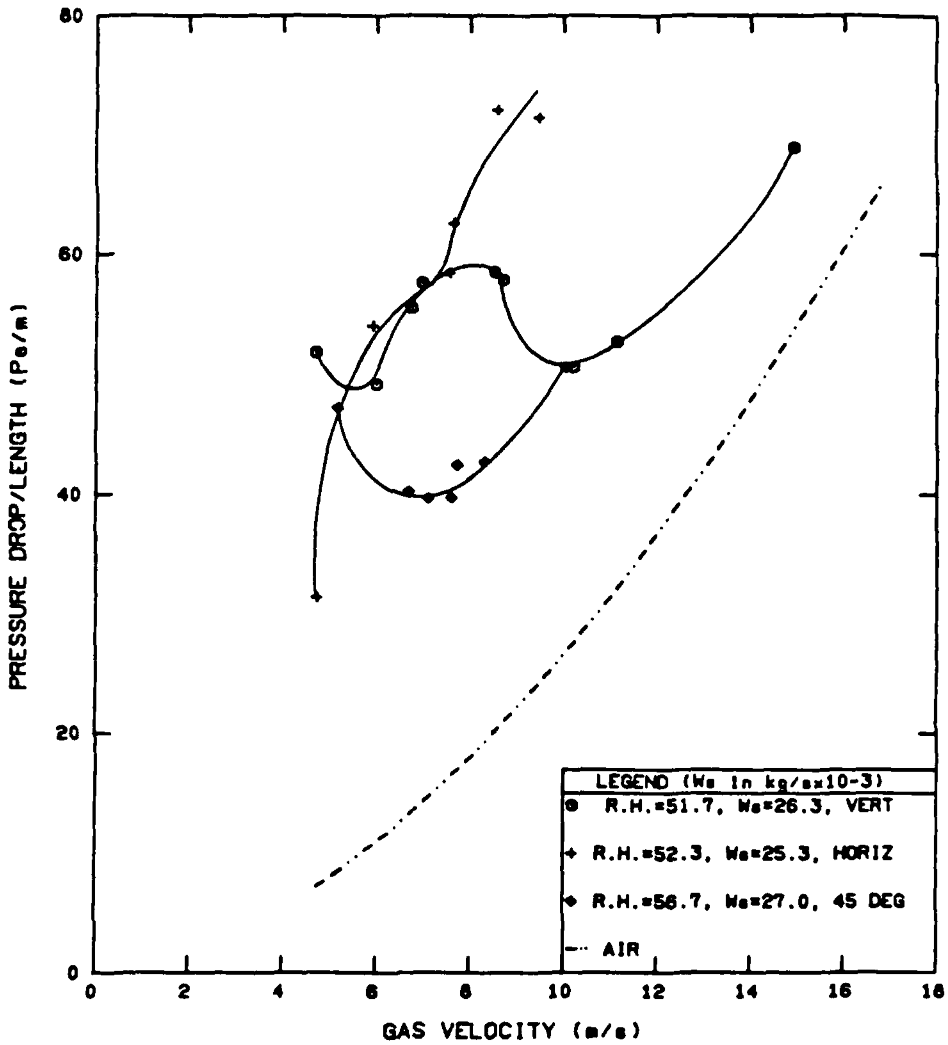

Figure A-21: Pressure Drop vs. Gas Velocity for 125μm Glass Beads for the Combined Orientations at the Higher Mass Flow Rate Without Electrostatics

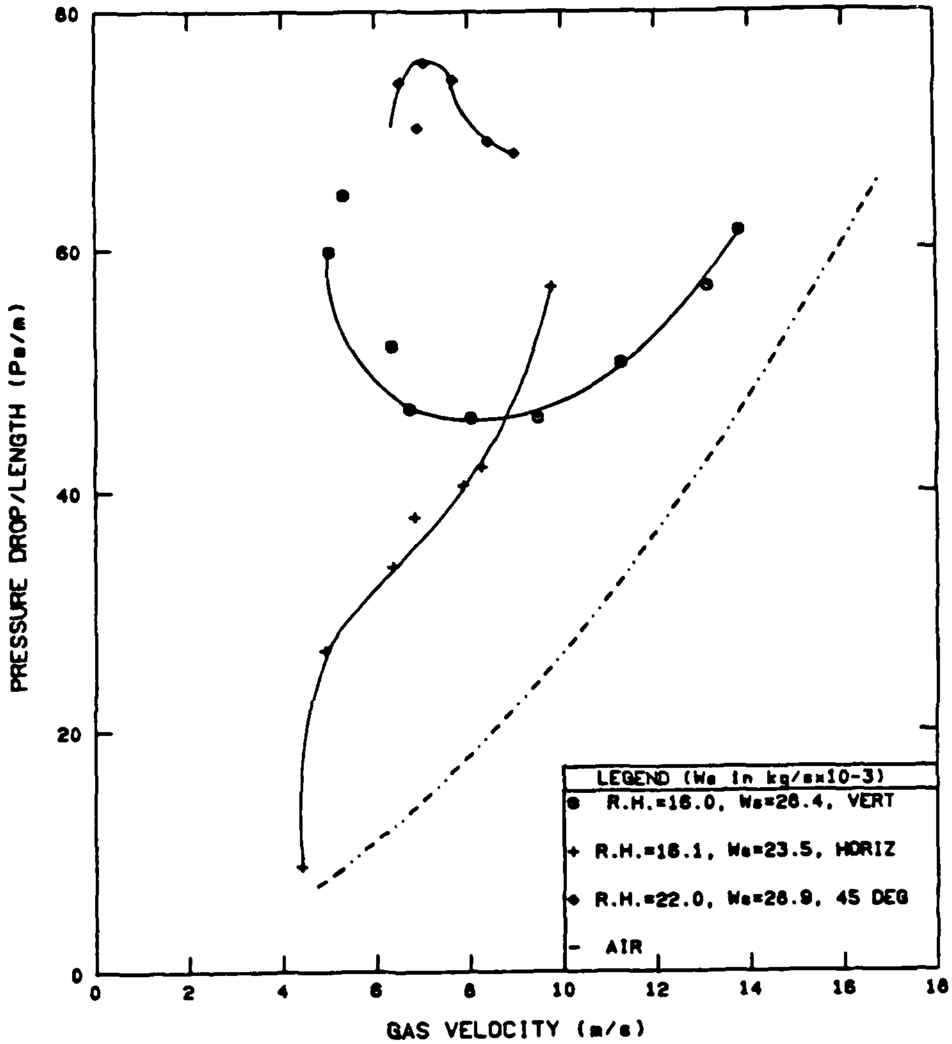

Figure A-22: Pressure Drop vs. Gas Velocity for 125μm Glass Beads for the Combined Orientations at the Higher Mass Flow Rate With Electrostatics

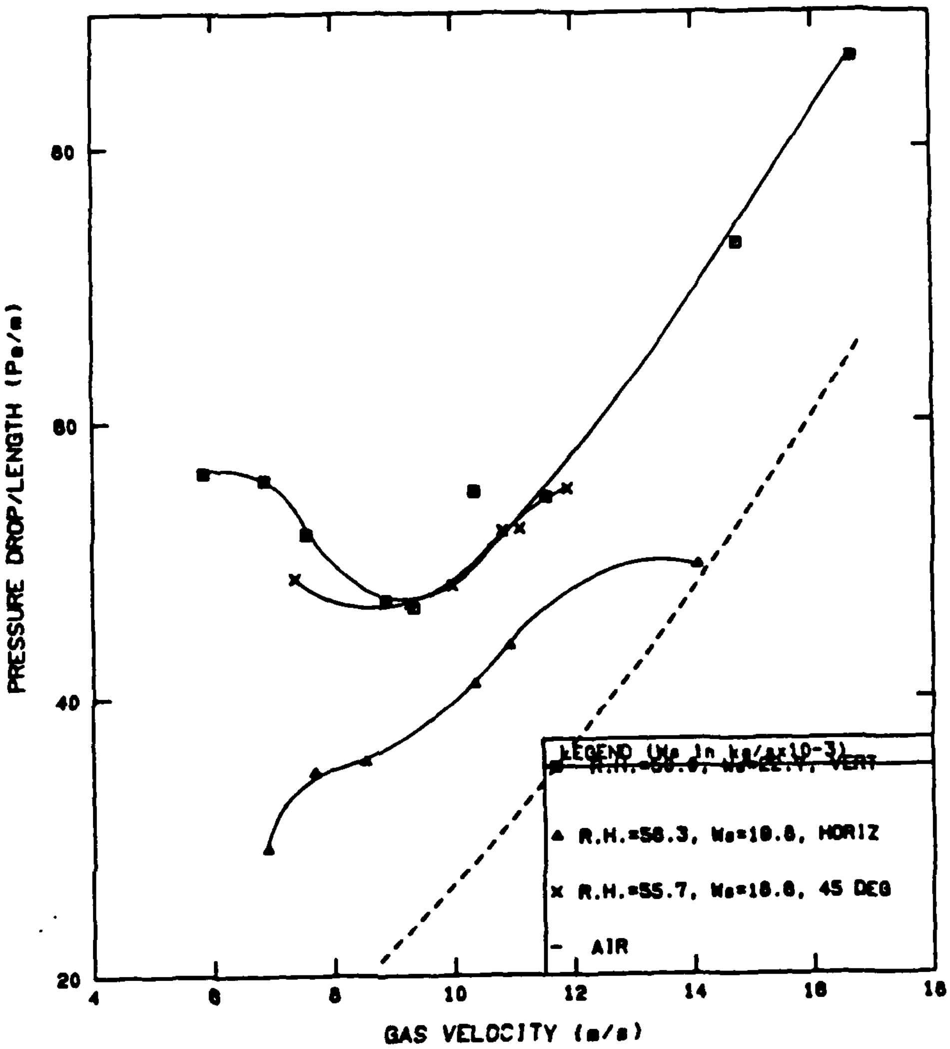

Figure A-23: Pressure Drop vs. Gas Velocity for 450μm Glass Beads for the Combined Orientations at the Lower Mass Flow Rate Without Electrostatics

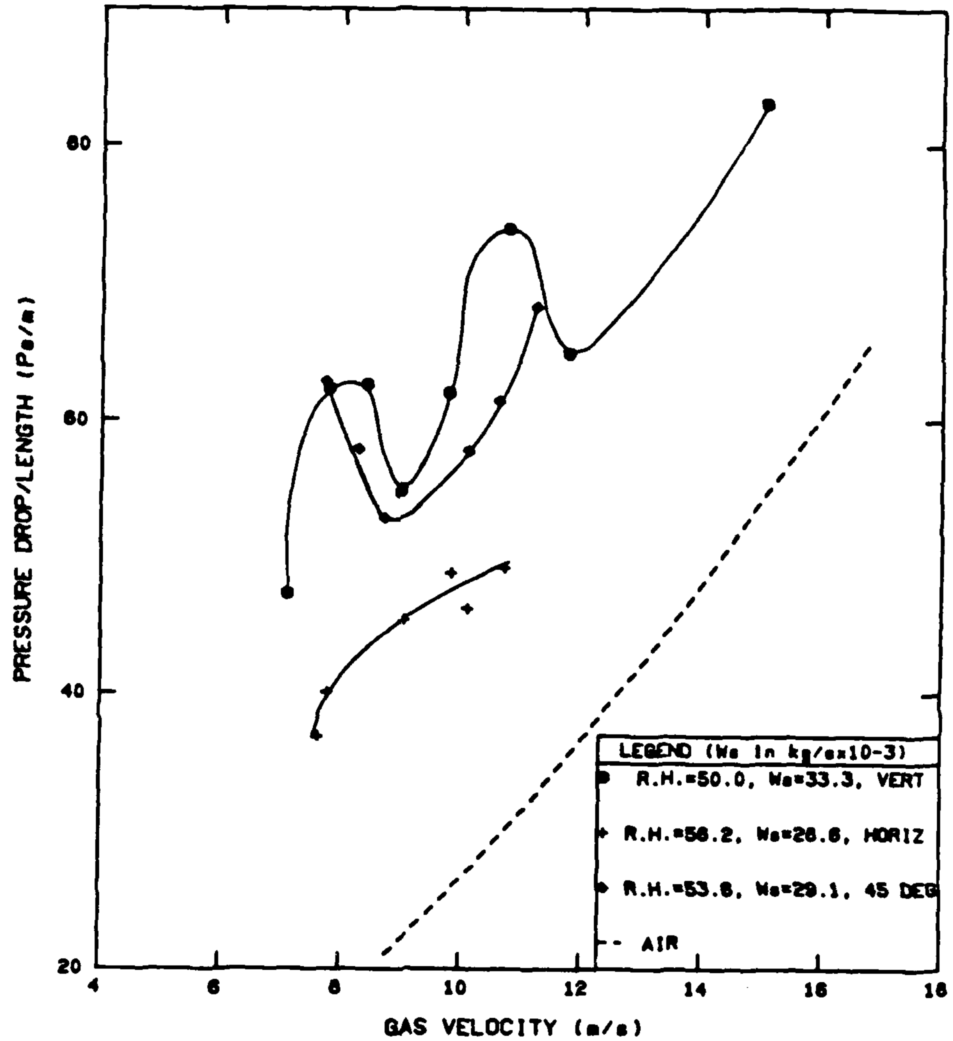

Figure A-25: Pressure Drop vs. Gas Velocity for 450μm Glass Beads for the Combined Orientations at the Higher Mass Flow Rate Without Electrostatics

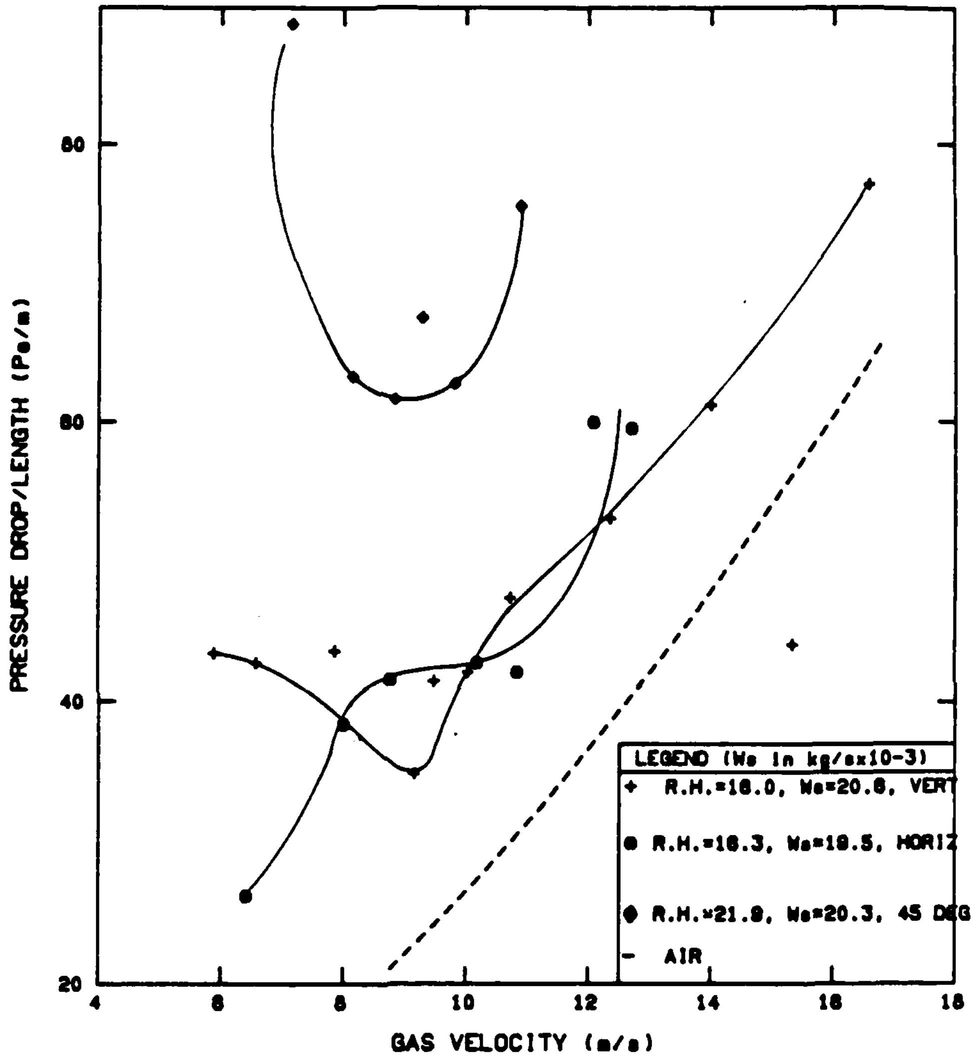

Figure A-24: Pressure Drop vs. Gas Velocity for 450μm Glass Beads for the Combined Orientations at the Lower Mass Flow Rate With Electrostatics

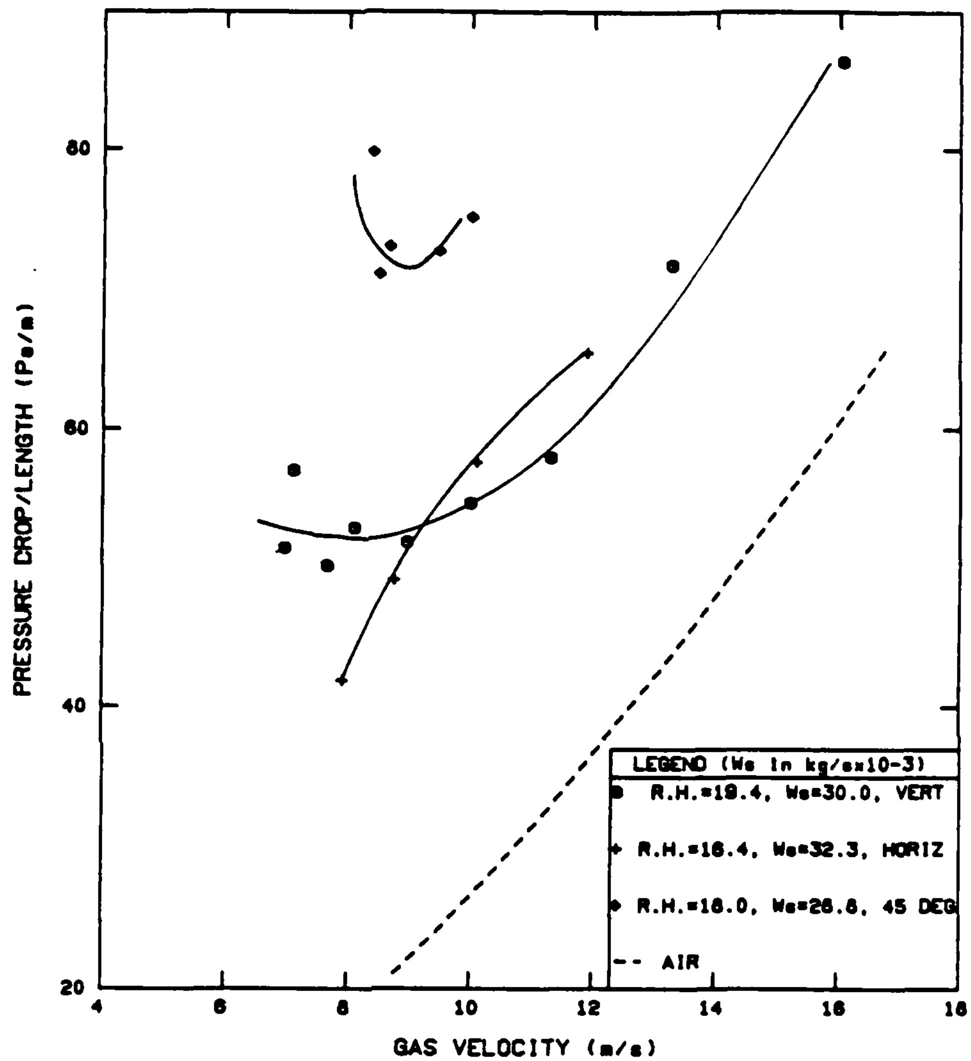

Figure A-26: Pressure Drop vs. Gas Velocity for 450μm Glass Beads for the Combined Orientations at the Higher Mass Flow Rate With Electrostatics

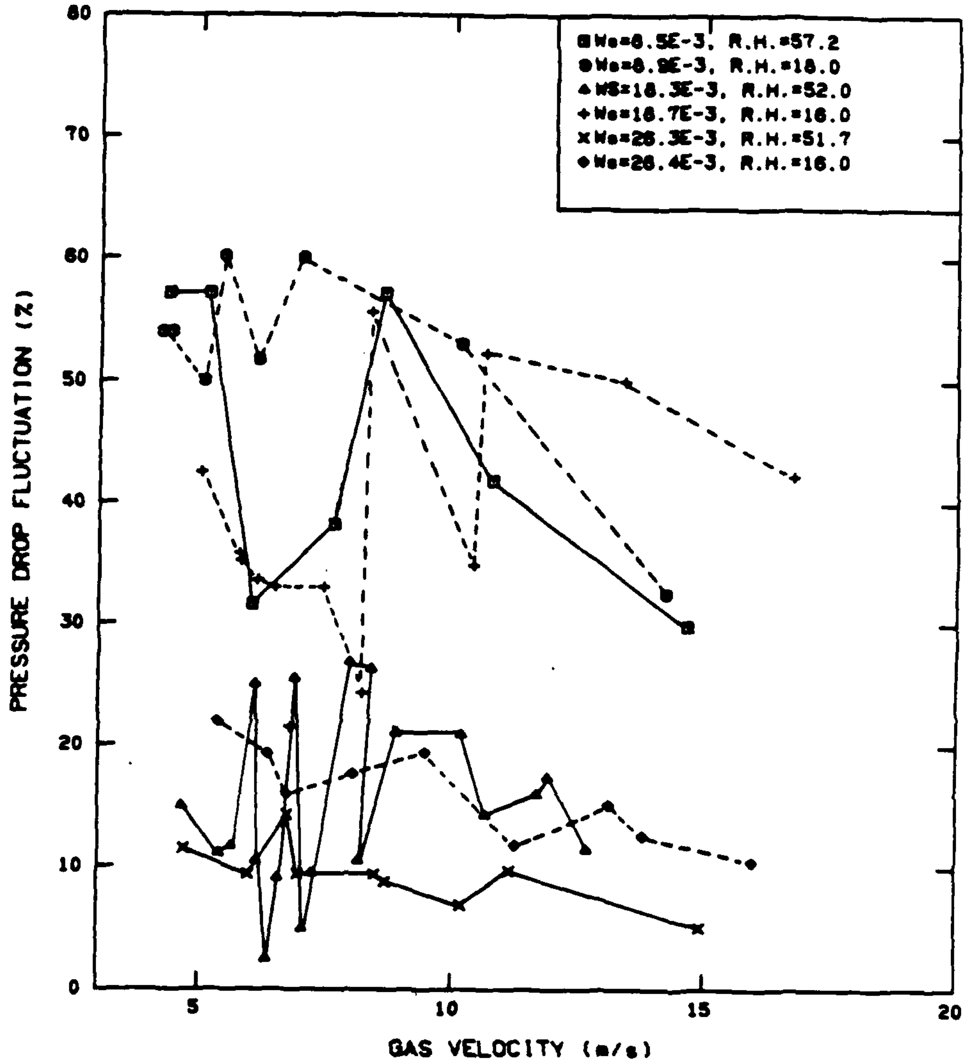

Figure A-27: Pressure Drop Fluctuation vs. Gas Velocity for 125μm Glass Beads in the Vertical Orientation

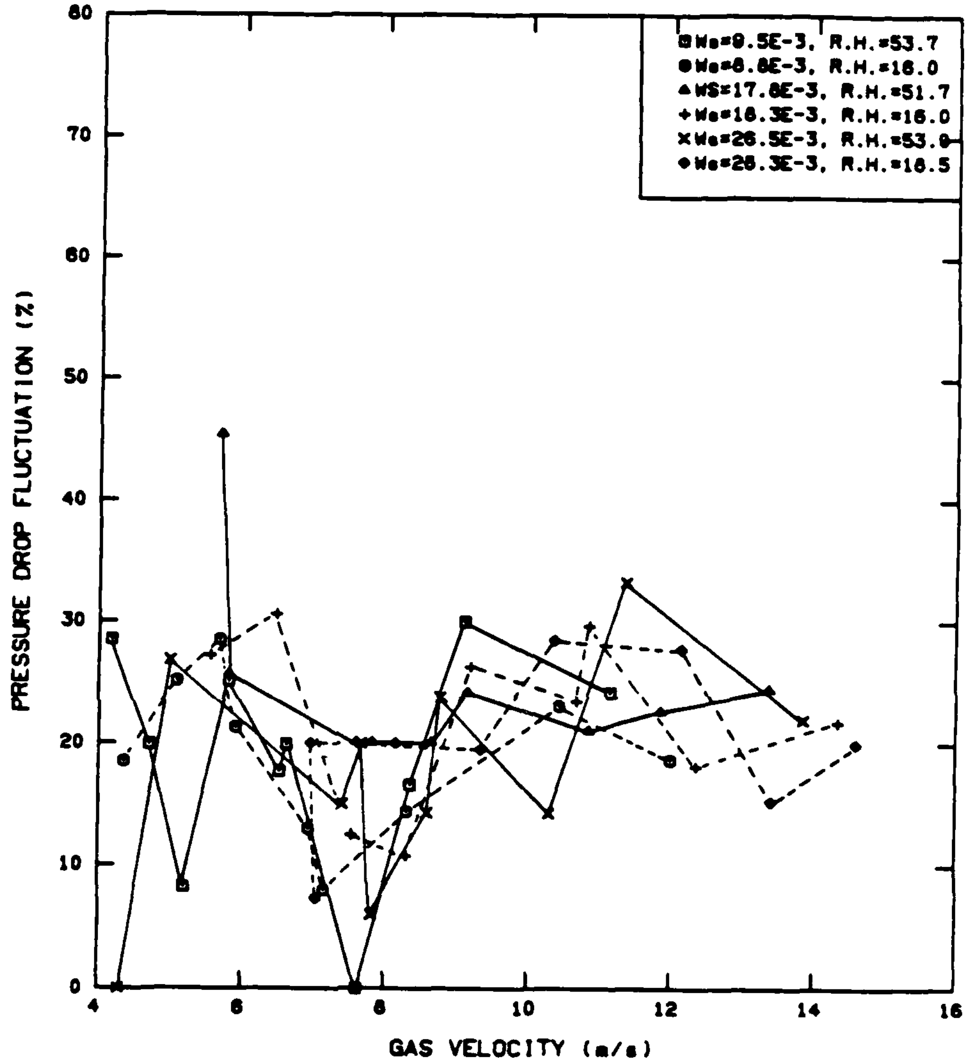

Figure A-28: Pressure Drop Fluctuation vs. Gas Velocity for 79μm Glass Beads in the Vertical Orientation

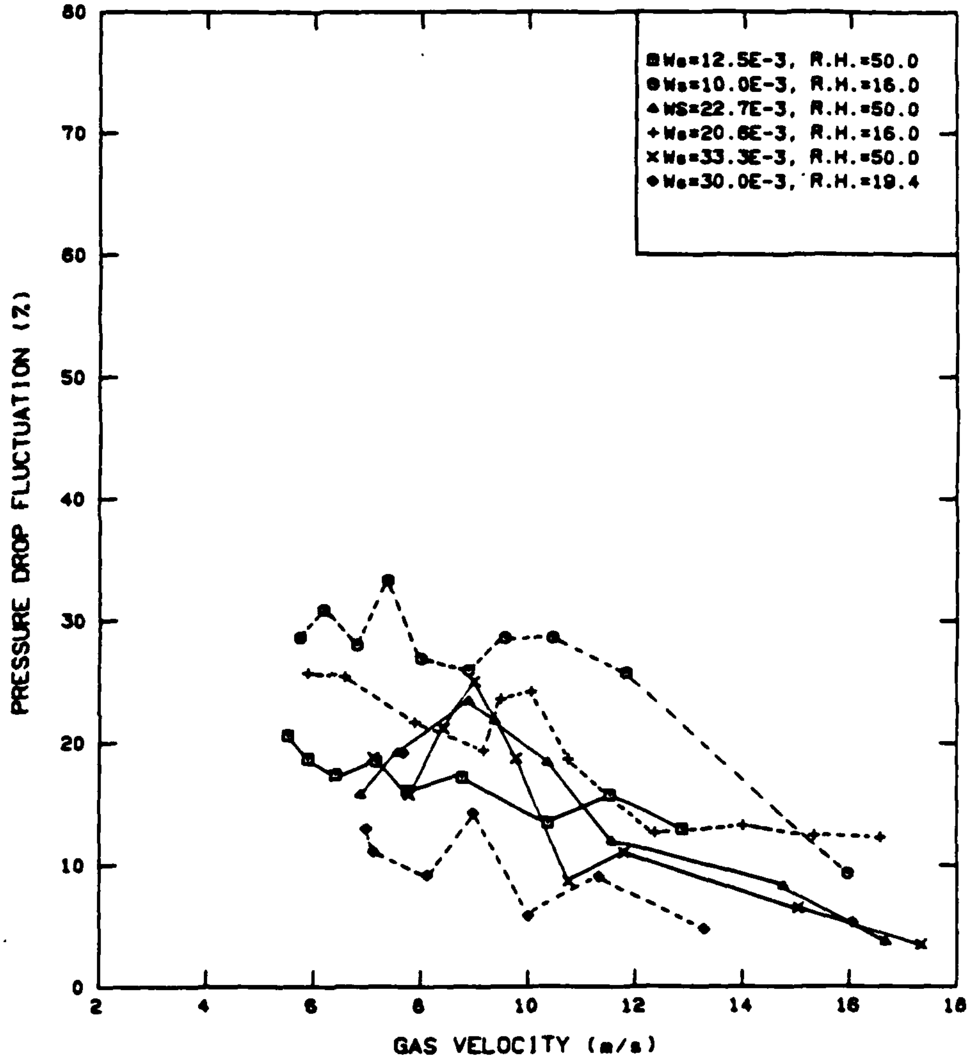

Figure A-29: Pressure Drop Fluctuation vs. Gas Velocity for 450μm Glass Beads in the Vertical Orientation

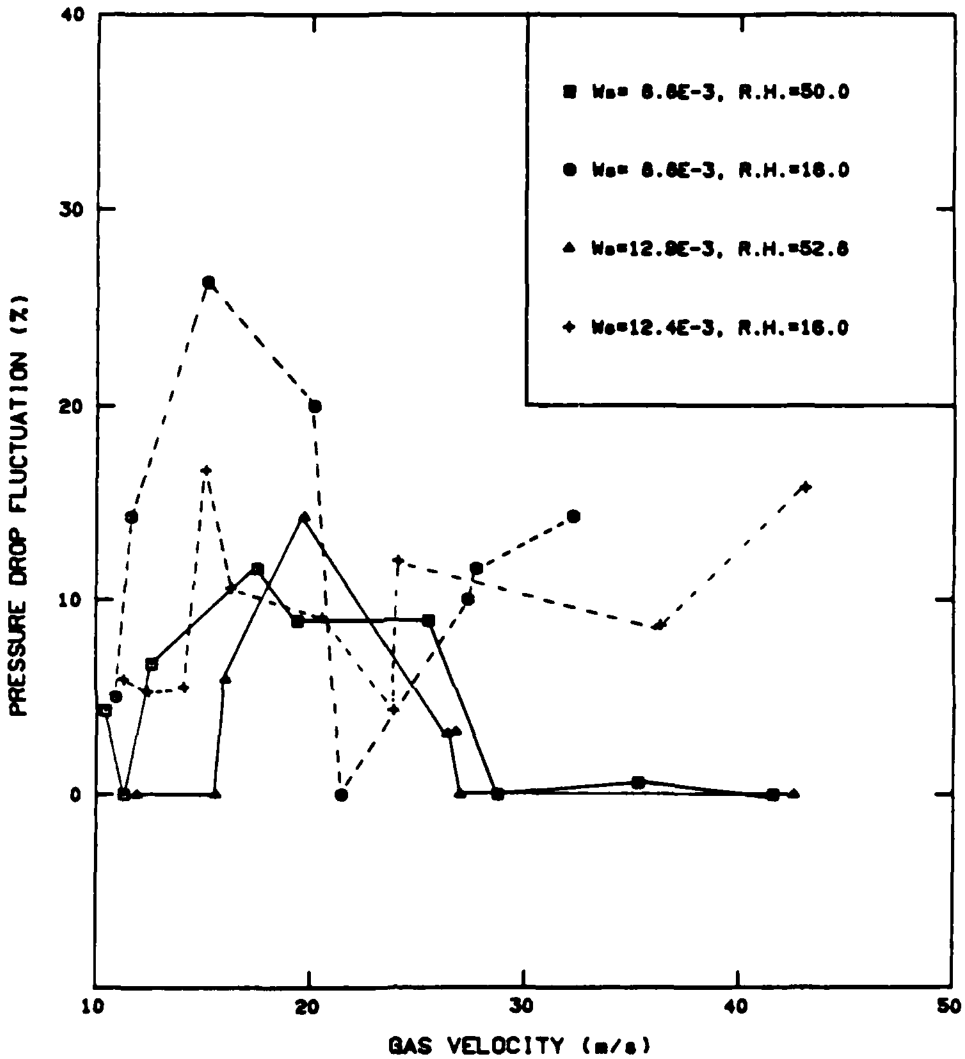

Figure A-30: Pressure Drop Fluctuation vs. Gas Velocity for 128μm Plexiglas Beads in the Vertical Orientation

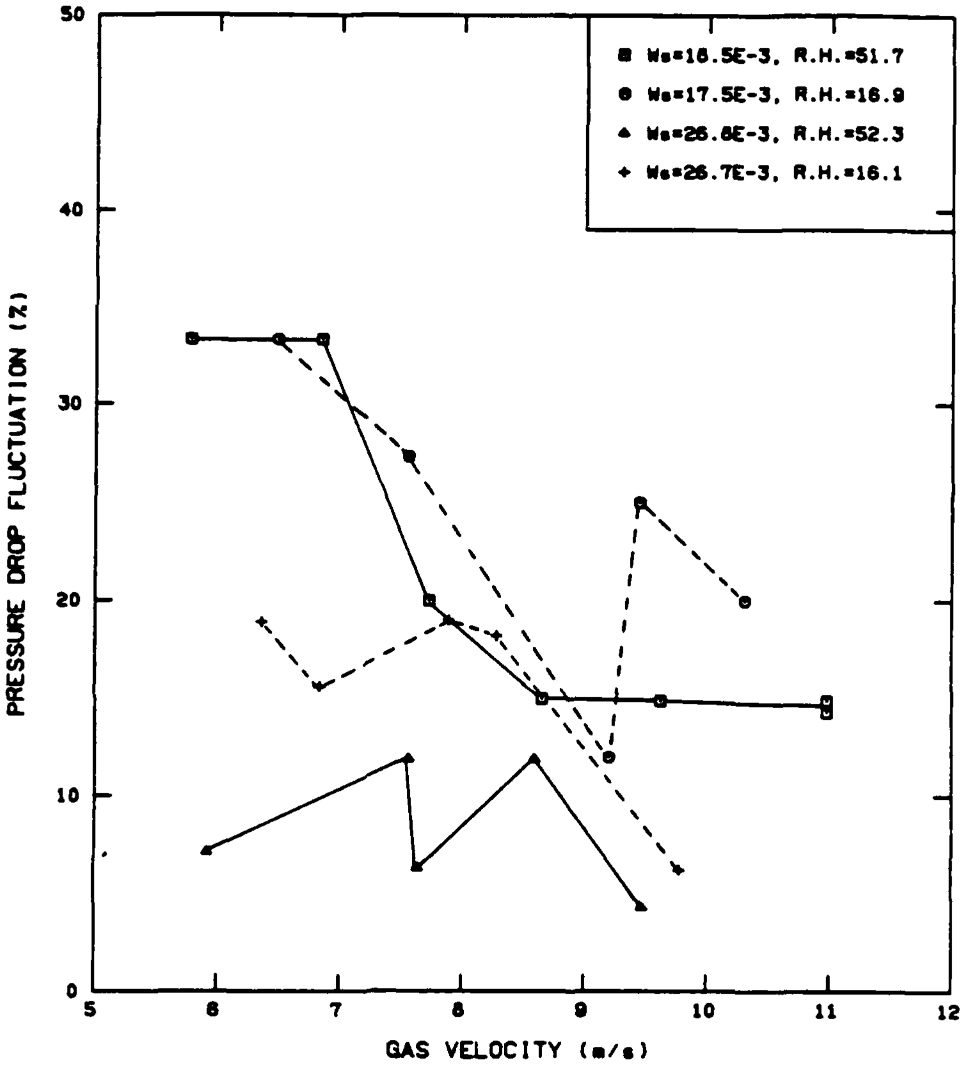

Figure A-31: Pressure Drop Fluctuation vs. Gas Velocity for 125µm Glass Beads in the Horizontal Orientation

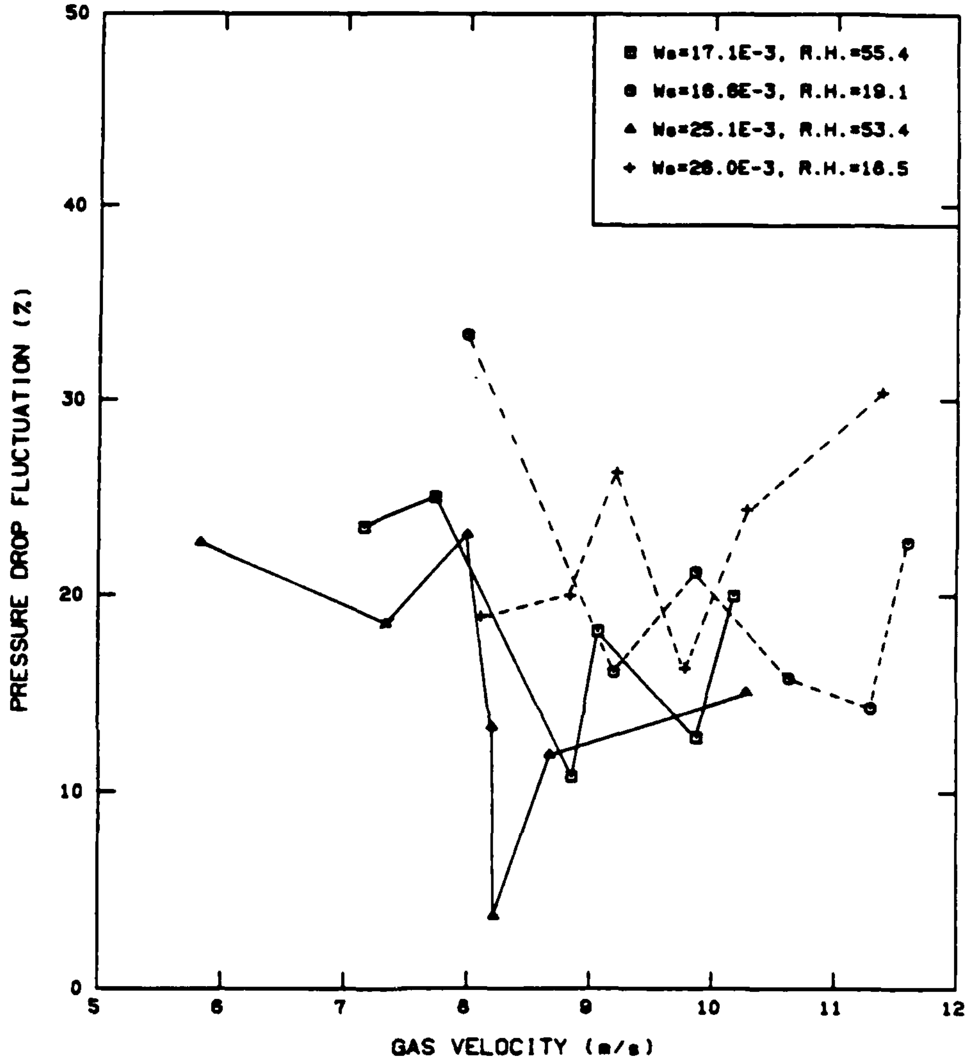

Figure A-32: Pressure Drop Fluctuation vs. Gas Velocity for 79μm Glass Beads in the Horizontal Orientation

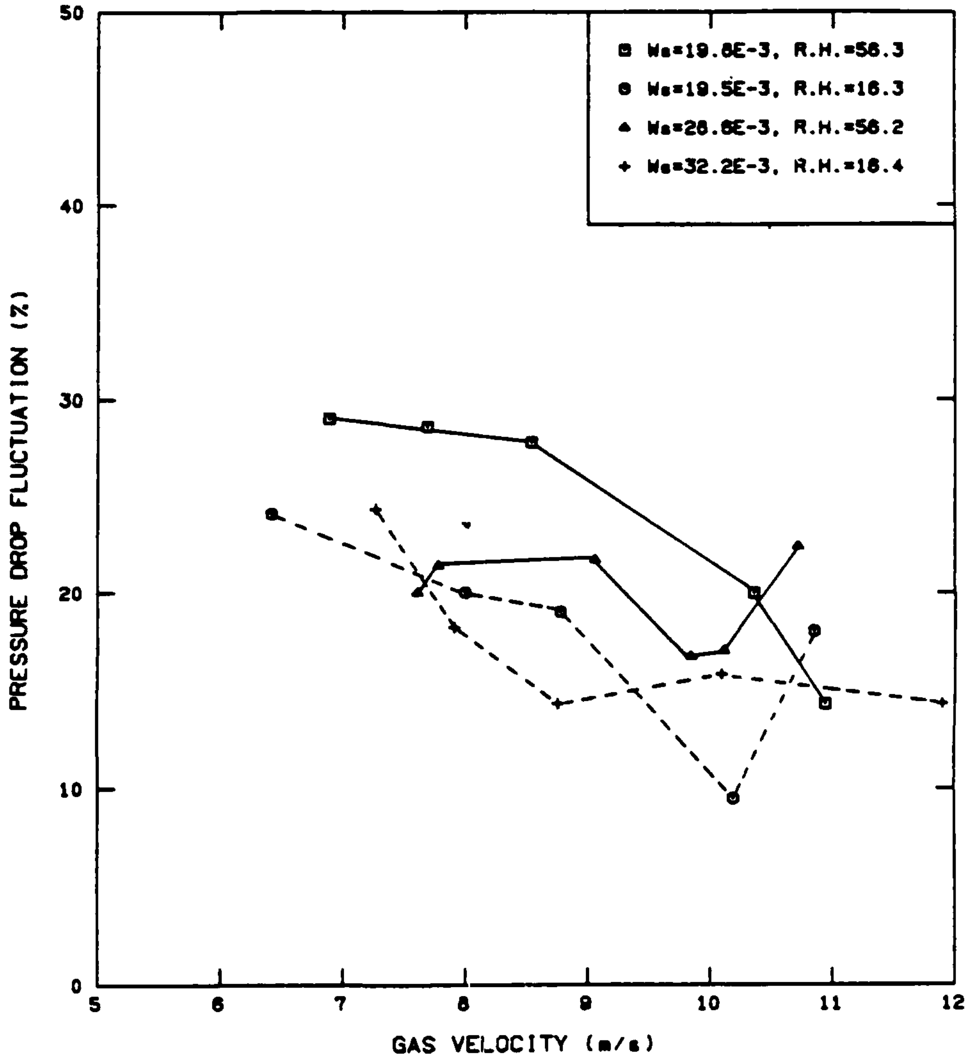

Figure A-33: Pressure Drop Fluctuation vs. Gas Velocity for 450μm Glass Beads in the Horizontal Orientation

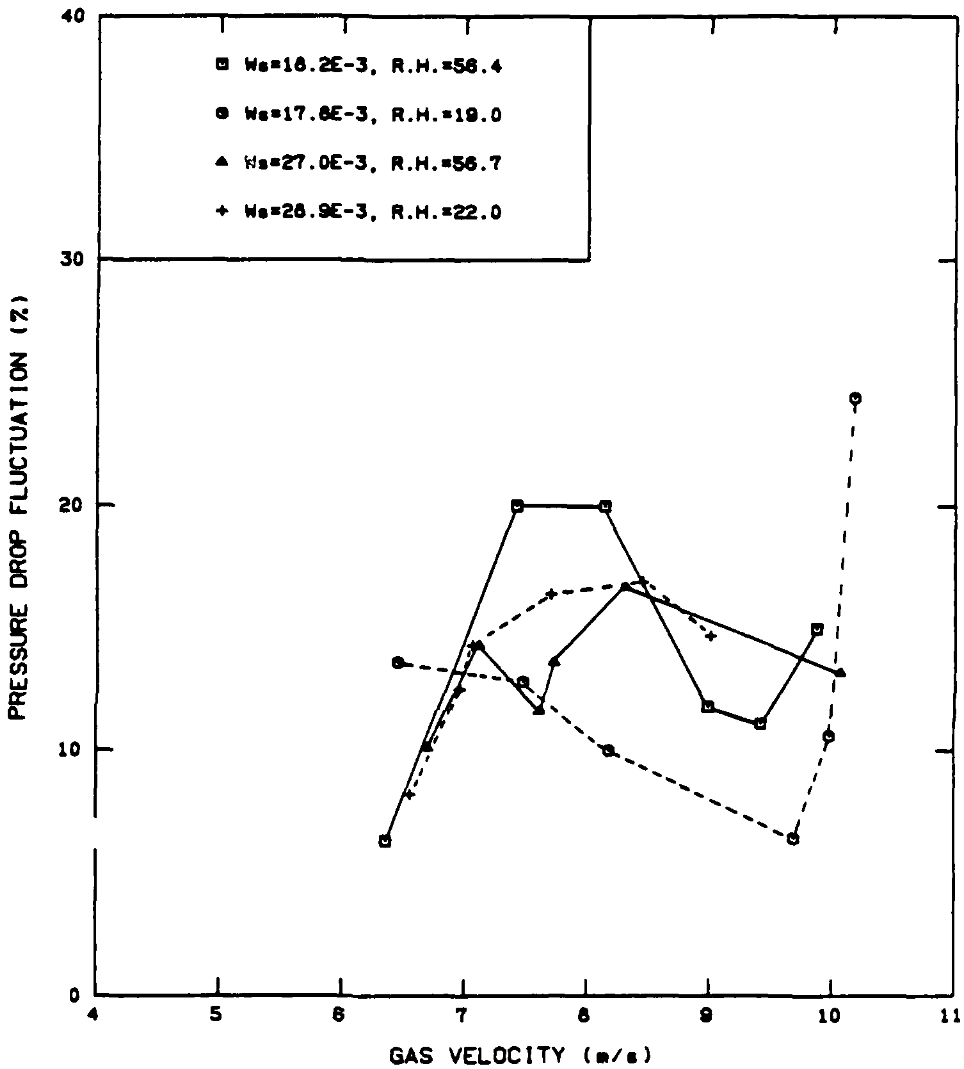

Figure A-34: Pressure Drop Fluctuation vs. Gas Velocity for 125μm Glass Beads in the Inclined Orientation

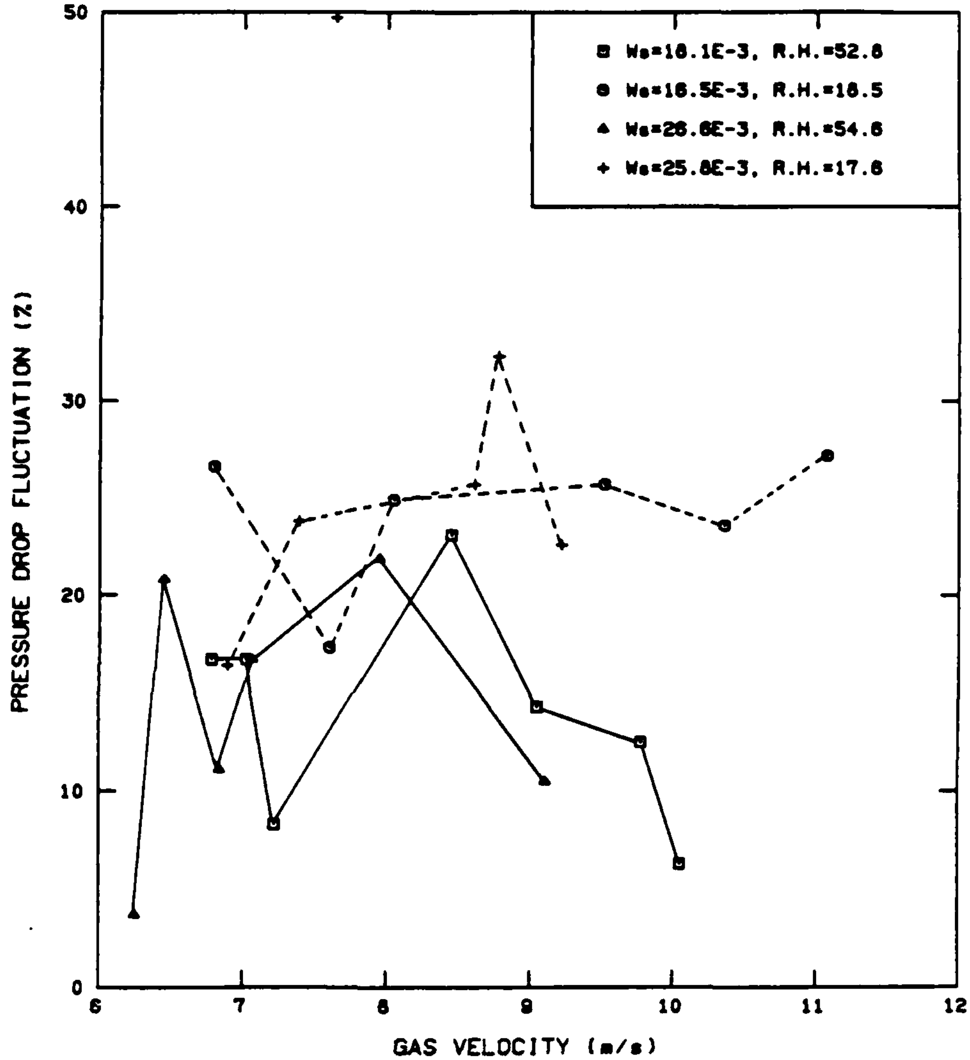

Figure A-35: Pressure Drop Fluctuation vs. Gas Velocity for 79μm Glass Beads in the Inclined Orientation

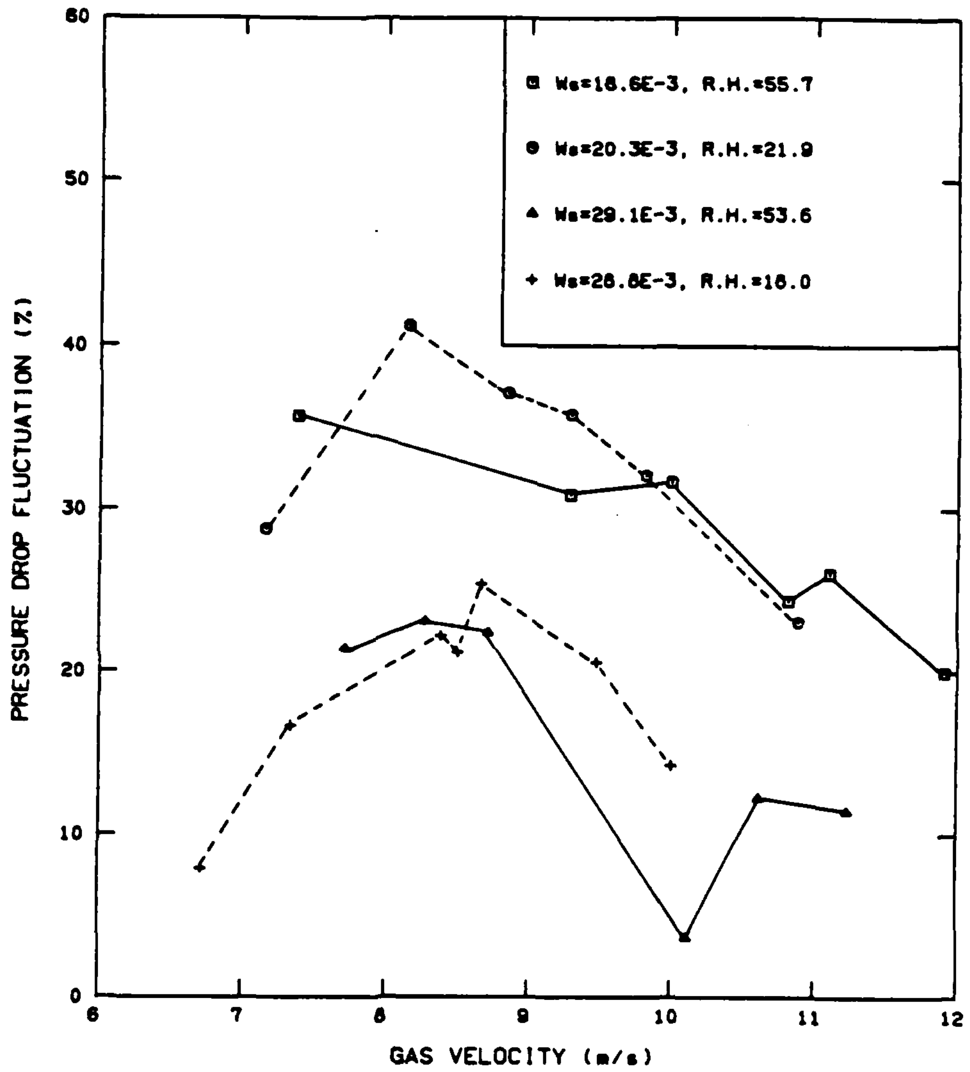

Figure A-36: Pressure Drop Fluctuation vs. Gas Velocity for 450μm Glass Beads in the Inclined Orientation

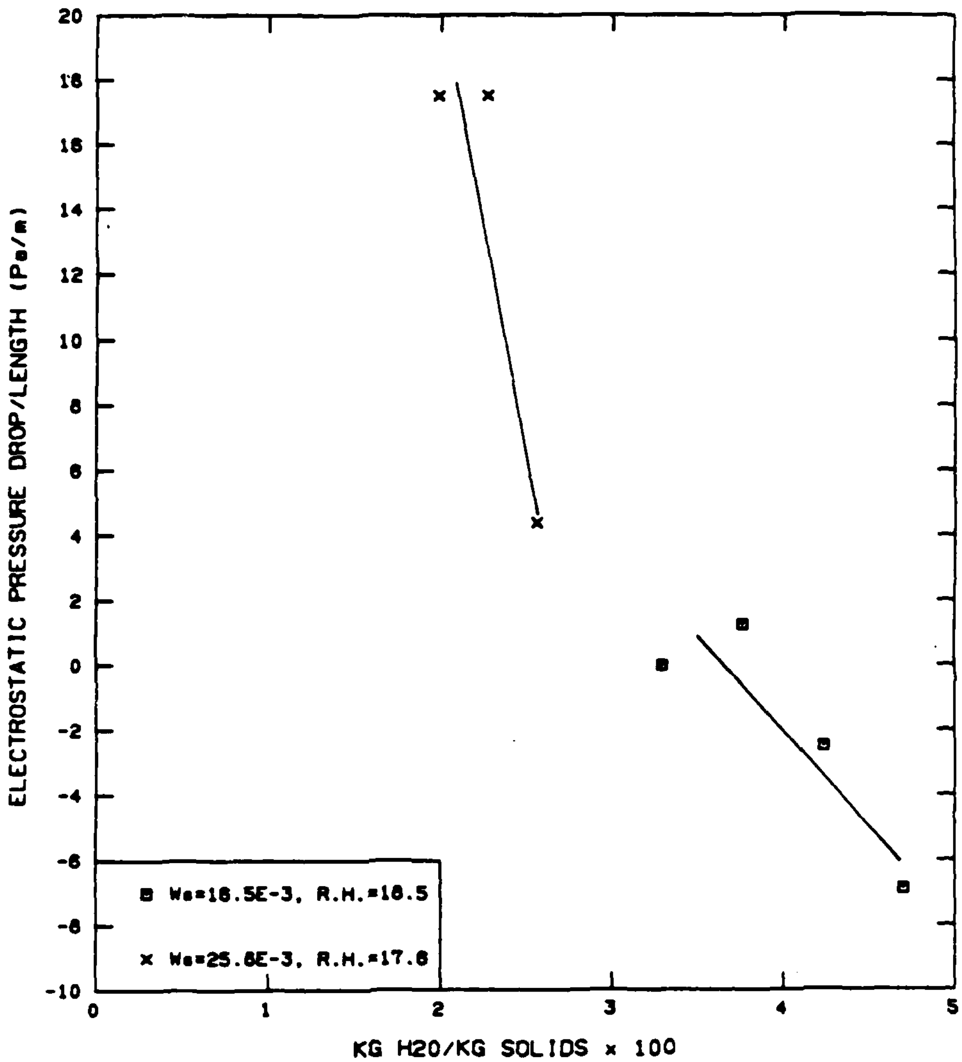

Figure A-37: Electrostatic Pressure Drop vs. kg H_2O/kg solids for the 79μm Glass Beads in the Inclined Orientation

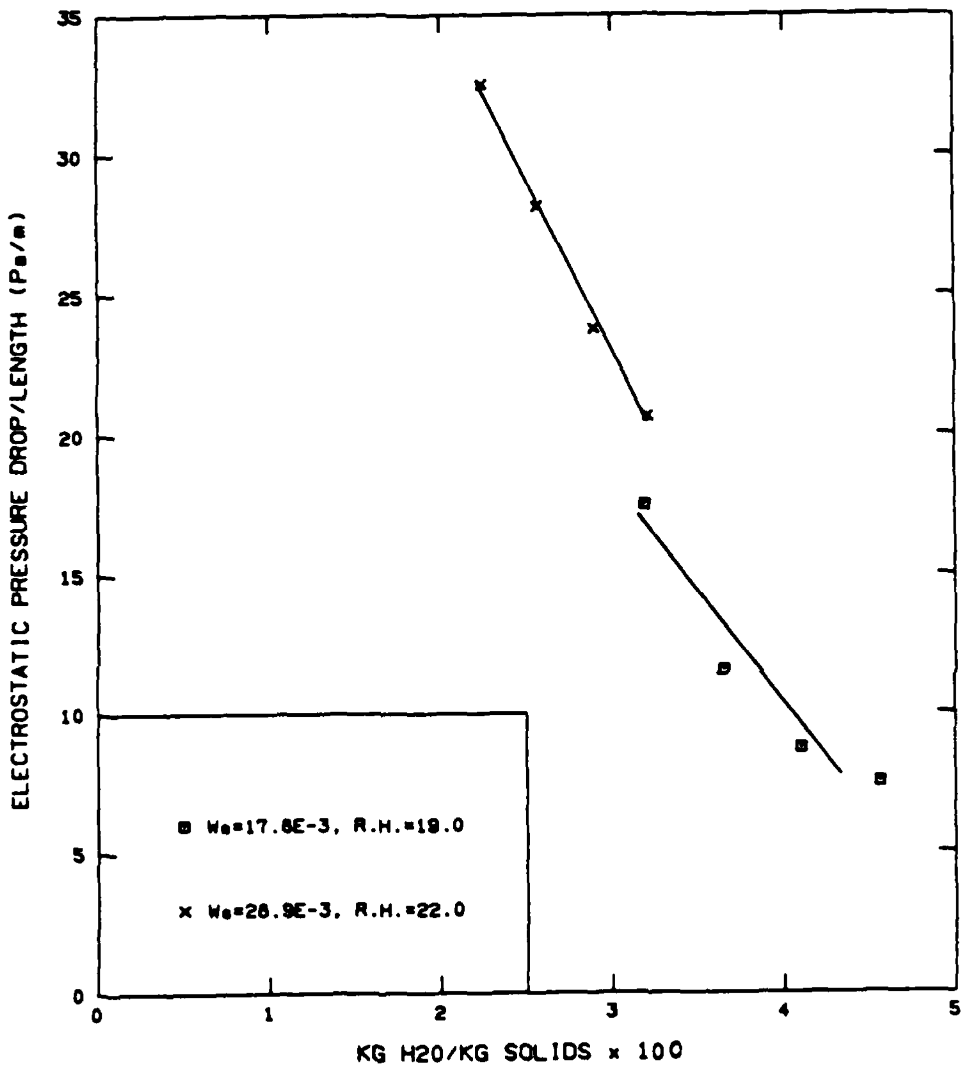

Figure A-38: Electrostatic Pressure Drop vs. kg H_2O/kg solids for the 125μm Glass Beads in the Inclined Orientation

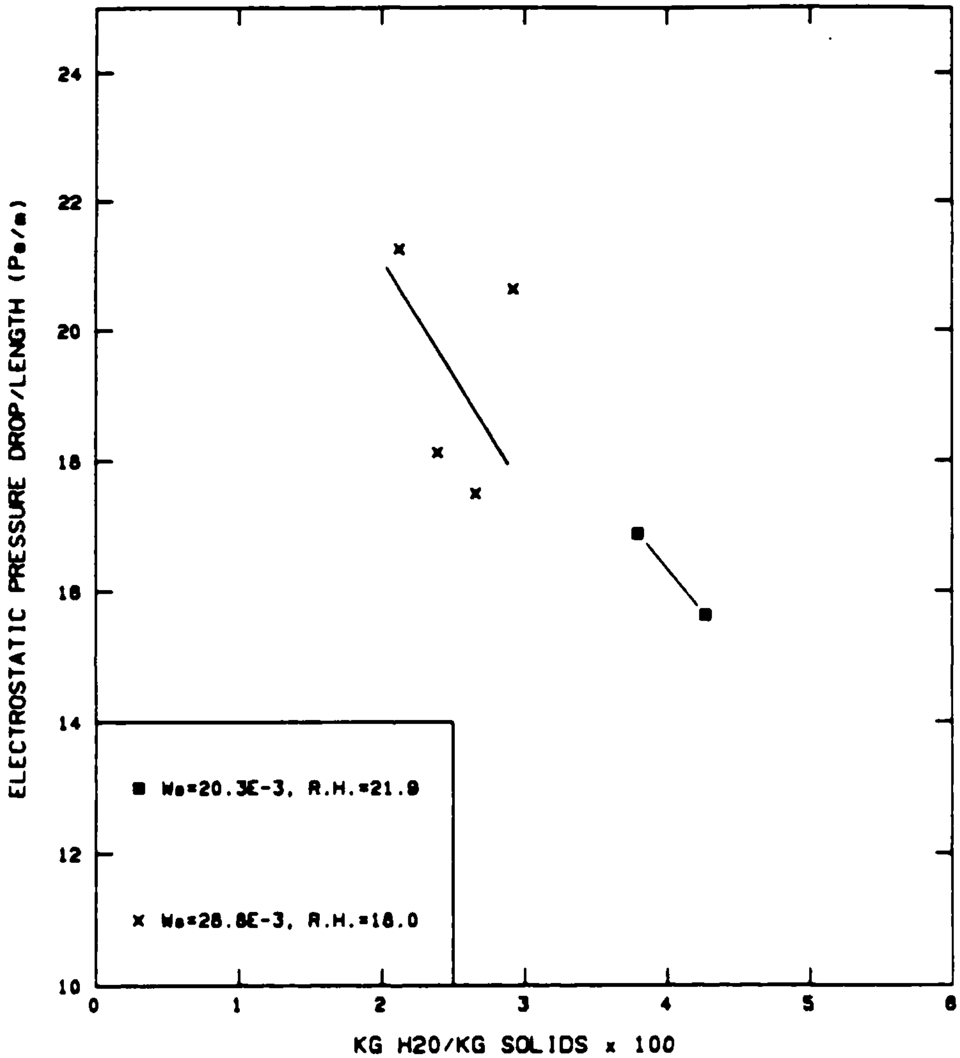

Figure A-39: Electrostatic Pressure Drop vs. kg H_2O/kg solids for the 450μm Glass Beads in the Inclined Orientation

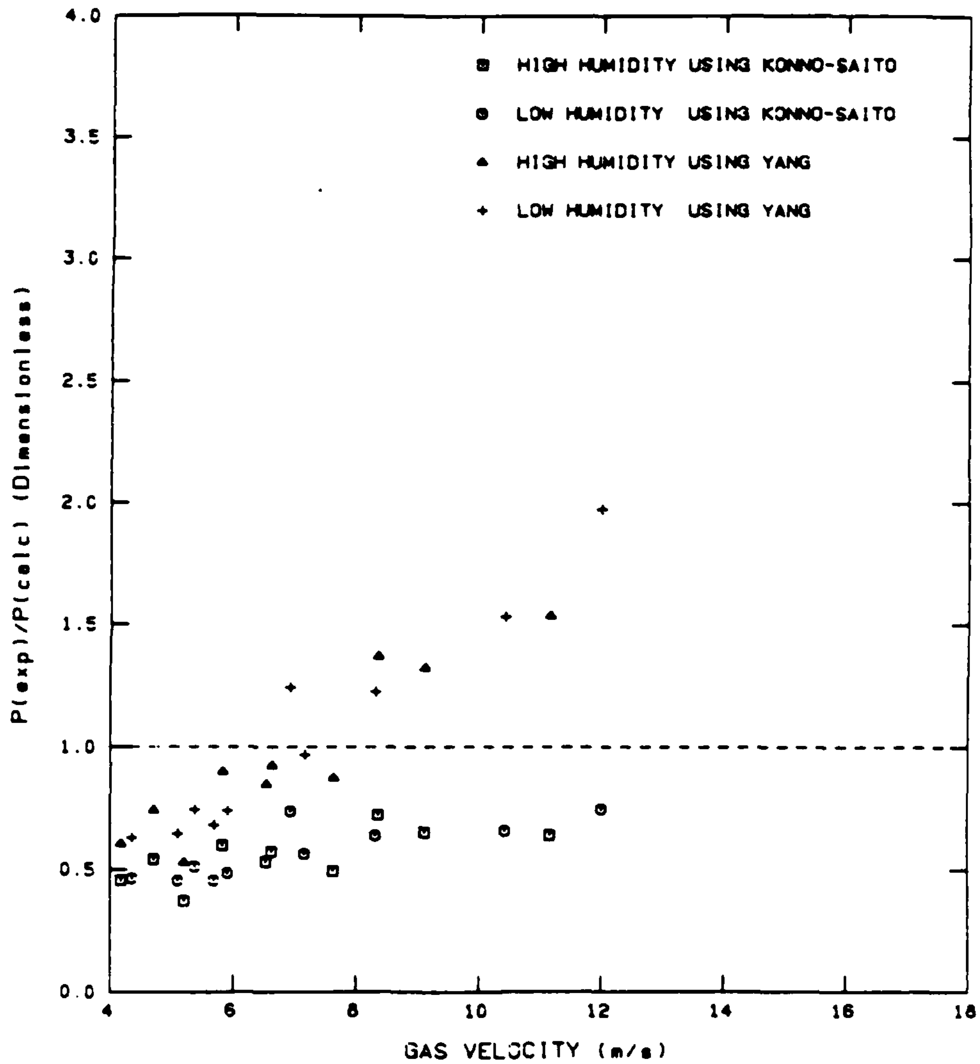

Figure A-40: Ratio of Experimental to Calculated Pressure Drop vs. Gas Velocity for 79μm Glass Beads in the Vertical Orientation with $W_s = 9. \times 10^{-3}$

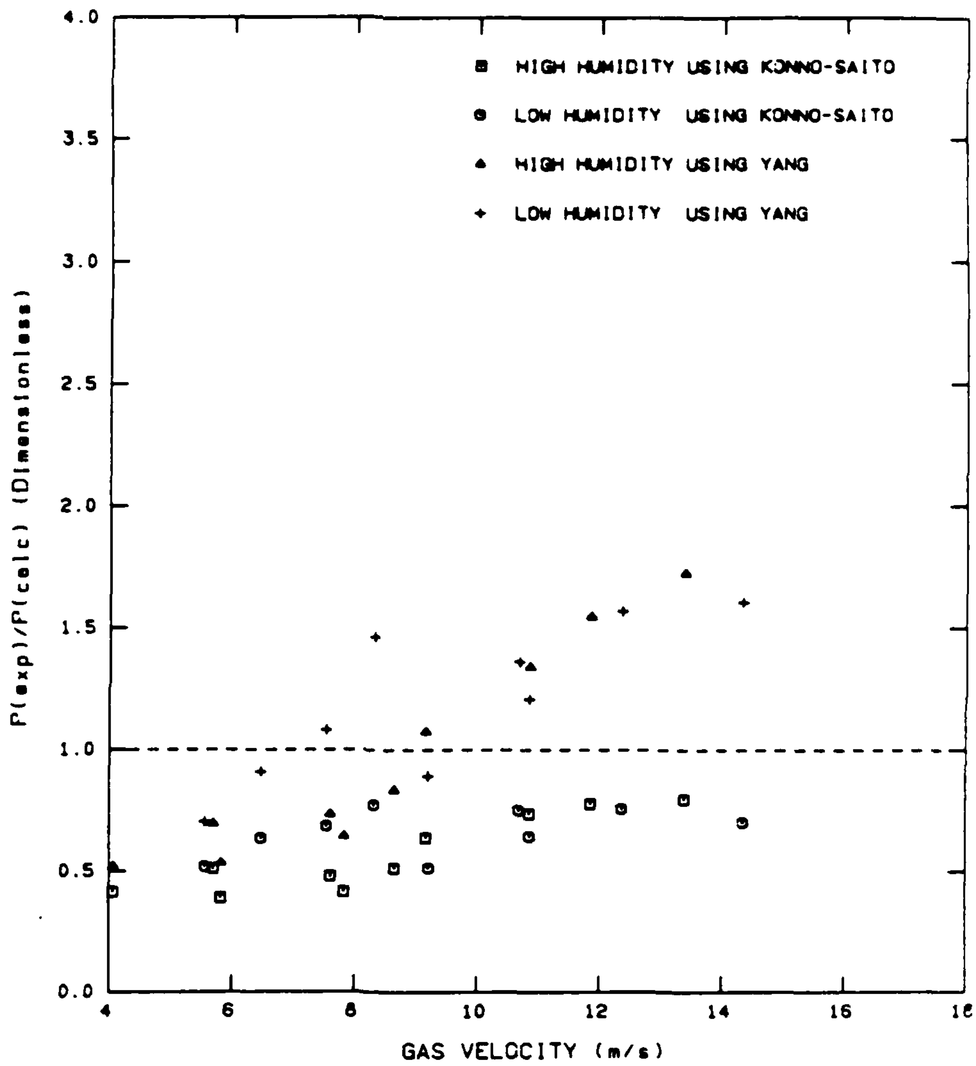

Figure A-41: Ratio of Experimental to Calculated Pressure Drop vs. Gas Velocity for 79µm Glass Beads in the Vertical Orientation with W_s =18. x10^{-3}

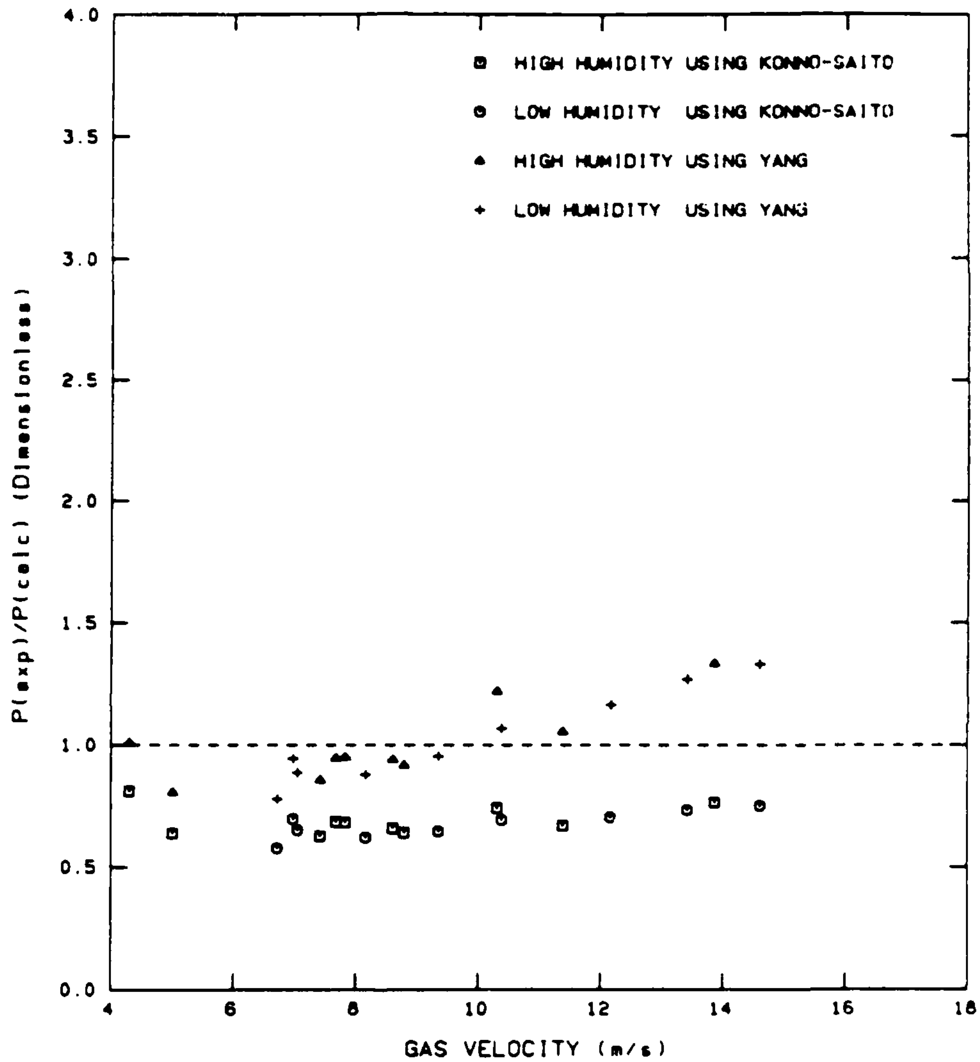

Figure A-42: Ratio of Experimental to Calculated Pressure Drop vs. Gas Velocity for 79μm Glass Beads in the Vertical Orientation with $W_s = 27. \times 10^{-3}$

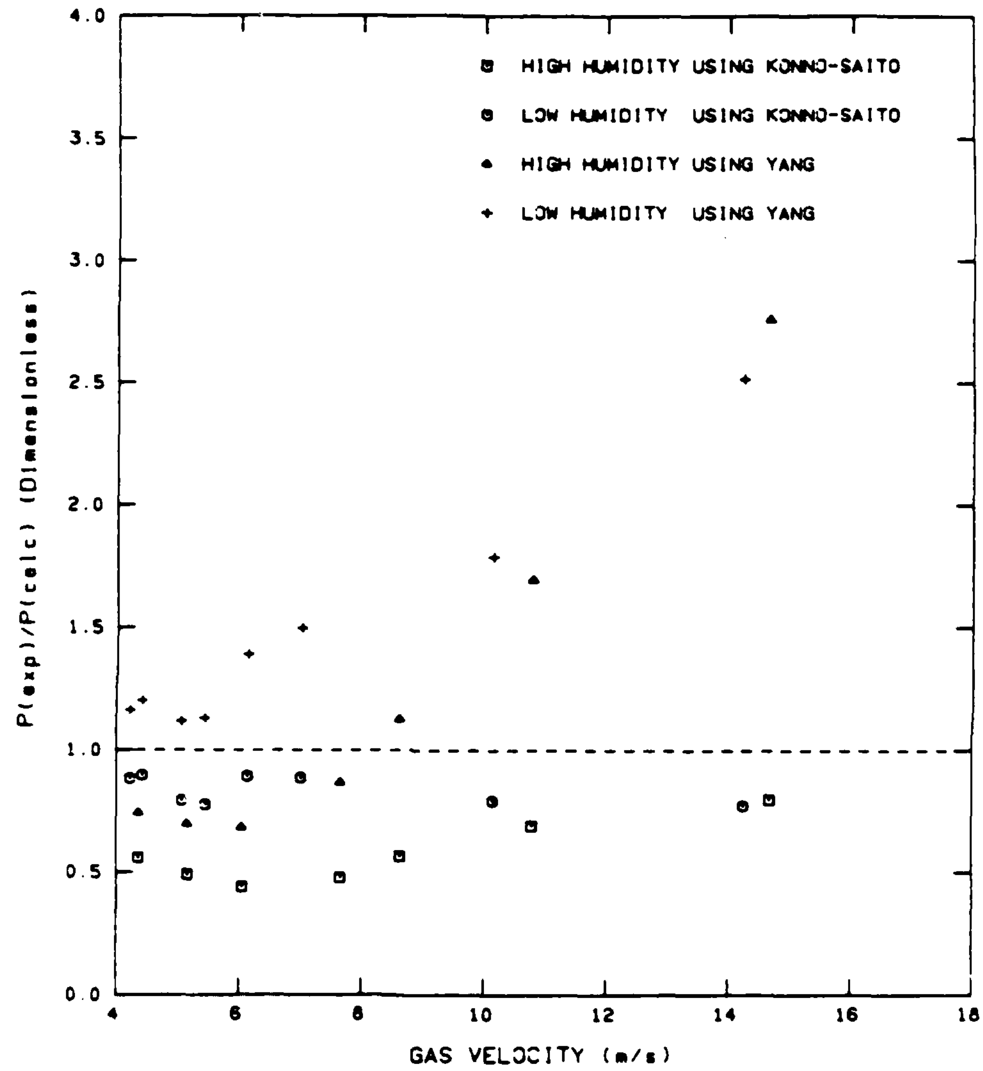

Figure A-43: Ratio of Experimental to Calculated Pressure Drop vs. Gas Velocity for 125μm Glass Beads in the Vertical Orientation with $W_s = 8. \times 10^{-3}$

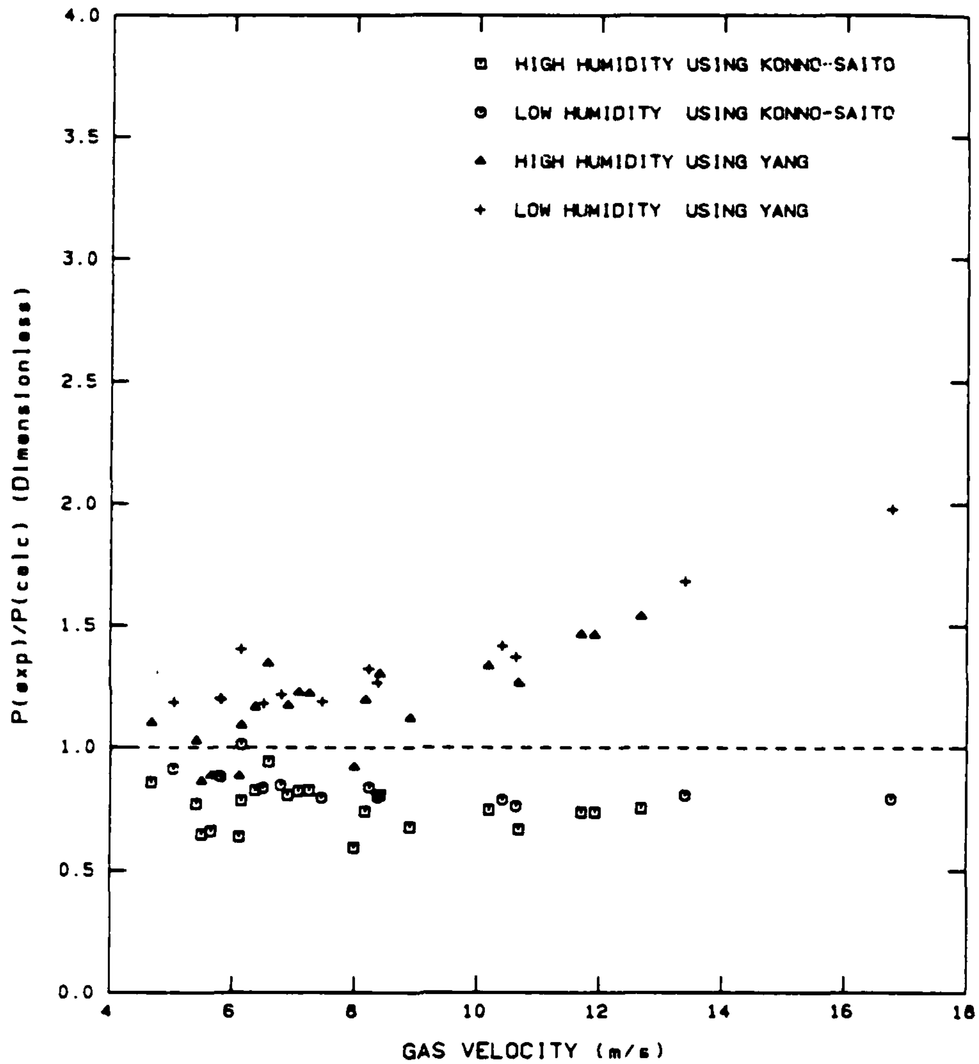

Figure A-44: Ratio of Experimental to Calculated Pressure Drop vs. Gas Velocity for 125μm Glass Beads in the Vertical Orientation with W_s=18. $x10^{-3}$

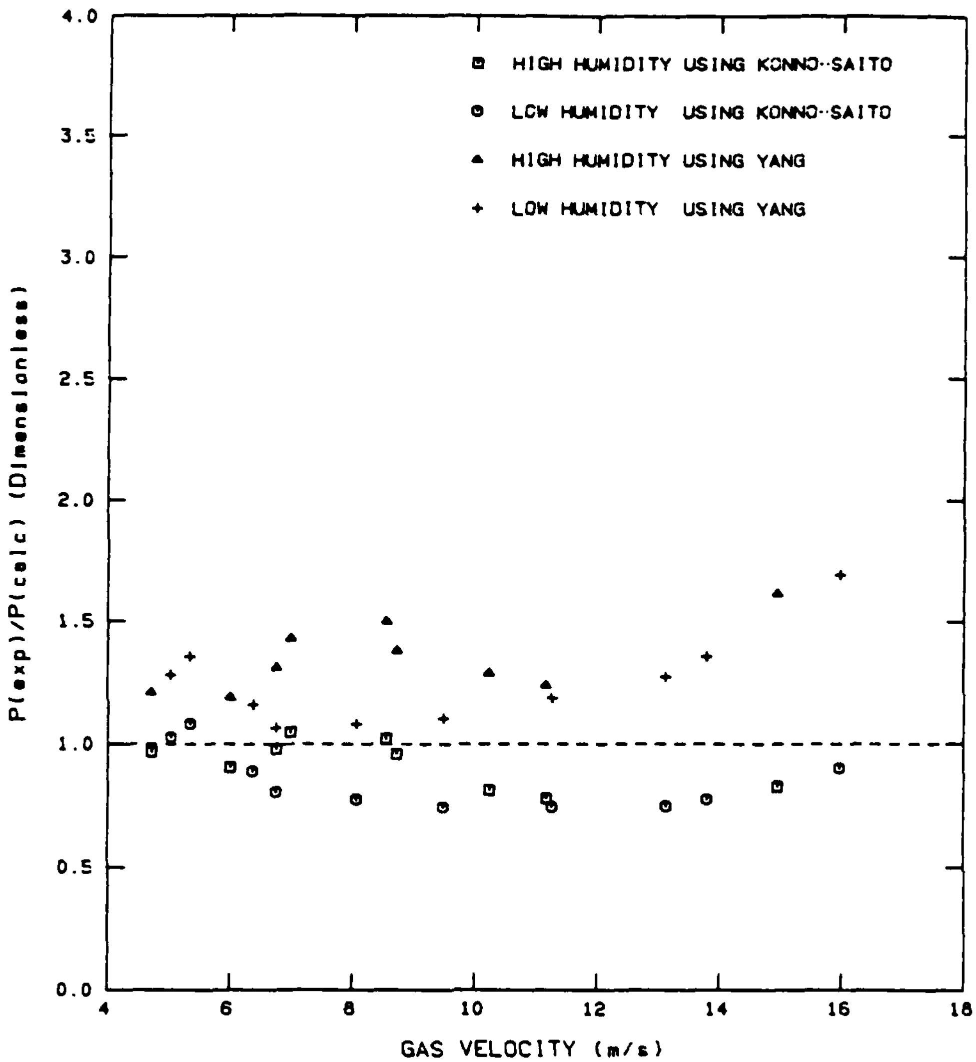

Figure A-45: **Ratio of Experimental to Calculated Pressure Drop vs. Gas Velocity for 125μm Glass Beads in the Vertical Orientation with W_s=27. x10^{-3}**

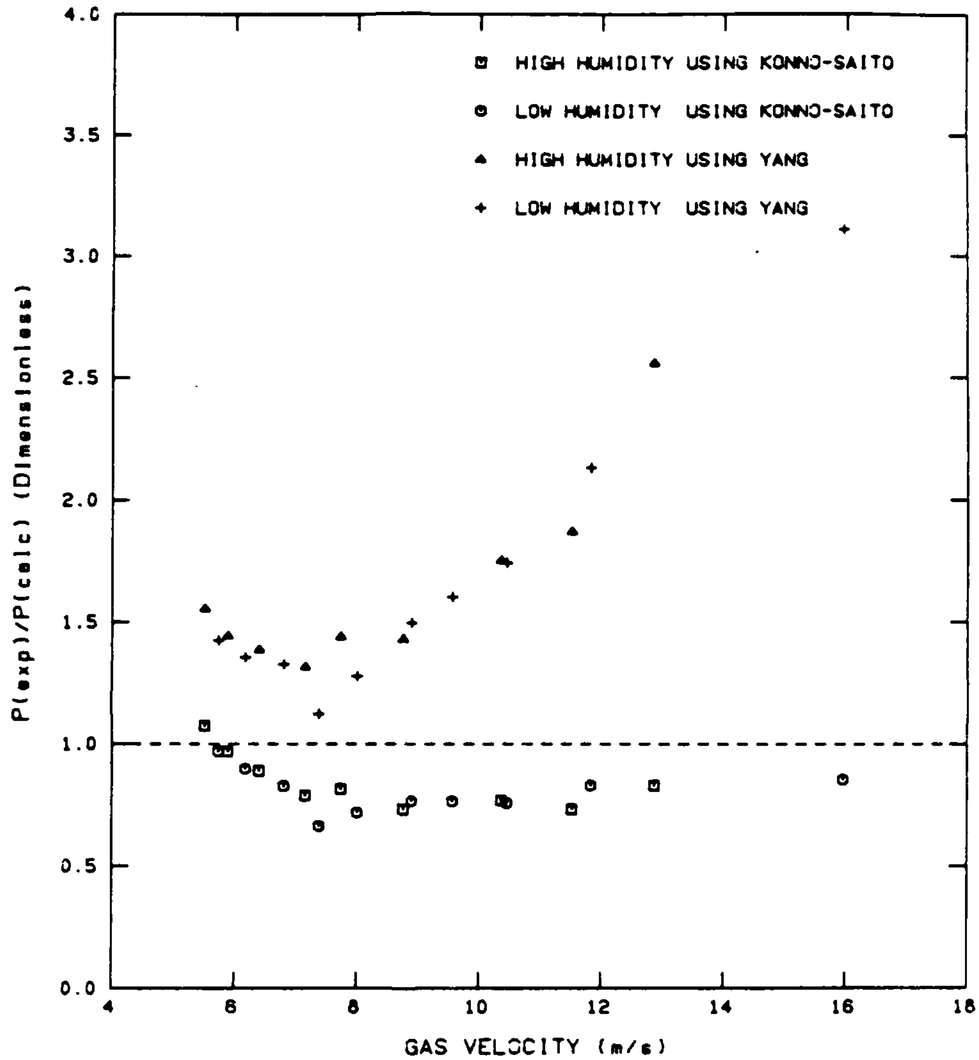

Figure A-46: Ratio of Experimental to Calculated Pressure Drop vs. Gas Velocity for 450µm Glass Beads in the Vertical Orientation with W_s=11. x10^{-3}

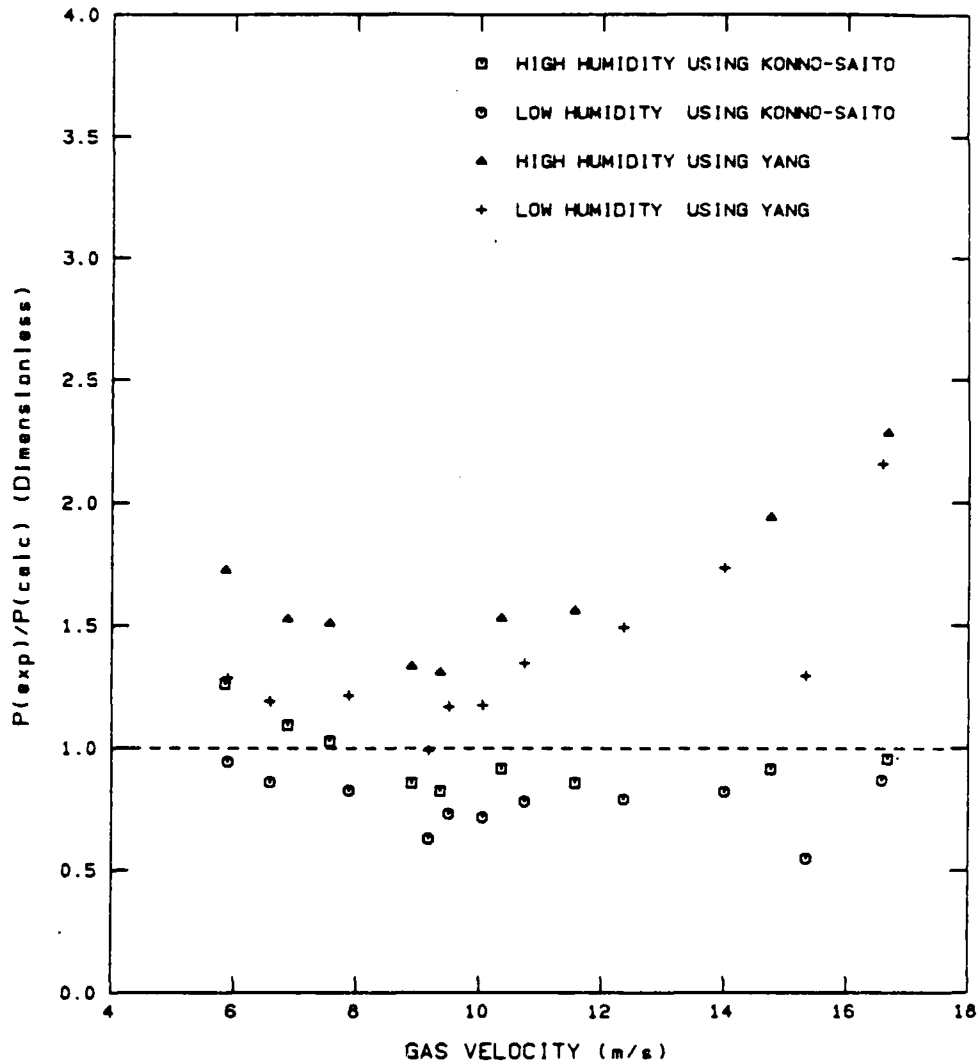

Figure A-47: Ratio of Experimental to Calculated Pressure Drop vs. Gas Velocity for 450μm Glass Beads in the Vertical Orientation with $W_s = 21. \times 10^{-3}$

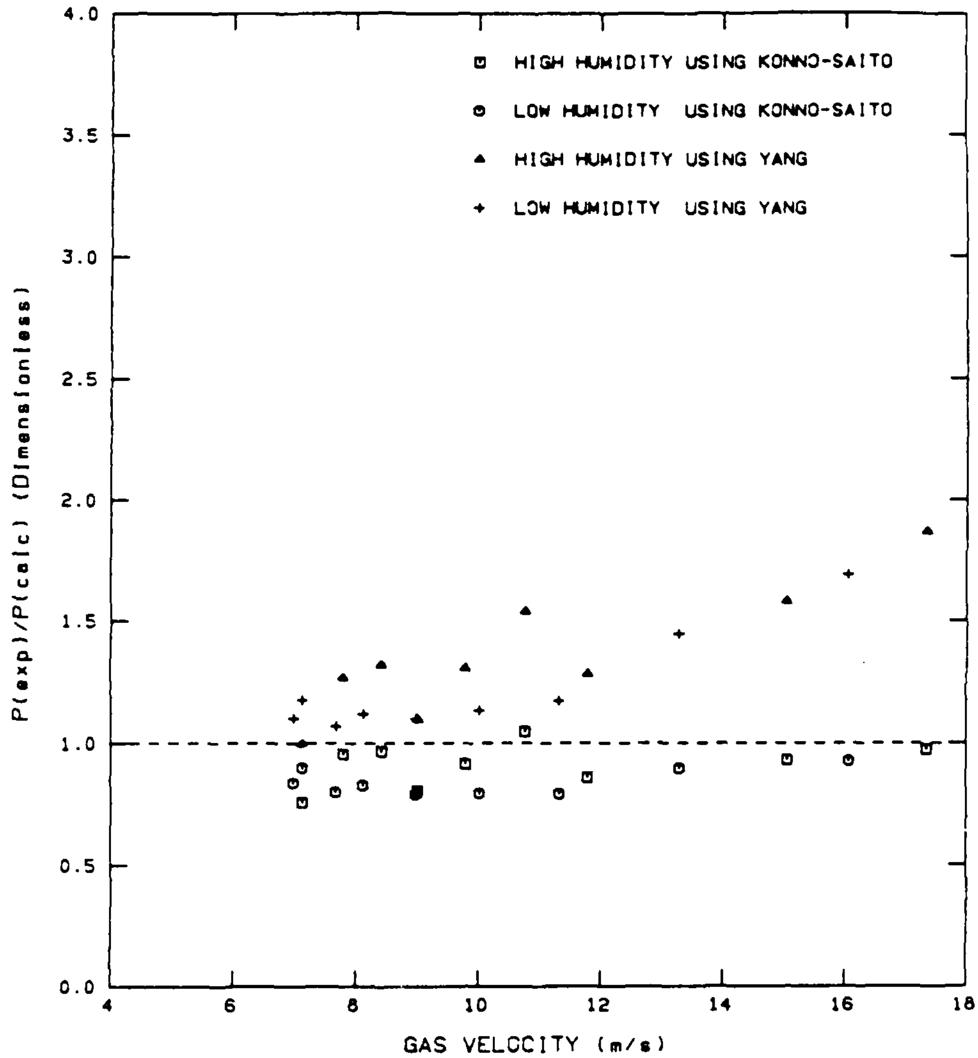

Figure A-48: Ratio of Experimental to Calculated Pressure Drop vs. Gas Velocity for 450μm Glass Beads in the Vertical Orientation with $W_s = 30. \times 10^{-3}$

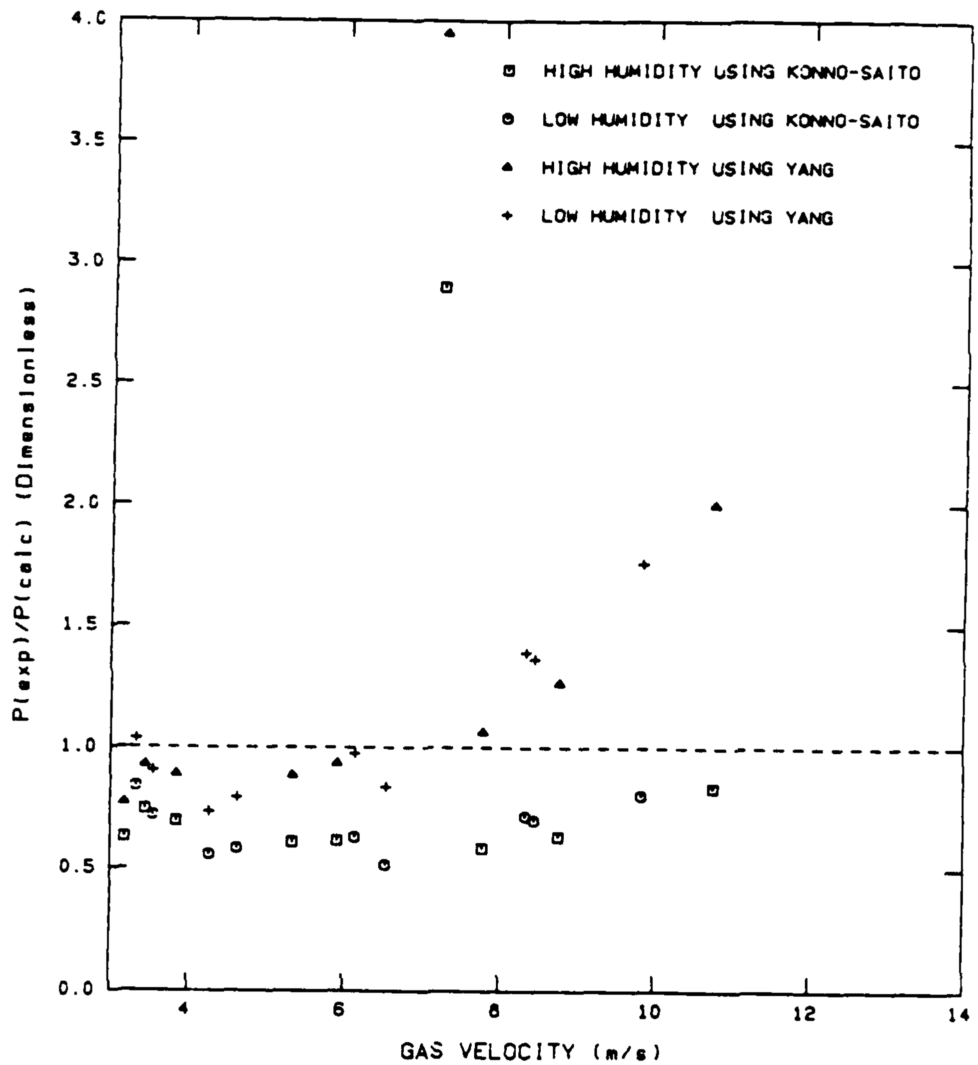

Figure A-49: Ratio of Experimental to Calculated Pressure Drop vs. Gas Velocity for 128μm Plexiglas Beads in the Vertical Orientation with $W_s = 8. \times 10^{-3}$

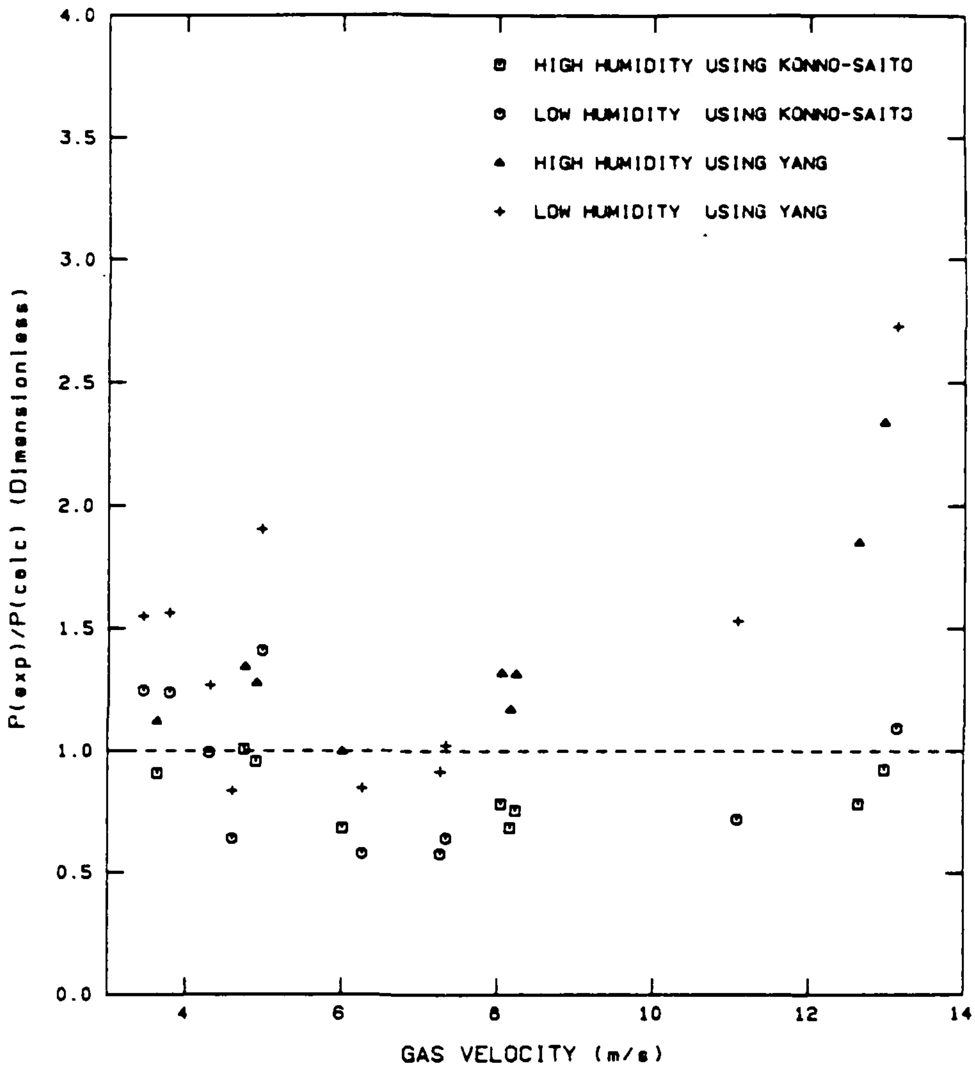

Figure A-50: Ratio of Experimental to Calculated Pressure Drop vs. Gas Velocity for 128µm Plexiglas Beads in the Vertical Orientation with $W_s = 12. \times 10^{-3}$

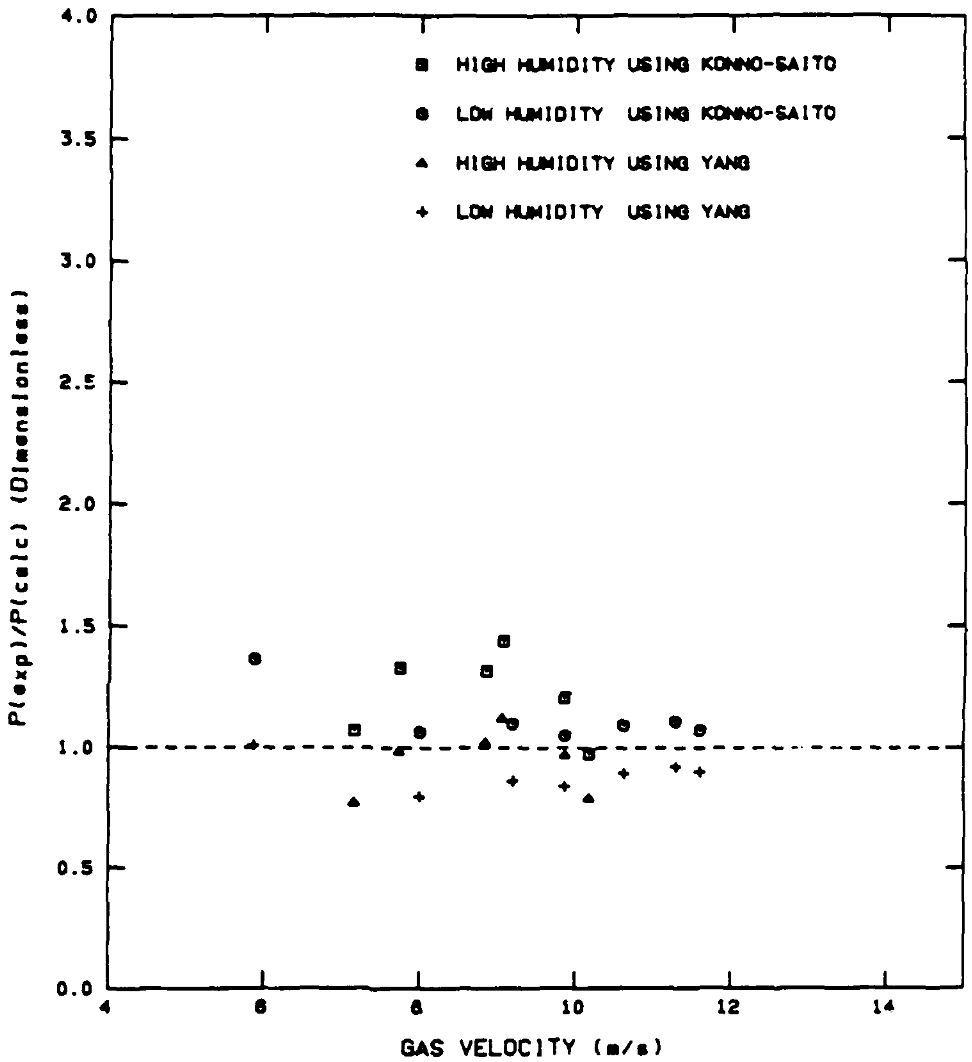

Figure A-51: Ratio of Experimental to Calculated Pressure Drop vs. Gas Velocity for 79μm Glass Beads in the Horizontal Orientation with W_s=17. x10^{-3}

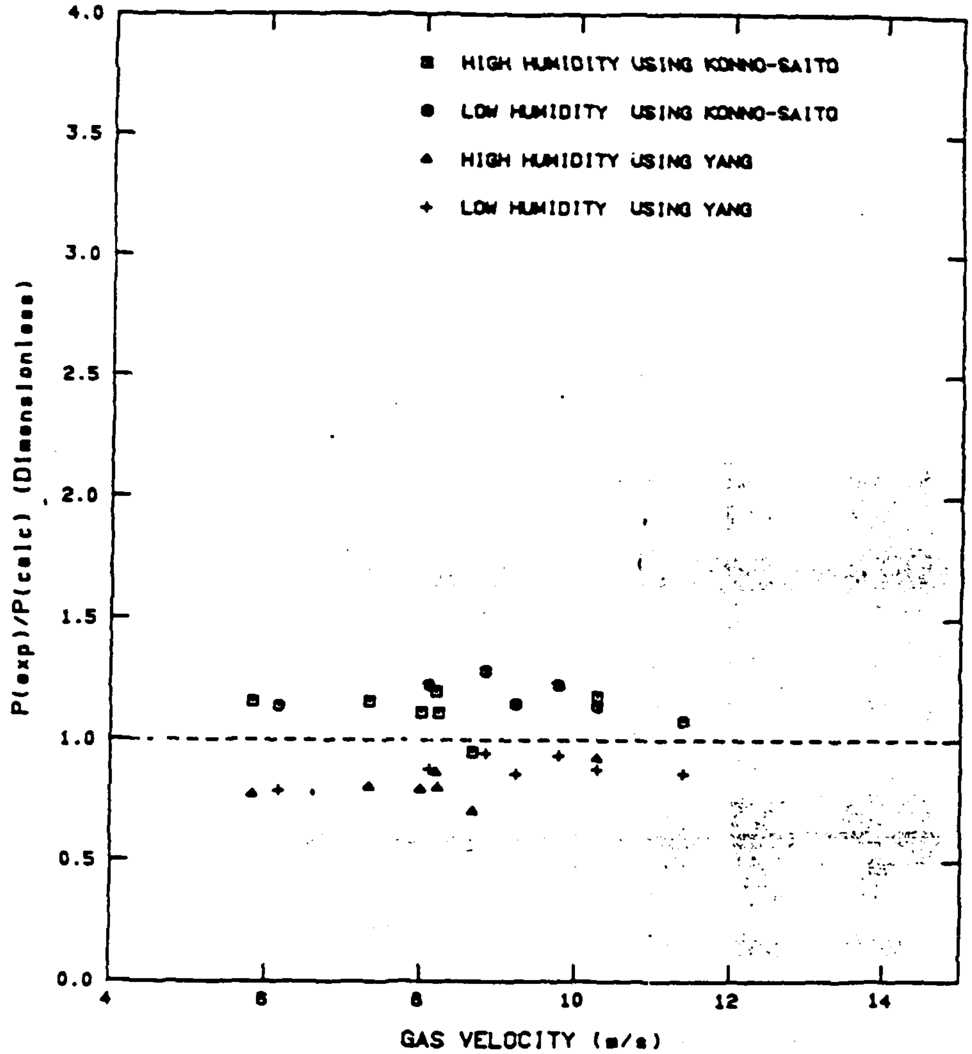

Figure A-52: Ratio of Experimental to Calculated Pressure Drop vs. Gas Velocity for 79μm Glass Beads in the Horizontal Orientation with $W_s = 24. \times 10^{-3}$

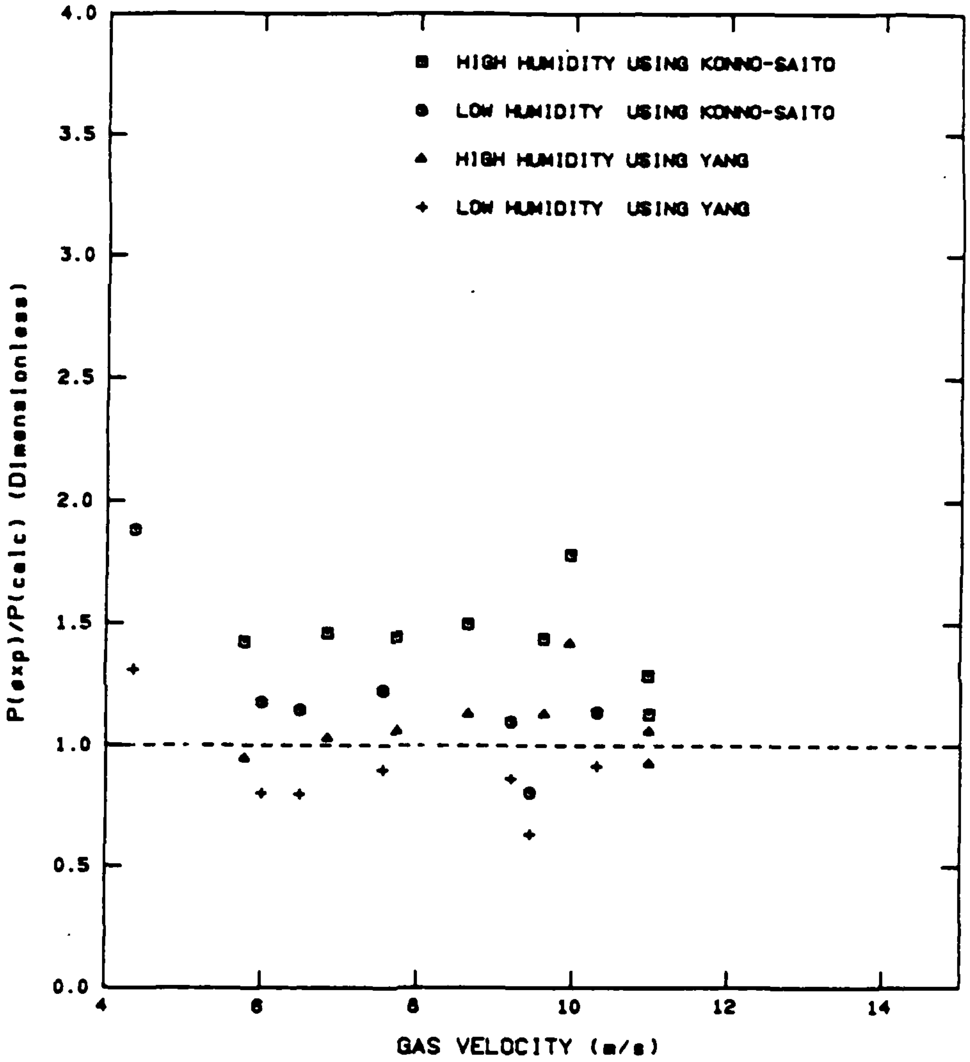

Figure A-53: Ratio of Experimental to Calculated Pressure Drop vs. Gas Velocity for 125μm Glass Beads in the Horizontal Orientation with $W_s = 17. \times 10^{-3}$

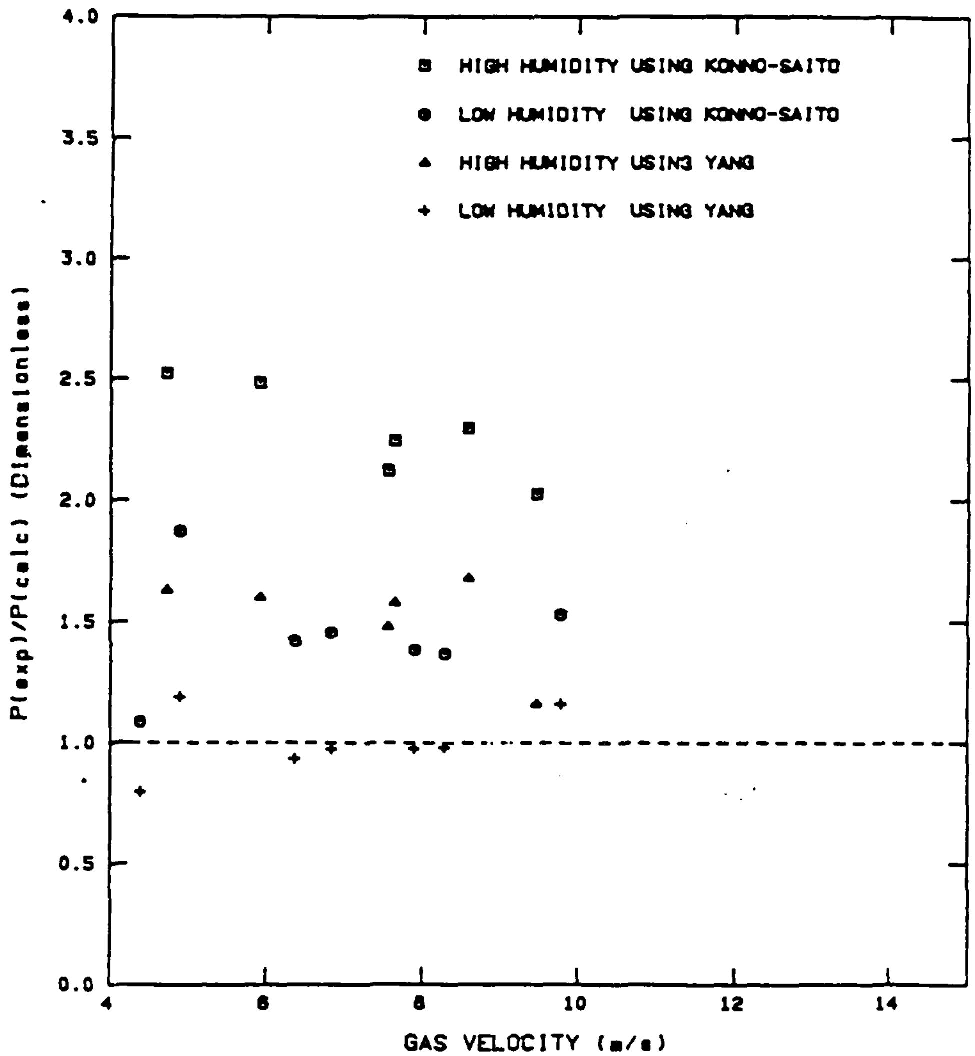

Figure A-54: Ratio of Experimental to Calculated Pressure Drop vs. Gas Velocity for 125µm Glass Beads in the Horizontal Orientation with W_s=24. x10^{-3}

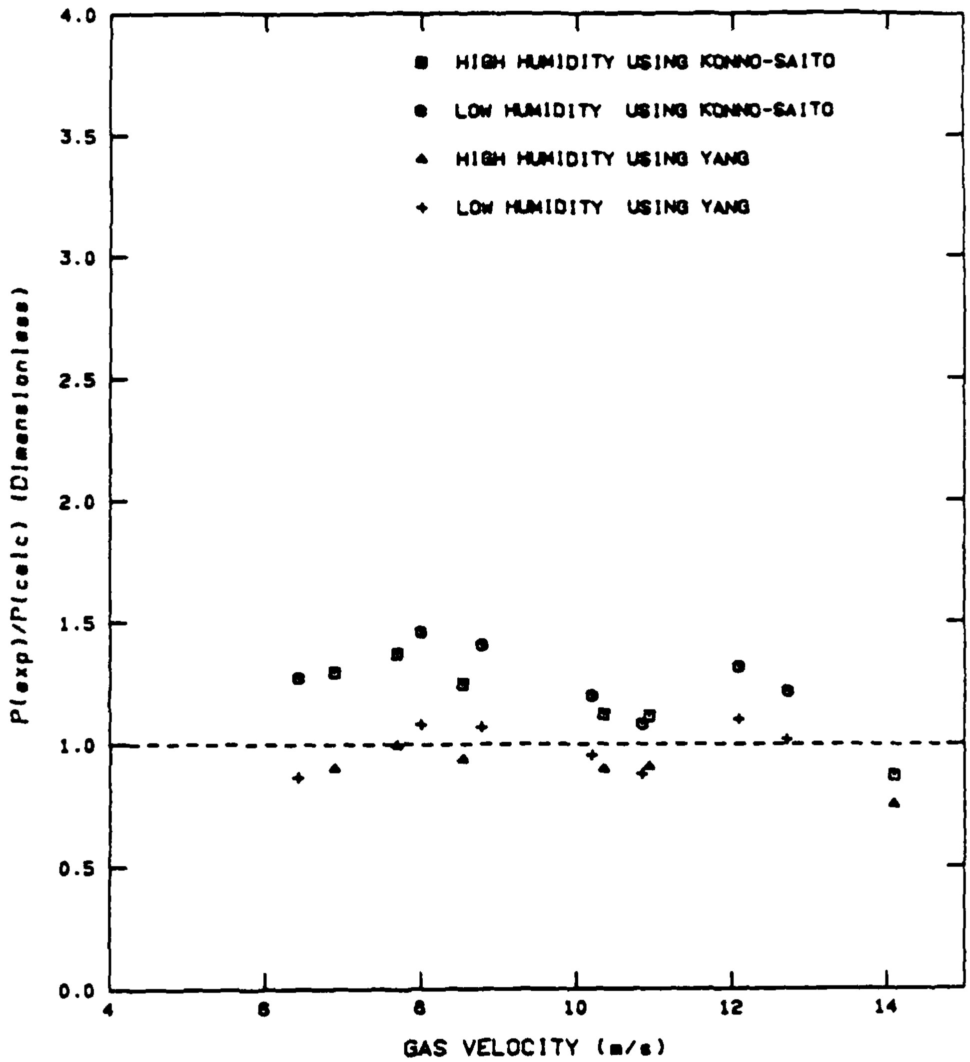

Figure A-55: Ratio of Experimental to Calculated Pressure Drop vs. Gas Velocity for 450µm Glass Beads in the Horizontal Orientation with W_s =19. x10^{-3}

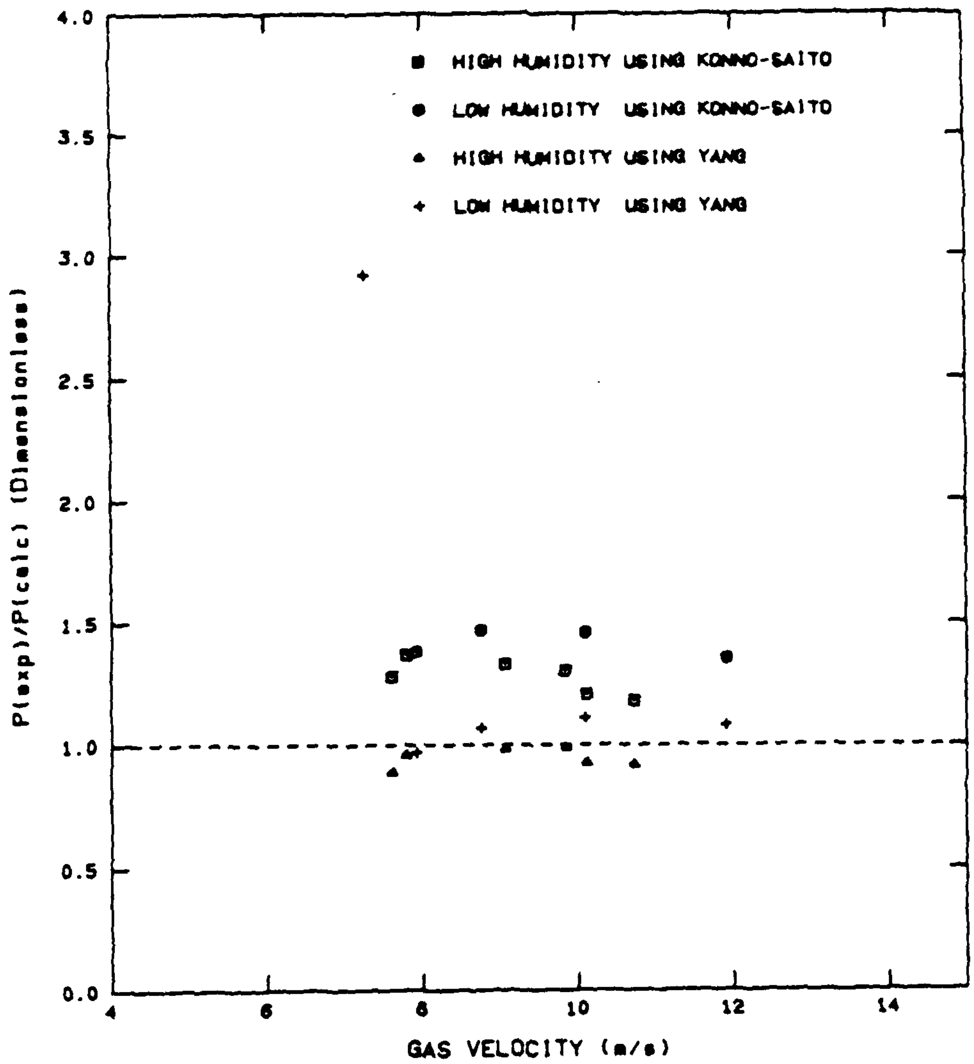

Figure A-56: Ratio of Experimental to Calculated Pressure Drop vs. Gas Velocity for 450μm Glass Beads in the Horizontal Orientation with $W_s = 30. \times 10^{-3}$

APPENDIX B.

TABLES REFERRED TO IN TEXT

Table B-1: Comparison of Absolute Mean Percent Error between the Correlation of Konno and Saito and that of Yang for 79μ Glass Beads in the Vertical Orientation

W_s	Humidity	Konno and Saito		Yang	
($x\ 10^{-3}$)		Abs. Mean Error (%)	Std Dev	Abs. Mean Error (%)	Std Dev
9.5	High	85.1	38.1	32.7	25.8
8.8	Low	81.2	34.6	35.4	17.7
17.8	High	88.1	49.2	44.3	27.3
18.3	Low	53.6	24.8	24.5	13.2
26.5	High	45.5	12.0	11.7	8.6
28.3	Low	49.3	12.7	14.7	8.5

Table B-2: Comparison of Absolute Mean Percent Error between the Correlation of Konno and Saito and that of Yang for 125μm Glass Beads in the Vertical Orientation

W_s ($\times 10^{-3}$)	Humidity	Konno and Saito Abs. Mean Error (%)	Konno and Saito Std Dev	Yang Abs. Mean Error (%)	Yang Std Dev
8.5	High	80.7	36.3	36.5	18.3
8.9	Low	20.1	8.26	27.3	17.8
18.3	High	34.6	15.7	17.7	8.7
18.8	Low	19.6	8.4	24.4	10.6
26.3	High	11.0	10.3	25.1	7.6
28.4	Low	21.9	12.3	18.8	10.7

Table B-3: Comparison of Absolute Mean Percent Error between the Correlation of Konno and Saito and that of Yang for 450μm Glass Beads in the Vertical Orientation

W_s	Humidity	Konno and Saito		Yang	
($x\ 10^{-3}$)		Abs. Mean Error (%)	Std Dev	Abs. Mean Error (%)	Std Dev
12.5	High	21.7	12.1	36.5	11.7
10.0	Low	25.7	13.9	34.8	16.5
22.7	High	12.2	6.9	37.1	10.5
20.6	Low	32.3	22.0	23.9	14.6
33.3	High	11.5	10.3	24.2	14.1
30.0	Low	19.3	7.4	16.5	11.6

Table B-4: Comparison of Absolute Mean Percent Error between the Correlation of Konno and Saito and that of Yang for 128μm Plexiglas Beads in the Vertical Orientation

W_s ($\times 10^{-3}$)	Humidity	Konno and Saito Abs. Mean Error (%)	Konno and Saito Std Dev	Yang Abs. Mean Error (%)	Yang Std Dev
8.7	High	51.8	17.5	18.4	15.1
8.8	Low	52.4	25.4	21.8	14.1
12.9	High	22.6	17.4	24.9	17.4
12.4	Low	37.5	26.2	28.7	18.3

Table B-5: Comparison of Absolute Mean Percent Error between the Correlation of Konno and Saito and that of Yang for 79μm Glass Beads in the Horizontal Orientation

W_s ($\times 10^{-3}$)	Humidity	Konno and Saito Abs. Mean Error (%)	Konno and Saito Std Dev	Yang Abs. Mean Error (%)	Yang Std Dev
19.0	High	17.6	11.0	12.4	12.9
15.4	Low	10.2	7.5	13.2	7.9
24.1	High	12.1	3.9	24.1	10.6
24.5	Low	14.8	5.1	14.0	6.9

Table B-6: Comparison of Absolute Mean Percent Error between the Correlation of Konno and Saito and that of Yang for 125μm Glass Beads in the Horizontcal Orientation

W_s	Humidity	Konno and Saito		Yang	
($x\ 10^{-3}$)		Abs. Mean Error (%)	Std Dev	Abs. Mean Error (%)	Std Dev
18.5	High	29.2	9.3	10.1	8.6
15.8	Low	19.8	12.9	24.1	16.4
25.3	High	55.9	3.8	36.7	2.8
23.5	Low	29.2	11.5	9.9	8.9

Table B-7: Comparison of Absolute Mean Percent Error between the Correlation of Konno and Saito and that of Yang for 450μm Glass Beads in the Horizontal Orientation

W_s	Humidity	Konno and Saito		Yang	
($x\ 10^{-3}$)		Abs. Mean Error (%)	Std Dev	Abs. Mean Error (%)	Std Dev
19.8	High	17.5	5.1	12.1	10.9
19.5	Low	21.0	8.1	8.4	4.7
28.6	High	21.5	4.5	6.0	4.4
32.3	Low	38.7	21.3	18.5	26.5

Table B-8: Eigenvalues for 125μm Glass Beads in the Vertical Orientation When $Ws=8.5x10^{-3}$ and R.H.= 57.2

RUN	U_g	U_f	m_1	m_2
34	14.67	12.01	−2.831	−36.963
35	10.78	6.60	−0.212	−56.710
36	8.62	7.26	0.440	−35.193
37	7.65	5.37	1.977	−49.059
38	6.05	4.37	2.671	−48.888
39	5.16	4.89	1.810	−22.455
40	4.36	3.32	2.438	−47.432

Table B-9: Eigenvalues for 125μm Glass Beads in the Vertical Orientation
When $Ws=8.9x10^{-3}$ and R.H.= 18.0

RUN	U_g	U_f	m_1	m_2
26	14.24	11.39	−2.413	−39.494
27	10.14	7.68	−1.692	−46.678
28	7.00	4.72	−1.133	−57.043
29	6.14	5.90	−1.749	−22.089
30	5.45	4.55	−0.332	−40.093
31	5.07	4.68	−0.591	−28.651
32	4.42	3.93	−1.015	−33.548
33	4.22	2.75	0.527	−61.098

Table B-10: Eigenvalues for 125μm Glass Beads in the Vertical Orientation When $Ws=18.3x10^{-3}$ and R.H.= 52.0

RUN	U_g	U_f	m_1	m_2
9	12.67	9.05	−1.536	−69.785
10	11.91	7.26	−0.763	−84.781
11	10.18	7.26	−0.937	−71.497
12	8.40	5.79	−0.778	−77.514
13	6.89	5.12	−0.505	−73.195
14	5.49	4.75	0.499	−54.585
16	7.98	5.04	1.149	−89.093
17	6.11	5.84	0.050	−32.033
48	11.69	7.59	−0.934	−77.454
49	8.89	6.61	−0.267	−67.992
50	7.25	6.29	−1.197	−51.951
51	6.58	5.64	−1.685	−54.300
52	6.14	5.28	−0.591	−53.521
53	5.40	4.62	−0.224	−55.671
54	4.67	4.57	−0.980	−24.574
82	10.67	7.59	−0.483	−67.684
83	8.16	6.29	−0.630	−62.335
84	7.07	6.60	−1.334	−36.584
85	6.36	5.20	−0.763	−60.795
86	5.64	4.86	0.384	−55.216

Table B-11: Eigenvalues for 125μm Glass Beads in the Vertical Orientation When $Ws=18.7x10^{-3}$ and R.H.= 52.0

RUN	U_g	U_f	m_1	m_2
19	16.76	12.23	-2.725	-64.098
20	13.38	7.59	-1.385	-92.192
21	10.63	10.16	-1.747	-30.931
22	8.36	6.17	-0.885	-71.308
23	6.14	5.04	-1.849	-61.962
24	5.80	5.74	-1.426	-19.581
25	5.02	4.68	-1.278	-41.258
76	10.40	8.36	-1.577	-58.488
77	8.22	7.86	-1.728	-31.751
78	7.45	5.69	-0.692	-69.590
79	6.78	6.74	-1.411	-16.090
80	6.49	4.97	-0.632	-71.135
81	5.78	5.69	-1.438	-22.182

Table B-12: Eigenvalues for 125μm Glass Beads in the Vertical Orientation

When $Ws=26.3x10^{-3}$ and R.H.= 51.7

RUN	U_g	U_f	m_1	m_2
56	14.94	12.95	−2.843	−53.698
57	10.22	7.86	−1.425	−76.838
58	8.54	7.68	−2.570	−53.694
59	6.98	6.60	−2.447	−43.353
60	6.00	5.74	−1.485	−40.397
61	4.71	4.65	−1.669	−26.041
63	6.75	6.74	−2.087	−15.246
64	8.71	7.18	−2.009	−73.655
65	11.16	7.18	−0.850	−104.549

Table B-13: Eigenvalues for 125μm Glass Beads in the Vertical Orientation

When Ws=28.4x10^{-3} and R.H.= 16.0

RUN	U_g	U_f	m_1	m_2
66	15.96	15.01	-3.593	-40.644
67	13.78	12.01	-2.173	-56.828
68	13.11	11.39	-1.854	-58.067
69	11.25	9.05	-1.298	-72.546
70	9.47	7.59	-0.909	-75.928
71	8.05	7.18	-1.025	-59.666
72	6.74	4.75	-0.061	-108.392
73	6.36	4.59	-0.507	-106.956
74	5.02	4.40	-1.651	-70.773
75	5.33	4.65	-2.011	-73.749

Table B-14: Eigenvalues for 450μm Glass Beads in the Vertical Orientation

When $Ws=12.5x10^{-3}$ and R.H.= 50.0

RUN	U_s	U_f	m_1	m_2
89	12.87	9.71	1.376	-7.554
90	11.52	9.71	2.500	-6.998
91	8.76	5.62	1.472	-9.199
92	7.16	6.41	0.099	-6.172
93	6.40	4.89	-0.693	-8.255
94	5.89	5.04	-1.643	-7.182
95	5.51	4.49	-2.326	-8.181
97	10.36	8.36	1.001	-7.321
98	7.74	5.55	0.083	-8.566

Table B-15: **Eigenvalues for 450μm Glass Beads in the Vertical Orientation When $Ws=10.0x10^{-3}$ and R.H.= 16.0**

RUN	U_g	U_f	m_1	m_2
119	15.96	12.95	1.298	-8.108
120	11.83	7.59	0.188	-9.341
121	10.45	7.59	1.297	-8.070
122	9.56	6.67	0.899	-8.552
123	8.89	5.55	1.059	-9.621
124	8.00	6.17	1.064	-7.901
125	7.38	6.17	1.711	-6.841
126	6.80	5.37	-0.183	-7.816
127	5.74	4.15	-1.082	-9.049
128	6.18	4.05	-0.159	-10.167

Table B-16: Eigenvalues for 450μm Glass Beads in the Vertical Orientation When $Ws=22.7 \times 10^{-3}$ and R.H.= 50.0

RUN	U_g	U_f	m_1	m_2
99	16.67	14.05	−3.123	−10.598
100	14.76	12.01	−2.320	−11.003
101	11.56	7.96	−1.137	−13.120
102	10.36	8.81	−1.861	−10.327
103	9.36	6.95	−0.706	−12.432
104	8.89	8.69	−1.117	−6.415
105	6.87	5.20	−2.138	−12.921
107	7.56	5.37	−1.733	−13.312
108	5.85	3.95	−2.741	−13.822

Table B-17: Eigenvalues for 450μm Glass Beads in the Vertical Orientation When $Ws=20.6x10^{-3}$ and R.H.= 16.0

RUN	U_g	U_f	m_1	m_2
129	15.34	12.01	4.012	-10.039
130	14.00	11.79	-1.009	-9.952
131	12.36	11.19	-0.674	-8.801
132	10.74	7.26	-0.281	-13.441
133	10.05	8.36	-0.068	-10.296
134	9.49	5.55	0.754	-15.969
135	9.16	4.37	2.508	-19.249
136	7.87	3.86	1.173	-19.938
137	6.58	3.51	1.059	-18.505
138	5.89	2.75	1.562	-19.867
139	16.58	14.05	-1.462	-9.934

Table B-18: Eigenvalues for 450μm Glass Beads in the Vertical Orientation When $Ws=33.3x10^{-3}$ and R.H.= 50.0

RUN	U_g	U_f	m_1	m_2
109	17.34	7.59	-2.066	-22.008
110	15.04	6.41	-0.975	-24.554
111	11.78	7.26	-0.868	-19.266
112	9.00	4.62	0.765	-25.278
113	7.78	4.49	-0.307	-22.827
115	7.11	4.89	0.438	-17.694
116	8.41	5.95	-1.301	-17.090
117	9.78	7.26	-1.401	-15.538
118	10.75	8.81	-2.642	-13.493

Table B-19: **Eigenvalues for 450μm Glass Beads in the Vertical Orientation When Ws=30.0x10^{-3} and R.H.= 19.4**

RUN	U_g	U_f	m_1	m_2
140	16.06	11.19	−2.399	−15.191
141	13.28	9.30	−1.711	−15.840
142	11.31	10.48	−1.039	−9.913
143	10.00	7.96	−0.786	−13.918
144	8.97	6.67	−0.443	−15.457
145	8.11	7.50	−1.024	−9.793
146	7.11	5.74	−0.990	−14.150
148	7.67	5.74	−0.255	−15.480
149	6.98	5.04	−0.211	−16.381

Table B-20: **Eigenvalues for 79μm Glass Beads in the Vertical Orientation When $Ws=9.5x10^{-3}$ and R.H.= 53.7**

RUN	U_g	U_f	m_1	m_2
150	11.16	8.36	−0.820	−100.078
151	9.11	6.11	−0.087	−118.126
152	8.36	3.86	1.164	−172.593
153	7.62	3.51	3.612	−175.384
154	6.62	3.77	2.181	−146.208
155	5.82	2.29	4.985	−213.789
156	6.53	5.69	0.731	−73.453
157	5.20	3.07	4.568	−143.880
158	4.18	3.37	2.986	−80.709
159	4.71	3.93	1.686	−81.802

Table B-21: Eigenvalues for 79μm Glass Beads in the Vertical Orientation When $Ws=8.8x10^{-3}$ and R.H.= 16.0

RUN	U_g	U_f	m_1	m_2
200	12.00	5.00	0.226	-171.283
201	10.43	6.60	-0.243	-119.470
202	8.31	6.60	-0.319	-88.570
203	7.16	4.89	1.171	-112.449
204	5.69	5.16	1.524	-60.401
205	5.91	4.23	2.110	-107.413
206	5.38	3.83	2.232	-108.191
207	5.10	2.71	4.700	-155.089
208	4.36	3.83	2.422	-60.254
209	6.94	5.74	-0.718	-82.480

Table B-22: Eigenvalues for 79μm Glass Beads in the Vertical Orientation When $Ws=17.8x10^{-3}$ and R.H.= 51.7

RUN	U_g	U_f	m_1	m_2
160	13.38	8.80	-1.951	-155.776
161	11.85	6.67	-0.916	-189.476
162	10.85	7.96	-1.190	-143.077
163	9.16	4.75	1.222	-219.420
164	8.65	7.96	0.060	-79.071
165	7.82	3.32	4.521	-281.476
166	7.60	6.60	0.691	-100.056
167	5.69	2.29	5.777	-328.035
168	4.07	2.23	6.009	-225.110
169	5.82	4.34	2.550	-149.925

Table B-23: Eigenvalues for 79μm Glass Beads in the Vertical Orientation When $Ws=18.3x10^{-3}$ and R.H.= 16.0

RUN	U_g	U_f	m_1	m_2
190	14.34	12.01	-2.105	-102.406
191	12.36	6.67	-0.738	-192.559
192	10.85	5.24	1.031	-221.892
193	10.67	5.04	0.335	-237.665
194	8.31	6.17	-1.103	-103.003
195	9.20	6.41	0.843	-144.561
196	7.54	5.37	0.082	-141.464
197	6.47	6.11	-0.138	-69.074
198	5.56	5.00	1.073	-89.761

Table B-24: Eigenvalues for 79μm Glass Beads in the Vertical Orientation When $Ws=26.5x10^{-3}$ and R.H.= 53.0

RUN	U_g	U_f	m_1	m_2
170	13.85	8.80	-1.366	-205.698
171	11.37	8.69	-0.808	-165.253
172	8.78	6.67	-0.043	-179.832
173	7.41	6.41	-0.021	-135.238
174	4.30	4.29	-0.587	-24.388
175	7.67	6.35	-0.276	-151.643
176	8.60	7.59	-0.556	-122.825
177	10.30	5.95	-0.183	-220.969
178	7.82	5.69	0.122	-195.892
179	5.00	4.23	0.849	-143.765

Table B-25: Eigenvalues for 79μm Glass Beads in the Vertical Orientation When Ws=28.3x10^{-3} and R.H.= 18.5

RUN	U_g	U_f	m_1	m_2
180	14.60	10.20	−1.701	−179.757
181	13.41	10.48	−1.683	−149.934
182	12.15	9.86	−1.348	−141.819
183	10.37	7.96	−0.758	−164.232
184	9.34	5.50	0.696	−251.283
185	8.15	6.67	−0.020	−150.757
186	6.96	4.86	0.481	−210.951
187	7.04	4.49	1.095	−239.068
189	6.71	4.34	1.614	−233.461

Table B-26: Eigenvalues for 128μm PLEXIGLAS BEADS in the Vertical Orientation When Ws= $8.6x10^{-3}$ and R.H.= 47.2

RUN	U_g	U_f	m_1	m_2
231	8.76	6.41	-0.078	-84.711
232	5.33	4.49	0.839	-65.872
233	3.85	2.58	2.298	-103.202
234	3.18	3.12	1.708	-24.296
236	3.45	2.95	0.871	-61.497
237	5.91	4.75	0.691	-75.356
238	7.78	5.95	0.437	-79.412
239	10.76	7.96	-2.313	-85.116

Table B-27: Eigenvalues for 128μm PLEXIGLAS BEADS in the Vertical Orientation When Ws= $8.8x10^{-3}$ and R.H.= 16.0

RUN	U_g	U_f	m_1	m_2
220	9.82	6.17	-1.300	-104.704
221	8.45	5.50	-0.117	-98.514
222	6.14	4.75	0.632	-80.790
223	4.62	3.25	2.279	-94.641
224	3.55	2.43	2.248	-92.672
225	4.27	2.90	3.012	-102.794
226	3.32	2.95	-0.034	-54.146
227	8.34	7.18	-1.064	-60.789
228	6.53	5.50	1.044	-64.348

Table B-28: Eigenvalues for 128μm PLEXIGLAS BEADS in the Vertical Orientation When $Ws=12.9x10^{-3}$ and R.H.= 52.8

RUN	U_g	U_f	m_1	m_2
240	12.97	6.88	-2.667	-137.974
241	12.63	7.96	-1.694	-121.708
242	8.22	7.59	-1.375	-56.763
243	6.00	3.92	1.055	-126.422
244	4.74	3.12	-0.704	-127.767
245	8.15	5.20	0.263	-126.677
246	3.63	3.18	-0.620	-76.412
248	8.04	5.95	-0.897	-105.060
249	4.89	3.18	-0.288	-136.043

Table B-29: Eigenvalues for 128μm PLEXIGLAS BEADS in the Vertical Orientation When Ws=12.4x10^{-3} and R.H.= 16.0

RUN	U_g	U_f	m_1	m_2
210	11.08	7.59	−0.888	−59.989
211	7.34	5.33	0.478	−58.984
212	7.26	5.95	0.548	−46.778
213	6.26	5.90	0.494	−28.826
214	4.59	4.37	0.679	−26.894
215	4.30	2.68	0.102	−84.097
216	3.45	3.24	−3.459	−26.504
217	13.13	12.01	−4.997	−35.777
218	4.96	3.06	−3.516	−78.796
219	3.78	3.37	−3.287	−35.872

Table B-30: Eigenvalues for 125μm Glass Beads in the Horizontal Orientation When $Ws=18.5x10^{-3}$ and R.H.= 51.7

RUN	U_g	U_f	m_1	m_2
269	10.98	7.26	−4.575	−80.759
270	10.98	6.67	−3.805	−87.783
271	9.96	8.69	−5.980	−51.978
272	9.62	6.11	−4.665	−87.534
273	8.65	3.24	−4.448	−160.639
274	7.73	3.53	−3.920	−133.033
275	6.85	3.46	−3.644	−123.811
276	5.78	2.33	−3.188	−164.382

Table B-30: Eigenvalues for 125μm Glass Beads in the Horizontal Orientation When $Ws=18.5x10^{-3}$ and R.H.= 51.7

RUN	U_g	U_f	m_1	m_2
269	10.98	7.26	−4.575	−80.759
270	10.98	6.67	−3.805	−87.783
271	9.96	8.69	−5.980	−51.978
272	9.62	6.11	−4.665	−87.534
273	8.65	3.24	−4.448	−160.639
274	7.73	3.53	−3.920	−133.033
275	6.85	3.46	−3.644	−123.811
276	5.78	2.33	−3.188	−164.382

Table B-31: Eigenvalues for 125μm Glass Beads in the Horizontal Orientation
When $Ws=15.8x10^{-3}$ and R.H.= 16.9

RUN	U_g	U_f	m_1	m_2
255	9.45	3.93	−1.614	−129.698
256	9.20	4.89	−3.139	−101.078
257	7.56	3.24	−3.103	−135.064
258	6.49	4.86	−2.682	−71.661
259	6.00	2.90	−2.578	−124.840
260	4.36	2.43	−4.621	−63.201
261	10.31	7.59	−3.718	−70.016

Table B-32: Eigenvalues for 125μm Glass Beads in the Horizontal Orientation When $Ws=25.3x10^{-3}$ and R.H.= 52.3

RUN	U_g	U_f	m_1	m_2
277	9.47	9.30	-5.857	-29.980
278	8.59	4.34	-6.796	-145.492
279	7.64	5.33	-5.788	-102.796
280	7.56	6.41	-5.289	-70.120
281	5.92	5.16	-5.309	-68.845
283	4.72	3.67	-5.451	-60.980

Table B-33: Eigenvalues for 125μm Glass Beads in the Horizontal Orientation When $Ws=23.5x10^{-3}$ and R.H.= 16.1

RUN	U_g	U_f	m_1	m_2
262	9.78	8.25	-4.526	-67.774
263	8.28	5.55	-3.477	-108.033
264	7.89	3.24	-3.338	-197.517
265	6.36	6.35	-3.092	-16.459
266	4.89	3.05	-4.058	-95.944
267	4.39	3.05	-2.405	-42.230
268	6.84	4.37	-3.249	-128.942

Table B-34: Eigenvalues for 79μm Glass Beads in the Horizontal Orientation When $Ws=19.0x10^{-3}$ and R.H.= 55.4

RUN	U_g	U_f	m_1	m_2
298	10.18	5.00	-2.756	-217.775
299	9.87	7.96	-3.980	-116.339
300	9.07	5.74	-4.528	-172.826
301	8.85	5.69	-3.945	-171.717
302	7.74	4.75	-3.600	-185.832
303	7.16	4.13	-2.536	-205.899

Table B-35: Eigenvalues for 79μm Glass Beads in the Horizontal Orientation When $Ws=15.4x10^{-3}$ and R.H.= 19.1

RUN	U_g	U_f	m_1	m_2
284	11.60	4.59	-3.510	-252.039
285	11.29	3.37	-3.454	-327.862
286	10.63	8.36	-3.755	-121.101
287	9.87	7.03	-3.277	-144.643
288	9.20	8.36	-3.410	-83.293
289	8.00	4.49	-2.711	-204.325
290	5.87	4.49	-3.526	-97.430

Table B-36: Eigenvalues for 79μm Glass Beads in the Horizontal Orientation When $Ws=24.1x10^{-3}$ and R.H.= 53.4

RUN	U_g	U_f	m_1	m_2
305	10.28	5.00	−3.459	−267.717
306	8.67	5.69	−2.356	−200.096
307	8.20	2.29	−2.779	−544.860
308	7.34	2.75	−2.520	−434.440
309	5.83	2.75	−2.447	−277.358
310	8.00	7.18	−2.813	−112.160
311	8.22	3.93	−2.610	−317.180

Table B-37: Eigenvalues for 79μm Glass Beads in the Horizontal Orientation When $Ws=24.5x10^{-3}$ and R.H.= 18.5

RUN	U_g	U_f	m_1	m_2
291	11.39	9.86	-3.584	-116.788
292	10.28	4.34	-3.069	-340.659
293	9.78	3.93	-3.343	-356.531
294	8.84	3.44	-3.288	-392.431
295	6.17	4.03	-2.611	-168.245
296	9.22	6.95	-3.164	-168.044
297	8.11	2.66	-2.871	-478.106

Table B-38: Eigenvalues for 450μm Glass Beads in the Horizontal Orientation When Ws=19.8x10^{-3} and R.H.= 56.3

RUN	U_g	U_f	m_1	m_2
319	14.09	10.48	−2.404	−11.995
320	10.94	7.26	−3.569	−14.038
321	10.36	4.86	−3.287	−19.096
322	8.54	5.90	−3.443	−13.878
323	7.69	4.75	−3.576	−16.060
324	6.89	3.44	−3.031	−20.199

Table B-39: Eigenvalues for 450μm Glass Beads in the Horizontal Orientation When Ws=19.5x10^{-3} and R.H.= 16.3

RUN	U_g	U_f	m_1	m_2
312	12.71	9.71	-4.684	-12.815
313	12.09	8.36	-4.995	-14.513
314	10.19	8.69	-3.834	-10.446
315	10.85	5.69	-3.248	-17.223
316	8.78	5.69	-4.108	-15.220
317	8.00	5.04	-4.007	-15.711
318	6.42	5.16	-2.913	-11.527

Table B-40: Eigenvalues for 450μm Glass Beads in the Horizontal Orientation When $Ws=28.6x10^{-3}$ and R.H.= 56.2

RUN	U_g	U_f	m_1	m_2
326	9.84	6.35	-3.693	-17.514
327	9.06	4.72	-3.506	-22.121
328	7.78	4.62	-3.266	-20.477
329	7.61	4.62	-2.954	-20.182
331	10.11	6.11	-3.405	-18.188
332	10.72	6.88	-3.441	-17.285

Table B-41: Eigenvalues for 450μm Glass Beads in the Horizontal Orientation When $Ws=32.3x10^{-3}$ and R.H.= 16.4

RUN	U_g	U_f	m_1	m_2
417	11.90	7.96	-4.498	-17.245
418	10.09	7.96	-4.292	-14.424
419	8.75	5.33	-3.861	-19.808
420	7.91	4.23	-3.290	-23.398
421	7.27	4.49	-9.571	-24.491

Table B-42: Eigenvalues for 125μm Glass Beads in the Inclined Orientation When $Ws=18.2x10^{-3}$ and R.H.= 56.4

RUN	U_g	U_f	m_1	m_2
375	9.87	5.55	-0.877	-97.403
376	9.42	6.41	-1.135	-79.783
377	8.98	6.67	-1.184	-70.007
378	8.14	7.96	-1.140	-24.521
379	7.42	5.74	-0.788	-68.204
380	6.36	4.86	-0.429	-71.975
381	4.85	3.44	-1.611	-68.151

Table B-43: **Eigenvalues for 125μm Glass Beads in the Inclined Orientation When $W_s = 17.8 \times 10^{-3}$ and R.H. = 19.0**

RUN	U_g	U_f	m_1	m_2
361	10.18	9.30	-2.515	-41.271
362	9.98	5.37	-1.999	-102.630
363	9.69	7.26	-2.872	-69.243
364	8.18	5.95	-2.061	-74.621
365	7.47	3.93	-1.386	-115.478
366	6.45	4.89	-3.531	-74.407
367	4.89	3.06	-20.342	-94.250

Table B-44: Eigenvalues for 125μm Glass Beads in the Inclined Orientation When $Ws=27.0x10^{-3}$ and R.H.= 56.7

RUN	U_g	U_f	m_1	m_2
382	8.31	7.26	−1.609	−62.477
383	7.72	5.55	−1.111	−98.450
384	7.11	5.16	−0.805	−99.051
385	7.61	5.37	−0.785	−101.748
386	5.17	4.72	−2.980	−48.651
387	6.70	5.20	−0.988	−88.804
388	10.06	7.86	−2.151	−77.011

Table B-45: Eigenvalues for 125μm Glass Beads in the Inclined Orientation When $Ws = 28.9 x 10^{-3}$ and R.H. = 22.0

RUN	U_g	U_f	m_1	m_2
368	9.00	7.50	−3.722	−72.218
369	8.45	6.41	−3.760	−88.661
370	7.70	3.93	−3.497	−156.845
371	6.95	5.20	−3.834	−96.698
373	6.56	5.74	−4.424	−68.021
374	7.06	6.41	−4.646	−58.133

AD-A184 074 GAS-SOLID TRANSPORT IN A 00508 M PIPE AT VARIOUS INCLINATIONS WITH AND WITHOUT ELECTROSTATICS(U) ARMY MILITARY PERSONNEL CENTER ALEXANDRIA VA C A MYLER AUG 85 3/3

UNCLASSIFIED F/G 13/11 NL

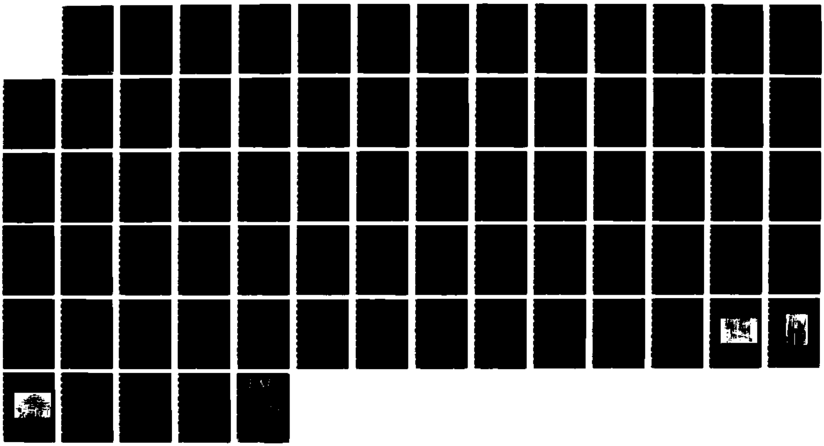

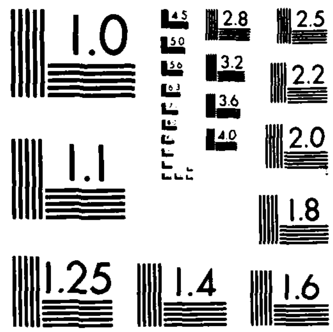

MICROCOPY RESOLUTION TEST CHART
NATIONAL BUREAU OF STANDARDS-1963-A

Table B-46: Eigenvalues for 450μm Glass Beads in the Inclined Orientation When $Ws=18.6 \times 10^{-3}$ and R.H.= 55.7

RUN	U_g	U_f	m_1	m_2
347	11.91	9.86	-2.581	-10.295
348	11.11	6.60	-2.100	-14.630
349	10.82	6.41	-2.151	-14.863
350	10.00	6.17	-1.925	-14.417
351	9.29	5.04	-1.575	-16.556
352	7.38	4.72	-2.457	-15.117

Table B-47: Eigenvalues for 450μm Glass Beads in the Inclined Orientation When $Ws=20.3x10^{-3}$ and R.H.= 21.9

RUN	U_g	U_f	m_1	m_2
333	10.89	5.90	−5.218	−17.784
334	9.82	4.59	−3.273	−19.685
335	9.29	5.33	−4.313	−17.444
336	8.85	5.37	−3.969	−16.101
337	8.16	3.59	−3.510	−21.504
339	7.16	4.37	−6.960	−19.263

Table B-48: Eigenvalues for 450μm Glass Beads in the Inclined Orientation When $Ws=29.1x10^{-3}$ and R.H.= 53.6

RUN	U_g	U_f	m_1	m_2
354	11.23	6.67	−2.868	−18.353
355	10.61	5.04	−1.694	−22.584
356	10.11	7.96	−2.450	−13.285
357	8.72	5.50	−1.581	−18.121
358	8.28	4.03	−1.379	−24.286
359	7.72	6.60	−3.122	−12.371

Table B-49: Eigenvalues for 450μm Glass Beads in the Inclined Orientation When Ws=28.8x10^{-3} and R.H.= 18.0

RUN	U_g	U_f	m_1	m_2
340	10.00	7.86	−4.148	−14.135
341	9.47	4.13	−2.706	−26.064
342	8.67	7.86	−4.250	−10.939
343	8.50	8.25	−4.139	−8.241
344	6.72	3.75	−9.565	−25.360
345	7.34	7.18	−5.461	−11.918
346	8.39	7.26	−4.771	−12.645

Table B-50: Eigenvalues for 79μm Glass Beads in the Inclined Orientation When Ws=18.1x10^{-3} and R.H.= 52.8

RUN	U_g	U_f	m_1	m_2
403	10.05	7.18	−2.216	−148.197
404	9.78	6.11	−2.055	−177.720
405	9.05	5.20	−2.100	−197.538
406	8.45	7.26	−1.751	−103.945
407	7.22	2.71	1.387	−325.563
408	7.02	2.39	1.738	−360.726
409	6.78	3.35	−0.454	−251.050

Table B-51: Eigenvalues for 79µm Glass Beads in the Inclined Orientation When $Ws=16.5x10^{-3}$ and R.H.= 18.5

RUN	U_g	U_f	m_1	m_2
389	11.08	8.81	−2.401	−99.369
390	10.36	4.13	−0.529	−271.150
391	9.52	5.69	−1.205	−183.498
392	8.05	7.59	−2.110	−70.350
393	7.60	6.11	−1.646	−123.537
394	6.80	5.16	−1.584	−140.582

Table B-52: Eigenvalues for 79μm Glass Beads in the Inclined Orientation When $Ws=26.6 \times 10^{-3}$ and R.H.= 54.6

RUN	U_g	U_f	m_1	m_2
410	9.11	6.88	−2.159	−169.376
411	7.95	5.95	−0.662	−179.888
412	7.06	5.20	−0.891	−186.387
413	6.84	3.44	0.769	−322.710
415	6.45	3.12	1.338	−332.440
416	6.25	4.75	−0.817	−179.629

Table B-53: Eigenvalues for 79μm Glass Beads in the Inclined Orientation When Ws=25.8×10^{-3} and R.H.= 17.6

RUN	U_g	U_f	m_1	m_2
396	9.22	8.36	-2.824	-107.020
397	8.61	6.17	-2.313	-194.539
398	8.78	5.20	-1.532	-254.876
399	6.89	4.89	-1.717	-200.346
400	6.06	4.75	-3.326	-130.947
401	7.39	4.75	-2.912	-239.469
402	7.64	5.90	-2.860	-174.742

APPENDIX C.
COMPUTER PROGRAMS

```
C
C                        CROS1.FOR
C                 CROSSCORRELATION PROGRAM
C
C     THIS IS THE FIRST PROGRAM IN A SERIES OF TWO WHICH
C     MUST BE EXECUTED IN ORDER TO CALCULATE THE PARTICLE
C     VELOCITY. THIS PROGRAM TAKES THE ANALOG SIGNAL FROM
C     THE TAPE RECORDER AND CONVERTS IT INTO A DIGITAL
C     SIGNAL. DATA IS INPUTED FROM THE FIRST TWO CHANNELS
C     ON THE A/D BOARD. THE UPSTREAM SIGNAL SHOULD BE
C     CONNECTED TO CHANNEL 0 AND THE DOWNSTREAM SIGNAL
C     SHOULD BE CONNECTED TO CHANNEL 1 ON THE A/D BOARD.
C     DATA SHOULD BE INPUTED FOR 8 SECONDS IN ORDER TO
C     COLLECT 8000 POINTS IN FILE 'FILE.DAT'.
C
C     THE EXAMPLE BEGINS BY DEFINING CERTAIN ARRAYS
C     REQUIRED BY THE SWEEP PROCESS. INFO IS USED AS THE
C     SWEEP-INFORMATION ARRAY AND IBUF(1,N+1) IS USED AS
C     THE Nth BUFFER.
C
C     IN ADDITION, ARRAY FBUF IS DEFINED. THIS ARRAY IS
C     USED FOR TEMPORARY STORAGE OF A/D CONVERTED VALUES.
C
      DIMENSION INFO(40),IBUF(1000,8),FBUF(1000)
C
C     THE FIRST OPERATION PERFORMED IN THIS EXAMPLE IS TO
C     CHECK THE STATUS AND READINGS OF A/D CHANNELS 0 AND
C     8. NOTE THAT CHANNEL 0 CAN NEVER RETURN ANY STATUS
C     OTHER THAN SINGLE-ENDED VOLTAGE INPUT WITH A GAIN
C     VALUE OF 1. CHANNEL 8, ON THE OTHER HAND, MAY HAVE A
C     PREAMPLIFIER (THAT IS, AN MNCAG) ASSOCIATED WITH IT,
C     THUS ALLOWING A VARIABLE STATUS AS WELL AS INPUT.
C
C     THIS SECTION LOOPS ON OPERATOR CONTROL SO THAT
C     VARIATIONS IN INPUT STATUS AND VALUE CAN BE
C     VERIFIED.
C
C     BEFORE PROCEEDING, SOME ADDITIONAL ARRAYS NEED TO BE
C     DEFINED.
C
      DIMENSION RANGE(5,3),LENG(3),GAIN(5)
      INTEGER*4 IDOUBL
      REAL*8 VALN
      LOGICAL*1 TYPE(10,3),ANS
```

```
      DATA RANGE/.01,.1,1.02,10.24,5.12,      !VOLTS
     1          .01,.1,1.02,10.24,0.0,        !MILLIAMPS
     1          .1,1.02,10.24,102.4,0.0/      !K OHMS
      DATA TYPE/' ','V','O','L','T','S',4*' ',
     1          ' ','M','I','L','L','I','A','M','P','S',
     1          ' ','K',' ','O','H','M','S',3*' '/
      DATA LENG/6,10,7/
      DATA GAIN/.5,5.,50.,500.,1./
C
    1 DO 10 I=0,8,8
C
C     NOW GET MNCAD #0 STATUS INFORMATION FOR THE
C     APPROPRIATE CHANNEL.
C
      CALL MADSTS(IND,I,INNER,IOUTER,NOMAG)
C
C     NOW READ AND CONVERT THE VALUE RECEIVED FROM THE
C     A/D CHANNEL.
C
      VAL=CAD2FP(IADINP(,I,IVAL))
C
C     NOW NORMALIZE THE CONVERTED VALUE AND SET THE DOUBLE
C     PRECISION RESULT TO A FLOATING POINT NUMBER.
C
      CALL KAD2DI(IVAL,IDOUBL)
      VALN=DJFLT(IDOUBL)
C
C     NOW PRINT RAW DATUM (IVAL), THE NORMALIZED DATUM
C     (VALN), AND THE ACTUAL DATUM (IVAL).
C
      TYPE 1000,I,IVAL,VAL,(TYPE(J,INNER),J=1,LENG(INNER))
 1000 FORMAT(/' THE RAW INPUT READ ON CHANNEL #'I1' IS
     1 '06' OCTAL.'/' THE ACTUAL INPUT IS THEREFORE 'F10.4,
     2 10A1)
      TYPE 1001,VALN
 1001 FORMAT(' THE NORMALIZED REPRESENTATION OF THE INPUT
     1 IS 'F10.0'.')
C
C     REPORT ON THE STATUS OF THE CHANNEL
C
      TYPE 1004
 1004 FORMAT(' THE INPUT IS '$)
      GO TO (14,15,16),NOMAG+2
   14 TYPE 1005
```

```
1005  FORMAT(' QUASI-DIFFERENTIAL '$)
      GO TO 30
  15  TYPE 1006
1006  FORMAT(' DIFFERENTIAL '$)
      GO TO 30
  16  TYPE 1007
1007  FORMAT(' SINGLE-ENDED '$)
  30  GO TO (21,22,22,22,22,22),IOUTER
  21  TYPE 1008
1008  FORMAT(' WITH THE GAIN SET TO PROGRAMMABLE.')
      GO TO 10
  22  TYPE 1009,RANGE(IOUTER-1,INNER),(TYPE(J,INNER),J-1,
     1 LENG(INNER))
1009  FORMAT(' WITH A RANGE OF + OR - 'F6.2,10A1)
      TYPE 1010,GAIN(IOUTER-1)
1010  FORMAT(' THE EFFECTIVE GAIN IS 'F5.1'.')
  10  CONTINUE
C
C      CHECK IF THE OPERATOR WISHES TO VERIFY INFORMATION
C      AGAIN.
C
      TYPE 1020
1020  FORMAT(/' SHOULD CHANNELS BE CHECKED AGAIN?   '$)
      ACCEPT 2000,ANS
2000  FORMAT(A1)
      IF(ANS.EQ.'Y')GO TO 1
C
C      THE EXAMPLE NOW GIVES THE OPERATOR THE OPTION TO
C      START A SWEEP OF CHANNEL SWEEPS ON ANY CHANNEL
C      BETWEEN 0 AND 8. UP TO A MAXIMUM OF FOUR CHANNELS
C      MAY BE SELECTED TO BE SAMPLED DURING EACH CHANNEL
C      SWEEP. AN AGGREGATE TOTAL OF 100 SAMPLES WILL BE
C      TAKEN IN THIS PROCESS.
C
C      THE OPERATOR MAY NOW ALSO CHOOSE THE INTERSAMPLE
C      INTERVAL TIME, OR DWELL, AS A INTEGRAL MULTIPLE OF
C      .01 SECONDS. THE VALUE CHOSEN MUST BE LESS THAN
C      65536 BUT GREATER THAN ZERO.
C
C      THE OPERATOR MAY ALSO CHOOSE TO HAVE THE INTERVAL BE
C      THE TIME BETWEEN SUCCESSIVE FIRINGS OF SCHMITT
C      TRIGGER 1 OF THE PRIMARY CLOCK BY CHOOSING ZERO (0)
C      AS THE LENGHT OF THE SAMPLE PERIOD.
C
```

```
 50   TYPE 1021
1021  FORMAT(' WHICH CHANNEL IS THE FIRST A/D CHANNEL TO
    1 BE SAMPLED AT THE END OF EACH'/' SAMPLE PERIOD(0-8)?
    2  '$)
      ACCEPT 2001,ICHN
2001  FORMAT(I5)
      IF(ICHN.LT.0.OR.ICHN.GT.8) GO TO 50
 51   TYPE 1022
1022  FORMAT(' HOW MANY CHANNELS SHOULD BE SAMPLED EACH
    1 SAMPLE PERIOD (1-4)?  '$)
      ACCEPT 2001,NCHN
      IF(NCHN.LT.1.OR.NCHN.GT.4) GO TO 51
C
C     NOTE THAT THE MODE INDICATES THAT THE SWEEP WILL NOT
C     START WHEN THE CALL TO THE ADSWP SUBROUTINE IS MADE
C     IF THE SWEEP IS DRIVEN BY THE PRIMARY CLOCK AT A
C     SPECIFIED RATE. THE PROGRAM WAITS FOR A COMMAND FROM
C     THE OPERATOR AND THEN CALLS THE DIGO SUBPROGRAM TO
C     START THE SWEEP IMMEDIATELY.
C
C     IF THE SWEEP IS EXTERNALLY DRIVEN, i.e., BY INPUT
C     DIRECTLY GIVE TO THE MNCAD MODULE, OR FROM INPUT TO
C     ST2 OF THE PRIMARY CLOCK (MNCKW), THE PROGRAM WAITS
C     TILL THE USER GIVES THE COMMAND BEFORE CALLING THE
C     SUBPROGRAM ADSWP. ADSWP ARMS AND ENABLES THE
C     SAMPLING PROCESS IMMEDIATELY IN THIS MODE.
C
      TYPE 1019
1019  FORMAT(5X,'SPECIFY NUMBER OF CYCLES(1,2,3,4,5 OR 6)
    1   '$)
      ACCEPT 2019,M
2019  FORMAT(I)
      TYPE 2222
2222  FORMAT(5X,'WHICH UNIT IS TO BE OPENED?'  $)
      ACCEPT 2223,IUNIT
2223  FORMAT(I)
      IF(IUNIT.EQ.3) GO TO 666
      OPEN(UNIT=2,NAME='FILE.DAT',TYPE='NEW',DISP='SAVE')
      GO TO 667
 666  OPEN(UNIT=3,NAME='FBUF1.DAT',TYPE='NEW',DISP='SAVE'
    1 )
 667  DO 31 I=1,M
      CALL SETIBF(INFO,IND,IBUF(1,1),IBUF(1,2),IBUF(1,3),
    1 IBUF(1,4),IBUF(1,5),IBUF(1,6),IBUF(1,7),IBUF(1,8))
```

```
      CALL RLSBUF(INFO,IND,0,1,2,3,4,5,6,7)
      CALL CLOCKA(4,,IND)
      MODE=256
      CALL ADSWP(INFO,1000,8,MODE,-1,,,ICHN,NCHN)
      IF(INFO(1).NE.0) STOP 'ADSWP - LIBGEN OR
     1 CONFIGURATION ERROR.'
C
C     THE DEFAULTED ARGUMENTS INDICATE THAT THE SWEEP HAS
C     NO DELAY FROM THE START EVENT, AND NO COMPLETION
C     ROUTINE IS ASSOCIATED WITH IT.
C
C     AT THE OPERATOR'S COMMAND THE SWEEP WILL BEGIN.
C
      TYPE 1024
 1024 FORMAT(' STRIKE THE "RETURN" KEY TO START THE SWEEP
     1 . '$)
      ACCEPT 2000,ANS
      CALL DIGO(,,,IND)
C
C     WAIT FOR EACH BUFFER, CONVERT THE INPUT TO ACTUAL
C     VALUES, TYPE THE ACTUAL VALUES, AND THEN GO GET
C     NEXT BUFFER.
C
   60 CALL CAD2FP(IBUF(1,(IWTBUF(INFO,,ID,IND)+1)),FBUF,
     1 1000)
      IF(IUNIT.EQ.3) GO TO 444
      WRITE(2,33)FBUF
      GO TO 445
  444 WRITE(3,33)FBUF
  445 CONTINUE
   33 FORMAT(F)
      IF(INFO(1).EQ.0) GO TO 60
   31 CONTINUE
      IF(IUNIT.EQ.3)GO TO 888
      CLOSE(UNIT=2,DISP='SAVE')
      GO TO 889
  888 CLOSE(UNIT=3,DISP='SAVE')
C
C     WHEN ALL DATA ARE ACQUIRED, PRINT THE RAW DATA AND
C     END.
C
  889 CONTINUE
      TYPE 1026,INFO(1)
 1026 FORMAT(/' A/D SWEEP ENDING CODE = 'I3)
```

```
STOP
END
```

```
C
C                         CROSS.FOR
C                  CROSSCORRELATION SEQUENCE
C       IN ORDER TO CROSSCORRELATE TWO SIGNALS,TWO
C       PROGRAMS MUST BE EXECUTED IN THE ORDER THAT THEY
C       APPEAR BELOW:
C
C              (1)...RUN CROS1
C              (2)...RUN CROSS
C
C       THE FIRST,'CROS1',CONVERTS A/D.DATA IS GATHERED FROM
C       THE FIRST TWO CHANNELS ON THE A/D BOARD AND 8,000
C       POINTS ARE STORED IN A SINGLE FILE CALLED FILE.DAT.
C       THE A/D BOARD SAMPLES AT A RATE OF 1MSEC.,THEREFORE
C       DATA MUST BE GATHERED FOR 8 SECONDS.
C
C       THE 2ND,'CROSS',IS THE ACTUAL CROSSCORRELATION.
C       TWO SIGNAL FILES ARE CREATED FROM THE ONE CREATED
C       BY CROS1.
C       THE TWO SIGNAL FILES ARE MULTIPLIED AND THEN
C       INTEGRATED EACH TIME THE PROGRAM GOES THROUGH ITS
C       MAIN LOOP ONE VALUE OF THE CROSS-CORRELATION
C       COEFFICIENT IS STORED IN THE VARIABLE LOCATION
C       SUMT.EACH POINT CORRESPONDS TO A DELAY TIME EQUAL
C       TO 1MSEC.EXCEPT FOR THE FIRST WHICH CORRESPONDS TO
C       A DELAY TIME EQUAL TO 0.0 MSEC. 300 VALUES OF THE
C       CROSS-CORRELATION COEFFICIENT ARE PRINTED,THEREFORE
C       A TOTAL DELAY TIME OF 299 MSEC IS SHOWN.THE PROGRAM
C       SEARCHES THE 300 POINTS AND LOCATES THE MAXIMUM
C       CROSS-CORRELATION VALUE AND THE TIME CORRESPONDING
C       TO THIS MAXIMUM.THE PROGRAM THEN CALCULATES A
C       PARTICLE VELOCITY BASED ON A 2.16 FT PROBE SEPARATION.
C       THIS PROGRAM ALSO CALCULATES THE VOIDAGE(E),THE GAS
C       VELOCITY(VG),THE SLIP VELOCITY(VS),THE ACTUAL GAS
C       RATE(SCFMA),THE SOLID FLOW RATE(WS),AND THE
C       THE LOADING.
C       DURING EXECUTION A NUMBER OF QUESTIONS ARE ASKED.
C
C
C
        DIMENSION FBUF(2500),FBUF1(2500),RMULT(2200),
     1  SUMT(300)
        TYPE 2990
2990    FORMAT(5X,'THIS MONTH IS? (1-12)'$)
```

```
      ACCEPT 2991,KMON
2991  FORMAT(I)
      TYPE 2992
2992  FORMAT(5X,'TODAYS DATE IS?'$)
      ACCEPT 2993,KDATE
2993  FORMAT(I)
      TYPE 2994
2994  FORMAT(5X,'THIS YEAR IS?'$)
      ACCEPT 2995,KYEAR
2995  FORMAT(I)
      TYPE 2996
2996  FORMAT(5X,'PRINT TRIAL NUMBER'$)
      ACCEPT 3001,KTN
3001  FORMAT(I)
      TYPE 3002
3002  FORMAT(5X,'PRINT TAPE NUMBER'$)
      ACCEPT 3003,KTAPN
3003  FORMAT(I)
      TYPE 3004
3004  FORMAT(5X,'TAPE FOOTAGE,BEGINNING NUMBER ?'$)
      ACCEPT 3005,KBTAF
3005  FORMAT(I)
      TYPE 3006
3006  FORMAT(5X,'TAPE FOOTAGE,END?'$)
      ACCEPT 3007,KENTA
3007  FORMAT(I)
      TYPE 3008
3008  FORMAT(5X,'TAPE SIDE ?'$)
      ACCEPT 3009,KTS
3009  FORMAT(I)
      TYPE 4000
4000  FORMAT(5X,'SOLID FLOW RATE (LBS/MIN) ?'$)
      ACCEPT 4001,WS
4001  FORMAT(F)
      TYPE 4002
4002  FORMAT(5X,'AIR HUMIDITY ?'$)
      ACCEPT 4003,AH
4003  FORMAT(F)
      TYPE 3010
3010  FORMAT(5X,'WHAT IS THE TURBINEMETER READING
     1 (SCFM) ?'$)
      ACCEPT 3011,SCFM
3011  FORMAT(F)
      DWELL=.001
```

```
      TYPE 2003
2003  FORMAT(5X,'SOLID DENSITY (LBS/FT-3) ?'$)
      ACCEPT 2004,DEN
2004  FORMAT(F)
C*******************************************************
C     THIS STATEMENT IS USED TO CALCULATE THE ACTUAL GAS
C     FLOW RATE.SCFM IS THE TURBINEMETER READING.
C
      SCFMA=SCFM
C
C*******************************************************
C
C*******************************************************
C     THIS STATEMENT IS USED TO CALCULATE THE ACTUAL
C     LOADING (ALOAD).
C
      ALOAD=379*WS/(SCFMA*29)
C
C
C
C*******************************************************
C
C*******************************************************
C     THE OPEN STATEMENT READ IN THE TWO SIGNAL FILES.FBUF
C     IS THE VARIABLE NAME FOR SIG1.DAT,AND FBUF1 IS THE
C     VARIABLE NAME FOR SIG2.DAT.
C
      OPEN(UNIT=2,NAME='FILE.DAT',TYPE='OLD',DISP='SAVE')
       DO 6 ID=1,2500
      READ(2,7)FBUF(ID)
      READ(2,7)FBUF1(ID)
6     CONTINUE
41    PRINT 42
42    FORMAT('RING PROBES WERE USED',/)
46    ADD1=0.0
      ADD2=0.0
      DO 45 I=1,2500
      ADD1=ADD1+FBUF(I)
      ADD2=ADD2+FBUF1(I)
45    CONTINUE
      IF(ADD1.GE.0.0)GO TO 47
      DO 48 I=1,2500
      FBUF(I)=-FBUF(I)
48    CONTINUE
```

```
47      IF(ADD2.GE.0.0)GO TO 49
        DO 145 I=1,2500
        FBUF1(I)=-FBUF1(I)
145     CONTINUE
        ADD1=0.0
        ADD2=0.0
49      DO 43 I=1,2500
        IF(FBUF(I).LE.0.0)FBUF(I)=0.0
        IF(FBUF1(I).LE.0.0)FBUF1(I)=0.0
43      CONTINUE
C*****************************************************
C
C*****************************************************
        DO 80 I=1,625
        TOTAL1=0.0
        TOTAL2=0.0
        DO 90 J=1,2
        M=J+(I-1)*2
        TOTAL1=TOTAL1+FBUF(M)
        TOTAL2=TOTAL2+FBUF1(M)
90      CONTINUE
        AVG1=TOTAL1/2.0
        AVG2=TOTAL2/2.0
        DO 100 K=1,2
        M1=K+(I-1)*2
        FBUF(M1)=AVG1
        FBUF1(M1)=AVG2
        ADD1=ADD1+FBUF(M1)
        ADD2=ADD2+FBUF1(M1)
100     CONTINUE
80      CONTINUE
        THRES1=0.5*ADD1/2500.0
        THRES2=0.5*ADD2/2500.0
C
C*****************************************************
C
C*****************************************************
C       THE FOLLOWING STATEMENT SET THE THRESHOLD VALUE.
C
        DO 10 I=1,2500
        IF(FBUF1(I).LE.THRES2)FBUF1(I)=0.0
        IF(FBUF(I).LE.THRES1)FBUF(I)=0.0
10      CONTINUE
C
```

```
C********************************************************
C
C********************************************************
C       THIS IS WHERE THE PROGRAM MULTIPLIES AND INTEGRATES
C       THE TWO SIGNAL FILES.
C
        DO 11 J=1,300
        DO 12 I=1,2200
        K=I+J
        RMULT(I)=FBUF(K)*FBUF1(I)
12      CONTINUE
        SUM=0.0
        DO 60 I=1,2199
        C12=(RMULT(I+1)+RMULT(I))*DWELL/2.0
        SUM=SUM+C12
60      CONTINUE
        SUMT(J)=SUM
11      CONTINUE
C
C*****************************************************
C
C*****************************************************
C       THIS STATEMENT TAKES THE GAS FLOW RATE AND DIVIDES
C       IT BY THE PRODUCT OF THE CROSS SECTIONAL AREA AND
C       THE REQUIRED TIME CONVERSION FROM MINUTES TO
C       SECONDS.
C
        GV=SCFMA/1.3712427
C
C*****************************************************
C
C*****************************************************
        PRINT 101,KMON,KDATE,KYEAR
101     FORMAT(/,'DATE',2X,I,2X,I,2X,I,//)
        PRINT 102,KTN
102     FORMAT('TRIAL NUMBER',2X,I,//)
        PRINT 103,KTAPN
103     FORMAT('TAPE NUMBER',2X,I,//)
        PRINT 104,KBTAF,KENTA
104     FORMAT('TAPE FOOTAGE',1X,I,'-',I,//)
        PRINT 105,KTS
105     FORMAT('TAPE SIDE',2X,I,//)
        PRINT 106
106     FORMAT(50X,'CROSSCORRELATION DATA',//)
```

```
      PRINT 369,SUMT
369   FORMAT(10(F10.7,2X),/)
C
C*****************************************************
C
C*****************************************************
C     THE FOLLOWING STATEMENTS SEARCH THE CROSS-
C     CORRELATION DATA TO LOCATE TIMES WHEN MAXIMUMS
C     OCCUR.
      TAU=2166.67/GV
      KOUNT=0
      TIME=0.0
      DO 500 I=1,298
      TIME=TIME+1.0
      IF(SUMT(I).GE.SUMT(I+1)) GO TO 134
      IF(SUMT(I).LT.SUMT(I+1)) GO TO 831
831   CONTINUE
      IF(SUMT(I+1).LT.SUMT(I+2)) GO TO 134
      IF(SUMT(I+1).GT.SUMT(I+2)) GO TO 832
832   PRINT 833,TIME,SUMT(I+1)
833   FORMAT('A MAXIMUM OCCURED,TIME(MSEC.)=',F5.1,5X,
     1 F11.7,/)
134   IF(TIME.LT.TAU) GO TO 500
      IF(KOUNT.EQ.1) GO TO 500
      N=I
      KOUNT=KOUNT+1
      T=TIME
500   CONTINUE
C
C*****************************************************
C
C*****************************************************
C     THESE STATEMENTS LOCATE THE MAXIMUM CROSSCORRELATION
C     VALUE AND THE CORRESPONDING DELAY INTERVAL.
C
900   PMAX=SUMT(N)
      KDT=1
      DO 368 I=N,300
      IF(SUMT(I).LT.PMAX) GO TO 350
      PMAX=SUMT(I)
      TIMAX=T
350   T=T+KDT
368   CONTINUE
C
```

```
C*******************************************************
C
C*******************************************************
C       THIS STATEMENT CALCULATES THE PARTICLE VELOCITY.
C       SINCE TIME IS IN SECONDS INSTEAD OF MSEC. A FACTOR
C       OF 1,000 APPEARS IN THE NUMERATOR.
C
        PV=2167.67/TIMAX
C
C*******************************************************
C
C*******************************************************
C       THE NEXT TWO STATEMENTS ARE USED TO CALCULATE THE
C       VOIDAGE(E).
C
        EA=0.72963*ALOAD*SCFMA/(PV*DEN)
        E=1-EA
C
C*******************************************************
C
C*******************************************************
C       THIS STATEMENT CALCULATES THE SLIP VELOCITY.
C
        SV=(GV/E)-PV
C
C*******************************************************
C
C*******************************************************
        PRINT 132,AH
132     FORMAT('AIR HUMIDITY(%)',2X,F5.2,//)
        PRINT 131,ALOAD
131     FORMAT('LOADING',2X,F6.3,//)
        PRINT 358,SCFMA
358     FORMAT('AIR FLOW RATE(SCFM)',2X,F6.3,//)
        PRINT 701,E
701     FORMAT('VOIDAGE',2X,'E=',F,//)
        PRINT 702,WS
702     FORMAT('SOLID FLOW RATE (LBS/MIN)',2X,'WS=',F5.3,//)
        PRINT 703,GV
703     FORMAT('GAS VELOCITY (FT/SEC)',2X,'VG=',F6.3,//)
        PRINT 704,PV
704     FORMAT('PARTICLE VELOCITY (FT/SEC)',2X,'VP=',
     1  F6.3,//)
        PRINT 705,SV
```

```
705     FORMAT('SLIP VELOCITY (FT/SEC)',2X,'VS=',F6.3,//)
        CLOSE(UNIT=3)
        CLOSE(UNIT=4)
        STOP
        END
```

```
C PROGRAM TO CALCULATE CHOKING AND SALTATION
C VELOCITIES
C
100     PRINT*,'INPUT THE PARTICLE DENSITY'
        READ*,RP
        RF=1.2
        XMU=1.E-5
        G=9.8
        D=.0508
        A=3.1415*D**2/4
        PRINT*,'INPUT THE PARTICLE DIAMETER'
        READ*,DP
        DP=DP*1.E-6
        PRINT*,'INPUT THE MASS FLOW RATE'
        READ*,WS
        FPC=6.81E5*(RF/RP)**2.2
        PRINT*,'INPUT AN INITIAL GUESS FOR UFC'
        READ*,GUESS
        UFL=GUESS
        DO 10 I=1,500
        UT=.153*G**.71*DP**1.14*(RP-RF)**.71
        UT=UT/(RF**.29*XMU**.43)
        UF=(2*G*D*((1-(WS/((UFL-UT)*RP*A)))**-4.7-1)/FPC)**.5
        UF=UF+UT
        ERR=ABS(UF-UFL)
        IF(ERR.LT..0001) THEN
        GOTO 20
        ENDIF
        UFL=UF
10      CONTINUE
        PRINT*,'DID NOT CONVERGE FOR YANG'
        GOTO 30
20      PRINT*,'UFC YANG = ',UF
30      CONTINUE
        DP=DP*1000.
        UGSALT=WS/(RF*A)*10.**(1.44*DP+1.96)
        UGSALT=UGSALT*(G*D)**((1.18*DP+2.5)/2)
        UGSALT=UGSALT**(1/(1.1*DP+3.5))
        PRINT*,'SALTATION VELOCITY BY RIZK= ',UGSALT
        DP=DP/1000.
        PRINT*,'INPUT AN INITIAL GUESS FOR OWENS SALTATION'
        READ*,UFLO
        DO 40 I=1,500
        FG=.0014+.125/((RF*D*UFLO)/XMU)**.32
```

```
      UGSALT=(.01*(2*RP*G*DP)/(RF*FG))**.5
      ERR=ABS(UGSALT-UFLO)
      IF(ERR.LT..0001) THEN
      GOTO 60
      ENDIF
      UFLO=UGSALT
40    CONTINUE
      PRINT*,'DID NOT CONVERGE FOR OWENS'
      GOTO 50
60    PRINT*,'SALTATION VELOCITY BY OWENS = ',UGSALT
50    CONTINUE
      PRINT*,' INPUT AN INITIAL GUESS FOR ROSE'
      READ*,UFL
      DO 70 I=1,500
      WG=RF*A*UFL
      UGCR=3.2*(WS/WG)**.2*(D/DP)**.6*(RP/RF)**-.7
      UGCR=UGCR*(UFL/(G*D)**.5)**.5
      UGCR=UGCR*UT
      ERR=ABS(UGCR-UFL)
      IF(ERR.LT..0001) THEN
      GOTO 80
      ENDIF
      UFL=UGCR
70    CONTINUE
      PRINT*,'DID NOT CONVERGE FOR ROSE AND DUCKWORTH'
      GOTO 90
80    PRINT*,'CHOKING VLOCITY BY ROSE AND DUCKWORTH = ',UGCR
90    CONTINUE
      PRINT*,'INPUT A 1 TO CONTINUE'
      READ*,Z
      IF(Z.EQ.1.) THEN
      GOTO 100
      ENDIF
      STOP
      END
```

```
C   LINEAR STABILITY
C       DT=PIPE DIAMETER
C       DP=PARTICLE DIAMETER
C       UPS=PARTICLE VELOCITY
C       UFS=GAS VELOCITY
C       RP=PARTICLE DENSITY
C       RF=FLUID DENSITY
C       PRESS=PRESSURE DROP
C       XM1,XM2 ARE THE EIGENVALUES
C       IRUN IS THE EXPERIMENTAL RUN NUMBER
C
        OPEN(UNIT=10,FILE='INPUT.DAT')
        DT=0.0508
        RF=1.2
        GRAV=9.8
        PRINT*,'INPUT PARTICLE DIAMETER IN MICRONS'
        READ*,DP
        DP=DP*1.E-6
        PRINT*,'INPUT ANGLE OF INCLINATION IN DEGREES'
        READ*,ANGLE
        THETA=ANGLE/180.*3.1415
        PRINT*,SIN(THETA),' IS THE SIN OF THETA'
C       GET CONSTANTS FOR PARTICLE VELOCITY AS FUNCTION
C       OF GAS VELOCITY (LINEAR)
        PRINT*,'INPUT THE SLOPE'
        READ*,SLOPE
        PRINT*,'INPUT THE INTERCEPT'
        READ*,INTER
        OPEN(UNIT=11,FILE='OUTPUT.DAT')
5       WRITE(11,200)
        WRITE(11,210)
        WRITE(11,220)
        WRITE(11,210)
        WRITE(11,200)
        WRITE(11,210)
200     FORMAT(5('_____________'))
210     FORMAT('  ')
220     FORMAT(4X,'RUN',7X,'Ug',8X,'Uf',10X,'M1',10X,'M2')
        READ(10,110)NDAT,RP,IRUN
110     FORMAT(I,F,I)
        IF(NDAT.EQ.999) THEN
        GOTO 1000
        ENDIF
        DO 10 I=1,NDAT
```

```
      READ(10,100)WS,UFS,UPS,PRE,DUMMY1,DUMMY2,DUMMY3
100   FORMAT(7F)
      RE=DT*UFS*3.28*0.07476/(1.24E-5)
      FG=0.0791/RE**0.25
      DPG=2*FG*UFS**2*0.07476*10/0.170583
      DPG=DPG*760/(32.174*14.696*144)
      DIFF=DUMMY2-DPG
      PRESS=PRE-DIFF
C     CONVERSION TO SI UNITS
      WS=WS*7.56E-3
      UFS=UFS*0.3048
      UPS=UPS*0.3048
      PRESS=PRESS*43.74097
      RP=RP*16.02
      UPS=SLOPE*UFS+INTER
      E=1-(4*WS/(3.1415*DT**2*UPS*RP))
C     CALC DRAG COEFF
      REP=RF*DP*(UFS/E-UPS)/1.E-5
      CDS=18.5*E**-4.7/REP**.6
      UFS=UFS/E
      FS=0.0285*(GRAV*DT)**.5/UPS
C     GET CONSTANTS FOR LINEAR ANALYSIS
      A=3*CDS*RF/(4*RP*DP)
      B=GRAV*SIN(THETA)+PRESS/RP
      C=2*FS/DT
      D=GRAV*SIN(THETA)+PRESS/RF
      EE=2*FG/DT
      A0=A*(UFS-UPS)**2-B-C*UPS**2
      A1=2*A*(UFS-UPS)
      A2=-2*C*UPS
      B0=-A*(UFS-UPS)**2-D-EE*UFS**2
      B1=-2*A*(UFS-UPS)
      B2=-2*EE*UFS
      XL1=(A1-B1-B2-A2)
      XL2=A2*B1+A2*B2-A1*B2
      XL3=A1*B0-A0*B1-A0*B2+A2*B1*UPS-A1*B2*UPS+A2*B2*UPS
C     D2+L1XD1+L2=L3
      XM1=-XL1+(XL1**2-4*XL2)**.5
      XM1=XM1/2
      XM2=-XL1-(XL1**2-4*XL2)**.5
      XM2=XM2/2
      UFS=UFS*E
      WRITE(11,250)IRUN,UFS,UPS,XM1,XM2
250   FORMAT(4X,I3,5X,F5.2,5X,F5.2,5X,F8.3,5X,F8.3)
```

```
          IRUN=IRUN+1
          RP=RP/16.02
10        CONTINUE
          WRITE(11,260)
260       FORMAT('1')
          GOTO 5
1000      STOP
          END
```

```
C   PROGRAM TO CALCULATE PRESSURE DROP
C   RATIOS WITH YANG AND KONNO SAITO
C       DT=PIPE DIAMETER
C       DP=PARTICLE DIAMETER
C       UPS=PARTICLE VELOCITY
C       UFS=GAS VELOCITY
C       RP=PARTICLE DENSITY
C       RF=FLUID DENSITY
C       PRESS=PRESSURE DROP
C       IRUN IS THE EXPERIMENTAL RUN NUMBER
C       DPKS = PRESSURE DROP BY KONNO-SAITO
C       DPY  = PRESSURE DROP BY YANG
C
C       OPEN INPUT FILE
C
        OPEN(UNIT=10,FILE='INPUT.DAT')
        DT=0.0508
        RF=1.2
        GRAV=9.8
C       GET DP AND ANGLE FROM SCREEN
        PRINT*,'INPUT PARTICLE DIAMETER IN MICRONS'
        READ*,DP
        DP=DP*1.E-6
        PRINT*,'INPUT ANGLE OF INCLINATION IN DEGREES'
        READ*,ANGLE
        THETA=ANGLE/180.*3.1415
C       OPEN OUTPUT FILES
        OPEN(UNIT=11,FILE='ROUT.DAT')
        OPEN(UNIT=12,FILE='ROUTY.DAT')
        OPEN(UNIT=13,FILE='MEAN.DAT',ACCESS='APPEND')
210     FORMAT('  ')
C       READ DATA AND CHEK FOR END OF FILE
5       READ(10,110)NDAT,RP,IRUN
        PRINT*,'NDAT IS ',NDAT
110     FORMAT(I,F,I)
        IF(NDAT.EQ.999) THEN
        GOTO 1000
        ENDIF
        DO 10 I=1,NDAT
        READ(10,100)WS,UFS,UPS,PRE,DUMMY1,DUMMY2,DUMMY3
100     FORMAT(7F)
        RE=DT*UFS*3.28*0.07476/(1.24E-5)
        FG=0.0791/RE**0.25
        DPG=2*FG*UFS**2*0.07476*10/0.170583
```

```
      DPG=DPG*760/(32.174*14.696*144)
      DIFF=DUMMY2-DPG
      PRESS=PRE-DIFF
C     CONVERSION TO SI UNITS
      WS=WS*7.56E-3
      UFS=UFS*0.3048
      UPS=UPS*0.3048
      PRESS=PRESS*43.73097
      RP=RP*16.02
      E=1-(4*WS/(3.1415*DT**2*UPS*RP))
      UFS=UFS/E
C     CALC TERMINAL VELOCITY
      UT=0.153*GRAV**.71*DP**1.14*(RP-RF)**.71
C     CALC PRESSURE DROP BY KONNO SAITO AND
C     GET THE RATIO RATIOK
      UPKS=E*UFS-UT
      FSKS=0.0285*(GRAV*DT)**.5/UPKS
      EKS=1-(4*WS/(3.1415*DT**2*(RP-RF)*UPKS))
      DPKS=(1-EKS)*GRAV*SIN(THETA)*RP+RF*EKS*GRAV*SIN(THETA)
      DPKS=DPKS+2*FG*RF*UFS**2/DT
      DPKS=DPKS+2*FSKS*RP*(1-EKS)*UPKS**2/DT
      RATIOK=PRESS/DPKS
      DEVKS=ABS((PRESS-DPKS)/PRESS)*100
C     DECIDE WHICH YANG CORRELATION TO USE
C     VERTICAL OR HORIZONTAL
      IF(ANGLE.LT.50.) THEN
      GOTO 200
      ENDIF
C     CALC PRESSURE DROP BY YANG
C     FOR VERTICAL PIPE AND
C     PRINT RESULTS TO THE OUTPUT
C     FILE
      UPY=1.
150   EY=1-4*WS/(3.1415*DT**2*(RP-RF)*UPY)
      FSY=((1-EY)*UT/(UFS-UPY))**-0.979
      FSY=FSY*(1-EY)*.00315/EY**3
      UPYC=UFS-UT*SQRT(((1+FSY*UPY**2/(2*GRAV*DT))*EY**4.7))
      ERROR=ABS(UPYC-UPY)
      IF(ERROR.LT.0.0001) THEN
      GOTO 180
      ENDIF
      UPY=UPYC
      GOTO 150
180   DPY=(1-EY)*GRAV*RP+RF*EKS*GRAV
```

```
      DPY=DPY+2*FG*RF*UF**2/DT
      DPY=DPY+2*FSY*RP*(1-EY)*UPY**2/DT
      RATIOY=PRESS/DPY
      DEVY=ABS((PRESS-DPY)/PRESS)*100
      RP=RP/16.02
      WRITE(11,350)UFS,RATIOK
      WRITE(12,350)UFS,RATIOY
      WRITE(13,370)DEVKS,DEVY
      GOTO 10
C     CALC PRESSURE DROP BY YANG FOR
C     THE HORIZONTAL PIPE AND PRINT
C     RESULTS TO THE OUTPUT FILES
200   UPY=1.
205   EY=1-4*WS/(3.1415*DT**2*(RP-RF)*UPY)
      IF(EY.GT.0.9999) THEN
      EY=.99999
      ENDIF
      FSY=.0293*(1-EY)/EY**3
      FSY=FSY*((1-EY)*UFS/(GRAV*DT)**.5)**-1.15
      UPYC=UFS-UT*SQRT(((1+FSY*UPY**2/(2*GRAV*DT))*EY**4.7))
      IF(UPYC.LT.0.0) THEN
      UPYC=ABS(UPYC)
      ENDIF
      ERROR=ABS(UPYC-UPY)
      IF(ERROR.LT.0.0001) THEN
      GOTO 300
      ENDIF
      UPY=UPYC
      GOTO 205
300   DPY=2*FG*RF*UFS**2/DT
      DPY=DPY+2*FSY*RP*(1-EY)*UPY**2/DT
      RATIOY=PRESS/DPY
      DEVY=ABS((PRESS-DPY)/PRESS)*100
      UFS=UFS*E
      WRITE(11,350)UFS,RATIOK
      WRITE(12,350)UFS,RATIOY
      WRITE(13,370)DEVKS,DEVY
350   FORMAT(F,',',F)
15    RP=RP/16.02
10    CONTINUE
      WRITE(11,360)IRUN
      WRITE(12,360)IRUN
      WRITE(13,360)IRUN
360   FORMAT('RUNS ABOVE BEGAN AT RUN ',I)
```

```
370    FORMAT(F,5X,F)
       GOTO 5
1000   END
```

APPENDIX D.
EXPERIMENTAL DATA

125 MICRON GLASS BEADS
VERTICAL ORIENTATION
HIGH HUMIDITY

RUN	GAS VELOCITY m/sec	SOLIDS VELOCITY m/sec	SOLIDS FLOW kg/sec	PRESS Pa/m	AIR PRESS Pa/m	VOIDAGE	LOADING
34	14.67	12.01	6.7E-3	55.74	51.91	.9999	.183
35	10.78	8.60	7.9E-3	34.11	30.27	.9998	.295
36	8.62	7.26	8.6E-3	23.04	20.49	.9998	.400
37	7.65	5.37	8.7E-3	17.87	16.60	.9997	.455
38	6.05	4.37	9.1E-3	14.83	11.00	.9996	.600
39	5.16	4.89	9.4E-3	15.99	8.33	.9996	.727
40	4.36	3.32	9.1E-3	17.69	6.20	.9994	.833

TEMP= 25.0 C HUMIDITY= 57.2 MASS RATE= 8.5E-3 kg/sec

125 MICRON GLASS BEADS
VERTICAL ORIENTATION
LOW HUMIDITY

RUN	GAS VELOCITY m/sec	SOLIDS VELOCITY m/sec	SOLIDS FLOW kg/sec	PRESS Pa/m	AIR PRESS Pa/m	VOIDAGE	LOADING
26	14.24	11.39	7.3E-3	52.21	49.29	.9999	.206
27	10.14	7.68	8.8E-3	37.39	27.18	.9998	.346
28	7.00	4.72	9.1E-3	32.10	14.23	.9996	.523
29	6.14	5.90	9.1E-3	30.44	11.29	.9997	.598
30	5.45	4.55	9.5E-3	25.76	9.16	.9996	.694
31	5.07	4.68	9.5E-3	25.96	8.08	.9996	.746
32	4.42	3.93	8.8E-3	28.08	6.37	.9996	.793
33	4.22	2.75	8.8E-3	27.58	5.87	.9994	.831

TEMP= 35.0 C HUMIDITY= 18.0 MASS RATE= 8.9E-3 kg/sec

125 MICRON GLASS BEADS
VERTICAL ORIENTATION
HIGH HUMIDITY

RUN	GAS VELOCITY m/sec	SOLIDS VELOCITY m/sec	SOLIDS FLOW kg/sec	PRESS Pa/m	AIR PRESS Pa/m	VOIDAGE	LOADING
9	12.67	9.05	18.1E-3	50.38	40.16	.9996	.570
10	11.91	7.26	17.8E-3	46.28	36.07	.9995	.597
11	10.18	7.26	18.1E-3	41.43	27.39	.9995	.713
12	8.40	5.79	18.2E-3	40.00	19.58	.9994	.867
13	6.89	5.12	19.0E-3	37.67	13.84	.9993	1.101
14	5.49	4.75	19.4E-3	29.72	9.29	.9992	1.410
16	7.98	5.04	18.9E-3	28.96	17.88	.9992	.947
17	6.11	5.84	18.9E-3	29.07	11.19	.9993	1.238
48	11.69	7.59	17.2E-3	45.11	34.90	.9995	.587
49	8.89	6.61	18.2E-3	34.38	21.61	.9994	.820
50	7.25	6.29	19.3E-3	39.36	15.10	.9994	1.064
51	6.58	5.64	18.8E-3	43.41	12.76	.9993	1.144
52	6.14	5.28	18.7E-3	35.55	11.29	.9993	1.217
53	5.40	4.62	18.5E-3	34.57	9.03	.9992	1.372
54	4.67	4.57	17.5E-3	37.64	6.99	.9992	1.497
82	10.67	7.59	16.6E-3	37.40	29.74	.9996	.623
83	8.16	6.29	17.0E-3	35.18	18.58	.9995	.834
84	7.07	6.60	17.6E-3	37.45	14.46	.9995	.997
85	6.36	5.20	18.6E-3	37.55	12.02	.9993	1.170
86	5.64	4.86	19.3E-3	30.19	9.76	.9992	1.366

TEMP= 22.5 C HUMIDITY= 52.0 MASS RATE= 18.3E-3 kg/sec

125 MICRON GLASS BEADS
VERTICAL ORIENTATION
LOW HUMIDITY

RUN	GAS VELOCITY m/sec	SOLIDS VELOCITY m/sec	SOLIDS FLOW kg/sec	PRESS Pa/m	AIR PRESS Pa/m	VOIDAGE	LOADING
19	16.76	12.23	18.3E-3	71.07	65.54	.9997	.388
20	13.38	7.59	18.3E-3	56.96	44.19	.9995	.547
21	10.63	10.16	18.9E-3	44.07	29.52	.9996	.712
22	8.36	6.17	18.9E-3	39.82	19.39	.9994	.905
23	6.14	5.04	19.0E-3	46.28	11.29	.9992	1.237
24	5.80	5.74	19.1E-3	40.24	10.23	.9993	1.319
25	5.02	4.68	19.1E-3	41.79	7.96	.9992	1.523
76	10.40	8.36	18.3E-3	44.40	28.44	.9996	.704
77	8.22	7.86	18.7E-3	41.32	18.85	.9995	.908
78	7.45	5.69	19.4E-3	38.32	15.84	.9993	1.044
79	6.78	6.74	19.3E-3	39.62	13.44	.9994	1.138
80	6.49	4.97	19.3E-3	38.77	12.46	.9992	1.188
81	5.78	5.69	18.7E-3	39.92	10.17	.9993	1.298

TEMP= 35.0 C HUMIDITY= 16.0 MASS RATE= 18.8E-3 kg/sec

125 MICRON GLASS BEADS
VERTICAL ORIENTATION
HIGH HUMIDITY

RUN	GAS VELOCITY m/sec	SOLIDS VELOCITY m/sec	SOLIDS FLOW kg/sec	PRESS Pa/m	AIR PRESS Pa/m	VOIDAGE	LOADING
56	14.94	12.95	23.2E-3	66.87	53.57	.9996	.622
57	10.22	7.86	25.6E-3	50.56	27.60	.9993	1.003
58	8.54	7.68	25.9E-3	58.44	20.12	.9993	1.214
59	6.98	6.60	26.5E-3	57.54	14.14	.9992	1.517
60	6.00	5.74	26.2E-3	49.18	10.86	.9991	1.745
61	4.71	4.65	24.3E-3	51.80	7.11	.9989	2.062
63	6.75	6.74	28.1E-3	55.47	13.35	.9992	1.666
64	8.71	7.18	28.6E-3	57.82	20.86	.9992	1.314
65	11.16	7.18	28.0E-3	52.71	32.16	.9992	1.003

TEMP= 25.0 C HUMIDITY= 51.7 MASS RATE= 26.3E-3 kg/sec

125 MICRON GLASS BEADS
VERTICAL ORIENTATION
LOW HUMIDITY

RUN	GAS VELOCITY m/sec	SOLIDS VELOCITY m/sec	SOLIDS FLOW kg/sec	PRESS Pa/m	AIR PRESS Pa/m	VOIDAGE	LOADING
66	15.96	15.01	25.7E-3	82.16	60.15	.9997	.644
67	13.78	12.01	26.9E-3	61.48	46.53	.9995	.782
68	13.11	11.39	27.4E-3	56.88	42.66	.9995	.836
69	11.25	9.05	28.0E-3	50.60	32.61	.9994	.995
70	9.47	7.59	28.3E-3	46.10	24.13	.9992	1.198
71	8.05	7.18	29.4E-3	46.09	18.15	.9992	1.461
72	6.74	4.75	29.7E-3	46.88	13.29	.9987	1.762
73	6.36	4.59	29.9E-3	51.96	12.01	.9987	1.879
74	5.02	4.40	28.3E-3	59.78	7.96	.9987	2.258
75	5.33	4.65	30.0E-3	64.52	8.84	.9987	2.249

TEMP= 35.0 C HUMIDITY= 16.0 MASS RATE= 28.4E-3 kg/sec

450 MICRON GLASS BEADS
VERTICAL ORIENTATION
HIGH HUMIDITY

RUN	GAS VELOCITY m/sec	SOLIDS VELOCITY m/sec	SOLIDS FLOW kg/sec	PRESS Pa/m	AIR PRESS Pa/m	VOIDAGE	LOADING
89	12.87	9.71	6.5E-3	48.92	41.25	.9999	.203
90	11.52	9.71	8.5E-3	39.09	33.98	.9998	.295
91	8.76	5.62	9.9E-3	31.26	21.04	.9996	.453
92	7.16	6.41	10.6E-3	30.10	14.78	.9997	.592
93	6.40	4.89	10.8E-3	32.59	12.16	.9996	.673
94	5.89	5.04	10.8E-3	34.52	10.52	.9996	.731
95	5.51	4.49	10.6E-3	37.46	9.37	.9995	.768
97	10.36	8.36	9.1E-3	37.16	28.22	.9998	.350
98	7.74	5.55	10.3E-3	32.26	16.94	.9996	.533

TEMP= 20.0 C HUMIDITY= 50.0 MASS RATE= 12.5E-3 kg/sec

450 MICRON GLASS BEADS
VERTICAL ORIENTATION
LOW HUMIDITY

RUN	GAS VELOCITY m/sec	SOLIDS VELOCITY m/sec	SOLIDS FLOW kg/sec	PRESS Pa/m	AIR PRESS Pa/m	VOIDAGE	LOADING
119	15.96	12.95	7.2E-3	66.85	60.15	.9999	.180
120	11.83	7.59	8.9E-3	45.82	35.60	.9998	.300
121	10.45	7.59	9.0E-3	36.83	28.66	.9998	.344
122	9.56	6.67	9.6E-3	34.74	24.53	.9997	.403
123	8.89	5.55	10.1E-3	33.10	21.61	.9996	.455
124	8.00	6.17	11.0E-3	29.46	17.97	.9996	.548
125	7.38	6.17	10.8E-3	25.81	15.59	.9996	.584
126	6.80	5.37	11.0E-3	31.15	13.53	.9996	.645
127	5.74	4.15	10.8E-3	34.30	10.04	.9995	.751
128	6.18	4.05	11.5E-3	33.26	11.43	.9994	.746

TEMP= 35.0 C HUMIDITY= 16.0 MASS RATE= 10.0E-3 kg/sec

450 MICRON GLASS BEADS
VERTICAL ORIENTATION
HIGH HUMIDITY

RUN	GAS VELOCITY m/sec	SOLIDS VELOCITY m/sec	SOLIDS FLOW kg/sec	PRESS Pa/m	AIR PRESS Pa/m	VOIDAGE	LOADING
99	16.67	14.05	17.8E-3	86.62	64.91	.9997	.426
100	14.76	12.01	19.8E-3	72.88	52.45	.9997	.535
101	11.56	7.96	20.9E-3	54.63	34.20	.9995	.723
102	10.36	8.81	22.6E-3	55.04	28.22	.9995	.872
103	9.36	6.95	22.8E-3	46.62	23.63	.9993	.974
104	8.89	8.69	22.6E-3	47.15	21.61	.9995	1.016
105	6.87	5.20	23.0E-3	55.89	13.75	.9991	1.338
107	7.56	5.37	21.5E-3	52.01	16.26	.9992	1.135
108	5.85	3.95	18.3E-3	56.36	10.40	.9991	1.249

TEMP= 23.0 C   HUMIDITY= 50.0   MASS RATE= 22.7E-3 kg/sec

450 MICRON GLASS BEADS
VERTICAL ORIENTATION
LOW HUMIDITY

RUN	GAS VELOCITY m/sec	SOLIDS VELOCITY m/sec	SOLIDS FLOW kg/sec	PRESS Pa/m	AIR PRESS Pa/m	VOIDAGE	LOADING
129	15.34	12.01	16.8E-3	74.09	56.11	.9997	.439
130	14.00	11.79	18.9E-3	61.25	47.84	.9997	.540
131	12.36	11.19	20.8E-3	53.14	38.46	.9996	.673
132	10.74	7.26	21.7E-3	47.42	30.05	.9994	.810
133	10.05	8.36	22.7E-3	42.08	26.78	.9995	.903
134	9.49	5.55	22.6E-3	41.46	24.23	.9992	.952
135	9.16	4.37	22.5E-3	34.89	22.76	.9990	.982
136	7.87	3.86	23.1E-3	43.63	17.45	.9988	1.172
137	6.58	3.51	22.1E-3	42.77	12.76	.9987	1.344
138	5.89	2.75	19.4E-3	43.46	10.52	.9986	1.315
139	16.58	14.05	16.4E-3	77.08	64.31	.9998	.397

TEMP= 35.0 C   HUMIDITY= 16.0   MASS RATE= 20.6E-3 kg/sec

450 MICRON GLASS BEADS
VERTICAL ORIENTATION
HIGH HUMIDITY

RUN	GAS VELOCITY m/sec	SOLIDS VELOCITY m/sec	SOLIDS FLOW kg/sec	PRESS Pa/m	AIR PRESS Pa/m	VOIDAGE	LOADING
109	17.34	7.59	26.0E-3	97.99	69.53	.9993	.600
110	15.04	6.41	30.2E-3	83.05	54.22	.9991	.804
111	11.78	7.26	34.2E-3	64.91	35.36	.9991	1.161
112	9.00	4.62	36.1E-3	54.73	22.08	.9984	1.603
113	7.78	4.49	35.3E-3	62.33	17.11	.9984	1.814
115	7.11	4.89	33.1E-3	47.27	14.62	.9986	1.860
116	8.41	5.95	33.9E-3	62.65	19.60	.9989	1.611
117	9.78	7.26	33.4E-3	62.01	25.53	.9991	1.366
118	10.75	8.81	33.1E-3	73.92	30.15	.9992	1.230

TEMP= 20.0 C   HUMIDITY= 50.0   MASS RATE= 33.3E-3 kg/sec

450 MICRON GLASS BEADS
VERTICAL ORIENTATION
LOW HUMIDITY

RUN	GAS VELOCITY m/sec	SOLIDS VELOCITY m/sec	SOLIDS FLOW kg/sec	PRESS Pa/m	AIR PRESS Pa/m	VOIDAGE	LOADING
140	16.06	11.19	27.4E-3	86.35	60.82	.9995	.683
141	13.28	9.30	31.1E-3	71.70	43.61	.9993	.936
142	11.31	10.48	33.8E-3	57.94	32.92	.9994	1.195
143	10.00	7.96	34.0E-3	54.65	26.56	.9991	1.360
144	8.97	6.67	33.5E-3	51.84	21.96	.9990	1.496
145	8.11	7.50	33.5E-3	52.88	18.41	.9991	1.654
146	7.11	5.74	34.0E-3	57.02	14.63	.9988	1.913
148	7.67	5.74	33.1E-3	50.14	16.68	.9988	1.725
149	6.98	5.04	32.3E-3	51.42	14.14	.9987	1.850

TEMP= 36.5 C   HUMIDITY= 19.4   MASS RATE= 30.0E-3 kg/sec

79 MICRON GLASS BEADS
VERTICAL ORIENTATION
HIGH HUMIDITY

RUN	GAS VELOCITY m/sec	SOLIDS VELOCITY m/sec	SOLIDS FLOW kg/sec	PRESS Pa/m	AIR PRESS Pa/m	VOIDAGE	LOADING
150	11.16	8.36	9.4E-3	33.43	32.16	.9998	.335
151	9.11	6.11	9.6E-3	28.54	22.56	.9997	.423
152	8.36	3.86	9.6E-3	29.61	19.39	.9995	.461
153	7.62	3.51	9.8E-3	19.07	16.51	.9994	.516
154	6.62	3.77	9.8E-3	20.57	12.91	.9995	.594
155	5.82	2.29	9.8E-3	20.52	10.31	.9991	.675
156	6.53	5.69	9.9E-3	18.99	12.61	.9996	.608
157	5.20	3.07	9.7E-3	12.29	8.46	.9994	.749
158	4.18	3.37	7.7E-3	13.43	5.77	.9995	.733
159	4.71	3.93	9.2E-3	17.33	7.11	.9995	.778

TEMP= 20.0 C HUMIDITY= 53.7 MASS RATE= 9.5E-3 kg/sec

79 MICRON GLASS BEADS
VERTICAL ORIENTATION
LOW HUMIDITY

RUN	GAS VELOCITY m/sec	SOLIDS VELOCITY m/sec	SOLIDS FLOW kg/sec	PRESS Pa/m	AIR PRESS Pa/m	VOIDAGE	LOADING
200	12.00	5.00	8.5E-3	41.64	38.54	.9997	.283
201	10.43	6.60	8.5E-3	31.61	28.55	.9997	.326
202	8.31	6.60	9.0E-3	25.60	19.21	.9997	.432
203	7.16	4.89	9.1E-3	20.53	14.78	.9996	.507
204	5.69	5.16	9.1E-3	15.00	9.90	.9996	.638
205	5.91	4.23	9.3E-3	16.33	10.58	.9996	.627
206	5.38	3.83	9.1E-3	16.63	8.97	.9995	.675
207	5.10	2.71	9.0E-3	14.55	8.17	.9993	.704
208	4.36	3.83	7.0E-3	13.22	6.20	.9996	.642
209	6.94	5.74	9.1E-3	26.50	13.99	.9997	.523

TEMP= 20.0 C HUMIDITY= 16.0 MASS RATE= 8.8E-3 kg/sec

79 MICRON GLASS BEADS
VERTICAL ORIENTATION
LOW HUMIDITY

RUN	GAS VELOCITY m/sec	SOLIDS VELOCITY m/sec	SOLIDS FLOW kg/sec	PRESS Pa/m	AIR PRESS Pa/m	VOIDAGE	LOADING
160	13.38	8.80	17.0E-3	55.68	44.19	.9996	.509
161	11.85	8.67	17.5E-3	48.48	35.71	.9995	.590
162	10.85	7.96	18.9E-3	43.37	30.60	.9995	.697
163	9.16	4.75	18.1E-3	32.97	22.76	.9992	.793
164	8.65	7.96	18.3E-3	25.69	20.58	.9995	.848
165	7.82	3.32	18.3E-3	19.83	17.28	.9989	.937
166	7.60	6.60	18.1E-3	22.56	16.43	.9994	.955
167	5.69	2.29	18.1E-3	22.66	9.90	.9984	1.276
168	4.07	2.23	14.9E-3	16.99	5.50	.9987	1.468
169	5.82	4.34	18.2E-3	17.33	10.31	.9992	1.253

TEMP= 20.0 C   HUMIDITY= 51.7   MASS RATE= 17.8E-3 kg/sec

79 MICRON GLASS BEADS
VERTICAL ORIENTATION
LOW HUMIDITY

RUN	GAS VELOCITY m/sec	SOLIDS VELOCITY m/sec	SOLIDS FLOW kg/sec	PRESS Pa/m	AIR PRESS Pa/m	VOIDAGE	LOADING
190	14.34	12.01	16.4E-3	52.41	49.86	.9997	.459
191	12.36	6.67	16.8E-3	48.67	38.45	.9995	.544
192	10.85	5.24	17.4E-3	36.99	30.60	.9993	.641
193	10.67	5.04	18.6E-3	43.52	29.73	.9993	.698
194	8.31	6.17	9.4E-3	31.34	19.21	.9997	.453
195	9.20	6.41	16.3E-3	25.63	22.95	.9995	.710
196	7.54	5.37	15.7E-3	30.48	16.18	.9994	.833
197	6.47	6.11	17.8E-3	28.34	12.38	.9994	1.099
198	5.56	5.00	17.1E-3	22.26	9.49	.9993	1.233

TEMP= 30.0 C   HUMIDITY= 16.0   MASS RATE= 18.3E-3 kg/sec

79 MICRON GLASS BEADS
VERTICAL ORIENTATION
HIGH HUMIDITY

RUN	GAS VELOCITY m/sec	SOLIDS VELOCITY m/sec	SOLIDS FLOW kg/sec	PRESS Pa/m	AIR PRESS Pa/m	VOIDAGE	LOADING
170	13.85	8.80	27.1E-3	61.01	46.96	.9994	.782
171	11.37	8.69	28.3E-3	46.02	33.25	.9993	.997
172	8.78	6.67	29.3E-3	39.01	21.14	.9991	1.335
173	7.41	6.41	28.7E-3	36.13	15.70	.9991	1.548
174	4.30	4.29	19.1E-3	37.97	6.05	.9991	1.774
175	7.67	6.35	28.5E-3	39.66	16.68	.9991	1.487
176	8.60	7.59	28.8E-3	39.52	20.37	.9992	1.342
177	10.30	5.95	23.0E-3	44.54	27.95	.9992	.893
178	7.82	5.69	28.3E-3	39.59	17.25	.9990	1.451
179	5.00	4.23	24.3E-3	33.69	7.89	.9988	1.940

TEMP= 20.0 C   HUMIDITY= 53.0   MASS RATE= 26.5E-3 kg/sec

79 MICRON GLASS BEADS
VERTICAL ORIENTATION
LOW HUMIDITY

RUN	GAS VELOCITY m/sec	SOLIDS VELOCITY m/sec	SOLIDS FLOW kg/sec	PRESS Pa/m	AIR PRESS Pa/m	VOIDAGE	LOADING
180	14.60	10.20	27.1E-3	62.94	51.45	.9995	.742
181	13.41	10.48	26.8E-3	56.49	44.36	.9995	.799
182	12.15	9.86	27.2E-3	50.10	37.33	.9994	.897
183	10.37	7.96	27.6E-3	44.48	28.30	.9993	1.063
184	9.34	5.50	28.0E-3	39.50	23.54	.9990	1.201
185	8.15	6.67	27.7E-3	35.92	18.56	.9992	1.361
186	6.96	4.86	27.1E-3	38.67	14.09	.9989	1.556
187	7.04	4.49	26.9E-3	36.06	14.36	.9988	1.531
189	6.71	4.34	26.3E-3	31.41	13.19	.9988	1.569

TEMP= 35.0 C   HUMIDITY= 18.5   MASS RATE= 28.3E-3 kg/sec

128 MICRON PLEXIGLAS BEADS
VERTICAL ORIENTATION
HIGH HUMIDITY

RUN	GAS VELOCITY m/sec	SOLIDS VELOCITY m/sec	SOLIDS FLOW kg/sec	PRESS Pa/m	AIR PRESS Pa/m	VOIDAGE	LOADING
231	8.76	6.41	8.7E-3	26.15	21.05	.9995	.397
232	5.33	4.49	8.8E-3	19.56	8.84	.9993	.659
233	3.85	2.58	8.6E-3	21.58	4.98	.9988	.895
234	3.18	3.12	6.8E-3	17.87	3.57	.9992	.856
236	3.45	2.95	7.6E-3	21.99	4.11	.9990	.878
237	5.91	4.75	9.4E-3	20.80	10.58	.9993	.633
238	7.78	5.95	8.9E-3	22.21	17.11	.9994	.457
239	10.76	7.96	8.3E-3	41.39	30.15	.9996	.309

TEMP= 18.0 C HUMIDITY= 47.2 MASS RATE= 45.7E-3 kg/sec

128 MICRON PLEXIGLAS BEADS
VERTICAL ORIENTATION
LOW HUMIDITY

RUN	GAS VELOCITY m/sec	SOLIDS VELOCITY m/sec	SOLIDS FLOW kg/sec	PRESS Pa/m	AIR PRESS Pa/m	VOIDAGE	LOADING
220	9.82	6.17	8.7E-3	36.67	25.74	.9995	.354
221	8.45	5.50	8.5E-3	27.93	19.75	.9994	.403
222	6.14	4.75	9.3E-3	21.50	11.29	.9993	.608
223	4.62	3.25	8.9E-3	18.37	6.88	.9990	.769
224	3.55	2.43	7.4E-3	20.92	4.32	.9989	.832
225	4.27	2.90	9.2E-3	17.73	5.98	.9988	.859
226	3.32	2.95	7.2E-3	24.29	3.86	.9991	.865
227	8.34	7.18	8.3E-3	28.24	19.30	.9996	.399
228	6.53	5.50	8.8E-3	17.72	12.61	.9994	.538

TEMP= 33.5 C HUMIDITY= 16.0 MASS RATE= 8.8E-3 kg/sec

128 MICRON PLEXIGLAS BEADS
VERTICAL ORIENTATION
HIGH HUMIDITY

RUN	GAS VELOCITY m/sec	SOLIDS VELOCITY m/sec	SOLIDS FLOW kg/sec	PRESS Pa/m	AIR PRESS Pa/m	VOIDAGE	LOADING
240	12.97	8.88	11.2E-3	58.42	41.82	.9994	.345
241	12.63	7.96	12.6E-3	48.89	39.95	.9994	.399
242	8.22	7.59	12.8E-3	32.90	18.85	.9994	.621
243	6.00	3.92	12.9E-3	26.18	10.86	.9988	.861
244	4.74	3.12	12.1E-3	36.56	7.19	.9985	1.023
245	8.15	5.20	13.4E-3	30.05	18.56	.9990	.657
246	3.63	3.18	12.1E-3	33.87	4.51	.9986	1.336
248	8.04	5.95	13.7E-3	34.37	18.12	.9991	.682
249	4.89	3.18	13.2E-3	36.19	7.59	.9984	1.082

TEMP= 20.0 C HUMIDITY= 52.8 MASS RATE= 12.9E-3 kg/sec

128 MICRON PLEXIGLAS BEADS
VERTICAL ORIENTATION
LOW HUMIDITY

RUN	GAS VELOCITY m/sec	SOLIDS VELOCITY m/sec	SOLIDS FLOW kg/sec	PRESS Pa/m	AIR PRESS Pa/m	VOIDAGE	LOADING
210	11.08	7.59	12.9E-3	39.40	31.74	.9997	.466
211	7.34	• 5.33	13.9E-3	26.92	15.43	.9995	.756
212	7.26	5.95	13.9E-3	24.10	15.16	.9995	.763
213	6.26	5.90	14.2E-3	23.19	11.70	.9995	.906
214	4.59	4.37	13.2E-3	24.17	6.81	.9994	1.152
215	4.30	2.68	14.2E-3	39.25	6.05	.9989	1.320
216	3.45	3.24	7.8E-3	37.31	4.11	.9995	.904
217	13.13	12.01	12.0E-3	70.71	42.75	.9998	.365
218	4.96	3.06	12.8E-3	52.48	7.79	.9992	1.028
219	3.78	3.37	9.6E-3	40.59	4.83	.9994	1.017

TEMP= 35.0 C HUMIDITY= 16.0 MASS RATE= 12.4E-3 kg/sec

125 MICRON GLASS BEADS
HORIZONTAL ORIENTATION
HIGH HUMIDITY

RUN	GAS VELOCITY m/sec	SOLIDS VELOCITY m/sec	SOLIDS FLOW kg/sec	PRESS Pa/m	AIR PRESS Pa/m	VOIDAGE	LOADING
269	10.98	7.26	17.7E-3	50.42	31.27	.9995	.643
270	10.98	6.67	17.5E-3	44.03	31.27	.9995	.636
271	9.96	8.69	17.9E-3	61.07	26.35	.9996	.717
272	9.62	6.11	18.3E-3	47.17	24.83	.9994	.759
273	8.65	3.24	19.8E-3	43.57	20.58	.9988	.918
274	7.73	3.53	19.1E-3	36.09	16.93	.9989	.985
275	6.85	3.46	19.1E-3	31.55	13.68	.9989	1.113
276	5.78	2.33	18.9E-3	25.49	10.17	.9984	1.306

TEMP= 29.4 C   HUMIDITY= 51.7   MASS RATE= 18.5E-3 kg/sec

125 MICRON GLASS BEADS
HORIZONTAL ORIENTATION
LOW HUMIDITY

RUN	GAS VELOCITY m/sec	SOLIDS VELOCITY m/sec	SOLIDS FLOW kg/sec	PRESS Pa/m	AIR PRESS Pa/m	VOIDAGE	LOADING
255	9.45	3.93	17.6E-3	25.30	24.02	.9991	.744
256	9.20	4.89	16.8E-3	33.17	22.95	.9993	.731
257	7.56	3.24	17.7E-3	29.03	16.26	.9989	.935
258	6.49	4.86	17.8E-3	22.67	12.46	.9993	1.095
259	6.00	2.90	17.1E-3	21.08	10.86	.9988	1.140
260	4.36	2.43	5.9E-3	16.44	6.22	.9995	.537
261	10.31	7.59	18.0E-3	40.79	28.02	.9995	.696

TEMP= 33.2 C   HUMIDITY= 16.9   MASS RATE= 15.8E-3 kg/sec

125 MICRON GLASS BEADS
HORIZONTAL ORIENTATION
HIGH HUMIDITY

RUN	GAS VELOCITY m/sec	SOLIDS VELOCITY m/sec	SOLIDS FLOW kg/sec	PRESS Pa/m	AIR PRESS Pa/m	VOIDAGE	LOADING
277	9.47	9.30	26.1E-3	71.38	24.14	.9994	1.101
278	8.59	4.34	26.2E-3	72.04	20.33	.9986	1.221
279	7.64	5.33	27.2E-3	62.54	16.58	.9990	1.425
280	7.56	6.41	27.2E-3	58.39	16.26	.9991	1.441
281	5.92	5.16	27.5E-3	54.01	10.60	.9989	1.856
283	4.72	3.67	12.9E-3	31.40	7.14	.9993	1.088

TEMP= 28.4 C HUMIDITY= 52.3 MASS RATE= 25.3E-3 kg/sec

125 MICRON GLASS BEADS
HORIZONTAL ORIENTATION
LOW HUMIDITY

RUN	GAS VELOCITY m/sec	SOLIDS VELOCITY m/sec	SOLIDS FLOW kg/sec	PRESS Pa/m	AIR PRESS Pa/m	VOIDAGE	LOADING
262	9.78	8.25	27.5E-3	56.81	25.53	.9993	1.123
263	8.28	5.55	28.2E-3	42.06	19.08	.9990	1.362
264	7.89	3.24	28.5E-3	40.52	17.54	.9982	1.444
265	6.36	6.35	29.0E-3	33.74	12.03	.9991	1.822
266	4.89	3.05	16.4E-3	26.74	7.59	.9989	1.340
267	4.39	3.05	4.3E-3	8.84	6.28	.9997	.391
268	6.84	4.37	30.5E-3	37.90	13.64	.9986	1.784

TEMP= 36.4 C HUMIDITY= 16.1 MASS RATE= 23.5E-3 kg/sec

79 MICRON GLASS BEADS
HORIZONTAL ORIENTATION
HIGH HUMIDITY

RUN	GAS VELOCITY m/sec	SOLIDS VELOCITY m/sec	SOLIDS FLOW kg/sec	PRESS Pa/m	AIR PRESS Pa/m	VOIDAGE	LOADING
298	10.18	5.00	16.6E-3	33.77	27.39	.9993	.654
299	9.87	7.96	16.4E-3	39.98	25.94	.9996	.666
300	9.07	5.74	17.0E-3	42.80	22.37	.9994	.750
301	8.85	5.69	17.4E-3	38.02	21.42	.9994	.786
302	7.74	4.75	17.4E-3	32.26	16.94	.9993	.899
303	7.16	4.13	17.8E-3	23.72	14.78	.9991	.993

TEMP= 22.4 C   HUMIDITY= 55.4   MASS RATE= 19.0E-3 kg/sec

79 MICRON GLASS BEADS
HORIZONTAL ORIENTATION
LOW HUMIDITY

RUN	GAS VELOCITY m/sec	SOLIDS VELOCITY m/sec	SOLIDS FLOW kg/sec	PRESS Pa/m	AIR PRESS Pa/m	VOIDAGE	LOADING
284	11.60	4.59	15.9E-3	44.65	34.43	.9993	.547
285	11.29	3.37	16.4E-3	44.58	32.83	.9990	.583
286	10.63	8.36	16.4E-3	40.24	29.52	.9996	.619
287	9.87	7.03	16.8E-3	34.88	25.94	.9995	.682
288	9.20	8.36	16.8E-3	33.17	22.95	.9996	.731
289	8.00	4.49	17.4E-3	26.91	17.97	.9992	.869
290	5.87	4.49	8.3E-3	19.13	10.44	.9996	.567

TEMP= 35.6 C   HUMIDITY= 19.1   MASS RATE= 15.4E-3 kg/sec

79 MICRON GLASS BEADS
HORIZONTAL ORIENTATION
HIGH HUMIDITY

RUN	GAS VELOCITY m/sec	SOLIDS VELOCITY m/sec	SOLIDS FLOW kg/sec	PRESS Pa/m	AIR PRESS Pa/m	VOIDAGE	LOADING
305	10.28	5.00	22.9E-3	44.46	27.86	.9991	.891
306	8.67	5.69	23.7E-3	28.97	20.67	.9992	1.092
307	8.20	2.29	25.7E-3	35.34	18.74	.9977	1.254
308	7.34	2.75	26.5E-3	30.50	15.43	.9981	1.443
309	5.83	2.75	18.1E-3	20.55	10.34	.9987	1.244
310	8.00	7.18	26.2E-3	32.02	17.97	.9993	1.310
311	8.22	3.93	26.0E-3	32.90	18.85	.9987	1.262

TEMP= 21.5 C   HUMIDITY= 53.4   MASS RATE= 24.1E-3 kg/sec

79 MICRON GLASS BEADS
HORIZONTAL ORIENTATION
LOW HUMIDITY

RUN	GAS VELOCITY m/sec	SOLIDS VELOCITY m/sec	SOLIDS FLOW kg/sec	PRESS Pa/m	AIR PRESS Pa/m	VOIDAGE	LOADING
291	11.39	9.86	24.7E-3	47.39	33.34	.9995	.867
292	10.28	4.34	26.5E-3	44.46	27.86	.9988	1.030
293	9.78	3.93	25.7E-3	44.68	25.53	.9987	1.051
294	8.84	3.44	26.7E-3	41.80	21.37	.9984	1.209
295	6.17	4.03	15.6E-3	20.33	11.40	.9992	1.013
296	9.22	6.95	25.7E-3	38.86	23.05	.9993	1.115
297	8.11	2.66	26.5E-3	36.03	18.41	.9980	1.305

TEMP= 36.8 C   HUMIDITY= 18.5   MASS RATE= 24.5E-3 kg/sec

450 MICRON GLASS BEADS
HORIZONTAL ORIENTATION
HIGH HUMIDITY

RUN	GAS VELOCITY m/sec	SOLIDS VELOCITY m/sec	SOLIDS FLOW kg/sec	PRESS Pa/m	AIR PRESS Pa/m	VOIDAGE	LOADING
319	14.09	10.48	18.9E-3	49.66	48.38	.9996	.536
320	10.94	7.26	18.9E-3	43.81	31.04	.9995	.691
321	10.36	4.86	19.3E-3	41.00	28.23	.9992	.744
322	8.54	5.90	19.8E-3	35.44	20.12	.9993	.930
323	7.69	4.75	20.4E-3	34.64	16.77	.9991	1.062
324	6.89	3.44	21.2E-3	29.16	13.83	.9988	1.229

TEMP= 25.2 C   HUMIDITY= 56.3   MASS RATE= 19.8E-3 kg/sec

450 MICRON GLASS BEADS
HORIZONTAL ORIENTATION
LOW HUMIDITY

RUN	GAS VELOCITY m/sec	SOLIDS VELOCITY m/sec	SOLIDS FLOW kg/sec	PRESS Pa/m	AIR PRESS Pa/m	VOIDAGE	LOADING
312	12.71	9.71	19.1E-3	59.56	40.41	.9996	.601
313	12.09	8.36	19.1E-3	59.99	37.01	.9995	.632
314	10.19	8.69	19.1E-3	42.77	27.45	.9996	.749
315	10.85	5.69	19.1E-3	42.09	30.60	.9993	.704
316	8.78	5.69	19.8E-3	41.56	21.13	.9993	.904
317	8.00	5.04	19.8E-3	38.40	17.97	.9992	.992
318	6.42	5.16	20.7E-3	26.26	12.22	.9992	1.288

TEMP= 36.8 C   HUMIDITY= 16.3   MASS RATE= 19.5E-3 kg/sec

450 MICRON GLASS BEADS
HORIZONTAL ORIENTATION
HIGH HUMIDITY

RUN	GAS VELOCITY m/sec	SOLIDS VELOCITY m/sec	SOLIDS FLOW kg/sec	PRESS Pa/m	AIR PRESS Pa/m	VOIDAGE	LOADING
326	9.84	6.35	27.7E-3	48.77	25.79	.9991	1.127
327	9.06	4.72	28.2E-3	45.31	22.32	.9988	1.246
328	7.78	4.62	29.7E-3	40.09	17.11	.9987	1.529
329	7.61	4.62	30.2E-3	36.90	16.47	.9987	1.589
331	10.11	6.11	26.7E-3	46.23	27.08	.9991	1.056
332	10.72	6.88	27.5E-3	49.15	30.00	.9992	1.024

TEMP= 26.4 C   HUMIDITY= 56.2   MASS RATE= 28.6E-3 kg/sec

450 MICRON GLASS BEADS
HORIZONTAL ORIENTATION
LOW HUMIDITY

RUN	GAS VELOCITY m/sec	SOLIDS VELOCITY m/sec	SOLIDS FLOW kg/sec	PRESS Pa/m	AIR PRESS Pa/m	VOIDAGE	LOADING
417	11.90	7.96	28.5E-3	65.38	36.01	.9993	.959
418	10.09	7.96	29.8E-3	57.61	26.97	.9992	1.180
419	8.75	5.33	29.9E-3	49.11	21.02	.9989	1.366
420	7.91	4.23	31.0E-3	41.88	17.62	.9985	1.567
421	7.27	4.49	31.2E-3	119.60	15.19	.9986	1.716

TEMP= 36.8 C   HUMIDITY= 16.4   MASS RATE= 32.3E-3 kg/sec

125 MICRON GLASS BEADS
45 DEGREE ORIENTATION
HIGH HUMIDITY

RUN	GAS VELOCITY m/sec	SOLIDS VELOCITY m/sec	SOLIDS FLOW kg/sec	PRESS Pa/m	AIR PRESS Pa/m	VOIDAGE	LOADING
375	9.87	5.55	18.3E-3	38.71	25.94	.9993	.743
376	9.42	6.41	19.1E-3	36.70	23.93	.9994	.810
377	8.98	6.67	18.9E-3	34.76	21.99	.9994	.842
378	8.14	7.96	19.3E-3	30.25	18.50	.9995	.948
379	7.42	5.74	19.5E-3	30.57	15.76	.9993	1.049
380	6.36	4.86	19.5E-3	28.61	12.01	.9992	1.225
381	4.85	3.44	13.0E-3	31.99	7.47	.9992	1.077

TEMP= 28.3 C HUMIDITY= 56.4 MASS RATE= 18.2E-3 kg/sec

125 MICRON GLASS BEADS
45 DEGREE ORIENTATION
LOW HUMIDITY

RUN	GAS VELOCITY m/sec	SOLIDS VELOCITY m/sec	SOLIDS FLOW kg/sec	PRESS Pa/m	AIR PRESS Pa/m	VOIDAGE	LOADING
361	10.18	9.30	18.5E-3	43.99	27.39	.9996	.728
362	9.98	5.37	18.3E-3	48.16	26.45	.9993	.735
363	9.69	7.28	18.7E-3	49.39	25.13	.9995	.772
364	8.18	5.95	19.1E-3	41.66	18.68	.9994	.934
365	7.47	3.93	19.3E-3	42.74	15.93	.9990	1.033
366	6.45	4.89	19.5E-3	52.15	12.31	.9992	1.208
367	4.89	3.06	11.0E-3	138.81	7.59	.9993	.897

TEMP= 38.6 C HUMIDITY= 19.0 MASS RATE= 17.8E-3 kg/sec

125 MICRON GLASS BEADS
45 DEGREE ORIENTATION
HIGH HUMIDITY

RUN	GAS VELOCITY m/sec	SOLIDS VELOCITY m/sec	SOLIDS FLOW kg/sec	PRESS Pa/m	AIR PRESS Pa/m	VOIDAGE	LOADING
382	8.31	7.26	28.2E-3	42.68	19.19	.9992	1.359
383	7.72	5.55	28.5E-3	42.43	16.89	.9990	1.475
384	7.11	5.16	28.5E-3	39.65	14.62	.9989	1.602
385	7.61	5.37	28.5E-3	39.71	16.47	.9989	1.496
386	5.17	4.72	20.4E-3	47.18	8.36	.9991	1.580
387	6.70	5.20	28.5E-3	40.23	13.16	.9989	1.701
388	10.06	7.86	26.7E-3	50.57	26.82	.9993	1.062

TEMP= 30.8 C HUMIDITY= 56.7 MASS RATE= 27.0E-3 kg/sec

125 MICRON GLASS BEADS
45 DEGREE ORIENTATION
LOW HUMIDITY

RUN	GAS VELOCITY m/sec	SOLIDS VELOCITY m/sec	SOLIDS FLOW kg/sec	PRESS Pa/m	AIR PRESS Pa/m	VOIDAGE	LOADING
368	9.00	7.50	28.7E-3	68.05	22.08	.9992	1.277
369	8.45	6.41	28.5E-3	69.04	19.75	.9991	1.349
370	7.70	3.93	28.5E-3	74.24	16.79	.9985	1.480
371	6.95	5.20	29.0E-3	70.21	14.03	.9989	1.669
373	6.56	5.74	29.0E-3	73.97	12.68	.9990	1.768
374	7.06	6.41	28.7E-3	75.71	14.42	.9991	1.628

TEMP= 38.2 C HUMIDITY= 22.0 MASS RATE= 28.9E-3 kg/sec

450 MICRON GLASS BEADS
45 DEGREE ORIENTATION
HIGH HUMIDITY

RUN	GAS VELOCITY m/sec	SOLIDS VELOCITY m/sec	SOLIDS FLOW kg/sec	PRESS Pa/m	AIR PRESS Pa/m	VOIDAGE	LOADING
347	11.91	9.86	18.5E-3	55.22	36.07	.9996	.622
348	11.11	6.60	18.3E-3	52.36	31.93	.9994	.660
349	10.82	6.41	18.7E-3	52.20	30.49	.9994	.691
350	10.00	6.17	19.1E-3	48.26	26.56	.9994	.763
351	9.29	5.04	19.7E-3	46.96	23.34	.9992	.846
352	7.38	4.72	20.6E-3	48.79	15.60	.9991	1.117

TEMP= 30.0 C HUMIDITY= 55.7 MASS RATE= 18.6E-3 kg/sec

450 MICRON GLASS BEADS
45 DEGREE ORIENTATION
LOW HUMIDITY

RUN	GAS VELOCITY m/sec	SOLIDS VELOCITY m/sec	SOLIDS FLOW kg/sec	PRESS Pa/m	AIR PRESS Pa/m	VOIDAGE	LOADING
333	10.89	5.90	18.4E-3	75.51	30.82	.9994	.677
334	9.82	4.59	20.0E-3	62.76	25.74	.9991	.816
335	9.29	5.33	20.7E-3	67.50	23.34	.9992	.893
336	8.85	5.37	19.8E-3	61.64	21.42	.9993	.897
337	8.16	3.59	20.2E-3	63.28	18.59	.9989	.992
339	7.16	4.37	20.2E-3	88.84	14.78	.9991	1.130

TEMP= 39.6 C HUMIDITY= 21.9 MASS RATE= 20.3E-3 kg/sec

450 MICRON GLASS BEADS
45 DEGREE ORIENTATION
HIGH HUMIDITY

RUN	GAS VELOCITY m/sec	SOLIDS VELOCITY m/sec	SOLIDS FLOW kg/sec	PRESS Pa/m	AIR PRESS Pa/m	VOIDAGE	LOADING
354	11.23	6.67	27.5E-3	68.24	32.49	.9992	.979
355	10.61	5.04	27.7E-3	61.38	29.46	.9989	1.045
356	10.11	7.96	28.2E-3	57.72	27.08	.9993	1.116
357	8.72	5.50	29.5E-3	52.83	20.91	.9989	1.352
358	8.28	4.03	29.7E-3	57.89	19.08	.9985	1.437
359	7.72	6.60	30.7E-3	62.86	16.89	.9991	1.592

TEMP= 29.6 C HUMIDITY= 53.6 MASS RATE= 29.1E-3 kg/sec

450 MICRON GLASS BEADS
45 DEGREE ORIENTATION
LOW HUMIDITY

RUN	GAS VELOCITY m/sec	SOLIDS VELOCITY m/sec	SOLIDS FLOW kg/sec	PRESS Pa/m	AIR PRESS Pa/m	VOIDAGE	LOADING
340	10.00	7.86	28.5E-3	75.06	26.56	.9993	1.139
341	9.47	4.13	29.0E-3	72.67	24.15	.9986	1.223
342	8.67	7.86	29.0E-3	73.02	20.67	.9993	1.337
343	8.50	8.25	29.2E-3	71.06	19.98	.9993	1.376
344	6.72	3.75	28.0E-3	138.21	13.25	.9985	1.664
345	7.34	7.18	29.2E-3	109.90	15.43	.9992	1.594
346	8.39	7.26	29.0E-3	79.80	19.53	.9992	1.381

TEMP= 38.5 C HUMIDITY= 18.0 MASS RATE= 28.8E-3 kg/sec

79 MICRON GLASS BEADS
45 DEGREE ORIENTATION
HIGH HUMIDITY

RUN	GAS VELOCITY m/sec	SOLIDS VELOCITY m/sec	SOLIDS FLOW kg/sec	PRESS Pa/m	AIR PRESS Pa/m	VOIDAGE	LOADING
403	10.05	7.18	18.1E-3	44.28	26.76	.9995	.722
404	9.78	6.11	18.1E-3	45.00	25.53	.9994	.742
405	9.05	5.20	18.0E-3	45.63	22.28	.9993	.794
406	8.45	7.26	18.1E-3	35.33	19.75	.9995	.859
407	7.22	2.71	18.1E-3	32.54	15.03	.9987	1.005
408	7.02	2.39	18.1E-3	33.77	14.31	.9985	1.033
409	6.78	3.35	18.1E-3	36.80	13.45	.9989	1.071

TEMP= 24.6 C HUMIDITY= 52.8 MASS RATE= 18.1E-3 kg/sec

79 MICRON GLASS BEADS
45 DEGREE ORIENTATION
LOW HUMIDITY

RUN	GAS VELOCITY m/sec	SOLIDS VELOCITY m/sec	SOLIDS FLOW kg/sec	PRESS Pa/m	AIR PRESS Pa/m	VOIDAGE	LOADING
389	11.08	8.81	11.2E-3	39.18	31.75	.9997	.404
390	10.36	4.13	17.6E-3	44.03	28.23	.9991	.679
391	9.52	5.69	17.5E-3	38.28	24.34	.9994	.734
392	8.05	7.59	18.1E-3	36.73	18.15	.9995	.902
393	7.60	6.11	18.0E-3	35.01	16.43	.9994	.945
394	6.80	5.16	17.8E-3	35.25	13.52	.9993	1.045

TEMP= 38.0 C HUMIDITY= 18.5 MASS RATE= 16.5E-3 kg/sec

APPENDIX E.

MISCELANEOUS

RUN # TAPE # ___ TAPE SIDE ___

Procedure to calibrate Pressure Transducers

Date ______________ Time: Begin __________ End ___________

Test section orientation:

Particle ______________ Density __________ Size ____________ μm

Temperature __________/__________ Pressure __________/__________

Humidity Scale Reading __________/__________ Probe Color ___________

Turbine Meter Stop ______________ Time ______________
Start ______________

Bead Feeder Setting ______________

Solids ________________ lbs. Time ______________

Tape Footage Begin ______________ End ______________

Observations:

Pressure Drop Data:

Figure E-1: Sample Data Acquisition Form

SIZE RANGE	NO % RANGE	WEIGHT % RANGE
2.0- 4.0	10.000	.001
4.0- 6.3	8.000	.006
6.3- 10.0	3.000	.008
10.0- 12.6	0.000	0.000
12.6- 15.8	0.000	0.000
15.8- 19.9	0.000	0.000
19.9- 25.1	1.000	.058
25.1- 31.6	1.000	.117
31.6- 39.8	6.000	1.396
39.8- 50.1	25.000	11.611
50.1- 63.1	28.000	25.962
63.1- 79.4	13.000	24.046
79.4-100.0	0.000	0.000
100.0-125.8	5.000	36.795

LENGTH DIAMETER= 45.6
VOLUME DIAMETER= 57.8
SURFACE DIAMETER= 52.9
SURFACE-VOLUME DIAMETER= 70.0
WEIGHT DIAMETER= 79.1

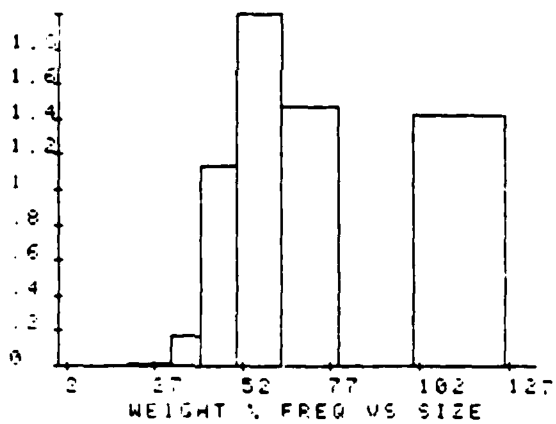

Figure E-2: **Particle Analysis for 79μm Glass Beads Before Experiments**

LENGTH MEAN SIZE:	6.9
VOLUME MEAN SIZE:	26.9
SURFACE MEAN SIZE:	16.1
SURFACE-VOLUME MEAN SIZE:	76.3
WEIGHT MEAN SIZE:	90.8

LENGTH-MEAN DIA. =	3.3459
LENGTH-SURF DIA. =	45.5540
SURFACE-VOL DIA. =	59.4621
VOLUME-MASS DIA. =	67.7688

Figure E-3: Particle Analysis for 79μm Glass Beads After Experiments

SIZE RANGE	NO % RANGE	WEIGHT % RANGE
2 0- 4 0	7 515	000
4 0- 6 3	9 827	002
6 3- 10 0	12 139	012
10 0- 12 6	6 358	016
12 6- 15.8	6 936	036
15.8- 19 9	4 046	.041
19 9- 25 1	578	012
25 1- 31 6	578	024
31 6- 39.8	1 156	.094
39 8- 50 1	1 156	188
50 1- 63 1	3 468	1 128
63 1- 79.4	16 185	10.497
79 4-100 0	16 185	20 945
100 0-125 8	5 202	13 424
125 8-158 4	6 936	35 687
158 4-200 0	1 734	17 893

LENGTH DIAMETER= 52 2
VOLUME DIAMETER= 82 0
SURFACE DIAMETER= 70.3
SURFACE-VOLUME DIAMETER= 112 7
WEIGHT DIAMETER= 125 0

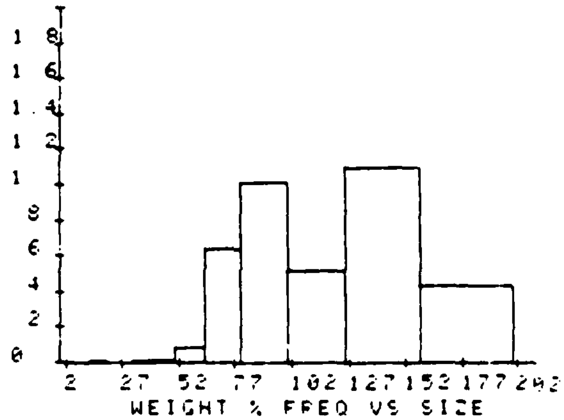

Figure E-4: Particle Analysis for 125μm Glass Beads Before Experiments

LENGTH MEAN SIZE:	14.2
VOLUME MEAN SIZE:	42.3
SURFACE MEAN SIZE:	27.7
SURFACE-VOLUME MEAN SIZE:	100.0
WEIGHT MEAN SIZE:	133.8

LENGTH-MEAN DIA.	=	9.7281
LENGTH-SURF DIA.	=	48.6002
SURFACE-VOL DIA.	=	76.0933
VOLUME-MASS DIA.	=	100.7184

Figure E-5: Particle Analysis for 125μm Glass Beads After Experiments

SIZE RANGE	NO % RANGE	WEIGHT % RANGE
2.0- 4.0	6.024	.000
4.0- 6.3	12.048	.000
6.3- 10.0	15.663	.001
10.0- 12.6	7.229	.001
12.6- 15.8	8.434	.002
15.8- 19.9	8.434	.003
19.9- 25.1	4.819	.004
25.1- 31.6	0.000	0.000
31.6- 39.8	1.205	.004
39.8- 50.1	3.615	.023
50.1- 63.1	1.205	.015
63.1- 79.4	3.615	.091
79.4-100.0	4.819	.243
100.0-125.8	1.205	.121
125.8-158.4	0.000	0.000
158.4-200.0	0.000	0.000
200.0-251.1	0.000	0.000
251.1-316.1	7.229	11.507
316.[illegible]-400.[illegible]	6.024	19.297
400.[illegible]-500.0	6.024	38.310
500.0-630.6	2.410	30.378

LENGTH DIAMETER= 100.5
VOLUME DIAMETER= 241.6
SURFACE DIAMETER= 185.4
SURFACE-VOLUME DIAMETER= 416.8
WEIGHT DIAMETER= 446.3

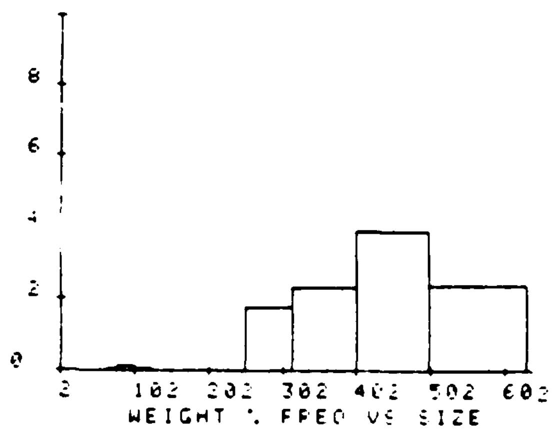

Figure E-6: **Particle Analysis for 450μm Glass Beads Before Experiments**

LENGTH MEAN SIZE:	40.2
VOLUME MEAN SIZE:	141.7
SURFACE MEAN SIZE:	87.9
SURFACE-VOLUME MEAN SIZE:	373.9
WEIGHT MEAN SIZE:	447.0

LENGTH-MEAN DIA. =	31.2593
LENGTH-SURF DIA. =	152.2733
SURFACE-VOL DIA. =	288.4763
VOLUME-MASS DIA. =	343.1080

Figure E-7: Particle Analysis for 450μm Glass Beads After Experiments

SIZE RANGE	NO % RANGE	WEIGHT % RANGE
2.0- 4.0	9.910	.000
4.0- 6.3	7.207	.002
6.3- 10.0	1.802	.002
10.0- 12.6	1.802	.005
12.6- 15.8	2.703	.014
15.8- 19.9	2.703	.028
19.9- 25.1	2.703	.055
25.1- 31.6	2.703	.111
31.6- 39.8	4.505	.369
39.8- 50.1	2.703	.442
50.1- 63.1	9.910	3.237
63.1- 79.4	27.027	17.608
79.4-100.0	11.712	15.225
100.0-125.8	6.306	16.346
125.8-158.4	5.405	27.937
158.4-200.0	0.000	0.000
200.0-251.1	.901	18.619

LENGTH DIAMETER= 53.3
VOLUME DIAMETER= 81.8
SURFACE DIAMETER= 71.8
SURFACE-VOLUME DIAMETER= 107.7
WEIGHT DIAMETER= 128.6

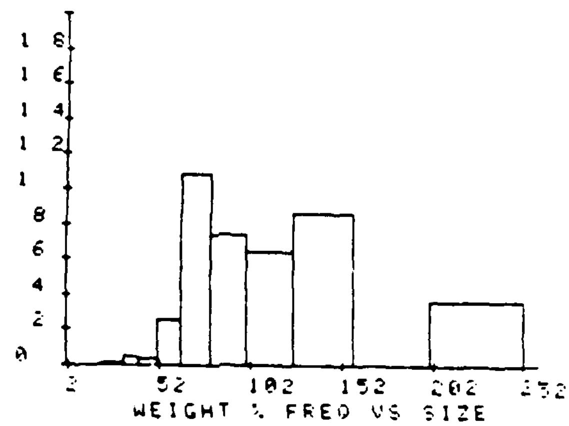

Figure E-8: Particle Analysis for 128μm Plexiglas Beads Before Experiments

LENGTH MEAN SIZE:	10.1
VOLUME MEAN SIZE:	55.7
SURFACE MEAN SIZE:	38.3
SURFACE-VOLUME MEAN SIZE:	119.3
WEIGHT MEAN SIZE:	120.7

LENGTH-MEAN DIA. = 10.7269

LENGTH-SURF DIA. = 84.8237

SURFACE-VOL DIA. = 95.0214

VOLUME-MASS DIA. = 100.8843

Figure E-9: Particle Analysis for 128μm Plexiglas Beads After Experiments

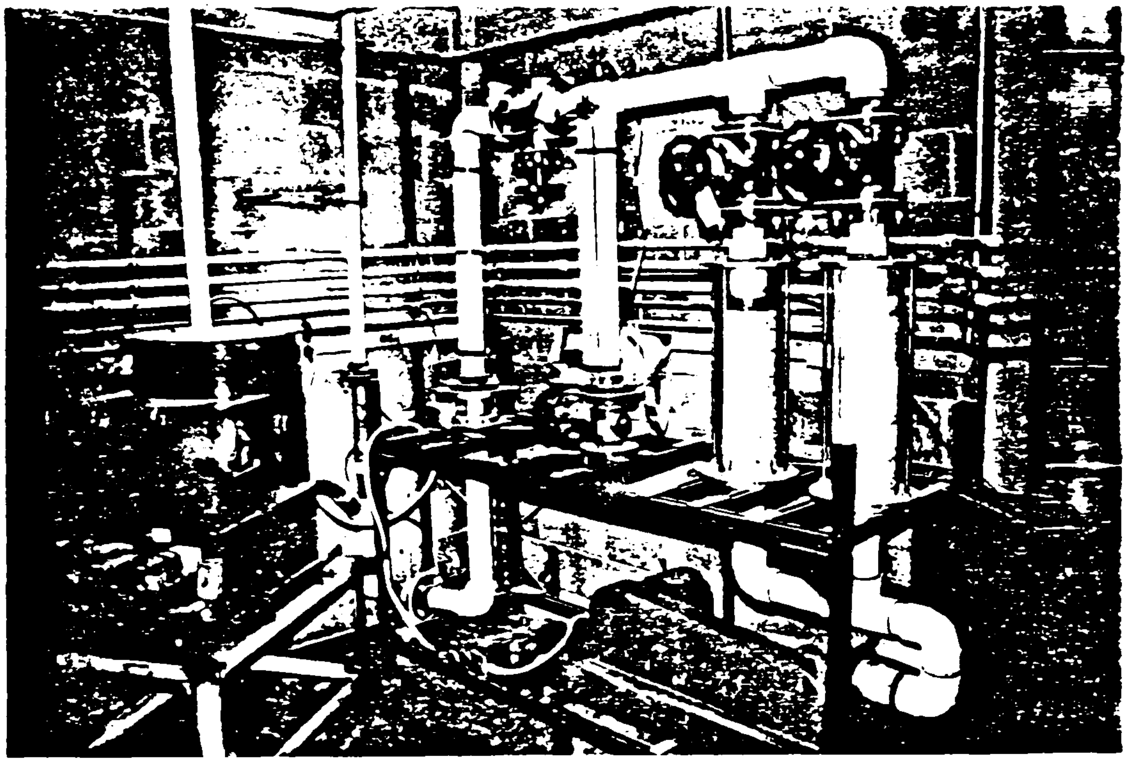

Figure E-10: Air Delivery Unit and Solids Feeder

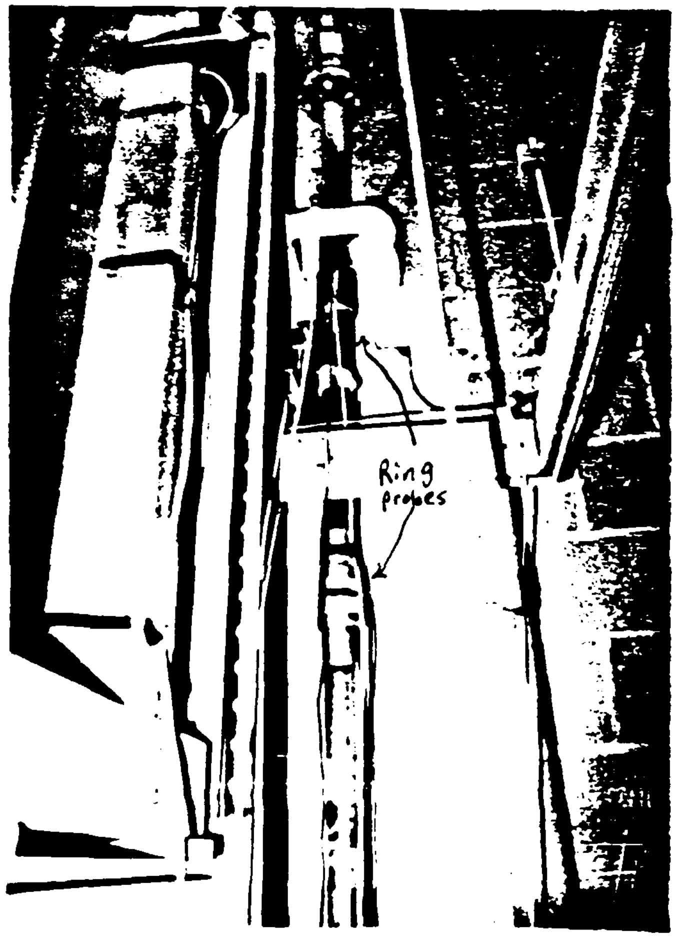

Figure E-11: Vertical Test Section Showing Electrostatic Ring Probes

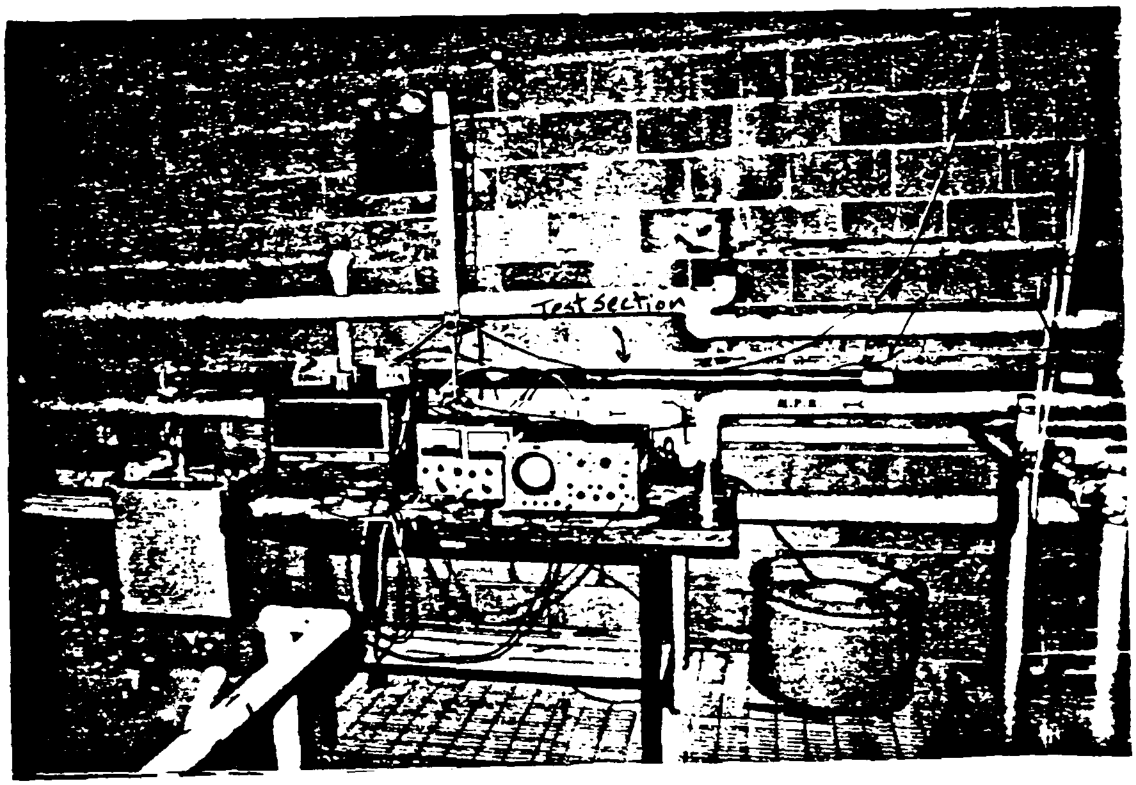

Figure E-12: Horizontal Test Section Showing Electrostatic Ring Probes

Bibliography

1. Wen,C.Y. and Yu,Y.H., "Mechanics of Fluidization", *Chem. Eng. Prog. Sym.*, Vol. 62, 1966, pp. 100.

2. Soo, S.L., *Fluid Dynamics of Multiphase Systems*, Blaisdell Pub. Co., Waltham, Mass., 1967.

3. Owen, P.R., "Pneumatic Transport", *J. Fluid Mech.*, Vol. 39, 1969, pp. 407–432.

4. Marcus, R. D., Meyers, S., Sellschop, F., Gordon, G. M., "Slip Velocity Measurement in a Dilute Phase Pneumatic Conveying System Using a Single Radio Active Tracer", University of Witwatersrand

5. Smith, R.A. and Klinzing, G.E., "Investigation of Particle Velocities in a Gas/Solid System", Chem/Pet Eng. Dept., U. of Pittsburgh

6. *PARTICLE VELOCITY AND PRESSURE DROP IN HORIZONTAL AND VERTICAL PIPES*, THIRD INTL. CONF. ON THE PNEU. TRANS. OF SOLIDS IN PIPES, 1976, by J.A. Ottjes, C.G. Meeuse, and G.J.L. van Kuijk

7. *An Electrostatic Probe for Measuring Particle Velocity in Suspension Flow*, 14th Annual FPS Meeting, 1983, by S. Nieh, B.T. Chao, and S.L. Soo

8. Sheen,S.H. and Raptis,A.C., "Tech. Memorandum #TM07", Tech. report, Argonne Natl. Laboratory, 1979.

9. Tsuji, Y., Morikawa, Y., Shiomi, H., "LDV Measurements of an Air_Solid Two Phase Flow in a Vertical Pipe", *J. Fluid Mech.*, Vol. 139, 1984, pp. 417–434.

10. Molerus, O., " Description of Pneumatic Conveying", *International Chemical Engineering*, Vol. 20, 1980, pp. 7–18.

11. Tuba,S.T., "Phen. of Vertical Gas-Solid Transport", Master's thesis, University of Pittsburgh, 1983.

12. Konno, H., Saito, S., " Pneumatic Conveying of Solids Through Straight Pipes", *Chem. Eng. Japan*, Vol. 2, 1969, pp. 211–217.

13. Yang, W. C., "Estimating the Solid Particle Velocity in Vertical Pneumatic Conveying Lines", *Ind. Eng. Chem. Fundamentals*, Vol. 12, 1973, pp. 349–352.

14. Leung, L. S., Wiles, R. J., "A Quantitative Design Procedure for Vertical Pneumatic Conveying Systems", *Ind. Eng. Chem. , Process Des. Dev.*, Vol. 15, 1976, pp. 552-557.

15. Van Swaaij,W.P.M.,Buurman,C. and van Breugel,W.J., "Shear Stresses on the Wall of a dense gas-solid Riser", *Chem. Eng. Sci.*, Vol. 25, 1970, pp. 1818-1820.

16. Reddy, K. V. S., Pei, D. C. T., "Particle Dynamics in Solid-Gas Flow in a Vertical Pipe", *I.E.C. Fund.*, Vol. 8, 1969, pp. 490-497.

17. Capes, C. E., Nakamura, K., "Vertical Pneumatic Conveying : An Experimental Study with Particles in the Intermediate and Turbulent Flow Regimes", *Can. J. Chem. Eng.*, Vol. 51, 1973, pp. 31-38.

18. Stemerding,S., "The pneumatic transport of craking catalyst in vertical risers", *Chem. Eng. Sci.*, Vol. 17, 1962, pp. 599-608.

19. Molerus, O., " Prediction of Pressure Drop with Steady State Pneumatic Conveying of Solids in Horizontal Pipes", *Chem. Eng. Sci.*, Vol. 36, 1981, pp. 1977-1984.

20. Morikawa, Y. and Tsuji,Y., "Zweiphasenstromung von Luft-Festoff-Gemischen", *Pneumatische Forderung*, Vol. 29, 1979, pp. 1027-1031.

21. Institute of Gas Technology, "Coal Conversion Systems Technical Data Book", Section IVC.50.1, HCP/t2286-01/4

22. Cheng and Soo, "Charging of Dust Particles", *J. of App. Physics*, Vol. 41, 1970, pp. 585.

23. Klinzing, G. E., *Gas-Solid Transport*, Mc. Graw Hill Book Co., New York, 1981.

24. Ally, M. R., Klinzing, G. E., "Electrostatic Effects in Gas-Solid Pneumatic Transport with Loadings to 100", *Journal of Powder & Bulk Solids Technology*, Vol. 7, 1983, pp. 13-20.

25. Yang, W. C., "Criteria for Choking in Vertical Pneumatic Conveying Lines", *Powder Technology*, Vol. 35, 1983, pp. 143-150.

26. *Estimation of Saltation Velocity in Horizontal Pneumatic Conveying*, Fourth Int. Conf. on the Pneu. Trans. of solids in Pipes, 1978, by P.J. Jones and L.S. Leung

27. Klinzing, G. E., "Linearized Stability Analysis For Gas-Solid Flow", University of Pittsburgh

28. Joseph, S., " Vertical Gas-Solid Transition Flow with Electrostatics", Master's thesis, University of Pittsburgh, 1982.

29. Zaltash, A., "Stability Analysis of Gas Solid Transport with Electrostatics", Master's thesis, University of Pittsburgh, 1985.

30. Ally, M. R., *Electrostatic Effects in Dilute and Dense Phase Gas-Solid Pneumatic Transport*, PhD dissertation, University of Pittsburgh, 1981.

END

10-87

DTIC